Annual Report 1993

Institute of Nuclear and Hadronic Physics

Editors: F. Dönau
H. Prade

Editorial staff: W. Enghardt
K. Möller
J. Mösner
G. Winter
R. Wünsch

Cover Picture

The front cover displays the start detector system of the Time-of-Flight Spectrometer for COSY experiments developed in Rossendorf. The system consists of two rings of 16 hollow light guides each, which transfer the light pulses generated in thin scintillator layers to PM tubes.

The use of the cover picture was permitted by PTD Präzisionstechnik Dresden GmbH.
Photograph: Michael Lange, Dresden

FZR-35
März 1994

Forschungszentrum Rossendorf e.V.
Postfach 51 01 19 · D-01314 Dresden
Bundesrepublik Deutschland
Telefon (0351) 591 3270
Telefax (0351) 591 3700

Preface

This annual report of the Institute of Nuclear and Hadronic Physics (IKH) of the Research Center Rossendorf Inc. (FZR) summarizes the research activities, the results and the progress achieved in the year 1993.

The present scientific profile of the IKH is predominantly determined by the participation in national or international research projects. The scientific activities of our experimental groups concentrated in 1993 on the preparations of a number of experiments at COSY in Jülich, SIS in Darmstadt, U400M in Dubna and at the S-DALINAC in Darmstadt. In this way the close and fruitful collaborations within the TOF, 0° Facility, FOPI, ALADIN, FOBOS and EUROBALL projects have been continued.

In parallel, experimental data obtained in measurements of the FOPI collaboration, from in-beam spectroscopic studies performed at VICKSI and the Cologne Tandem accelerator as well as in-beam PET experiments at SIS and the fragment separator FRS have been analyzed and succesfully interpreted.

The theoretical investigations performed in the last year dealt with the study of nuclear and subnuclear degrees of freedom, high-spin phenomena and the dynamics of open quantum systems. The results of our research and developments are presented in numerous publications, conference contributions and talks documented in this report.

In the following some prominent results of the last year are mentioned.

Applying the Tilted Cranking Theory, developed in the IKH, to experiments carried out by the spectroscopy group of the University of Bonn has led to the discovery of the "Shears Bands", which represent a new type of collective excitation showing up as regular bands of very fast magnetic and slow electric γ-transitions. This phenomenon is characterized by a tilt of the rotational axis with respect to the deformation axis, which does not occur in classical systems.

Velocity correlations of intermediate-mass fragments produced in central Au + Au collisions at 100 - 400 AMeV have been analyzed. They provide for the first time a clue on the space-time extent of the exploding and multifragmenting system in this energy range. While the data are taken by the FOPI collaboration in GSI, our interpretation benefits from common efforts of the experimental and theory groups in the Institute for Nuclear and Hadronic Physics.

A first implementation of the 4π fragment spectrometer FOBOS consisting of 10 of the 30 detector modules in its final stage has been taken into operation at the U400M in Dubna. First experiments aiming at the study of the ternary fission process in the reaction 43 AMeV $^{7}Li + ^{233}Th$ have been performed at the end of 1993.

The COSY/TOF start detector system was finally assembled and succesfully tested. Thus, an essential contribution is made to the completion of the COSY Time-of-Flight Spectrometer and for future COSY experiments.

In a series of experiments with a small positron camera at light ion beams at the GSI Darmstadt the PET-group of the IKH was able to demonstrate that the positron emitter distributions generated by nuclear fragmentation in thick targets show a pronounced structure. This may offer the possibility for in-vivo dose localization and therapy control without the necessity of producing radioactive beams.

Concerning the infrastructure of the Institute of Nuclear and Hadronic Physics further improvements were achieved during 1993, especially with respect to new installations for the computational network and new equipments for the detector laboratory.

Finally, we gratefully acknowledge the close and fruitful collaboration with our colleagues from other institutes in Germany and abroad as well as the financial support provided by the Federal Ministry for Research and Technology (BMFT), the German Research Community (DFG), the Ministry for Science and Art (SMWK) of Saxony, the KFA Jülich and the GSI Darmstadt.

The support of our collaboration partners and the institutions mentioned before was of vital importance for the scientific work in our institute.

Harald Prade

CONTENTS

I. Results of Research and Development

Explanation of special symbols:

Numerous research projects were funded by the Federal Ministry for Research and Technology (BMFT) , the German Research Community (DFG), the GSI Darmstadt and the KFA Jülich. The support of theses institutions is indicated by using the letters "B", "D", "G", "K", respectively, after the title of the corresponding contributions.

1. Theoretical Nuclear Physics

Asymmetric Flow Extracted from BUU calculations[B]

H.W. Barz [1] and B. Heide

The search for collective phenomena in intermediate energy heavy ion collisions is one of the interesting goals. In recent experiments [1,2] colliding *Au* on *Au* with bombarding energies of 150 MeV, 250 MeV and 400 MeV per nucleon, mean kinetic energies of fragments were measured as a function of the fragment mass. This mass dependence cannot be interpreted without assuming a large radial flow.

We have investigated the occurence of flow within the frame of the BUU model. This model generates the phase space distributions of the nucleons interacting through the mean field and two-body collisions. We assume that fragments are formed from a source consisting of sufficiently dense matter ($n > n_{crit} = 0.1\,n_0$) at a break-up time of about 70 fm/c. Since the source is not spherical in coordinate neither in momentum space we analyse the phase space distribution in a coordinate system which is oriented along the main axes $e^{(i)}$ of the energy flow tensor. The flow energies F_i in the main axes are given by

$$F_i = \frac{1}{2m_N}\left[\frac{1}{A}\sum_n (p^{(n)}e^{(i)})(r^{(n)}e^{(i)})\right]^2 \Big/ \left[\frac{1}{A}\sum_n (r^{(n)}e^{(i)})^2\right]. \qquad (1)$$

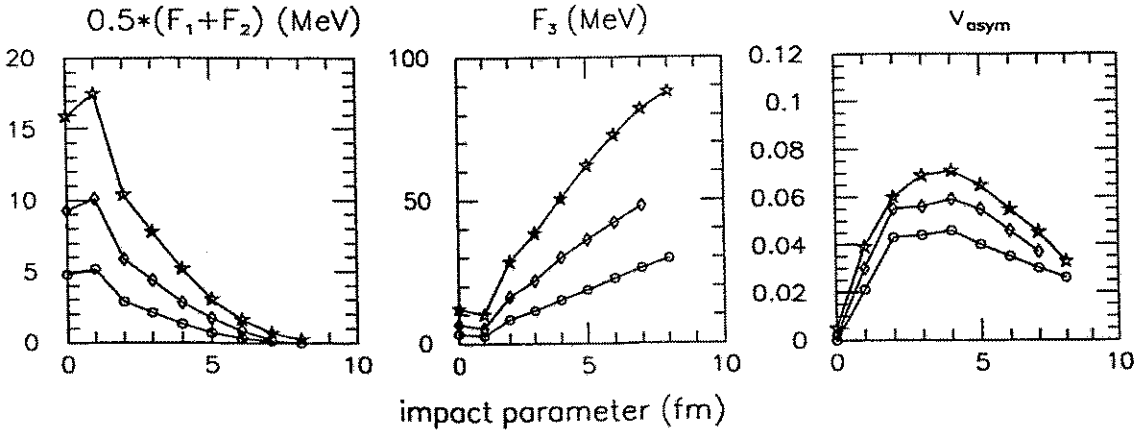

Fig. 1. Transverse, longitudinal and mean sideways flow as a function of the impact parameter for bombarding energies of 150 MeV (circles), 250 MeV (diamonds) and 400 MeV (stars), respectively.

Fig. 1 presents the results for *Au* on *Au* collisions at the three bombarding energies. For central collisions the flow ellipsoid is oblate and most of the nucleons flow sidewards. Flow energies of 14 MeV, 26 MeV and 45 MeV, respectively, are obtained. With increasing impact parameter the flow becomes more forward directed and the transverse flow diminishes. This might explain why only small flow values were found in peripheral collisions by the ALADIN collaboration. The mean sideways velocity $v_{asym} = (2\sqrt{F_3} - \sqrt{F_2} - \sqrt{F_1})/\sqrt{2m_N}\,sin\alpha$ is also shown, where α is the flow angle. The maximum values coincide well with the values of $v_{proj}\sqrt{F_S}$ in ref. [2] measured for intermediate mass fragments.

[1] Institut für Theoretische Physik, TU Dresden and Institut für Kern- und Hadronenphysik, FZ Rossendorf

REFERENCES:

[1] B. Kämpfer, R. Kotte , J. Mösner, W. Neubert, D. Wohlfahrt for FOPI-collaboration, Phys. Rev. C46(1992)R955

[2] T. Wienold, Ph. D. thesis, GSI preprint(1993), GSI-93-28

HBT Analysis of an Expanding Ultrarelativistic Pion Gas[B]

H.W. Barz[1], G. Bertsch[2,3], P. Danielewicz[2], H. Schulz[4] and G.M. Welke[5]

In ultrarelativistic collisions of heavy ions a hot central region is formed that subsequently decays mostly into π mesons. One of the primary goals in these experiments is the search for collective phenomena. We show that the degree of collectivity affects sensitively the two-pion correlations and the extracted source size calculated on the basis of the Hanbury-Brown and Twiss (HBT) effect.

For this pupose we have calculated the expansion of a mesonic cloud, where the resonances decay finally into pions. The process is described by the Boltzmann equation including Bose-Einstein statistics (see ref. [1]) and simulates the collision of ^{16}O on Au at 200 A GeV bombarding energy. The degree of collectivity is controlled by the initial density determined by the effective pionic hadronization time τ. We investigate the correlation as a function of the total momentum P_t of a pion pair. The result is shown in fig. 1.

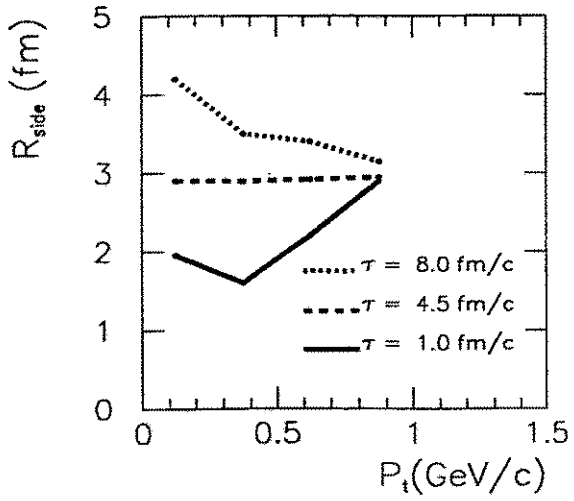

Fig. 1. Radii R_{side} extracted from the correlation function using pion pairs with total momentum around P_t.

On the first view the result is surprising, because the most strongly interacting pions exhibit the smallest radius. However, in a collective motion of cooling matter the pions with momenta around $\frac{1}{2}P_t$ come from a small region. For large transverse momenta the extracted radii are nearly independent of the initial density. This means that the fast pions do not collide frequently. The value of the radius is only slightly larger than the initial radius of the source. Obviously the fast pions leave the surface region in an early stage evading the reaction zone. However for small momenta the behaviour is quite different. For small τ, i.e. high density, we expect a highly collective behaviour which results in small radii. On the other hand the relatively independent motion of pions for large τ together with those coming from the ρ decay gives larger radii.

[1] Institut für Theoretische Physik, TU Dresden and Institut für Kern- und Hadronenphysik, FZ Rossendorf
[2] NSCL and Dpt. of Physics and Astronomy, Michigan State University, East Lansing, MI 48824, USA
[3] Department of Physics FM-15,University of Washington, Seattle, WA 98195, USA
[4] The Niels-Bohr Institute, Blegdamsvej 17, DK-2100 Copenhagen, Denmark
[5] Department of Physics and Astronomy, Wayne State University, Detroit, MI 48202, USA

References

[1] H.W. Barz, P. Danielewicz, H. Schulz and G. Welke, Phys. Lett. 287B(1992)40

A BUU-Copenhagen Hybrid Model[B]

B. HEIDE AND H.W. BARZ[1]

The description of heavy ion collisions at intermediate energies is hampered by the fact that, although the evolution of a nucleus-nucleus system from the initial stages of the collision until its maximum expansion can adequately be treated within a dynamical model, the break-up into fragments cannot. However, the fragmentation process can be described quite successfully by a statistical model. Hence, we have constructed a BUU-Copenhagen Hybrid (BCH) model which consists of both the dynamical Boltzmann-Uehling-Uhlenbeck (BUU) model and the statistical Copenhagen model.

To build up the BCH model one has to transform the "output" of the BUU model, namely the positions and momenta of the nucleons (test particles), into the "input" of the Copenhagen model, namely nucleon number, fragment velocity distribution, volume as well as excitation energy per nucleon of the fragmenting source. Further, the break-up time must be estimated.

For the determination of the nucleon number we just count the nucleons within a region in which the density is higher than one-tenth of the ground state density of nuclear matter.

In order to construct the fragment velocity distribution we make an ansatz for the Wigner function for a fragment with mass number A:

$$w_{\pm}(\vec{r},\vec{p}) = \frac{f_{\pm}(\vec{r})}{c_{\pm}} \; \mathrm{e}^{-\frac{A}{2}[\frac{\vec{p}}{A} - B_{\pm}(\vec{r}-\vec{R}_{\pm}) - \vec{b}_{\pm}]^T \Lambda_{\pm} [\frac{\vec{p}}{A} - B_{\pm}(\vec{r}-\vec{R}_{\pm}) - \vec{b}_{\pm}]} \quad . \tag{1}$$

Notation: We consider the distribution function in a system oriented according to the main axes of the energy flow tensor. We put a plane at $\vec{r} = 0$ perpendicular to the flow axis of the position distribution (cf. fig. 1a). Then the $+$ $(-)$ sign indicates that the corresponding quantity is related to the upper (lower) region of this plane, $\vec{R}$ is the centre of gravity above (below) the half plane and $\vec{b}$ is the average momentum. The elements of matrix B are connected with flow energies ($E_{flow,x}$, $E_{flow,y}$, $E_{flow,z}$), the ones of matrix Λ with temperatures. The function f is 1 if $\vec{r}$ is within a cylinder, otherwise 0, and c is a normalization factor. The quantities $\vec{b}$, A and Λ are determined by comparison with BUU calculation.

Radius R_{cyl} and length H_{cyl} of the volume of the fragmenting source are calculated by use of $\langle r_x^2 \rangle$ and $\langle r_z \rangle$.

The dependence of eq. (1) on the fragment mass A means that all fragments flow within the same velocity field but their random motion is governed by a common temperature.

For the computation of the excitation energy E^* per nucleon, we subtract the ground state energy E_0 per nucleon from the average internal energy:

$$E^* = \left(\frac{V}{N} + \frac{1}{N} \sum_{k<i}^{Z} \frac{e^2}{|\vec{r}_i - \vec{r}_k|} + \frac{1}{2mN} \sum_{i=1}^{N} \vec{p}_i^{\,2} - \sum_{j=x,y,z} E_{flow,j} \right) - E_0 \quad . \tag{2}$$

The equation holds in the CM system. Notation: V = potential energy, N = nucleon number of the fragmenting source, Z = proton number, e = elementary charge, m = nulceon mass.

Finally, we determine the break-up time in accordance with fig. 1b to be 80 fm/c.

We have applied our BCH model to semi-central (PM3-PM5) Au on Au collisions at 150 A·MeV. We found that the peak of the correlation function C_2 (see fig. 1f) is mainly caused by transverse flows. Further results are represented in fig. 1b,c,d,e.

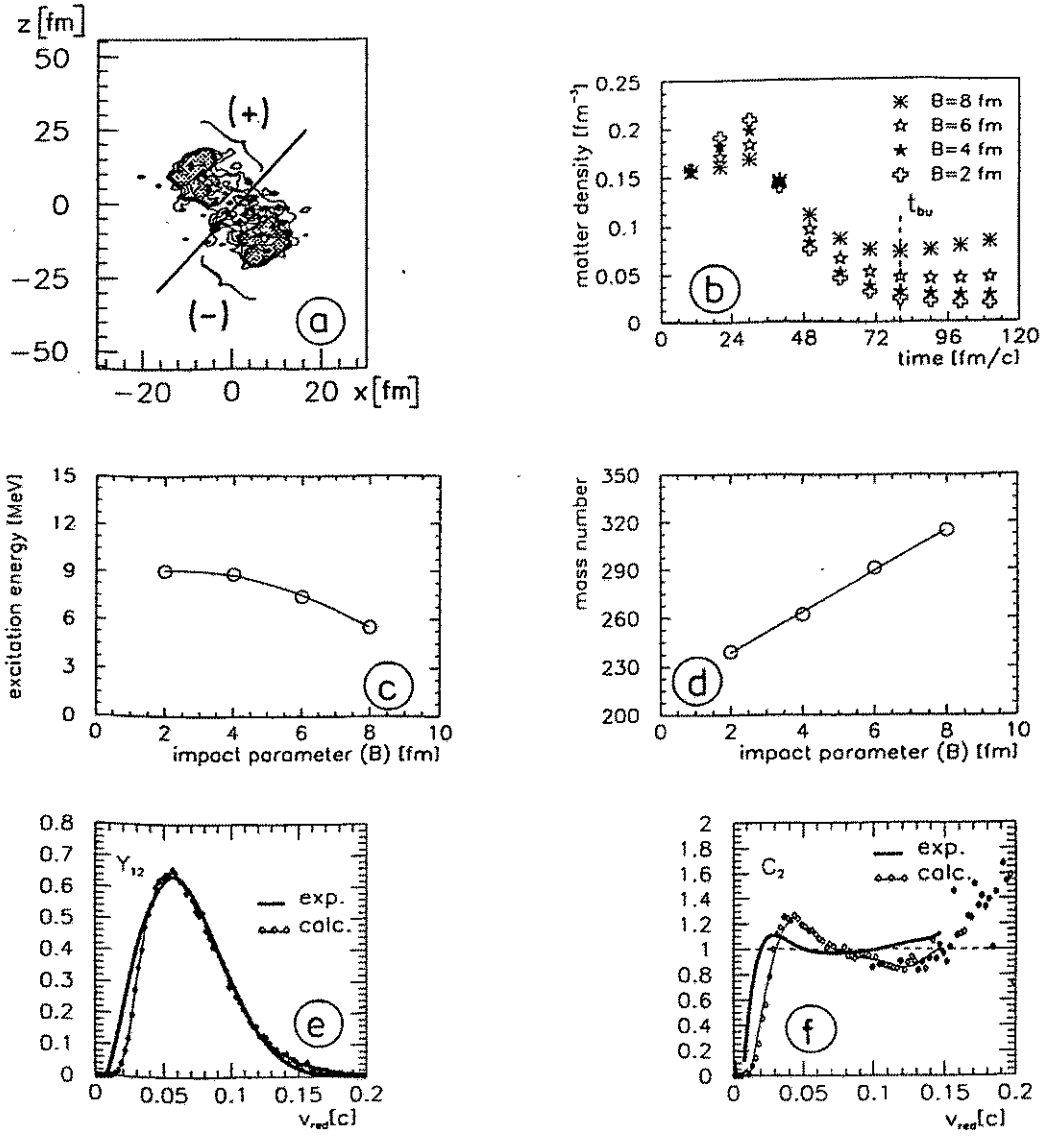

Fig. 1: Characteristics of Au on Au collisions at 150 A·MeV. (a) Contour plot of the position distribution (for impact parameter B = 6 fm and break-up time of t = t_{bu} = 80 fm/c). (b) Averaged matter density versus time for several impact parameters. (c) Excitation energy per nucleon of the fragmenting source as a function of the impact parameter at t = t_{bu}. (d) Mass number of the fragmenting source versus impact parameter at t = t_{bu}. (e) Velocity distribution versus the reduced relative velocity $v_{red} = v/\sqrt{z_1 + z_2}$ of two fragments each of them having a charge number larger than 2 according to both, the model (diamonds) and the experiment (full line, from [1]). (f) Two-particle correlation function as a function of the reduced relative velocity compared to exp. [1].

[1]Institut für Theoretische Physik, TU Dresden and Institut für Kern- und Hadronenphysik, FZ Rossendorf

REFERENCES:

[1] B. Kämpfer, R. Kotte, J. Mösner, W. Neubert, D. Wohlfarth and FOPI-collaboration, Phys. Rev. C 46 (1993) R 955.

Kaons in nuclear matter[B]

E.E. KOLOMEIZEW, B. KÄMPFER[1], D.N. VOSKRESENSKY[2]

The possibility of meson condensation in compressed and heated nuclear matter has been theoreticaly investigated in the last two decades. After focusing on π-condensation now one is interested in kaonic excitations. A condensate of K^--mesons can occure because of the scaling of kaon mass with nucleon density $m_K^2(\rho) = m_K^2(1 - \frac{\rho}{\rho_c})$, $\rho_c \approx 3 - 4\rho_o$, as suggested in ref. [1]. The knowledge of the kaon dispersion relation is important for the description of kaon production in heavy-ion collisions [2]. The presence of a K-condensate would also influence the properties of neutron stars.

Most of papers concerning kaonic excitations and K-condensate in nuclear matter consider the s-wave interaction of kaons with nucleons. We extend this investigation and consider also, in non-relativistic approximation, the p-wave contributions in the self-energy of K^--mesons formed by $\Lambda - p^{-1}$, $\Sigma^o - p^{-1}$ and $\Sigma^- - n^{-1}$ loops. We have included graphs with pions in intermediate states. A minimal relativistic correction is taken into account too. New graphs correspond to p-wave attraction. Relativistic corrections give contributions to the s-wave part of the polarization operator. In restoring the residual interaction in the off-shell polarization operator we use the Adler consistency condition [3].

The analysis of the dispersion equation $\omega(k)$, which can be written as

$$\omega^2 - k^2 - \tilde{m}_K^2 - \frac{\tilde{A}\nu k^2 \frac{\rho}{\rho_o}}{\omega - \omega_\Lambda - \frac{k^2}{2m_N}} = 0,$$

$$\tilde{m}_K^2 = m_K^{o2}\frac{1 + \rho/\rho_c}{1 + 2\rho/\rho_c}, \quad \tilde{A} = \frac{2.2}{1 + 2\rho/\rho_c}, \quad \nu = \rho_p/\rho, \quad \omega_\Lambda = m_\Lambda - m_N \approx 1.4 m_\pi,$$

shows that the spectrum of K^--mesons in nuclear matter possesses accordingly two branches of excitations, one of which, i.e. the upper one, evolves into the vacuum branch at $\rho \to 0$, and the second one corresponds to mixed $\Lambda - p^{-1}$-states with quantum numbers of the K^--meson.

At proton density $\rho_p = \nu\rho > 0.6 - 0.7\rho_o$ a roton-like minimum with momentum $k = k_o \neq 0$ appears on the low-lying branch. With growing density the effective kaonic gap $\omega_2(k_o, \rho)$ decreases and vanishes at $\rho = \rho_c^1 \simeq 5.5\rho_o$. The second branch, occupied with maximal probability $\sim exp(-\omega_2(k_o, \rho)/T)$, enhances the kaon yield in heavy-ion collisions [4]. The analysis of the equation of state of nuclear matter with taking into account the possibility of a K-condensate shows that at $\rho \geq \rho_c^1$ it becomes energetically favorable to create a proton-enriched system ($\nu \approx 1$), with charge compensated by the charge of condensed K^--mesons. By analogy with K^--mesons we investigate the properties of $\bar{K}^o$-mesons in nuclear matter. We argue on the possibility of $\bar{K}^o$-condensation. The consequences of K^- and $\bar{K}^o$-condensation for neutron stars and possible phase transition in nuclear matter will be considered in further investigations. Also the impact on dilepton yields [5] needs further studies

[1]Institut für Theoretische Physik, TU Dresden; Institut für Kern- und Hadronenphysik, FZR
[2]Moscow Engineerig-Physical Institute, Moscow, Russia

REFERENCES

[1] D. Kaplan, A. Nelson, Phys. Lett. **B175** (1987) 156
[2] E. Grosse et al. (KaoS Collab.), Prog. Part. Nucl. Phys. **30** (1993) 89
[3] S.L. Adler, Phys. Rev. **137** (1965) B1022
[4] D.N. Voskresensky, E.E. Kolomeitsev, Yad. Fiz. **56** (1993) 192
[5] B. Kämpfer, A.I. Titov, E.L. Bratkovskaya, Phys. Lett. **B301** (1993) 123

Photon production in an expanding and chemically equilibrating gluon-enriched plasma[B]

B. KÄMPFER[1], O.P. PAVLENKO[2]

We consider the photon radiation from strongly interacting matter in the framework of a complete scenario including the chemical equilibration of the initial parton matter and its transition through a mixed phase into a hadron gas. Chemical equilibration in a thermalized gluon-enriched plasma is followed within a schematic model of rate equations which includes $gg \rightleftharpoons q\bar{q}$, $gg \rightleftharpoons ggg$ channels and longitudinal and transverse expansion [1,2]. By variations of the corresponding rates we try to simulate higher order QCD processes.

We find that mainly the soft part of the photon spectrum is somewhat sensitive (within factor two) to variations of the equilibration rates (when keeping the initial temperature fixed). For fixed initial energy density there is no dependence on the initial phase space saturation, supposed equilibration is fast enough to achieve full local equilibrium at confinement temperature.

Provided that deconfined and hadron matter shine equally bright at given temperature, we find that the photons from deconfined matter dominate over hadron matter-created photons in case of a weakly first-order confinement transition, independently of the initial phase space saturation (see Fig. 1). This provides a good chance to observe thermal photon radiation from early parton matter at energies densities which are presumably achieved in future RHIC experiments.

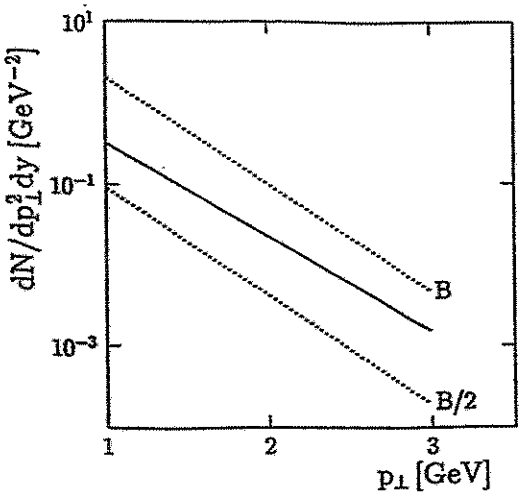

Figure 1: The photon yield from deconfined matter (full line) and hadron matter (dotted lines; the curve labeled by B [B/2] uses the standard bag model equation of state with $B^{1/4} = 235$ MeV [equation of state with halved latent heat but the same critical temperature]). The initial temperature is $T_0 = [(g_Q + g_g)/(\lambda_Q^0 g_Q + \lambda_g^0 g_g)]^{1/4} 550$ MeV, where λ and g are the fugacities and degeneracities, and the subscripts Q and g refer to quarks and gluons. For more details consult Refs. [1,2].

[1]Institut für Theoretische Physik, TU Dresden; Institut für Kern- und Hadronenphysik, FZR
[2]Institute for Theoretical Physics, Kiev, Ukraine

REFERENCES

[1] B. Kämpfer, O.P. Pavlenko, FZR-93-09, Yad. Fiz. in print
[2] B. Kämpfer, O.P. Pavlenko, FZR-93-29, Z. Phys. C (1994) in print

Quasi-particle description of a strongly interacting pion gas[B]

G.G. BUNATIAN[1], B. KÄMPFER[2]

In ultrarelativistic collisions of heavy nuclei a dense and hot hadronic system is formed. For large enough nuclei and high enough energies such a hadron gas might even achieve local equilibrium irrespectively whether it emerges from a previously deconfined matter state. The conjectured increase of nuclear transparency at high bombarding energy provides the colliding nuclei to go through each other, and a meson cloud is produced in the middle region between the receding nuclei. Therefore, one gets a possibility to investigate rather extended meson systems. This new opportunity stimulated a series of theoretical works devoted to the investigation of properties of such systems.

Unlike to previous work, in our approach [1] the considered system of interacting pions is described by Weinberg's pion field Lagrangian. We carry out our investigation of an interacting pion system by using the temperature Greens functions and take into account only the first term in the pion self-energy expansion and arrive at the Hartree approximation. The pion propagator has poles at $\omega^2(k) = \mathrm{k}^2 + \tilde{m}_\pi^2$, where

$$\tilde{m}_\pi^2 = \frac{1-10\lambda d(T)}{1-12\lambda d(T)}, \quad d(T) = \frac{1}{2\pi^2}\int_0^\infty \frac{dk\, k^2 \chi(\omega(k))}{\omega(k)(1-6d(T)\lambda)}, \quad \chi(\omega) = \left[\exp\left\{\frac{\omega(k)}{T}\right\} - 1\right]^{-1}. \tag{1}$$

with residues $\gamma/2\omega(k)$ ($\gamma = (1-6\lambda d(T))^{-1}$). The pion polarization operator is real, and the propagator has simple poles only. Therefore, for the pion spectrum $\omega(k)$ the formulae for the particle density ϱ, and entropy density $\mathcal{S}$ look like for the free pion gas, but with effective mass $\tilde{m}_\pi(T)$. The thermodynamical potential Ω and the energy density $\mathcal{E} = \partial(\Omega/T) \,/\, \partial(1/T)$ can be written, after some cumbersome algebra, as

$$\Omega(T) = \tilde{\Omega}(T) - \tilde{\Omega}(0) = \frac{3T}{2\pi^2}\int_0^\infty dk\, k^2 \ln[1 - exp(-\omega(k)/T)] + \Delta(T), \tag{2}$$

$$\mathcal{E}(T) = \tilde{\mathcal{E}}(T) - \tilde{\mathcal{E}}(0) = \frac{3}{2\pi^2}\int_0^\infty dk\, k^2 \omega(k)\chi(\omega(k)) + \Delta(T), \tag{3}$$

$$\Delta(T) = -\frac{3\lambda\gamma(T)d(T)}{4\pi^2(1-12\lambda d(T))}\int_0^\infty \frac{dk\, k^2}{\omega(k)}\chi(\omega(k)). \tag{4}$$

Since the effective mass becomes larger than the vacuum mass at $T > m_\pi$ the thermodynamical properties of a pion gas suffers minor modifications due to strong interaction in the used approximation.

[1]Laboratory of Neutron Physics, JINR Dubna, Russia
[2]Institut für Theoretische Physik, TU Dresden, und
Institut für Kern- und Hadronenphysik, FZR

RERERENCES

[1] G.G. Bunatian, B. Kämpfer, FZR-93-28

The spin-dependent deuteron structure function within an effective meson-nucleon theory[B]

L.P. KAPTARI[1], K.YU. KAZAKOV[1,2], A.YU. UMNIKOV[2], B. KÄMPFER[3]

One of the topics of the present experimental and theoretical investigation of deep inelastic scattering (DIS) of leptons from hadronic targets is the determination of the electromagnetic interaction characteristics of the neutron. The proton and neutron properties together will allow one to verify sum rules of Quantum Chromodynamics and predictions of QCD-motivated models. In previous experiments some indications of a breakdown of the fundamental symmetries are found (e.g., the famous spin crisis, the isospin symmetry violation), and the validity of the Bjorken and Gottfried sum rules are called into question. New experiments are aimed to clarify this subject.

Some collaborations have recently obtained first results on the spin-dependent structure functions (SSF). These data can now be used for consistency checks. From SLAC data on polarized ^3He one can extract the neutron SSF and compute the Bjorken sum rule integral. It is found that the Bjorken sum rule is slightly violated, whereas the first moment of the neutron SSF is in good agreement with the Ellis-Jaffe sum rule. This result seems to be in conflict with the conclusions drawn from the EMC experiments, that is, there is no room for a spin crisis in the SLAC results. At the same time, the SM Collaboration performs the first measurements on polarized deuterons [1]. From these data one can estimate the SSF of the "isoscalar" nucleon. Combining these data with EMC proton data one finds the validity of the Bjorken sum rule. It is worth stressing here that the SLAC and SMC measurements are performed with *nuclear* targets, and the interpretation of the data requires an accurate theory describing DIS off polarized nuclei.

In the previous papers [2] we suggest a theoretical model to analyze the DIS off unpolarized targets by using the operator product expansion method within an effective meson nucleon theory with one-boson-exchange interaction. Within this approach a good description of DIS off unpolarized nuclei is achieved. The recent paper [3] extends the proposed model to the polarized processes of DIS off a deuteron target. Results are displayed in Figs. 1 and 2.

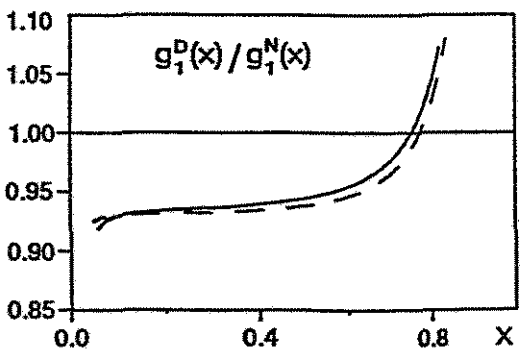

Figure 1: The ratio of the deuteron to isoscalar nucleon spin structure functions. Full (dashed) line - the contribution of impulse approximation + contribution of bound nucleons to the deuteron SSF (only impulse approximation).

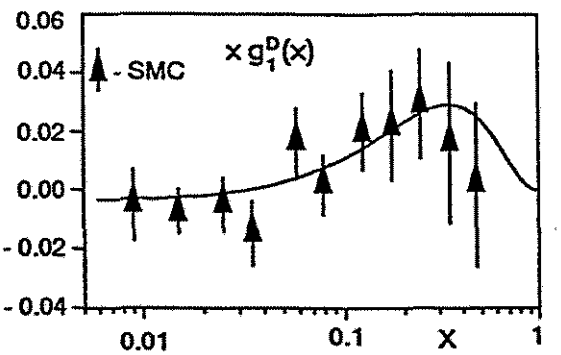

Figure 2: The weighted deuteron spin structure function $x\, g_1^D(x)$. Full line - the result of computation within the present approach; the experimental data are taken from ref. [1].

[1]Laboratory of Theoretical Physics, JINR Dubna, Russia
[2]Theoretical Physics Institute, University of Alberta, Edmonton; TRIUMF, Vancouver, Canada
[3]Institut für Theoretische Physik, TU Dresden, und Institut für Kern- und Hadronenphysik, FZR

REFERENCES

[1] B. Adeva et al. (SM Collaboration), Phys. Lett. **B302** (1993) 534
[2] L.P. Kaptari, K.Yu. Kazakov, A.Yu. Umnikov, Phys. Lett. **B293** (1992) 219
L.P. Kaptari, A.Yu. Umnikov, B. Kämpfer, Phys. Rev. **D47** (1993) 3804
[3] L.P. Kaptari, K.Yu. Kazakov, A.Yu. Umnikov, B. Kämpfer, Phys. Lett. **B321** (1994) 271

Transverse momentum dependence of dileptons from parton matter in ultrarelativistic heavy-ion collisions[B]

B. KÄMPFER[1], O.P. PAVLENKO[2]

Dileptons are considered as useful tool to investigate the dynamics and the state of matter in the course of ultrarelativistic heavy-ion collisions. In particular, the lepton pairs are thought to represent direct messengers from the early stages where the transient creation of deconfined matter is prejudiced. Whether the energy density and lifetime are large enough to achieve a locally equilibrated quark-gluon plasma is a question to be decided experimentally. The presently available estimates and simulation codes predict the possibility of creating deconfined parton matter in future experiments at RHIC.

Under certain conditions the dilepton yield from a locally equilibrated quark-gluon plasma depends only on the transverse mass, i.e., $dN/dM_\perp^2 dq_\perp^2 dY \propto F(M_\perp)$, that is it scales with $M_\perp$ ($M_\perp$, and $q_\perp$, and Y are the transverse mass and momentum and rapidity of the pair, respectively). This property has been proposed to be used as a unique signature of the formation of a quark-gluon plasma. In particular, the yield from hadron matter [1] is shown to display strong violation of the scaling.

In the recent paper [2] we extend the approach of previous studies and also include pre-equilibrium parton matter [3]. It is quite obvious that the partonic matter needs some time to evolve from the overlapping nuclear distributions towards a locally thermalized state. It might be suspected that the early stages just give a substantial contribution to the dilepton yield, or even might dominate it.

We study possible origins of the $M_\perp$ scaling violation of the dilepton spectrum from pre-equilibrium parton matter in a kinetic framework. We show that under certain conditions strong off-equilibrium parton matter displays approximate scaling, as also the Drell-Yan contribution does at $M_\perp > 2$ GeV. Otherwise we find that the inclusion of essentially additional parameters, such as a low-momentum cut-off and parton masses, gives rise to a noticeable violation of scaling. Strong scaling violations have been observed in the ambitious parton cascade simulations and are there attributed to higher twist effects which cause effective parton masses and form factors.

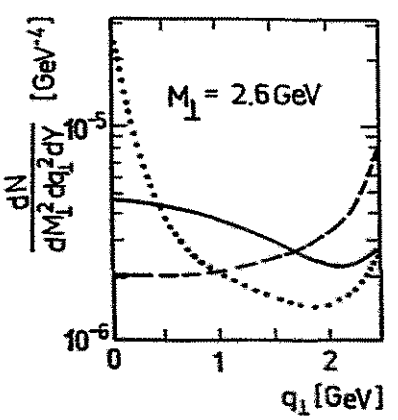

Figure 1: The transverse momentum dependence of the dilepton spectrum from free-streaming parton matter at $M_\perp = 2.6$ GeV. The initial distributions are: (i) highly anisotropic (full curve; Gaussian [sharply peaked] distribution in transversal [longitudinal] direction), (ii) highly anisotropic (dotted curve; power-law [sharply peaked] distribution in transversal [longitudinal] direction), and (iii) thermalized (dashed curve). For further details and thermalization effects consult Ref. [2].

[1] Institut für Theoretische Physik, TU Dresden; Institut für Kern- und Hadronenphysik, FZR
[2] Institute for Theoretical Physics, Kiev, Ukraine

REFERENCES

[1] B. Kämpfer, P. Koch, O.P. Pavlenko, FZR-93-07, Phys. Rev. C49[1] (1994) in print
[2] B. Kämpfer, O.P. Pavlenko, FZR-93-23, Phys. Rev. C49[4] (1994) in print
[3] B. Kämpfer, O.P. Pavlenko, NATO ASI, B303, p. 649, Plenum Press New York 1993

Thermal masses in a strongly interacting gluon gas[B]

A. PESHIER[1], B. KÄMPFER[2], G. SOFF[1]

Available QCD lattice calculations of thermodynamical properties of strongly interacting matter are not very illustrative with respect to an understanding of the equation of state. One therefore tries to interpret the outcome of such lattice calculations by simpler models. E.g., the data of pure gauge theory of ref. [1] are interpreted in ref. [2] by a thermodynamical model with low-momentum cut-off. Here we follow another interpretation ref. [3] of the SU(3) gluon plasma data ref. [1], which we later want to apply to fermionic systems, too.

We use the concept of quasi-particles and replace the strongly interacting massless gluons by free massive bosons with an effective thermal (screening) mass $m(T) = \alpha\, g(T)\, T$, where $g = 4\pi[11 \log[(T - T_s)/T_c]^2]^{-1/2}$ is the temperature dependent running coupling constant, and the parameter α accounts for the effective number of degrees of freedom. To avoid a singular behaviour of the thermal mass at the confinement temperature T_c we also introduce a temperature shift parameter T_s to regulate for reasonable values near T_c. Our fit (see fig. 1) gives a good agreement with the lattice data [1], especially at larger values of T. Although the gluon system clearly does not display the behaviour of an ideal gas (in the temperature range considered) there is a certain approach to asymptotic freedom. In a plot $p(e)$ (fig. 2) one observes some limited analogy to the bag model.

The cooling of a gas within the Bjorken picture is governed by the time evolution equation $de/d\tau = -[p(e) + e]/\tau$ (τ is the proper time) and depends on the equation of state $p(e)$. The bag model ($e = 3AT^4 + B$, $p = AT^4 - B$) yields the known cooling $T \propto \tau^{-1/3}$ while for our fit of the gluon medium we find a substantial slowing down of the cooling curves $T(\tau)$ near T_c. This might compensate for the reduced latent heat found in recent lattice data and might apply to Shuryaks 'hot glue scenario'.

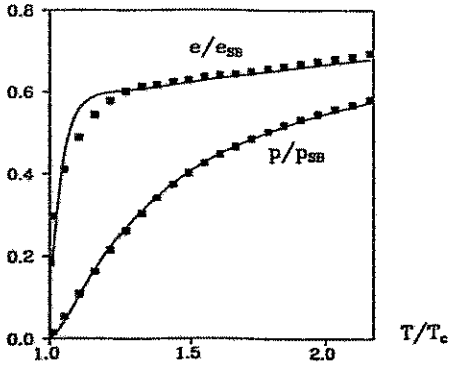

Figure 1: Fit of the energy density and pressure data (dots from ref. [1], scaled by the Stefan-Boltzmann values) by our thermal gluon mass model with $\alpha = 0.551$ and $T_s/T_c = 0.023$. Observe the striking deviation from the bag model equation of state, which would give $e/e_{SB} > 1$.

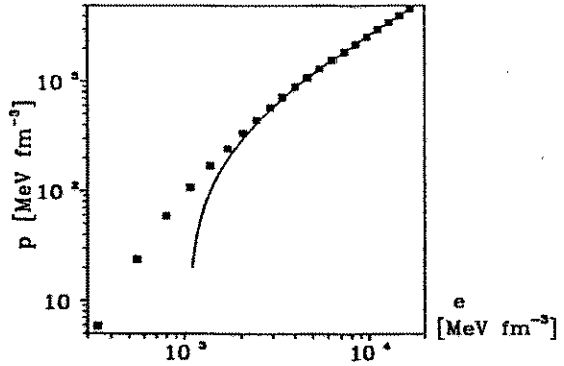

Figure 2: Pressure as function of energy density (dots from ref. [1]). At sufficiently large energy density (or temperature) a bag model-like equation of state (full line) emerges in the form $p = ae - 4/3B$ with $a = 0.297$ and $B^{1/4} = 205MeV$.

[1]Institut für Theoretische Physik, TU Dresden
[2]Institut für Theoretische Physik, TU Dresden und Institut für Kern- und Hadronenphysik, FZR

REFERENCES

[1] J. Engels, J. Fingberg, F. Karsch, D. Miller, M. Weber, Phys. Lett. **B252** (1990) 625
[2] D. Rischke, M. Gorenstein, A. Schäfer, H. Stöcker, W. Greiner, Phys. Lett. **B278** (1992) 19
[3] B. Kämpfer, O.P. Pavlenko, FZR-93-16, Nucl. Phys. **A566** (1994) 351c

A Reference Profile for the Average Meson Field of the Semibosonized Nambu & Jona-Lasinio Model[B]

R. WÜNSCH, K. GOEKE[1], TH. MEIßNER[2]

We have considered the average meson field of the bosonized Nambu & Jona-Lasinio model for u and d quarks. Restricting the meson fields to hedgehog shape and to the chiral circle they can uniquely be described by a single scalar function, the profile function $\Theta(r)$. Classical self-consistent meson fields are obtained by minimizing the effective Euclidean action $S_{eff}[\Theta(r)]$ and solving the resulting equation of motion [1].
We have evaluated a series of meson profiles (Fig. 1) in dependence on the constituent quark mass M, which is the only free parameter in the model [2]. We have shown that the numerically determined self-consistent profiles

- do practically not depend on the constituent quark mass M,
- can be approximated by a reference profile

$$\Theta^{Ref}(R;r) = \begin{cases} -\pi\left(1-\frac{r}{2R}\right) & \text{if } r \le R_M \\ -\pi\left(1-\frac{R_M}{2R}\right)\left(\frac{R_M}{r}\right)^2 \frac{1+m_\pi r}{1+m_\pi R_M} e^{-m_\pi(r-R_M)} & \text{if } r \ge R_M. \end{cases} \quad (1)$$

The reference profile interpolates between the correct asymptotic behavior of the self-consistent profile for small and large radii. A smooth interpolation is obtained with a matching point at $R_M = \frac{4}{3}R\left(1+\frac{8}{27}m_\pi^2R^2+O[(m_\pi R)^3]\right)$. Fig. 1 demonstrates that the self-consistently determined profiles do not substantially deviate from each other and can - at least visually - be fairly well approximated by a common reference profile with the empirically determined radius parameter $R = (0.42 \pm 0.05)\,fm$.

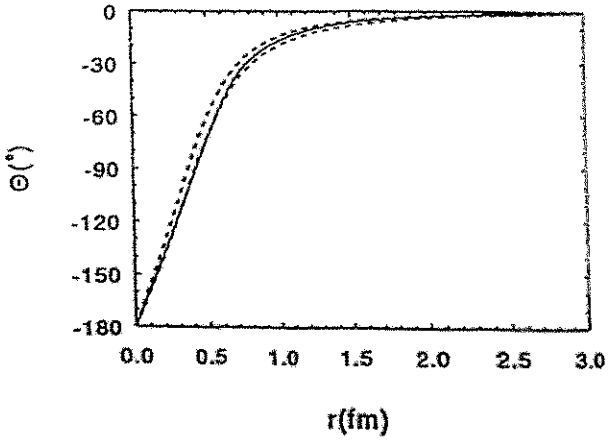

Fig. 1: *Self-consistently determined profiles $\Theta(r)$ in the mass region $350\,MeV \le M \le 1000\,MeV$. All numerically calculated profiles fit in the corridor marked by the broken lines.*
The full line represents the reference profile (1) with $R = 0.42\,fm$.

To test the quality of the reference profile we have calculated the expectation values of several observables and compared them with the corresponding values obtained for the self-consistent profiles [3]. The agreement was found to be quite good. Hence many of the properties of the Nambu & Jona-Lasinio Lagrangian can be studied using the reference profile instead of applying the time-consuming determination of the self-consistent profile. If a more accurate determination of the self-consistent profile is necessary, the reference profile may serve as a suitable starting profile in an iteration procedure.

[1] Institut für Theoretische Physik II, Ruhr-Universität Bochum, Postfach 102148, 44780 Bochum
[2] Institute for Nuclear Theory, University of Washington, HN-12 Seattle, WA 98195, USA

REFERENCES:

1. H. Reinhardt, R. Wünsch *Phys. Lett.* B215 (1988) 577; B230 (1989) 93;
   Th. Meißner, F. Grümmer, K. Goeke Phys. Lett. B227 (1989) 296
2. Th. Meißner, K. Goeke Nucl. Phys. A524 (1991) 719
3. R. Wünsch, K. Goeke, Th. Meißner *Z. Phys.* A (in print)

CMM and Rotational Corrections in the semibosonized Nambu & Jona-Lasinio Model for Interacting Quarks[B]

M. SCHLEIF AND R. WÜNSCH

We consider the two-flavor (u,d) Nambu & Jona-Lasinio Model [1] involving scalar-isoscalar and pseudoscalar-isovector quark-quark interactions as an effective model of describing nucleons and delta resonances. Introducing appropriate mesonic fields, the Lagrangian can be linearized. Using hedgehog ansatz, chiral circle and spherical symmetry the mesonic fields are uniquely determined by the profile function $\Theta(r)$. The total energy E_{HH} of the field configuration consists of a fermionic and a mesonic part. Contributions of the Dirac sea to the fermionic energy diverges and are regularized using Schwinger's proper-time scheme. The corresponding cut-off parameter is adjusted to the experimental value of the weak pion decay constant. The constituent quark mass M is the only parameter of the model.
In mean-field (Hartree) approximation, static mesonic fields minimize the total energy E_{HH}. Solitonic configurations have been obtained for masses $M \gtrsim 350\,MeV$. Due to mean field approximation and hedgehog ansatz this solution is neither an eigenstate of the total momentum operator $\vec{P}$ nor of the isospin operator $\vec{T}$. This lack can be corrected by means of the classical "pushing" and "cranking" approaches giving rise to the modified expression [2]

$$E_{T,\vec{P}=0} = E_{HH} - \frac{\langle \vec{P}^{\,2} \rangle_{HH}}{2E_{HH}} + \frac{T(T+1)}{2\mathcal{I}} - \frac{\langle \vec{T}^{\,2} \rangle_{HH}}{2\mathcal{I}} \qquad (1)$$

for the total energy, where $\langle \vec{P}^2 \rangle_{HH}$ and $\langle \vec{T}^2 \rangle_{HH}$ are the expectation values of the square of the center-of-mass momentum and of the isospin, respectively, calculated for the hedgehog configuration. E_{HH} denotes the unmodified hedgehog energy. The second term corrects for the center-of-mass (CMM) motion, while the last terms "cranks" the hedgehog to the correct values of spin and isospin. $\mathcal{I}$ is the moment of inertia of the corresponding quark configuration. We have calculated modified profile function by minimizing the energy (1) instead of the pure hedgehog energy E_{HH}. In particular, the CMM correction depends strongly on the mass parameter M. In fig. 1, we have selected a quite large quark mass M with sizeable corrections in the profile function. Pushing corrections modify the slope of the profile at small distances and are almost equal for nucleons and delta resonances. Cranking corrections modify the asymptotic behaviour at large distances. To keep the calculation feasible we insisted in spherical symmetry of the rotating hedgehog and spread the effect of the centrifugal force over all spatial directions. In the physically relevant mass region around 400 MeV the effects are roughly half as large.

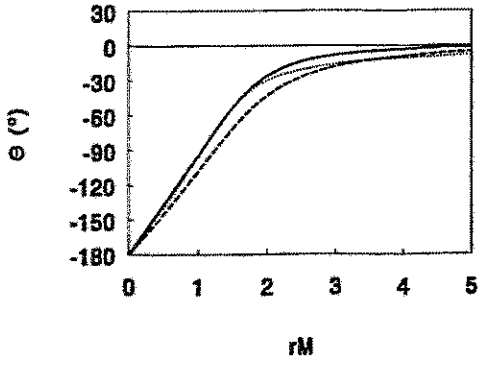

Fig. 1: Profile function of the uncorrected hedgehog (dashed line), the nucleon (fulled line) and the delta (dotted line) calculated for a constituent quark mass of $M = 600\,MeV$.

REFERENCES:

1. J. Nambu, G. Jona-Lasinio *Phys. Rev.* **122** (1961) 345; **124** (1961) 246

2. P.V. Pobylitsa, E. Ruiz Arriola, Th. Meißner, F. Grümmer, K. Goeke, W. Broniowski *J. Phys. G* **18** (1992) 1455

Tilted Bands in the even-even Xe and Ba Nuclei

F. DÖNAU AND S. FRAUENDORF
O. VOGEL[1], A. GELBERG[1] AND P. VON BRENTANO[1]

Excited bands characterized by strong $\Delta I = 1$ transitions and relatively weak crossover $\Delta I = 2$ transitions have been identified in several even-even Xe and Ba nuclei [1,2]. The similarity of the transition energies in different nuclides suggests a common intrinsic structure of these bands. The theoretical investigation is based on the Tilted Axis Cranking Model [3] which allows one to treat the case of a non-principal axis of rotation. The calculation for ^{128}Ba specifies so-called t-bands which carry substantial quasiparticle angular momentum along both the symmetry and the collective axis in an oblate shaped configuration. The intrinsic orientation of the calculated angular momentum $\vec{J}$ is shown in Fig.1. The experimental energy and spin sequence can be reasonably reproduced for a negative parity configuration $(\nu h^2_{11/2})(\pi h_{11/2} d_{5/2})$. Within the same approach the B(M1) and B(E2) values of intra band transitions are calculated. Strong M1 rates are found as a consequence of the tilted quasiparticle spins. The calculated branching ratios B(M1)/B(E2) for the t-band are consistent with the observation of relatively strong M1 and weak E2 transitions. An excitation energy of 5-6 MeV is estimated for the band head having an effective K-value of approximately 10 $\hbar$. Experimentally the decay out of the t-band was not seen which indicates that the available final states possess rather different intrinsic structure.

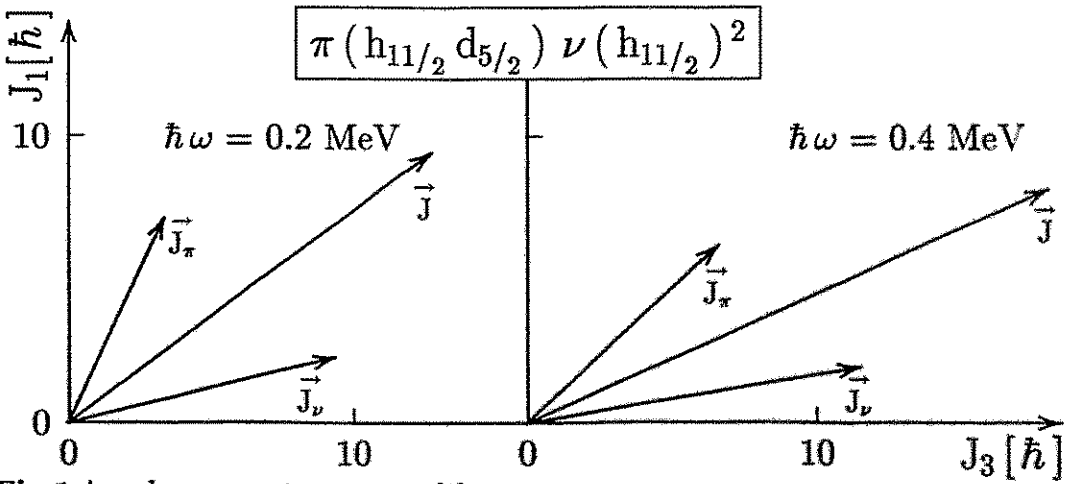

Fig.1 Angular momentum composition in the tilted 4qp configurations for two frequencies. In the considered case the intrinsic 1-axis is the symmetry axis.

[1] Institut für Kernphysik der Universität zu Köln

REFERENCES:

[1] U. Neuneyer et al., Z. Phys. **A336** (1990) 245
[2] D. Ward et al., Nucl. Phys. **A529** (1991) 315
[3] S. Frauendorf, Nucl. Phys. **A 557** (1993) 259c

Investigation of the Validity of Tilted Axis Cranking Approximation

STEFAN FRAUENDORF, JIE MENG[1]

Tilted Axis Cranking (TAC) is a systematic microscopic approach to high spin physics[2], which provides a semiclassical description of both the energies and the intra band transition matrix elements. It has turned out to be very successful in the description of the γ-spectra of rapidly rotating nuclei[2]. In addition to all the virtues the standard principal axis cranking has for the description of ΔI=2-bands with good signature, the TAC approach permits to calculate the rotational bands with ΔI=1 and fixed parity which are quite common in deformed nuclei. However, as it is based on the assumption of classical angular momentum and uniform rotation, it has some restrictions. Therefore it seems necessary to invesitgate how important and serious these restriction turn out to be in the description of the experimental observables. To study this question, typical cases of two quasi particles coupled to a rotor have been treated exactly by the means of the particle-rotor model (PRM) and approximately by means of the TAC. As an example, the BM1 values for PRM and TAC are given in figure 1. They depend sensitively on the angular momentum geometry. It can be seen that the TAC reproduces the PRM rather well, except at the begining of the band (i.e. at low spin) where the assumption of the uniform rotation is not correct. This is also the case for the smaller deformation where signature splitting has set in. Another restriction of the TAC turns out to be the transition to rotation about a principal axis where the signature quantum number is restored. The TAC gives zero BM1 in such a case, where the PRM gives small but finite BM1 values. So one could say that TAC is reliable and accurate except for situation where it is not expected to work.

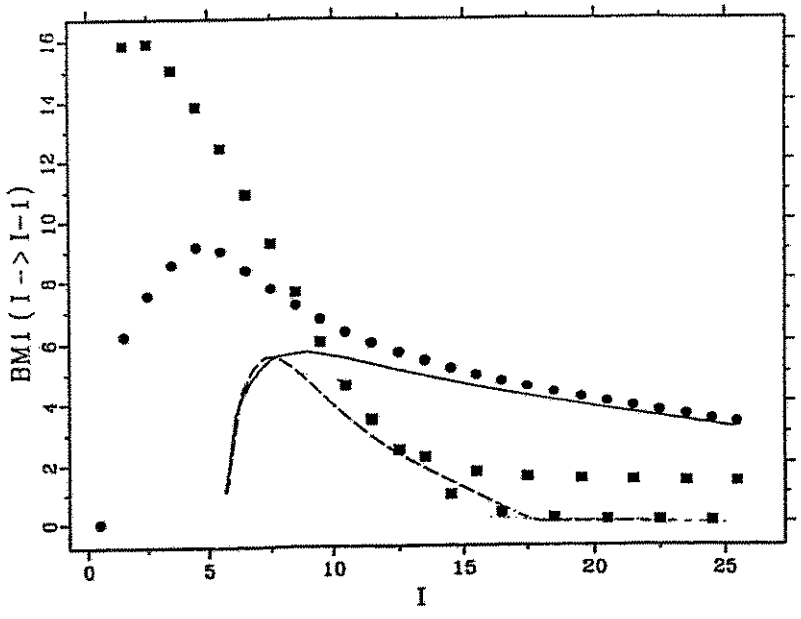

Fig. 1 The BM1 values for one proton (g-factor = 1) and one neutron hole (g-factor = -1) coupled to a rotor in the PRM and TAC. The squares describe PRM at small deformation, and the dots at large deformation. The dashed line gives the TAC at small deformation, and the solid line at large deformation.

[1] Institute for Theoretical Physics, Academia Sinica

REFERENCES:

[1] S. Frauendorf and J. Meng, Nucl. Phys. A, to be published .
[2] S. Frauendorf, Nucl. Phys. A557 (1993) 259.

Shears-Bands in the Light Pb - Isotopes

S. FRAUENDORF, J. MENG[2], G. BALDSIEFEN[1], H. HÜBEL[1]

The recently discovered $\Delta I = 1$-bands in the light Pb nuclei (c.f. e.g. [1,2]) are a challenge to standard nuclear structure theory, since the measured deformations turn out to be very small ($\beta < 0.07$). How can a long regular band appear in an almost shperical nucleus? The possible mechanism has been suggested in ref. [3] and is illustrated in the figure. The relevant proton states are $h_{9/2}$ and $i_{13/2}$ with a torus like density distribution. The relevant neutron orbitals are $i_{13/2}$ holes with a dumbbell like density distribution. The maximal overlap between the proton and neutron density distributions is reached at the band head when the angular momenta stand perpendicular to each other. Moving up the band, most of the angular momentum is gained by gradually tilting $\vec{i}_\pi$ and $\vec{i}_\nu$ towards $\vec{J}$. The two vectors rotate around $\vec{J}$ with the inertial forces balancing the counter forces generated by the decreasing overlap with the deformed field. Since this gradual motion reminds of the closing of the blades of a pair of shears, we suggest the name "Shears Bands". Using the Tilted Axis Cranking (TAC) approach, we have studied the energies, BM1- values and BE2- values of Shears Bands in ^{198,199,200}Pb. The energies and branching ratios are well reproduced, there is some discrepancy with the measured M1 - lifetimes.

The shears mechanism is an example of new type of rotation ("Magnetic Rotation"), which is expected in weakly deformed nuclei, when the high spin proton levels are of particle type and the high spin neutron levels are of hole type, or vice versa. It is characterized by: regular ΔI=1-sequences with a low but rather constant $\mathcal{J}^{(2)}$, large BM1- values and very small BE2 - values.

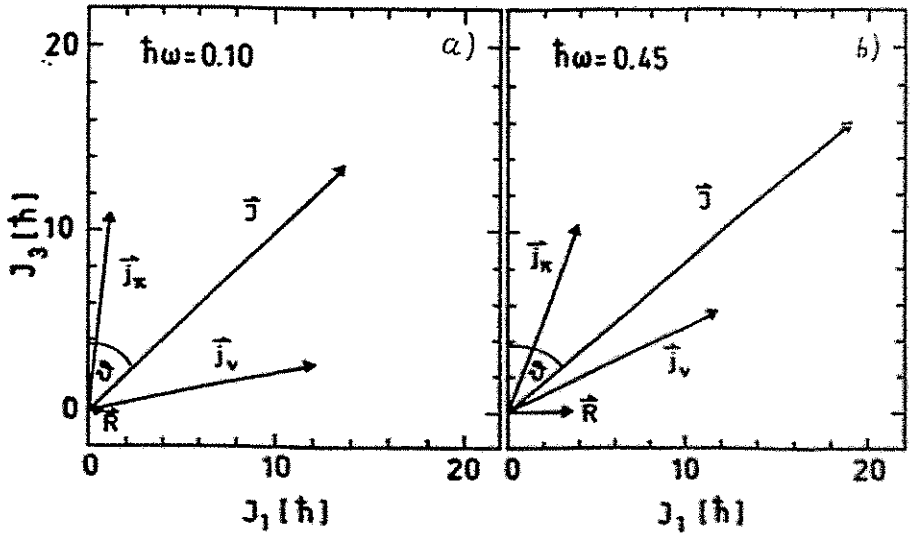

Fig. 1 A TAC calculation of the angular momentum composition in the lowest Shears Band of ^{198}Pb. The vector diagrams show how the proton and neutron "blades" close with increasing angular momentum .

[1]Institut für Strahlen- und Kernphysik, Universität Bonn
[2]Institute for Theoretical Physics, P. O. 2735, Beijing, China

Dynamics of the Spin Orientation

S. FRAUENDORF

The Tilted Axis Cranking model (TAC) permits to calculate the orientation ϑ of the angular momentum vector with respect to the body fixed system of coordinates. Each orientation found thus is associated with a particular rotational band. Transitions between the bands may be viewed as a motion in ϑ. Of particular interest is the decay of high - K- isomers into bands with low K, representing large amplitude motion in the orientation degree of freedom. The intrinsic structure changes rapidly with the orientation angle ϑ. As a consequence the adiabatic concepts of a potential energy and a mass coefficient fail. An appropriate fomulation for the dynamics is the hopping concept of solid state physics (fig. 1). Different orientations (bands) are considered as sites. There is a probability to hop from one to another site. The hopping matrix is determined by the detailed structure of the nucleon states near the Fermi surface and also by the number of possible pathes to final state. The relation between the structural and combinatorial aspects is beeing investigated. The fig. 2 demonstrates that the "normal" isomer decay in ^{178}Hf and "anormal" decay in the adjacent isotope ^{174}Hf can be accounted for by calculating the available sites by means of the TAC and assuming a stochastic hopping matrix that exponentially falls off with the length of the hop.

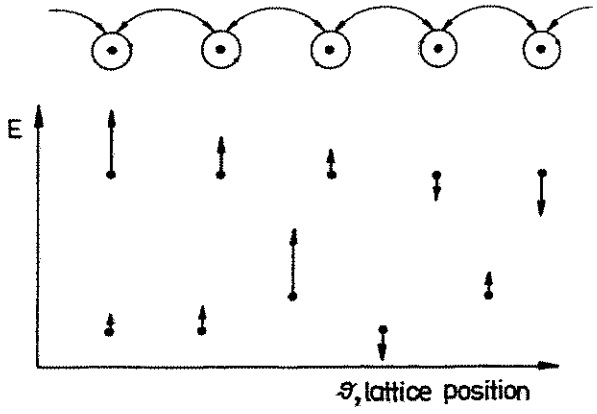

Fig. 1 Hopping dynamics in a lattice and in the spin orientation ϑ. The top illustrates how electrons hop in a one dimensional lattice. The lower part shows the site energies and the wave function. The nuclear case does not correspond to the Bloch waves of conductors (middle) but to the Andersson localization of insulators (bottom).

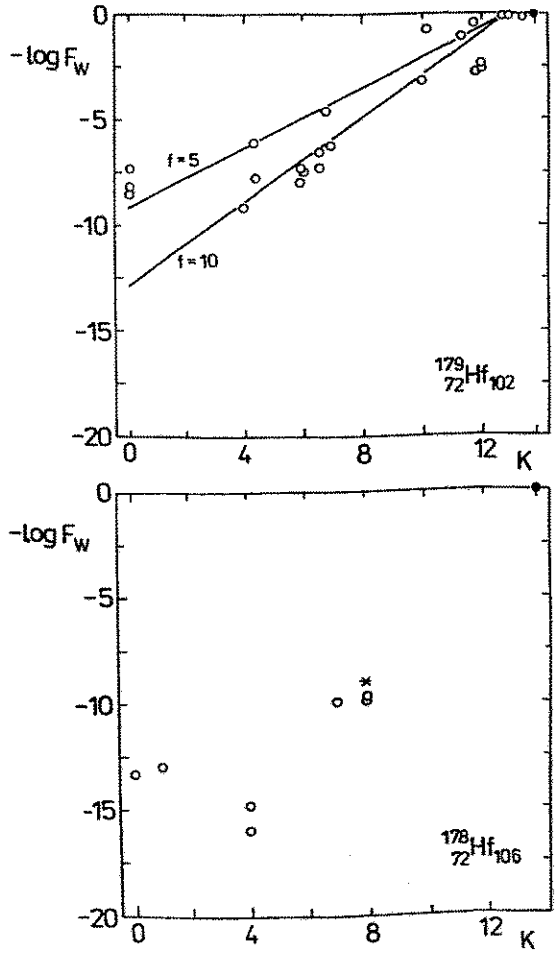

Fig.2 Transition probablities in Weißkopf units for the decay of K=16 isomers into bands with different K. The calculations are the open circles. Experimentally, ^{178}Hf shows "normal" decay into one K=8 band (star), ^{174}Hf "anormal" decay many bands with different K (the probability lying between the lines).

REFERENCES:

S. Frauendorf, Proceedings of the International Conference on the Future of Nuclear Spectroscopy, Invited Lectures, in print and Nucl. Phys. to be published

Consequences of Neutron-Proton Interactions on Backbending

S. FRAUENDORF, J.A. SHEIKH[1], N. ROWLEY[2]

The influence of neutron-proton correlations on backbending is investigated in a single-j-shell model with a surface δ interaction. If the shell is filled symmetrically with protons and neutrons there are strong correlations between the two kinds of nucleons, resulting in a favoured T=0 s- band and an unfavoured T=1 s -band. The correlations make the crossing frequency of double s -band (2 quasiproton 2 quasineutron) lower than the one of the T=0 s- band. This is a behaviour very different from the familiar scenario of an independent neutron and proton backbend. It permits to obtain information about the high multipoles of the p-n interaction. The p-n correlations are quenched very quickly, if the neutrons and protons fill a high-j intruder orbital asymmetrically. This is due to the repulsive neutron-proton correlation energy in these configurations. Thus, new insight into the large angular momentum components of the proton neutron correlations can be obtained by studying high spin states in medium mass N=Z nuclei. Such experiments become possible with the advent of large multidetector arrays, like EUROBALL and the radioactive beam facilities.

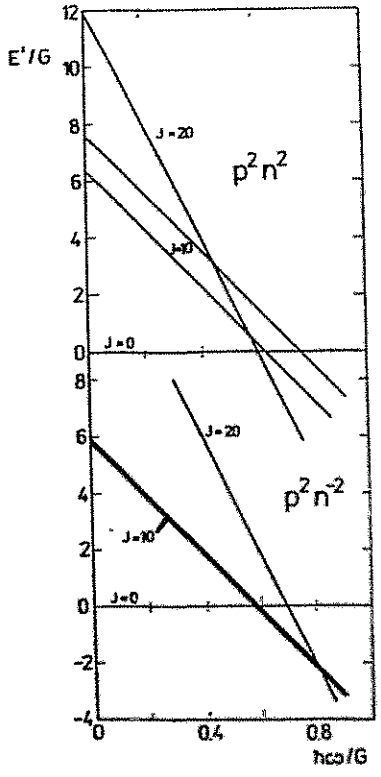

Fig. 1 Energy in the frame rotating with the frequency ω for two protons and two neutrons (p^2n^2) and two protons and two neutron holes (p^2n^{-2}) in the $h_{11/2}$ shell. The energy is measured in units G of the surface δ interaction. The ground band is used as a reference. Inclusion of deformation will make the crossings less sharp.

[1] Joint Institute for Heavy Ion Research, Oak Ridge National Laboratory, Oak Ridge, Tennessee 37831, USA

[2] Department of Physics, University of Manchester, Manchester M13 9PL, UK and Department of Physics, University of Surrey, Guildford, GU2 5XH, UK

REFERENCES:

[1] S. Frauendorf, J.A. Sheikh, N. Rowley Phys. Rev. D, to be published

Transfer Operator Approach to the Semiclassical Baker Map[M]

F.-M. Dittes and U. Smilansky[1]

The transfer operator approach proposed recently for the semiclassical description of chaotic systems is based on the fact that sums over N-periodic orbits can be identically rewritten as traces over phase space of a correspondingly chosen (classical) operator. For a map $r' = T(r)$ this operator is given by

$$V^{(N)}(r,r') = \Omega^{-1}\delta(r - T^{-N}r')\sqrt{|\det(I - M(r))|}e^{2\pi i/hS(r)} ,$$

where Ω denotes the phase space volume, $S(r)$ — the action of an N-step classical trajectory starting at point r (including, if necessary, the Maslov index) and $M(r)$ is the monodromy matrix of such a trajectory. For hyperbolic systems, this N-step operator can be approximated by an N-fold convolution of the 1-step operator allowing, therefore, the treatment of arbitrary long periodic orbits in terms of a single operator, the transfer operator $V(r,r') \equiv V^{(1)}(r,r')$.

In Ref. [1], this technique has been developed for a simple chaotic system, the baker map. The latter one is defined as a mapping of the unit square onto itself: $x' = \{2x\}$, $y' = y/2 + [2x]/2$, where $[x]$ and $\{x\}$ represent the integer and fractional parts of x, respectively. A convenient representation of V has been derived and applied in order to calculate the eigenvalues and eigenfunctions of the transfer operator.

For a given integer value of $L = 1/h$, the spectrum of V has L eigenvalues in the vicinity of the unit circle, in analogy to the spectrum of the quantum one-step evolution operator. The semiclassical spectrum appears, however, to be smeared out to both sides of the unit circle, indicating a violation of unitarity introduced by the semiclassical approximation (Fig. 1). In particular, over a wide range of h, V has eigenvalues whose absolute values are greater than one. This causes a breakdown of the semiclassical description after a time t_c which depends on h approximately as $h^{-1/2}$ (Fig. 2).

The obtained information about the spectrum of V has been used to check the existence of correlations between classical actions of chaotic systems for high lengths of trajectories, not directly accessible to periodic orbit calculations (Ref. [2]).

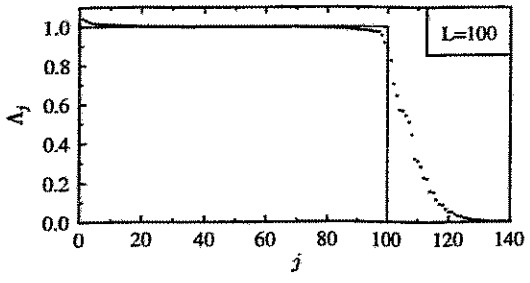

Figure 1: Absolute values Λ_j of the eigenvalues of V, in descending order for $L = 100$, in comparison with the quantum spectrum (full line).

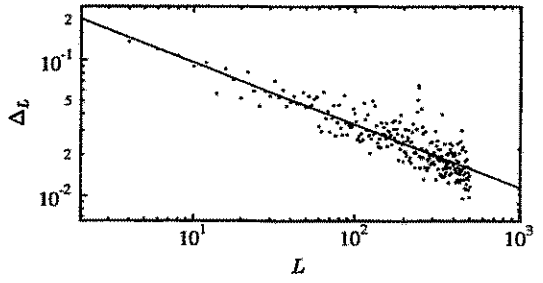

Figure 2: Distance Δ_L of the leading eigenvalue of V from the unit circle. The straight line is the best powerlike fit through all data points and is given by $\Delta_L = 0.29\, L^{-0.47}$.

[M] Supported by *Minerva* and by the *Minerva Center for Nonlinear Physics of Complex Systems*

[1] The Weizmann Institute of Science, Department of Physics of Complex Systems, 76100 Rehovot, Israel

References:

[1] F.-M. Dittes, E. Doron and U. Smilansky, *Phys. Rev. E* **49** (1994) R963

[2] N. Argaman, F.-M. Dittes, E. Doron, J. P. Keating, A. Yu. Kitaev, M. Sieber and U. Smilansky, *Phys. Rev. Lett.* **71** (1993) 4326

Radial extension of the amplitudes of partial widths[D,B]

W. ISKRA[1], M. MÜLLER AND I. ROTTER[2]

The continuum shell model (CSM) describes the nucleus in a realistic manner as an open quantum mechanical system [1]. Its properties are determined by an nonhermitian effective Hamiltonian with eigenfunctions $\tilde{\Phi}_R$. The amplitudes of the partial widths are the transition matrix elements $\tilde{\gamma}_{Rc} = < \tilde{\Phi}_R | V | \xi^c_E >$ between the complex $\tilde{\Phi}_R$ and the channel wavefunctions ξ^c_E. V is the residual interaction. The radial profile of the amplitudes of the partial widths is given by an integration of

$$\tilde{\gamma}^r_{Rc} = (2\pi)^{1/2} < \tilde{\Phi}_R | V \delta(r - r') | \xi^c_E > \qquad (1)$$

over r'. All the formulas are derived without pertubation theory. A detailed description of the model is given in [1].

In the framework of the CSM, the radial profile of the partial widths amplidudes in ^{16}O is calculated as a function of the coupling strength to the continuum for $N = 70$ 1^- resonances with $2p-2h$ nuclear structure with the $1s$, $1p_{3/2}$, $1p_{1/2}$, $2s$, $1d_{5/2}$ shells. In this calculation the energy of the system is chosen to be $E = 34$ MeV and the number of open decay channels is $K = 2$ which are either two proton or two neutron channels. The inelastic channels open at $E = 6.30$ MeV in the proton decay and at $E = 6.15$ MeV in the neutron decay. The parameters for the Woods-Saxon potential and for the residual interaction V^0 are the same as in [2]. The calculations are performed for $\alpha^{ex} = .2$ up to 8 where α^{ex} determines the coupling strength to the continuum ($V = \alpha^{ex} \cdot V^0$). The trapping effect appears at $\alpha^{ex}_{cr} \approx 2.5$.

The wavefunctions $\tilde{\Phi}_R$ and the matrix elements $\tilde{\gamma}_{Rc}$ are complex. In figures 1.a to h, $Re\{\tilde{\gamma}^r_{Rc}\}$ for the inelastic neutron decay channel is drawn for $\alpha^{ex} = .2$ to 8. The $\tilde{\gamma}^r_{Rc}$ for the two states $R = 1$, 2 with the largest widths are represented by dashed lines while the $\tilde{\gamma}^r_{Rc}$ of all the other states $R = 3, ..., 70$ are shown by points at the radii r for which the calculations are performed. The solid curves in figure 1 are drawn for a typical trapped state.

The results of our calculations show the following: With increasing α^{ex} the amplitudes $\tilde{\gamma}^r_{Rc}$ increase for all states. Further the transition matrix elements for the broad states get dominant peaks at small radii for large coupling strenghts. That means the fast decays arise mostly from the inner part of the nucleus. In contrast to that, the decay probability for the trapped states is distributed over the whole nucleus. In other words, most nucleons which originate from the short-lived resonances are emitted in the internal region. The nucleons emitted in the surface region originate mostly from the long-lived states.

[D,B] *Supported by the* DFG (Ro 922/1) *and* BMFT (WTZ X081.39).

[1] *On leave of absence from* Soltan Institute for Nuclear Studies, 00-681 Warszawa, Poland
[2] Institut für Theoretische Physik, TU Dresden *and* Institut für Kern- und Hadronenphysik, FZ Rossendorf

REFERENCES

[1] I. Rotter, Rep. Progr. Phys. 54, 635 (1991) and references therein
[2] W. Iskra, M. Müller and I. Rotter, J. Phys. G 19, 2045 (1993)

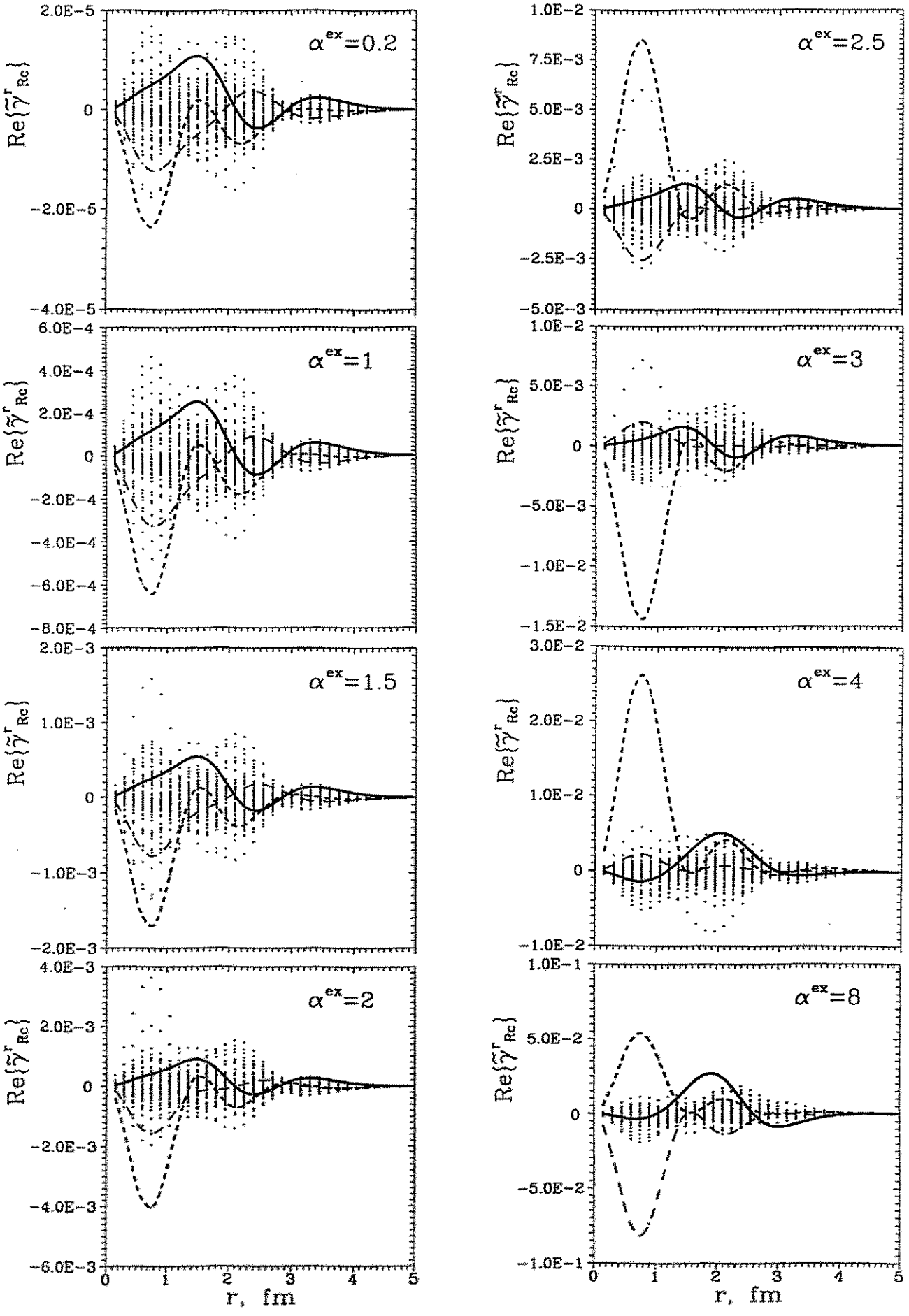
α^ex=0.2
α^ex=2.5
α^ex=1
α^ex=3
α^ex=1.5
α^ex=4
α^ex=2
α^ex=8
Re{γ̃^r_Rc}
r, fm

The interplay of different time scales at high excitation energy [D,B]

W. Iskra [1], M. Müller and I. Rotter [2]

At high level density, the properties of the resonance states of a nucleus are described by means of a Hamilton operator H_{QQ}^{eff} which is non-Hermitean due to the coupling to the continuum of decay channels. Its eigenvalues $\tilde{\mathcal{E}}_R = \tilde{E}_R - \frac{i}{2}\tilde{\Gamma}_R$ and eigenfunctions $\tilde{\Phi}_R$ are complex. It holds

$$\langle\tilde{\Phi}_R|H_{QQ}^{eff}|\tilde{\Phi}_R\rangle = \tilde{\mathcal{E}}_R\langle\tilde{\Phi}_R|\tilde{\Phi}_R\rangle \tag{1}$$

and $\langle\tilde{\Phi}_R|\tilde{\Phi}_R\rangle \geq 1$, in general. The wavefunctions of the resonance states are

$$\tilde{\Omega}_R = (1 + G_P^{(+)}V)\tilde{\Phi}_R \tag{2}$$

where V is the residual interaction and $G_P^{(+)}$ is the Green function for the motion of a particle in the continuum.

Numerical calculations have shown [1] that at high level density a redistribution takes place inside the nucleus. Here, K short-lived states are formed together with $N-K$ long-lived states where K is the number of open decay channels and N the total number of resonance states. The redistribution is the consequence of interferences to which all N resonance states contribute.

In further investigations, the $\langle\tilde{\Phi}_R|\tilde{\Phi}_R\rangle$ are calculated [2]. They are large (up to 10) for all resonances in the critical region where the redistribution takes place. Beyond that redistribution region, it is $\langle\tilde{\Phi}_R|\tilde{\Phi}_R\rangle \approx 1$ for the short-lived resonance states. That means, these resonances behave like isolated resonances although they result from an interference of all N resonances and overlap the $N-K$ long-lived resonances.

In contrast to the behaviour of the short-lived resonances, $\langle\tilde{\Phi}_R|\tilde{\Phi}_R\rangle > 1$ remains for the long-lived resonances also beyond the critical region [2]. That means, the long-lived resonances do *not* behave like isolated resonances but are *correlated* with each other. This result is true although the long-lived resonances may appear as well isolated resonances in the cross section on the background of the short-lived resonances and the direct reaction part.

Further, the wavefunctions of all resonance states are correlated due to the term $G_P^{(+)}V\ \tilde{\Phi}_R$ which is an integral over the energy of the decay channels. It is important for the long-lived states which are (weakly) coupled to *all* open decay channels in contrast to the short-lived states where one decay channel is preferred.

In order to prove whether correlations of the type discussed above exist in the (long-lived) neutron resonances, it should be investigated whether their lifetimes obey, indeed, the Porter-Thomas distribution. Deviations of the type discussed in [3] may appear as a consequence of the (nonlinear) correlations involved in $\langle\tilde{\Phi}_R|\tilde{\Phi}_R\rangle$ and in $\tilde{\Omega}_R$.

[D,B] *Supported by* DFG (Ro 922) *and* BMFT (WTZ X081.39)

[1] *On leave of absence from* Soltan Institute for Nuclear Studies, 00-681 Warszawa, Poland
[2] Institut für Theoretische Physik, TU Dresden *and* Institut für Kern- und Hadronenphysik, FZ Rossendorf

References:

[1] I. Rotter, Rep. Progr. Phys. 54, 635 (1991) and references therein
[2] W. Iskra, M. Müller, I. Rotter, J. Phys. G 19, 2045 (1993)
[3] F.M. Dittes, I. Rotter and T.H. Seligman, Phys. Lett. A 158 (1991) 14

Resonance phenomena in multi-channel scattering [D]

E. SOBESLAVSKY, W. CASSING [1], F.-M. DITTES AND I. ROTTER [2]

Experimental investigations of the resonance phenomena in heavy-ion reactions indicate the existence of different time scales. In the present note, we study this phenomenon in a simple many-channel model for nuclear reactions [1]. The model allows us to consider an arbitrary number of resonance states and of channels.

By changing the coupling strength between different channels, we simulate the transition from isolated to overlapping resonances. Extending our previous study [2], we present data for $\Lambda = 15$ channels. The threshold energies are chosen in such a manner that one or two of them are open in the energy region considered. For details of the parametrization see [2]. The S-matrix is determined by the mean field potentials V_{mm} in the channels $m (m = 1, ..., \Lambda)$ and by the channel coupling matrix elements V_{mn}. We use the V_{mm} so as to have one bound state in each channel. The number of resonances seen in the elastic channel is then given by the number of closed channels.

We consider the S-matrix as a function of the coupling strength α between the open and closed channels. In the case of one open channel, this coupling is chosen to be the same for all channels: $V_{1m} \propto \alpha$ for $m = 2, ..., \Lambda$. In the case of two open channels, we take V_{1m}, V_{2m} as independent random numbers uniformly distributed between 0 and α.

The positions and widths of the resonances are determined by the poles of the S-matrix in the complex energy plane. Fig. 1a shows the relative widths $\Gamma_i / \sum_k \Gamma_k$ (width Γ_i of a given resonance divided by the sum of the widths of all resonances) as a function of α in the case of one open channel. One clearly sees that with increasing α more and more of the total width is accumulated on one state whereas the widths of the other resonances decrease. This can be seen also in the landscape pictures (Figs. 1b, 1c). The 120 contour lines shown are equidistant.

In the case of two open channels, analogous results are found (Fig. 1d,e,f). Here, two states with increasing widths appear. Note, however, that for still larger coupling, the widths of *all* resonances decrease. This can be attributed to the finite number of channels we are able to take into account as well as to the fact that the states with large widths leave the resonance region.

Summarizing, our results provide a further example for the redistribution of spectroscopic properties at large coupling strength.

[1] Institut für Theoretische Physik, Universität Giessen
[2] Institut für Theoretische Physik, TU Dresden *and* Institut für Kern- und Hadronenphysik, FZ Rossendorf

References:

[1] H.A. Weidenmüller, Ann. Physics (New York) 28, 60 (1964)
[2] F.-M. Dittes, W. Cassing and I. Rotter, Z. Phys. A 337, 243 (1990)

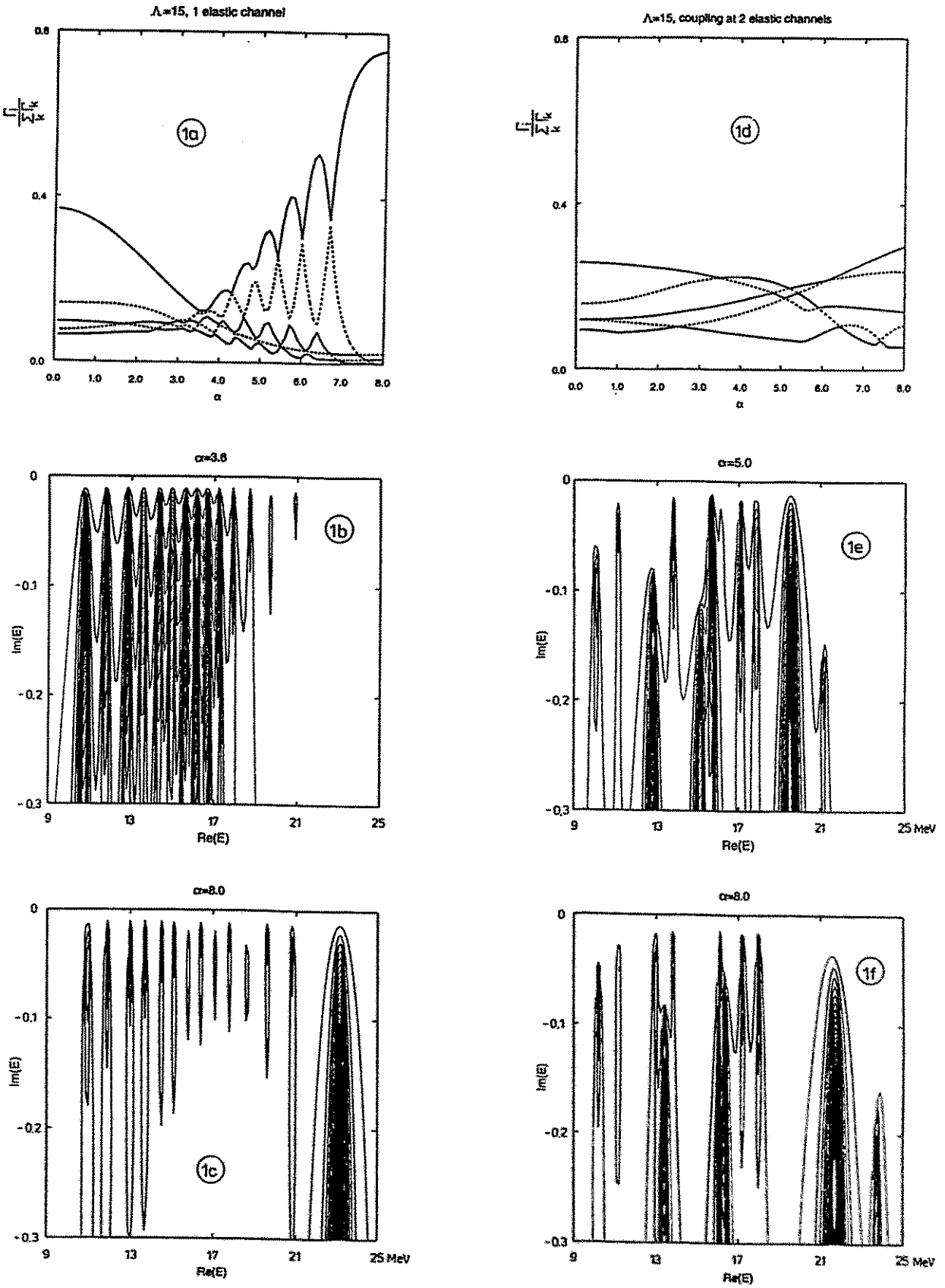

Fig. 1.
The five largest relative widths $\Gamma_i/\sum_k \Gamma_k$ as a function of α for 1 **(1a)** and 2 **(1d)** open channels and the S-matrix landscape at $\alpha = 3.6$ **(1b)** and 8.0 **(1c)** for 1 open channel and at $\alpha = 5.0$ **(1e)** and 8.0 **(1f)** for 2 open channels. The contour lines shown are equidistant, $1.04 < |S_{11}| < 12.00$.

Axial Deformations of Na Clusters at Finite Temperature

S. Frauendorf, V. V. Pashkevich[1]

The shell correction method developed in nuclear physics has been adapted to study the shape of Na clusters at zero temperature [1]. The method has been extended to treat clusters at finite temperature [2]. It is important to calculate the thermodynamic properties of the system of delocalized valence electrons for a fixed electron number (canonical partition function) since clusters are mass selected. It turns out that this can be done efficiently by evaluating the expression

$$F = \lambda N - T ln \left[\frac{1}{L} \sum_{l=1}^{L} e^{i\frac{2\pi l N}{L}} \prod_j [1 + e^{-\frac{e_j - \lambda}{T} - i\frac{2\pi l}{L}}] \right] \quad (1)$$

which becomes for $L \rightarrow \infty$ the exact free energy of N independent electrons in a potential with the energies e_j. The shapes of clusters in the range of 10 to 700 atoms have been calculated. For clusters with mass up to 310 the most general axial shape has been found. Cluster deformation has a strong influence on the separation energies. The calculated clustershapes correlate well with the splitting of the plasmon resonances (analog to the GDR in nuclei), measured recently [3]. Light clusters have a shape that reminds of big molecules. The principles governing cluster deformation are of great interest for a deeper understanding of the shapes of deformed nuclei.

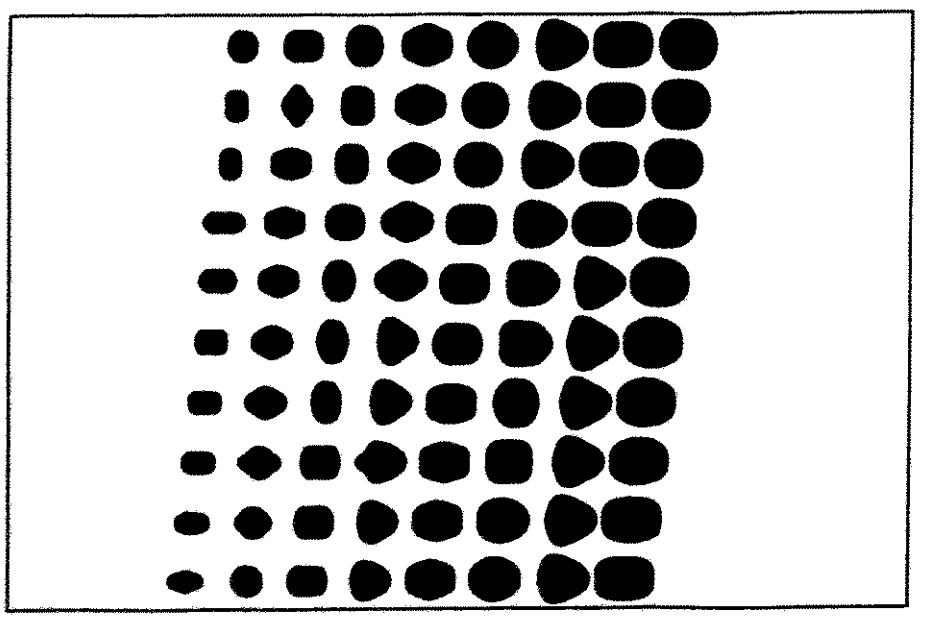

Fig. 1 The shapes of Na Clusters with 10 (lower left corner) to 89 (upper right corner) atoms. The clusters are ordered with ascending number of atoms from the left to the right.

[1] Laboratory for Theoretical Physics, Joint Institute for Nuclear Research Dubna, Russia

REFERENCES:

[1] S. Frauendorf, V. V. Pashkevich, Z. f. Physik **D26** (1993) S 98 and Phys. Rev. **B**, to be published

[2] S. Frauendorf, V. V. Pashkevich, Phys. Rev. **B**, to be published

[3] J. Borggreen et al., Phys. Rev. **B48** (1993) 17 507

Correlations in the Actions of Periodic Orbits Derived from Quantum Chaos
(Phys. Rev. Lett. 71 (1993) 4326)

Argaman, N., F.-M. Dittes, E. Doron, J.P. Keating, A.Yu. Kitaev, M. Sieber and U. Smilansky

Abstract: We discuss two-point correlations of the actions of classical periodic orbits in chaotic systems. For systems where the semiclassical trace formula is exact and the spectral statistics follow Random Matrix Theory, there exist non-trivial correlations between actions, which we express in a universal form. We illustrate this result with the analogous problem of the pair-correlations between prime numbers. We also report on numerical studies of three chaotic systems where the semiclassical trace formula is only approximate, but nevertheless these unexpected action correlations are observed.

First observation of a crossing of oblate dipole bands in the A = 200 region
(Phys. Lett. B298 (1993) 54)

Baldsiefen, G., U. Birkental, H. Hübel, N. Nenoff, B.V. Thirumala Rao, P. Willsau, J. Heese, H. Kluge, K.H. Maier, R. Schubart and S. Frauendorf

Abstract: High-spin states in ^{199}Pb were populated in the ^{186}W(^{18}O, 5n) reaction at a beam energy of 94 MeV. The analysis of the γ-ray coincidences revealed a new oblate rotational band of strong dipole transitions which shows a pronounced backbending. The connection between this band and the normal spherical states is established. Thus, spin and excitation energy of an oblate collective band in the Pb isotopes are determined for the first time. The backbending is interpreted as a crossing of bands with different numbers of aligned $i_{13/2}$ neutrons.

Charged-particle correlations in 600 A·MeV gold induced disassembly reactions, a statistical multifragmentation analysis
(Nucl. Phys. A561 (1993) 466)

Barz, H.W., W. Bauer, J.P. Bondorf, A.S. Botvina, R. Donangelo, H. Schulz, K. Sneppen

Abstract: The correlations between the charges emitted in the collision of 600 A·MeV Au nuclei on different targets are analysed by using a statistical multifragmentation model. Those correlations in partition space can be well reproduced by adjusting source sizes and excitation energies as a function of the total bound charge. The source sizes and excitation energies obtained are consistent with BUU calculations and from these we estimate the time at which the system reaches the break-up configuration. We suggest to measure the transverse flow energy carried by the intermediate mass fragments in order to further constrain the conditions causing the disassembly of matter.

Interpretation of bands in ^{163}Er within the tilted rotation scheme
(Nucl. Phys. A557 (1993) 469c)

Brockstedt, A., J. Lyttkens-Lindén, M. Bergström, L.P. Ekström, H. Ryde, J.C. Bacelar, S. Frauendorf, J.D. Garrett, G.B. Hagemann, B. Herskind, F.R. May, P.O. Tjom

Abstract: High-spin data are presented for levels in ^{163}Er and their structure is interpreted within the tilted rotation scheme.

A nonperturbative transport approach including particle collisions and density fluctuations
(Nucl. Phys. A561 (1993) 133)

Cassing, W., A. Peter, A. Pfitzner

Abstract: The dynamical description of correlated nuclear motion is based on coupled equations of motion for the one-body density matrix $\rho(11'; t)$ and the two-body correlation function $c_2(12, 1'2'; t)$ as obtained from the density-matrix hierarchy. The resulting equations nonperturbatively describe particle-particle collisions as well as particle-hole interactions. We propose an approximate solution of the equation of motion for the two-body correlation function c_2 which nonperturbatively accounts for the renormalization of the bare interaction, for in-medium nucleon-nucleon scattering as well as for the coupling to density fluctuations or collective phonons. By performing a Wigner transformation and conventional semiclassical limits we obtain a transport equation of the Vlasov-Uehling-Uhlenbeck type (VUU) coupled to a respective transport equation for the density fluctuations. We present explicit solutions for the ground-state density fluctuations of ^{40}Ca in phase space and compare them with the corresponding fluctuations in case of collective monopole excitations.

Tilted Cranking
(Nucl. Phys. A557 (1993) 259c)

Frauendorf, S.

Abstract: Within the QQ-model the existence of TDHF solutions is demonstrated that rotate uniformly about an axis tilted with respect to the principal axes of the quadrupole mean field. These TAC solutions represent ΔI=1-bands of fixed parity. Energies and intraband transition matrix elements of ΔI=1-bands deviating significantly from strong coupling are studied. As examples two bands in ^{179}W containing Fermi Aligned $i_{13/2}$ quasineutrons and the M1-bands discovered recently in nuclides around ^{198}Pb are discussed. For the latter the dynamical moment of inertia is almost purely quantal generated by the $i_{13/2}$, $h_{9/2}$ protonpair and the few $i_{13/2}$ quasineutrons excited from the paired neutron ground band.

Shapes of Na Clusters
(Z. Phys. D26 (1993) 98)

Frauendorf, S. and V.V. Pashkevich

Abstract: Quadrupole, octupole and hexadecapole deformations of Na clusters are calculated. The quadrupole deformations correlate well with the splittings of the plasmonresonances. Octupole deformation is predicted for clusters around 46, 64, 104, ..., which creates a static dipole moment. Rotational lines in the microwave spectrum are expected.

Evidence for trapping and collectivization of resonances at strong coupling
(Nucl. Phys. A556 (1993) 107)

Herzberg, R.-D., P. von Brentano and I. Rotter

Abstract: The behavior of 22 neutron resonances in ^{53}Cr is investigated as a function of the coupling-strength parameter μ and of the degree of overlapping. Starting from a doorway picture at small μ, the widths of 21 resonances increase with increasing μ at the cost of the width of the original "single-particle doorway resonance". At $\mu \approx 1$, the widths of most states decrease again. At $\mu \rightarrow 10$ the widths of these "trapped" states vanish while "collective" states are formed which gather the widths. Thus we again observe a doorway picture at strong coupling. At $\mu = 1$, the energies and widths of the resonances are fitted to the experimental data. At this coupling strength, most resonances investigated resemble trapped modes.

Selforganization in the nuclear system
I: The slaving principle
(J. Phys. G: Nucl. Part. Phys. 19 (1993) 2045)

Iskra, W., M. Müller and I. Rotter

Abstract: The properties of the atomic nucleus are investigated from the point of view of selforganization. The nucleus is described as an open quantum mechanical many-body system embedded in the continuum of decay channels. The transition from low to high level density is traced as a function of the coupling strength between the discrete nuclear states and the environment of decay channels. A redistribution inside the nucleus takes place in a small region around some critical value of the coupling strength. As a result of the redistribution, the effective number of degrees of freedom is reduced. The analogy of the results obtained numerically for the nuclear system to the laws of synergetics is investigated. The slaving principle is shown to hold in the open quantum system.

Hierarchical trapping of resonance states at high level density
(Phys. Rev. C47 (1993) 1086)

Iskra, W., I. Rotter and F.-M. Dittes

Abstract: On the basis of a simple S-matrix model we show that, at high average level density, local fluctuations in the density of states of an open quantum mechanical system create locally a few broad resonance states together with a larger number of narrow (trapped) ones. The widths of the broad states are of the order of the length which characterizes the local fluctuations in the spectrum. They serve as a background for the narrow "fine-structure resonances". If the spectrum shows a hierarchical fluctuation pattern in energy, this behavior repeats on all energy scales. From these results, we conjecture that the well-known intermediate structures in nuclei at high level density, described by the doorway mechanism, are formed due to such a trapping effect.

Barrier penetration effect on the angular momentum dependence of the parity splitting in actinide nuclei
(J. Phys. G: Nucl. Part. Phys. 19 (1993) L151)

Jolos, R., P. von Brentano and F. Dönau

Abstract: Experimental data on the angular momentum dependence of the parity splitting of the yrast band in actinide nuclei are interpreted in the framework of a one-dimensional model of octupole vibrations with axial symmetry. The tunnelling effect as a main source of the parity splitting is calculated in the quasiclassical approximation.

Velocity correlations of intermediate mass fragments produced in central collisions of Au + Au at E = 100, 150, 250, 400 A MeV
(Nachrichten GSI 10-93)

Kämpfer, B., R. Kotte for the FOPI collaboration

Abstract: Velocity correlations of intermediate mass fragments (IMFs) with $Z \geq 3$, produced in central and semi-central collisions of Au + Au at 100, 150, 250 and 400 A MeV beam energy, are extracted from measurements with the FOPI (phase I) detector system. Shown is the correlation function 1 + R as function of the scaled relative velocity υ_{red} (see contribution). The IMF correlation functions for semi-central events (open symbols) are found to be affected by the directed sideward flow. When rotating the events into a unique reaction plane an enhancement of correlations in the low-υ_{red} region, resulting from event mixing effects, vanishes (full symbols). Selecting violent collisions with a high degree of azimuthal symmetry the correlation function appears nearly independent of additional event or single particle gate conditions. The comparison of the data with a Coulomb dominated final-state interaction model points to time scales of τ ~ 25 fm/c or less for emitting IMFs from an expanding and fast-multifragmenting source with radius R ~ 14 fm.

Estimates of dielectron production in pp and pd reactions at 1 - 2 GeV
(Phys. Lett. B301 (1993) 123)

Kämpfer, B., A.I. Titov and E.L. Bratkovskaya

Abstract: Estimates of elementary cross sections for dielectron production in pN and pd reactions are presented. We use the vector dominance model for all hadron-photon vertices. A dynamical suppression mechanism (off-shell behavior of the two-body T-matrix, mass dependent Δ production rate) brings the elementary rate near to previous estimates which did not use vector meson dominance. However, near to the ρ mass a characteristic shoulder apprears in our approach. We consider Δ,η Dalitz decays and bremsstrahlung at 1-2 GeV as dominant sources of dielectrons. At higher energies to bremsstrahlung contribution is only a subclass of direct vector meson decays. Relying on a realistic deuteron wave function we predict the ratio of dielectron production in pd to pp reactions.

Kinetics of pre-equilibrium parton matter probed by dilepton radiation
(NATO ASI B303 (1993) 649)

Kämpfer, B. and O.P. Pavlenko

Nuclear structure function F_2^A: Moments $M_n(F_2^A)$ and kinematics beyond x = 1
(Phys. Rev. D47 (1993) 3804)

Kaptari, L.P., A.Yu. Umnikov and B. Kämpfer

Abstract: An analysis of the behavior of nuclear structure functions F_2^A at large x and their moments M_n^A at large n has been performed within two theoretical approaches: (i) the QCD-motivated Q^2-rescaling model and (ii) the operator product expansion method within an effective meson-nucleon theory which is prompted by nuclear physics. Our theoretical estimates of the nuclear structure function at $x \geq 1$ are in good agreement with existing data. The moments, derived from experimental data, are found to depend essentially on the behavior of the respective structure functions beyond x = 1. A relation between the Q^2-rescaling parameter ε_A and nuclear averages, i.e., mean kinetic energy and chemical potential of nucleons, as well as a dependence of ε_A on n are established.

Poisson and Porter-Thomas fluctuations in off-yrast rotational transitions
(Nucl. Phys. A564 (1993) 345)

Matsuo, M., T. Dossing, B. Herskind, S. Frauendorf

Abstract: Fluctuations associated with stretched E2 transitions from high-spin levels in nuclei around ^{168}Yb are investigated by a cranked shell model extended to include residual two-body interactions. In the cranked mean-field model without residual interactions, it is found that gamma-ray energies behave like random variables and the energy spectra show Poisson fluctuation. With two-body residual interactions included, the discrete transition pattern with unmixed rotational bands is still valid up to around 600 keV above yrast, in good agreement with experiments. At higher excitation energy, a gradual onset of rotational damping emerges. At 1.8 MeV above yrast, complete damping is observed with GOE-type fluctuations for both energy levels and transition strengths (Porter-Thomas fluctuations).

Chaotic Behavior in Warm Deformed Nuclei Induced by Residual Two-body Interactions
(Nucl. Phys. A557 (1993) 211c)

Matsuo, M., T. Dossing, B. Herskind, S. Frauendorf, E. Vigezzi and R.A. Broglia

Abstract: Band mixing calculations in rapidly rotating well-deformed nuclei are presented, investigating the properties of energy levels and rotational transitions as a function of excitation energy. Substantial fragmentation of E2 transitions is found for $E_x > 800$ keV above yrast, which represents the onset of rotational damping. Above $E_x \approx 2$ MeV, energy levels and E2 strengths display fluctuations typical of quantum chaotic systems, which are determined by the high multipole components of the two-body residual interaction.

Rotation-induced transition from superfluid to normal phase in mesoscopic systems: ^{168}Yb and adjacent nuclei
(Phys. Rev. C47 (1993) R 926)

Oliveira, J.R.B., S. Frauendorf, M.A. Deleplanque, R.M. Diamond, F.S. Stephens, C.W. Beausang, J.E.Draper, C. Duyar, E. Rubel, J.A. Becker, E.A. Henry and N. Roy

Abstract: The transition from strong static pairing to weak static pairing and its consequences to the excitation spectrum of a mesoscopic (medium number of particles) system are investigated. New levels have been measured in ^{168}Yb. A reasonable description of the A ≈ 168 isotopes spectra is obtained. The adequacy of the phase transition concept is discussed.

Band crossings in intruder configurations of odd-A nuclei: A probe of the neutron-proton interaction?
(Nucl. Phys. A565 (1993) 573)

Satula, W., R. Wyss and F. Dönau

Abstract: The routhian diagrams calculated by means of the cranked shell model are known to be a rather succcessful tool for describing the experimental alignment pattern observed for rotational band structures. However, this mean-field approach seems to fail when applied to band structures built on intruder configurations. It is investigated whether the observed anomalies are affected by the neutron-proton interaction which is only partly and indirectly included in the standard mean-field approach.

First Identification of Dipole Excitations to a $2^+ \otimes 3^-$ Particle Multiplet in an Odd-A Nucleus
(Phys. Rev. Lett. 70 (1993) 2880)

Zilges, A., R.-D. Herzberg, P. von Brentano, F. Dönau, R.D. Heil, R.V. Jolos, U. Kneissl, J. Margraf, H.H. Pitz and C. Wesselborg

Abstract: A photon scattering experiment has been performed on the odd-A nucleus ^{143}Nd. Strong dipole excitations have been detected in the energy region around 3.2 MeV. This is near the expected position of the two-phonon ($2^+ \otimes 3^-$) multiplet in the even-even neighboring nucleus ^{142}Nd. The summed dipole strength between 2.8 and 3.6 MeV in ^{143}Nd is in agreement with the sum rule for weak particle coupling to the core nucleus ^{142}Nd. Model calculations in a harmonic approximation are in very good agreement with the experiment and they suggest a two-phonon ($2^+ \otimes 3^-$) particle structure of the excitations in ^{143}Nd.

2. Experimental Medium Energy Physics

Estimate of the Total Cross Section of the Proton-Proton-Bremsstrahlung near Pion Threshold[B,K]

E. KUHLMANN[1], H. MÜLLER, B. NAUMANN, L. NAUMANN

The COSY-TOF-collaboration plans the investigation of the proton-proton-Bremsstrahlung ($pp\gamma$) with a sufficiently high precision to study off-shell effects of the nucleon-nucleon scattering near the pion threshold [1]. To understand the influence of the background reactions on the investigated nuclear process it is important to know the order of magnitude of their total cross sections. The aim of this study was to estimate the total cross section of $pp\gamma$ at proton beam energies of about 300 MeV. By Rothe et al. [2] a total cross section for $pp\gamma$ of $\sigma_{tot} = (0.7 \pm 0.15)\ \mu$b was obtained at 204 MeV for a photon energy of $E_\gamma \geq 35$ MeV. At TRIUMF [3] and Bloomington IUCF [4] differential cross sections had been measured at 280 MeV and 294 MeV, respectively. The TRIUMF data were obtained with the help of a coplanar spectrometer, where all three scattered particles had been detected. The IUCF data were measured with a noncoplanar spectrometer geometry. Both outgoing protons were constrained to angles from 4.8° to 12° and kinetic energies between 20 and 120 MeV. The Bremsstrahlung had been selected by a missing mass procedure. Authors of the IUCF data noted a good agreement between the pure phase space distribution and the shape of the data [4]. We generated phase space distributed events for the IUCF kinematic conditions taking into account a scattering angle straggling of 1.2°, a momentum resolution of 8% and the quadrupole character of the radiation. For the three angular distributions the calculated differential cross sections are shown in Fig.1. They were normalized with an averaged total cross section of $\sigma_{tot} = 9\mu$b. The averaged error of this value has been obtained to 3μb. The result of simular calculations for the TRIUMF data at proton scattering angles about 12° is in a good agreement with the above one. The estimate of the total cross section has been carried out in the framework of the program AFKINE [5] based on the General Simulation program FOWL of the CERN Program Library.

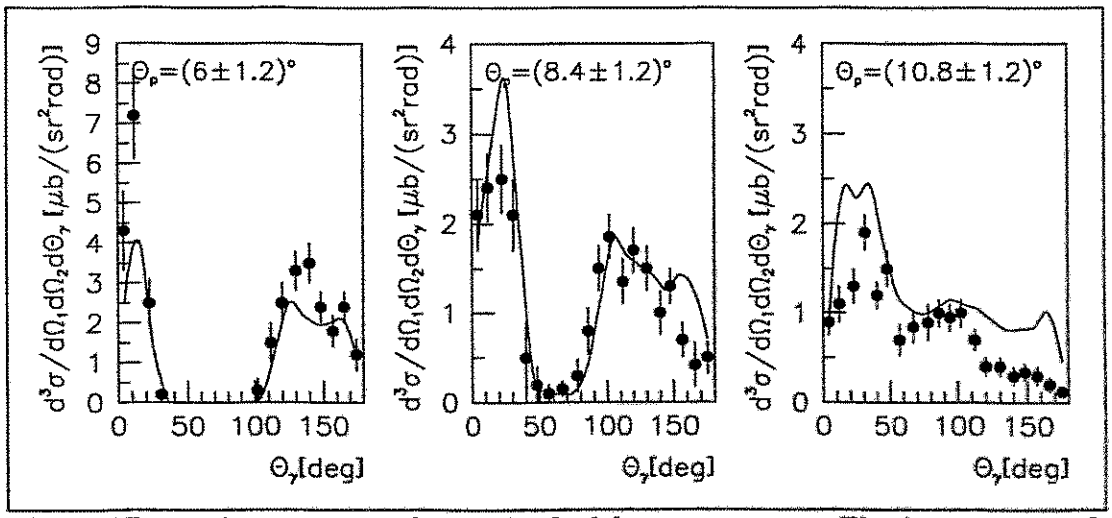

Fig.1 Differential cross section for $pp\gamma$ in the laboratory system. The data correspond to [4] and the curves to a phase space distribution, normalized with the averaged total cross section $\sigma_{tot} = 9\mu$b.

[1] *Ruhr-Universität Bochum, Institut für Experimentalphysik I*

REFERENCES:

[1] W. Amian et al.,COSY Proposal No.9(1989)
[2] K.W. Rothe et al., Phys. Rev.**157**(1967) 1247
[3] K. Michaelian et al., Phys. Rev.**D41**(1990) 2689
[4] B. v. Przewoski et al., Phys. Rev.**C45**(1992) 2001
[5] B. Naumann et al., Annual report 1992,FZR 93-10(1993) 69

Missing Mass Measurements $pp \rightarrow ppX$ at COSY-Energies[B]

E. KUHLMANN[1], H. MÜLLER, E. RODERBURG[2], K. SISTEMICH[2]

A study of η and η' production as well as an investigation of pp bremsstrahlung (COSY–Proposals #12 [1] and #9 [2]) is planned to be carried out at the TOF spectrometer. The process of interest is to be selected via momentum measurement of two protons in order to determine the invariant mass of the particles accompanying the two protons. In the case of η and η' production the ratio of the produced $\eta^{(\prime)}$ mesons to groups of other particles with invariant masses near the $\eta^{(\prime)}$ mass will be decisive for the accuracy of the experimental results. For the investigation of the bremsstrahlung above the pion threshold or even in the vicinity of the two-pion threshold it will be important to achieve a momentum resolution sufficient to resolve the γ and the pion peak in the missing mass spectrum. These two problems can be studied in the framework of a statistical model, whose ability to reproduce the energy dependence of the reaction channels with meson production at COSY energies has been demonstrated recently [3].

In Fig. 1 the calculated missing mass spectra $pp \rightarrow ppX$ at 2.5 GeV are shown as expected under various conditions. An "ideal" missing mass spectrum is plotted in Fig. 1a with the mass resolution given by the bin width of the histogram, which is chosen such that the line width of the ω meson can be observed. The neutral mesons are clearly visible except the η' meson which obviously disappears in the background (see the dashed line in Fig. 1a which does not show any signature from the η'). In Fig. 1b it is demonstrated that the peak to background ratio for the η' meson can be improved by triggering on six charged particles in the final state. The reduction of the background due to the selection of channels with production of four charged mesons in addition to the two protons is stronger than the reduction of the η' peak caused by selecting the particular decay chain $\eta' \rightarrow \pi^-\pi^+\eta$ (44 %) with subsequent $\eta \rightarrow \pi^-\pi^\circ\pi^+$ (24 %) or $\eta \rightarrow \gamma\pi^-\pi^+$ (5 %).

In order to get an impression how a realistic measurement may look like the same spectra are plotted in the Figs. 1c) and d), but now folded with a momentum resolution (see ref. [4]) as expected for the TOF spectrometer to be installed at the external COSY beam. From the spectra shown in Figs. 1c) and d) one can expect that a measurement of the η production cross section should yield reasonable results in spite of the large physical background, while the determination of the η' cross section will probably be difficult.

At the 0° Facility (ZDF) to be installed at the internal beam of COSY the momentum measurement is based on a separation of the different ejectile momenta by a magnetic field in connection with a time-of-flight measurement for particle identification. This method results in a momentum resolution $\Delta p/p$ nearly independent of the ejectile momentum. The angular acceptance of the ZDF is restricted to the forward direction $\Theta < 10°$. Although this detector is dedicated [5] to the investigation of proton-nucleus interactions a measurement of well defined peaks in the missing mass spectra from pp reactions is considered as very helpful for tuning and calibration of the set-up. A measurement of the missing mass spectra at the ZDF should give spectra as shown in Figs. 1e) and f). Due to the limited angular acceptance the yield is much smaller but due to the better momentum resolution the peaks are more pronounced. Even a measurement of the η' production cross section might be possible, because the energy is near the threshold and all reaction products are emitted in forward direction. Thus, the ZDF approaches a 4π detector under these specific conditions.

In order to compare the suitability of the TOF spectrometer and the ZDF with respect to the measurement of bremsstrahlung the reaction channel $pp \rightarrow pp\gamma$ has been implemented in the statistical model [3]. The phase-space of this channel is multiplied by an empirical matrix element squared of the form $1/3 + \cos^2\Theta^*_\gamma$ with Θ^*_γ being the emission angle of the γ in the

center-of-mass system. The phase space distribution is normalized to the total cross section for which a value of 30 μb [2] has been assumed for the three energies in the region up to the two-pion threshold considered in Fig. 2. Again the lower yield but the better resolution of the ZDF compared to the TOF spectrometer can be seen. For a comprehensive investigation of bremsstrahlung it is reasonable to supplement the TOF measurements of the full phase-space at lower energies by an investigation of the especially interesting high-momentum part of the γ spectrum at higher energies by means of the ZDF.

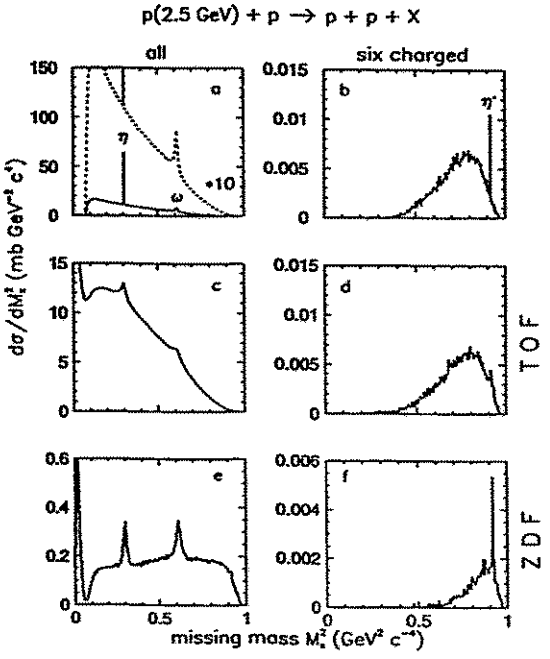

Fig.1: Missing mass spectra from pp interactions at 2.5 GeV. In a) and b) an "ideal" 4π detector is assumed. In c) and d) the calculated momenta are folded with a resolution as expected [4] for the TOF spectrometer, namely $\Delta p/p = 0.03p^2$ for $\tan\Theta < 0.2$, $\Delta p/p = 0.05p^2$ for $0.2 \leq tan\Theta \leq 0.6$ and $\Delta p/p = 0.1p^2$ for $\tan\Theta > 0.6$. In e) and f) an angular acceptance of $\pm 10°$ in horizontal and $\pm 6°$ in vertical direction, a momentum and angular resolution of $\Delta p/p = 1.5\%$ FWHM and $\Delta\Theta = 0.2°$, respectively, as expected for the ZDF [5] is taken into account. A trigger on six charged particles in the final state is simulated in b), d) and f).

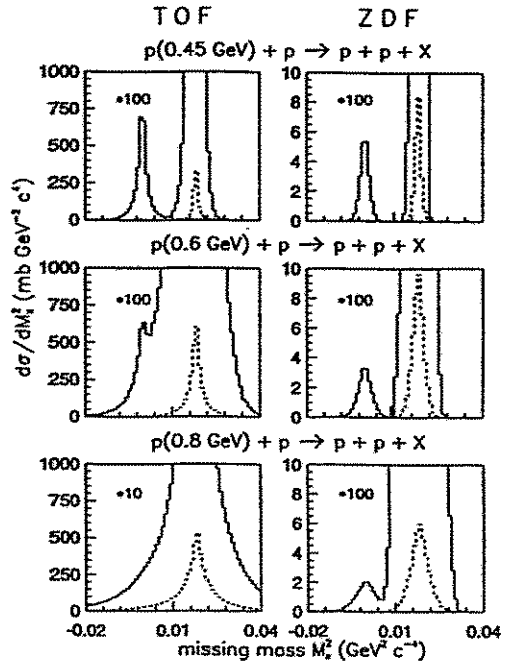

Fig.2: Missing mass spectra from pp interactions at different energies. The full curves are multiplied by the factors indicated. For the TOF spectrometer and the ZDF the same experimental conditions are assumed as described in the caption of Fig. 1.

[1] Ruhr-Universität Bochum, Germany
[2] Forschungszentrum Jülich, Institut für Kernphysik

REFERENCES:

[1] D. Bour et al., Study of η and η' Production and Interaction, COSY Proposal #12, 1989

[2] W. Amian et al., Investigation of proton-proton bremsstrahlung, COSY Proposal #9, 1989

[3] H. Müller, Proceedings of the 105th WE-Heraeus-Seminar (1993) 117

[4] E. Kuhlmann, Phys. Scripta 48 (1993) 226

[5] W. Borgs et al., Study of the Subthreshold K^+ Production with the 0° Facility at TP2 in COSY, Cosy Proposal #18, 1991

Tests of the COSY-TOF Startdetector MARS with Electrons and 13 MeV-Protons[B]

P. MICHEL, K. MÖLLER[1], A. SCHAMLOTT AND A. SCHÜLKE

The basic design of the Rossendorf start detector MARS for the COSY-Time-of- Flight Spectrometer TOF is described in [1],[2]. In 1993 the mechanical construction was completed and test measurements for calibrations with electrons from a ^{90}Sr-source and with protons from the Rossendorf Cyclotron were carried out. In order to use the full geometrical and momentum accuracy of the COSY beam the geometrical adjustment of the small start detector segments (2x16 trapezium-like scintillators) has to be very precise. Fig.1 shows part of the elements of the two 16-fold segmented start detector rings A and B. In the first appliccation of the start detector, the measurement of ppγ-bremsstrahlung ([3]), the B-Ring will be operated as a veto counter to rejectelastic pp-scattering events. Due to the large cross section of elastic scattering in comparison to the bremsstrahlung reaction it is necessary to suppress elastic protons with an efficiency of 100%. Therefore the B-segments have to overlap their neighbours to reject particles coming from any possible point of the target. Small gaps of the order of 100μm between the A-segments are acceptable because this reduces the efficiency of the detector only by a few percent. A small overlap between ring A and B is also required to ensure that despite of the finite size of the target each ejectile is registered at least by one of the two rings (exept for the small loss due to the ring A gaps). A precise adjustment of the start detector elements is very important for track measurement, since due to geometrical conditions (target to start distance: 4cm, start to stop distance: 7.5m) a small displacement of a start segment in the order of 100μm corresponds to an error in the stop detector plane of a few cm's. The procedure of adjusting the hollow light guides by means of a laser beam and theodolite is described in [4]. The hollow light guides are housing the small scintillator elements. Because the scintillators are covered by light guide tubes made from aluminized mylar, additional investigations were carried out to measure the scintillator positions using charged particles. First a β-source (diameter 2 mm, 50 kBq) was installed at the position corresponding to the back egde of the liquid hydrogen target. For particles coming from this region maximum gaps should be observed. Overlaps between neighbouring B segments or between corresponding A and B segments were determined by means of coincidence corellation analysis. Fig.2 shows the coincidence correlation matrix for ring A. Lines and columns characterize the detector segment number, and the matrix elements are filled by 2-fold coincidences between any pair of counters. The main diagonal is filled by single events. By comparing the number of coincidences of neighbouring channels with the number of single events the geometrical overlap can be calculated. The accuracy of this method is limited to about 10% since in addition to the true coincidences corresponding to the geometrical overlap there are background coincidences originating from electron scattering in air and in the foils of the hollow light guides. To improve the accuracy of this method the measurement was repeated with 13 MeV protons at the Rossendorf Cyclotron U-120 [5]. The start detector chamber was mounted at the vacuum beam line system. A pipe with a 2 mm diameter hole was inserted in the target position to reproduce the geometrical conditions of the cooled COSY beam as shown in Fig.3. Protons passing this collimator are scattered on a 15μm tungsten target mounted near the hole. Fig.4 shows the coincidence matrix of the B segments. Since the p-A-scattering cross section increases strongly with decreasing scattering angles the number of single events

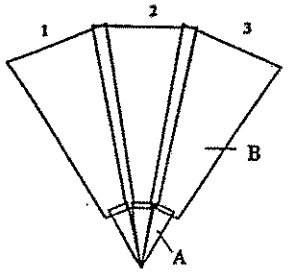

Fig.1 Arrangement of scintillators in the MARS start detector

	1	2	3	4	5	6	7	8	9	10	11	12	13			
1	416	12	2	1	3			1	2		2		3	2	2	18
2		513	13	1		1		2	1	1	1	1			2	2
3			516	24	2	1	1				2	3	1	1		3
4				510	11	1	1		2				1	1	2	1
5					534	10	2	2	1	1	1	2	2	3		
6						552	9		2	2	2	1			2	
7							452	8	1	2	2	2	1		1	1
8								472	22	5	2	1	1	1		
9									413	16	2	1		1		
10										475	10	1	2	1		
11											399	12	2		1	
12												472	12	2		1
13													449	10	3	
14														481	19	2
15															488	12
16																374

Fig.2 Coincidence matrix for the A-ring bombarded with electrons

is very sensitive to the distance of the trapezium-like scintillators from the target as well as from the beam axis. Due to the overlap of neighbouring elements this distance is changing alternately and so does the number of single events. From the numbers of coincidences between neighbouring elements the size of overlaps can be evaluated and can be corrected by readjustment. It should be noted that in the 8th diagonal in Fig.4 the coplanar hits can be observed which are due to elastic pp-scattering on surface hydrogen of the tungsten target.

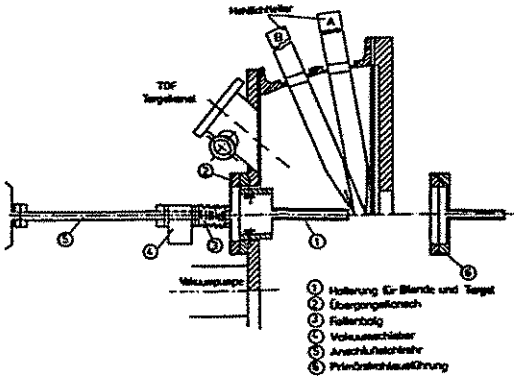

Fig.3 Setup for test measurements with the MARS detector at the Rossendorf Cyclotron

	1	2	3	4	5	6	7	8	9	10	11	12	13	14	15	16
1	42241	6610	2	3	3	2	2	3	17	4	0	4	3	2	3	5675
2		24828	3752	5	7	2	2	6	2	37	5	5	2	7	1	3
3			30510	3425	4	2	1	2	0	1	20	6	1	1	3	3
4				17673	2283	4	4	5	0	0	3	26	2	2	2	2
5					36239	4106	3	4	2	1	1	4	24	8	1	1
6						16656	3451	4	3	2	0	1	2	30	4	1
7							28808	6092	3	0	5	4	0	2	14	5
8								17671	4795	5	3	6	2	1	3	34
9									17041	2771	4	4	3	1	4	2
10										19845	2382	6	1	0	1	0
11											31824	4977	4	2	2	0
12												18647	5918	2	4	0
13													33149	3313	1	5
14														18830	6530	3
15															41379	6704
16																26764

Fig.4 Coincidence matrix for the B-ring bombarded with 13 MeV Protons

[1] Institut für Kern- und Teilchenphysik, TU Dresden und
Institut für Kern- und Hadronenphysik, FZR

REFERENCES:

[1] P. Michel et al., Annual Report 1991 FZR 92 - 09, 48

[2] P. Michel et al., Annual Report 1991 KFA, IKP, 5

[3] COSY proposal #9

[4] A. Schülke et al., Annual Report 1992 FZR 93 - 10, 67

[5] P. Michel et al., COSY-TOF-NOTES RO-1-1993

Simulation of Momentum Resolution at the 0° -Facility[B]

S. Dshemuchadse, L.v. Horn[1], V. Kruglov[2], H. Müller, H. Ohm[1],
Ch. Schneider and Ch. Schneidereit

The side detector of the 0° -Facility will be equipped with two multiwire chambers with anode readout for measuring the particle tracks of the ejectiles. By reconstructing the tracks through the magnetic field of the analysing magnet D2 their momentum and angular distributions are received. From the study [1] of the side detector it is known that the momentum resolution is restricted mainly due to small angle scattering in the vacuum window of the magnet and the start scintillator. Since the particle trajectories are reconstructed using the position information from the wire chambers W1 and W2, it is important to know how the wire spacing influences the momentum resolution.

For this purpose GEANT simulations are performed for chambers consisting of three anode and four cathode planes. Mylar foils are used as cathodes and the distance between cathode and anode is 6 mm. The three anode planes contain wires with diameters of 20 μm arranged at angles of 0° and ± 30° resp. to the vertical. The dimensions of the active areas of the chambers as well as their positions were chosen as in [1].

The error caused by the position resolution is simulated in a first step by folding the true position of the particle tracks in the middle planes of the two chambers with Gaussian distributions in x and y direction. These two "measured" points are then used for backward tracing of the trajectory, whereby the particle momentum is adjusted such that the track ends in the target. A target width of 0.1 mm is used in the calculations.

This procedure results in a reconstructed value for the ejectile momentum, whose deviation from the original one is related to the width of the position distribution assumed for the wire chamber.

In Fig. 1 the momentum resolution $\Delta p/p$ achieved for K^+ mesons with momentum p = 290 MeV/c is plotted versus the standard deviation σ_G of the Gaussian used for smearing out the particle position. The curve marked with squares is calculated with all physical processes switched off. It represents the influence of the position resolution of the chambers on the momentum resolution. The second curve marked with triangles shows that the physical processes (mainly small angle scattering, decay, hadronic interactions and δ-ray production) give the main contribution to the overall momentum resolution as long as σ_G remains smaller than about 1.5 mm. Therefore, the latter value should not be exeeded by the chamber.

The next step consists in finding the relation between σ_G and the wire spacing d in the anode planes of the chambers. The simplest anode chamber model assumes that only the wire closest to the particle trajectory responds. Then the error in the position for one anode plane is given by the standard deviation $\sigma_U = d / \sqrt{12}$ of a uniform distribution.

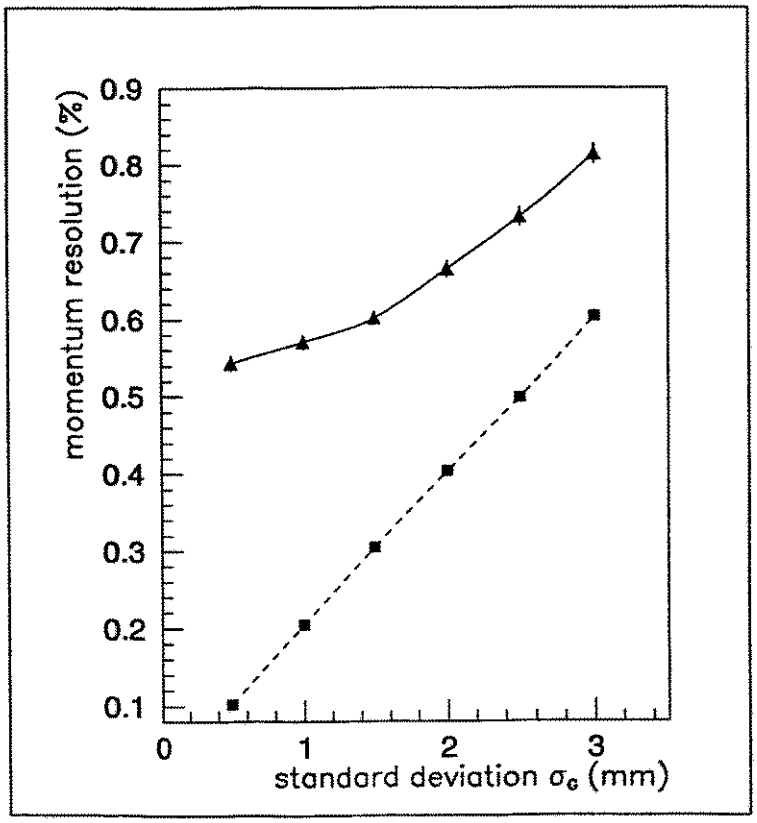

Fig.1 Momentum resolution (FWHM) versus assumed position resolution for K^+ mesons of momentum p = 290 MeV/c.
▲ : physical processes switched on
■ : physical processes switched off

Actually, the relation between σ and d is more complicated. If for example a particle crosses the chamber diagonally more than one wire could respond. In this case the resolution gets a bit worse. On the other hand there are three active anode planes in one chamber. This increases the accuracy of the position determination noticeably.

As a first estimate it is assumed that the relation $\sigma_U \leq \sigma_G$ holds from which a wire spacing of $d \leq \sqrt{12}\ \sigma_G \approx 5$ mm can be deduced.

[1] Forschungszentrum Jülich, Institut für Kernphysik
[2] Joint Institute for Nuclear Research, Dubna

REFERENCES:

[1] O. Schult et al., Annual Report 1993 KFA

Light Meson Production and pp-Bremsstrahlung at the COSY Time-of-Flight Spectrometer
(Physica Scripta 48 (1993) 226)

Kuhlmann, E. and the COSY-TOF Collaboration: H.Brand, S. Brand, P. Cloth, M. Dahmen, V. Drüke, W. Eyrich, D. Filges, H. Freiesleben, A. Fritsche, K. Kilian, M. Kirsch, H. Koch, R.A. Kraft, J. Krug, E. Kuhlmann, S. Lange, H. Machner, H. Matthäy, P. Michel, R. Mirz, K. Möller, H.P. Morsch, B. Naumann, L. Naumann, W. Oelert, A. Parsch, N. Paul, P. Ringe, E. Roderburg, K. Röhrich, A. Röser, M. Rogge, G. Schmidt, M. Schmidt, O. Schult, T. Sefzick, M. Steinke, F. Stinzing, R. Stratmann, P. Turek, R. Werding and S. Wirth

Abstract: Experiment on light meson production and pp-bremsstrahlung as planned for the initial stage at COSY are discussed. Special emphasis will be placed on near-threshold behaviour where due to kinematics all particles are forced into a rather narrow cone around the beam axis. A specially designed charged particle detector system will be used which not only covers the complete forward hemisphere of 2π in the laboratory system but additionally shows maximum resolution in the extreme forward direction with only moderate cuts in the minimally required energy of all ejectiles.

3. Experimental Nuclear Spectroscopy

Lifetimes in ^{83}Br

R. Schwengner, G. Winter, R. Wirowski[1], N. Nicolay[1] and P. von Brentano[1]

The nucleus ^{83}Br has been investigated in coincidence experiments with the six-detector array OSIRIS CUBE at the tandem accelerator in Köln [1]. Mean lifetimes of states in ^{83}Br were determined from Doppler shifts observed in coincidence spectra at 45° and 135° to the beam using the Doppler-shift attenuation (DSA) method. The coincidence spectra were extracted from two E_γ–E_γ matrices that contain γ–γ–α coincidence events of all Ge detector pairs with one detector at 45° or 135°, respectively. The γ–γ–α coincidence technique allowed especially lifetimes of levels fed by the μs isomer at 3068.5 keV to be determined as coincidences with the isomeric transition at 303.4 keV are suppressed. The lifetimes were deduced from a comparison of experimental lineshapes with calculated ones. The velocity distributions of the emitting nuclei were calculated with a Monte Carlo code in which reactions in different depths of the target, the kinematics of the reaction and the slowing down and deflection of the recoils were taken into account [2]. Examples of lineshape analyses are shown in figure 1. The lifetimes obtained from the present analysis and reduced $E2$ and $M1$ transition strengths derived from these lifetimes are given in table 1. The relatively small $E2$ transition strengths point to rather non-collective configurations of the level sequences in ^{83}Br.

Table 1. Mean lifetimes of states in ^{83}Br

E_i (keV)	E_γ (keV)	τ^a (ps)	$B(M1)$ (W.u.)^b	$B(E2)$ (W.u.)^b
1701.1	609.3	31(6)		15^{+4}_{-3}
2765.1	1064.3	2.0(3)		14^{+3}_{-2}
4221.8	1456.4	0.5(2)		12^{+7}_{-4}
2134.1	1042.3	0.5(3)	$0.022^{+0.032}_{-0.008}$	29^{+43}_{-11}
2788.6	654.5	1.4(6)	$0.036^{+0.020}_{-0.009}$	125^{+93}_{-38}
1438.7	572.0	2.1(6)	$0.055^{+0.022}_{-0.012}$	
1438.7	1082.2			$3.9^{+1.6}_{-0.9}$
2127.1	688.3	1.7(6)	$0.029^{+0.024}_{-0.008}$	
2127.1	1260.5			$3.5^{+1.8}_{-0.9}$

[a]) Mean lifetime deduced from DSA experiments. The error given in parentheses includes the statistical error, uncertainties of feeding times and feeding intensities and a 10% uncertainty of the nuclear and electronic stopping power.

[b]) Reduced transition probability in Weisskopf units: 1 W.u.($E2$) = 21.5 e^2fm^4; 1 W.u.($M1$) = 1.8 μ_K^2. Branching ratios and mixing ratios were taken into account.

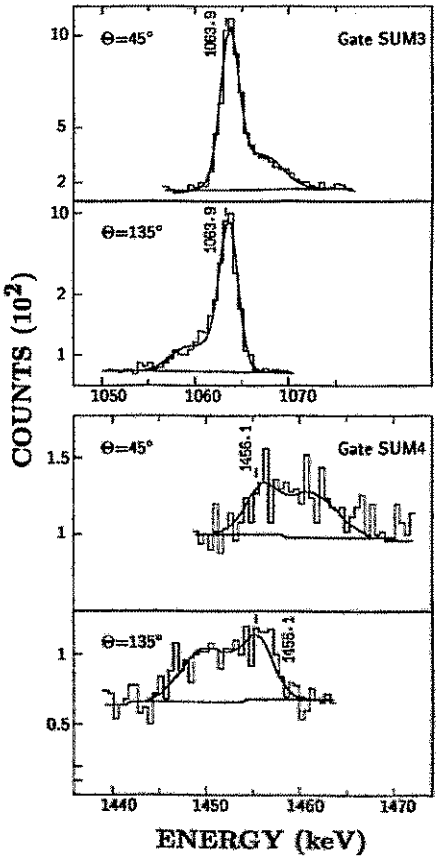

Figure 1. Lineshape analyses of the γ rays at 1064.3 and 1456.4 keV in γ–γ–α coincidence spectra. The lifetimes were deduced from a joint fit of the spectra at the complementary observation angles of 45° and 135°.

[1] *Institut für Kernphysik der Universität Köln*

REFERENCES:

[1] R. Schwengner et al., Annual report 1992, **FZR 93-10** (1993) p.82

[2] G. Winter, Nucl. Instr. Meth. **214** (1983) 537

Neutron–Core Excitations in the N=50 Nucleus ^{86}Kr [D]

J. Reif, G. Winter, H. Grawe[1], R. Schubart[1,2]

The N=50 isotones are particular systems for testing the nuclear shell model. Due to the shell closure of the neutron system the low-lying level structure of the N=50 nuclei can be explained by valence proton configurations only. However, at high excitation energies high-spin states might involve considerable contributions of neutron $0g_{9/2}^{-1}1d_{5/2}$ excitations. Recently, high-spin states of $^{86}_{36}Kr_{50}$ were investigated using in–beam γ–ray spectroscopy. A new level scheme of high-spin states with excitation energies up to 7.9 MeV and tentative spins up to (12) was observed [1].

In order to search for excitations of the neutron core shell-model calculations have been performed using a model space generated out of active $0f_{5/2}, 1p_{3/2}, 1p_{1/2}, 0g_{9/2}$ proton and $0g_{9/2}, 1d_{5/2}$ neutron orbitals relative to a hypothetic ^{68}Ni core. For details of the calculations see [1]. States of positive parity below 4 MeV and the negative-parity states with spins up to 9^- are dominated by proton configurations. They are only weakly shifted by inclusion of the neutron $g_{9/2}^{-1}d_{5/2}$ excitation. Considerable shifts are obtained for the 7^+, 9^+, 10^+, and 11^+ yrast levels. Dominating contributions to these states result from the coupling of the aligned neutron cluster $(g_{9/2}^{-1}d_{5/2})_{7+}$ to the proton excitation 0^+ and 4^+, respectively. Up to the experimentally observed I = (10) yrast state at 6248 keV the calculated level sequence is in good agreement with the experimental observations which is interpreted as a clear indication for the presence of particle–hole excitations of the closed neutron core in the positive-parity yrast states with spins $7\hbar$, $9\hbar$, and $10\hbar$.

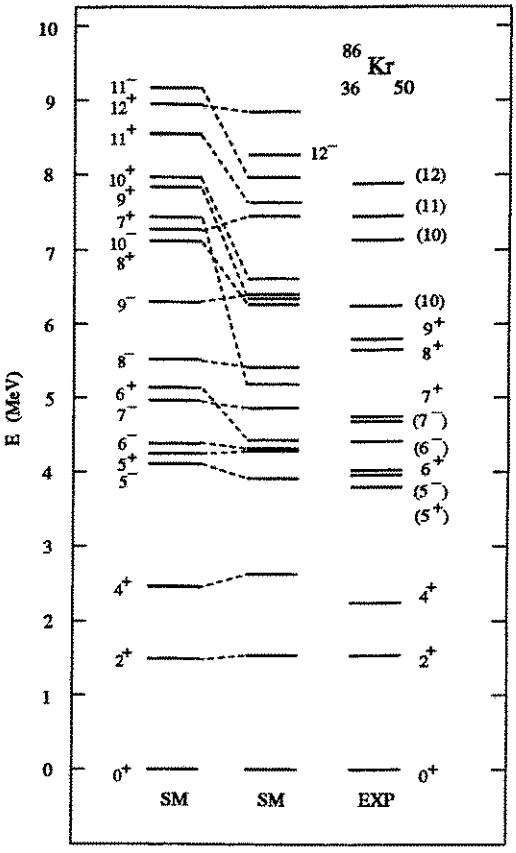

Fig. 1 Comparison of experimental and calculated level energies in ^{86}Kr considering only excitations of the proton system (first column) and with the additional inclusion of the neutron $g_{9/2}^{-1}d_{5/2}$ excitation (second column).

[D] Supported by the Deutsche Forschungsgemeinschaft

[1] *Hahn-Meitner-Institut Berlin*
[2] *II. Physikalisches Institut, Universität Göttingen*

REFERENCES:

[1] G. Winter et al., Phys. Rev. C 48 (1993) 1010

Excited states built on the 6^- isomer in $^{86}_{37}Rb_{49}$ [D]

G. WINTER, R. SCHWENGNER, J. REIF, H. PRADE, J. DÖRING[1], R. WIROWSKI[2], N. NICOLAY[2], P. VON BRENTANO[2], H. GRAWE[3] AND R. SCHUBART[3]

High-spin states of the doubly-odd nucleus ^{86}Rb containing 37 protons and 49 neutrons have been investigated via the reaction ^{82}Se(^{7}Li, $3n$) using ^{7}Li ions with energies between 30 and 35 MeV. Preliminary results have been published previously [1]. The new level scheme is based on prompt $\gamma\gamma$ coincidences, angular distributions and DCO ratios of γ rays as well as on linear polarizations of some strong γ rays and contains levels with excitation energies up to 7.9 MeV and tentative spins up to $16\hbar$ (see Fig. 1). For fifteen of the levels lifetimes in the ps region have been determined by analyzing the Doppler shift of γ rays. Several fast $M1$ transitions with $B(M1)\gtrsim 0.3$ W.u. have been identified.

The new high-spin level scheme of ^{86}Rb is interpreted on the basis of shell-model calculations in the configuration space $1p_{3/2}, 0f_{5/2}, 1p_{1/2}$, and $0g_{9/2}$ for the protons and $1p_{1/2}, 0g_{9/2}$, and $1d_{5/2}$ for the neutrons. The energies of the observed levels with $I > 5$ as well as most of the observed electromagnetic transition probabilities could be well described. The excitation of a $0g_{9/2}$ neutron over the N=50 shell gap into the $1d_{5/2}$ orbital is predicted to cause remarkable alterations only for states with $I^\pi \geq 15^+$. Some of the reduced $M1$ transition probabilities calculated within the shell model are found to depend critically on the parametrization used to describe the residual interaction.

[D] Supported by Deutsche Forschungsgemeinschaft (DFG)

[1] *Department of Physics, Florida State University, Tallahassee, Florida 32306, U.S.A.*
[2] *Institut für Kernphysik, Universität zu Köln, D-50937 Köln.*
[3] *Hahn-Meitner-Institut Berlin, D-14109 Berlin.*

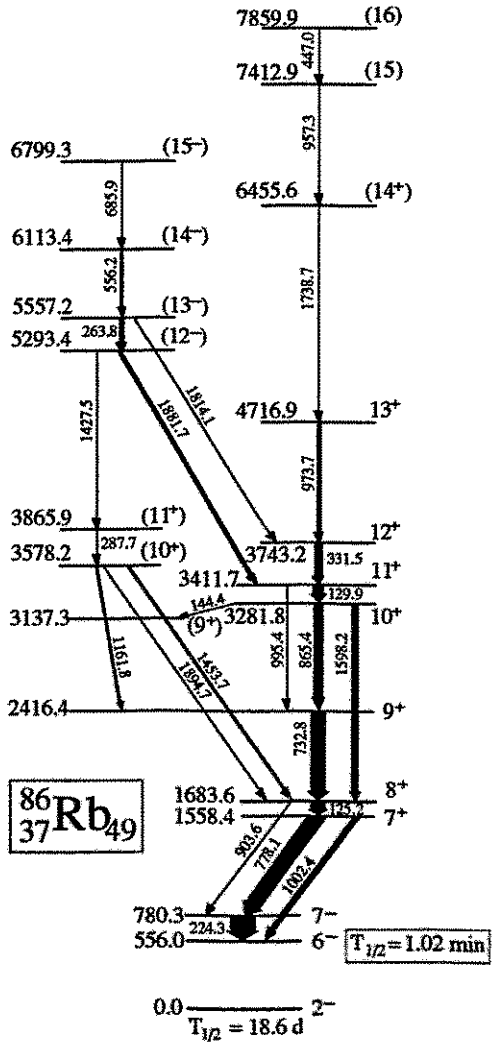

Fig.1 Level scheme of ^{86}Rb as found in the present in-beam study.

REFERENCES:

[1] G. Winter and J. Döring, *Abstracts of the Conference on Nuclear Structure in the Nineties*, edited by N.R. Johnson, (Oak Ridge National Laboratory, Oak Ridge, Tennessee, 1990), p. 103.

Proton–Neutron Interaction in the Nucleus $^{86}_{37}Rb_{49}$ [D]

J. Reif, G. Winter, H. Grawe[1], R. Schubart[1,2]

Recently, high-spin states of the N=49 nucleus ^{86}Rb were investigated via in-beam γ-ray spectroscopy. A new level scheme of high-spin states built on the 6^- isomer with excitation energies up to 7.9 MeV and tentative spins up to $16\hbar$ was established [1]. The new high-spin level scheme has been interpreted on the basis of shell-model calculations carried out in the configuration space $0f_{5/2}, 1p_{3/2}, 1p_{1/2}$, and $0g_{9/2}$ for the protons (π) and $1p_{1/2}$ and $0g_{9/2}$ for the neutrons (ν) considering a hypothetic ^{66}Ni core. For details of the used two-body matrix elements and single-particle energies see [2]. The residual interaction between active protons moving in the (fp)-subshell and the $\nu 0g_{9/2}$ hole is indicated in the low-lying states of negative parity. The 2^- ground state and the lowest 7^- level are dominated by the $\pi 0f_{5/2}^{-1} \otimes \nu 0g_{9/2}^{-1}$ configuration, whereas the 6^- isomer is mainly formed by the $\pi 1p_{3/2}^{-1} \otimes \nu 0g_{9/2}^{-1}$ configuration. The 8^- and 9^- levels are realized by the additional excitation of one proton to the $1p_{1/2}$ orbital resulting in the seniority–4 configuration $\pi(0f_{5/2}^{-1}, 1p_{3/2}^{-1}, 1p_{1/2}^{-1}) \otimes \nu 0g_{9/2}$.

The structure of levels with $I^\pi \geq 10^-$ is characterized by the excitation of two protons into the $0g_{9/2}$ orbital which explains the energy gap between the 8^- and 10^- states. The $\pi\nu$-interaction between particles occupying the $0g_{9/2}$ orbitals determines the structure of the yrast states with $7^+ \leq I^\pi \leq 15^+$. The 7^+, 8^+, and 9^+ levels are dominated by the configuration $\pi 0g_{9/2}^1 \otimes \nu 0g_{9/2}^{-1}$. The coupling of this configuration to the proton excitation $(0f_{5/2}^{-1} 1p_{3/2}^{-1})_{4+}$ generates the states with $10^+ \leq I^\pi \leq 13^+$. Positive-parity states with higher spin values can be formed by breaking an additional pair in the proton (fp)-subshell generating the $\pi(0f_{5/2}, 1p_{3/2}, 1p_{1/2})^8_{6+}$ configuration. Combining this cluster with the $\pi 0g_{9/2}^1 \nu 0g_{9/2}^{-1}$ structure results in states with maximal spin value $15\hbar$. The excitation of one proton to the $1p_{1/2}$ orbital explains the rather large energy separation between the 13^+ and 14^+ states. The structure of states with spins higher than 15^+ is dominated by the excitation of a $0g_{9/2}$ neutron over the $N = 50$ gap into the $1d_{5/2}$ orbital [2].

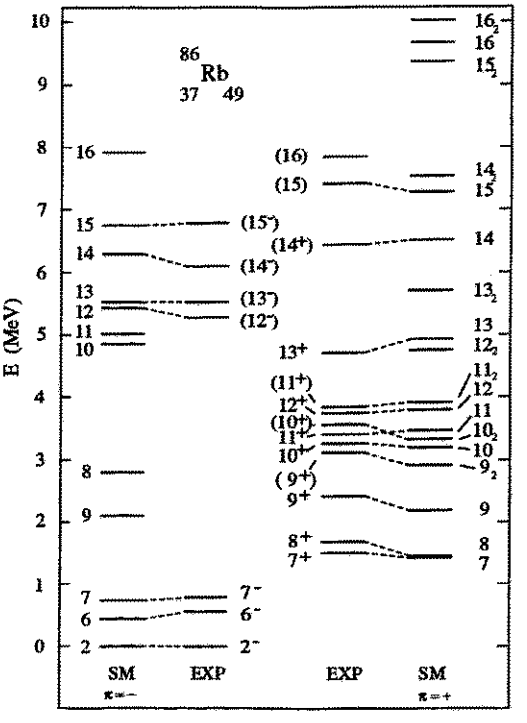

Fig. 1 Comparison of experimental and calculated level energies in ^{86}Rb.

[D] Supported by the Deutsche Forschungsgemeinschaft

[1] *Hahn-Meitner-Institut Berlin*
[2] *II. Physikalisches Institut, Universität Göttingen*

REFERENCES:

[1] G. Winter et al., contribution to this report
[2] G. Winter et al., submitted to Phys. Rev. C

Three-quasiparticle excitations in ^{77}Br
(Phys. Rev. C48 (1993) 2524)

Döring, J., L. Funke, R. Schwengner and G. Winter

Abstract: Excited states in ^{77}Br were investigated via the reactions ^{75}As (α,2n)^{77}Br and ^{73,74}Ge(^{7}Li,xn)^{77}Br at beam energies of 27 and 35 MeV, respectively. On the basis of coincidence and angular distribution data of the γ rays the known level sequences of positive and negative parity were extended to tentative spins of 25/2 h, and a new decay sequence beginning at spin and parity of (17/2$^-$) was found. This new sequence is discussed in terms of the 3-quasiparticle configuration ($\pi g_{9/2} \otimes \nu g_{9/2} \otimes \nu(p_{1/2},p_{3/2},f_{5/2})$). Moreover, the irregularity found in the moments of inertia at $\hbar\omega \approx 0.4$ MeV for the negative-parity band is attributed to a $g_{9/2}$ quasiproton alignment.

Energie of the $4^{(+)}$ isomer and new bands in the odd-odd nucleus ^{74}Br
(Phys. Rev. C47 (1993) 2560)

Döring, J., J.W. Holcomb, T.D. Johnson, M.A. Riley, S.L. Tabor, P.C. Womble and G. Winter

Abstract: High-spin states of the odd-odd nucleus ^{74}Br were investigated via the reactions ^{58}Ni(^{19}F,2pn)^{74}Br and ^{65}Cu(^{12}C,3n)^{74}Br at beam energies of 62 and 50 MeV, respectively. On the basis of coincidence data new levels have been introduced and partly grouped into rotational bands. Some of these new states decay to known levels of negative-parity bands built on both the ground state and the long-lived $4^{(+)}$ isomer. Thus, an excitation energy of 13.8 keV has been deduced for the long-lived isomer in ^{74}Br. The level sequences observed are interpreted in terms of Nilsson configurations in conjunction with collective excitations.

Identification of excited levels in the N = Z + 1 nucleus ^{73}Kr
(Phys. Lett. B302 (1993) 167)

Freund, S., J. Altmann, F. Becker, T. Burkardt, J. Eberth, L. Funke, H. Grawe, J. Heese, U. Hermkens, H. Kluge, K.H. Maier, T. Mylaeus, H. Prade, S. Skoda, W. Teichert, H.-G. Thomas, A. v.d. Werth and G. Winter

Abstract: Excited states of ^{73}Kr have been identified by in-beam γ-ray spectroscopy via the reaction ^{40}Ca(^{36}Ar, 2pn)^{73}Kr. A strongly coupled band is interpreted as a prolate band built on the Nilsson [312] 3/2$^-$ orbital at $\beta_2 \approx 0.4$, while a decoupled $g_{9/2}$ band is likely to correspond to a small deformation. Evidence for a large oblate deformation as discussed for ^{72}Kr has not been found.

Study of excited states in ^{85}Kr and ^{86}Kr: Evidence for neutron-core excitations in the N = 50 nucleus ^{86}Kr

(Phys. Rev. C48 (1993) 1010)

Winter, G., R. Schwengner, J. Reif, H. Prade, L. Funke, R. Wirowski, N. Nicolay, A. Dewald, P. v. Brentano, H. Grawe and R. Schubart

Abstract: High-spin states of the N = 49,50 nuclei ^{85,86}Kr have been investigated via the reactions ^{82}Se(^{7}Li,p3n) or ^{82}Se(^{7}Li,p2n), respectively, using 32 MeV ^{7}Li ions. In order to suppress γ rays arising from pure neutron evaporation the measurements of angular distributions and relative excitation functions of the γ rays as well as $\gamma\gamma$ coincidences have been performed in particle-γ coincidence modes. Additional information on excited states in ^{85}Kr has been obtained in connection with the ^{82}Se(α,n) reaction at beam energies between 13 and 21 MeV. The level scheme of ^{85}Kr has been extended by a new sequence of high-spin states with excitation energies up to 4.8 MeV and tentative spins up to (23/2) that is built on top of the $17/2^{+}$ μs isomer at 1991.8 keV. For ^{86}Kr a new level scheme of high-spin states with excitation energies up to 7.9 MeV and tentative spins up to (12) has been observed for the first time. The level sequences observed in ^{85,86}Kr are interpreted on the basis of shell-model calculations in the configuration space $1p_{3/2}$, $0f_{5/2}$, $1p_{1/2}$, and $0g_{9/2}$ for the protons and $0g_{9/2}$ or $0g_{9/2}$, $1d_{5/2}$ for the neutrons in ^{85}Kr or ^{86}Kr, respectively. The inclusion of neutron-core excitations in the calculations for ^{86}Kr results in a remarkably improved agreement between experimental and calculated level energies. In this way considerable contributions of neutron-core excitations are strongly suggested for the positive-parity yrast states with spins 7h, 9h, and 10h.

4. Experimental Heavy Ion Physics

Fission and IMF Emission in the Reaction 43 AMeV ^{7}Li on ^{232}Th Studied with FOBOS [B]

A.A. Aleksandrov[1], I.A. Aleksandrova[1], M. Andrassy, L. Dietterle[2], V.N. Doronin[1], P. Gippner[2], C.-M. Herbach, D. Hilscher[3], S.I. Ivanovskij[1], J. Krüger, A. Matthies[2], D. May[2], H.-G. Ortlepp[2], G. Pausch[4], Yu.E. Penionzhkevich[1], V.N. Pokrovskij[1], G. Renz[2], K.D. Schilling, D.I. Shishkin[1], V.E. Shuchko[1], O.V. Strekalovskij[1], V.V. Trofimov[1], C. Umlauf[2], D.V. Vakatov[1], V.M. Vasko[1], W. Wagner[2]

The study of the fission of hot nuclei is of considerable interest. Questions of time scales, the dissipation mechanism and others are extensively discussed /1/. The neck emission of intermediate mass fragments (IMF) recently reported in /2/ should give new insights into this complex process.

As a first experiment with the FOBOS detector /3/ at the beam of the new U-400M heavy ion cyclotron in Dubna, the study of fission induced by 43 AMeV ^{7}Li on ^{232}Th has been chosen. 10 modules each consisting of a position-sensitive avalanche counter (PSAC) and an axial ionisation chamber (BIC), two further BIC's without PSAC's and two arrays of 3 and 7 CsI(Tl) scintillation counters came into operation.

The geometrical arrangement (fig. 1) has been chosen after a series of Monte-Carlo simulations of triple events including the neck emission of IMF. Two triple groups of modules detect fission fragment (FF) pairs (5 and 17 or 27; 2 and 19 or 29) and cover the whole expected range of folding angles.

Since the U-400M beam parameters at present do not allow a precise time-of-flight measurement relative to the microbunches, two transmission avalanche counters were placed near the target in front of the modules 2 and 5 to deliver the START signals. The PSAC's were operated with 4 Torr of pentane at a voltage of 5 V below the onset of spark discharges. This allowed the efficient registration of fragments down to alpha particles. In the BIC's a pressure of 200 Torr of P-10 was utilized. This value was suggested by response simulations as an optimum for the identification of the expected IMF's. A ^{232}Th target of 270μg/cm^2 deposited on 50μg/cm^2 Al_2O_3 was bombarded with a ^{7}Li beam of $\approx$ 3 particle nA, pulsed with about 10% duty cycle. A FF in one of the START counters triggered the data acquisition with a rate of $\approx$ 300 events/s.

The analysis of FF coincidences is presently in progress. Fig. 2 shows a preliminary folding angle distribution. Masses and momenta of both fragments will be determined independently utilizing the algorithm developed for the TOF-E analysis with large corrections /4/. Our goal here are FF sum masses, mass splits and TKE's in dependence on the transferred momentum. Fig. 3 shows TOF-E plots, where 10% of the collected data have been included. For the analysis of ternary fission, triple coincidences (2 FF plus one particle in another gas module or in a CsI(Tl) counter) have been selected out of the huge amount of raw data ($\approx 10^8$ events). Alpha particles and IMF's were selected by windows in the Z-E plot of the BIC's.

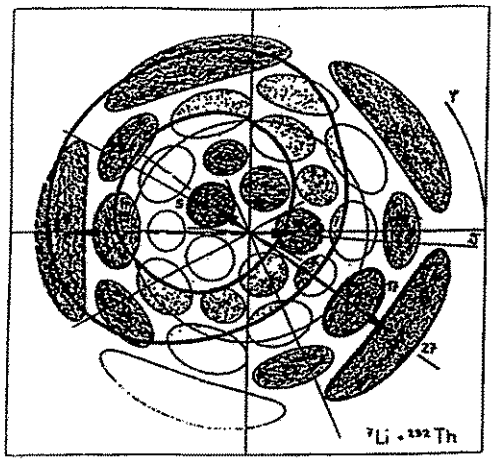

Fig. 1 FOBOS geometry. The numbers denote the module positions in this experiment (shaded). The dots illustrate simulated triple events as expected from neck emission of IMF's if the two FF hit modules 5 and 17 or 27.

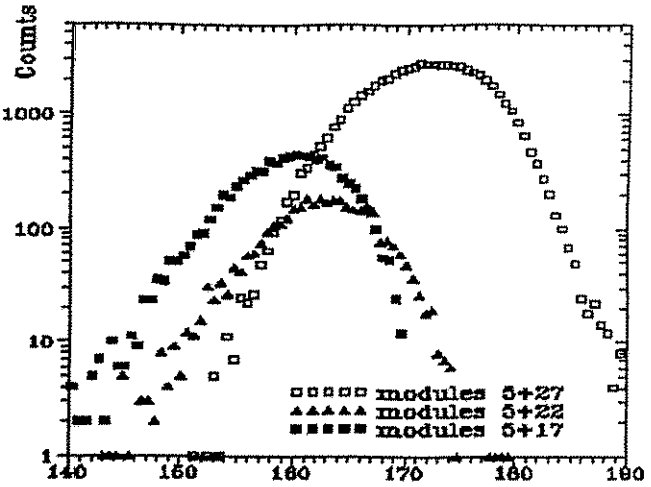

Fig. 2 Preliminary folding angle distribution (not corrected for acceptance)

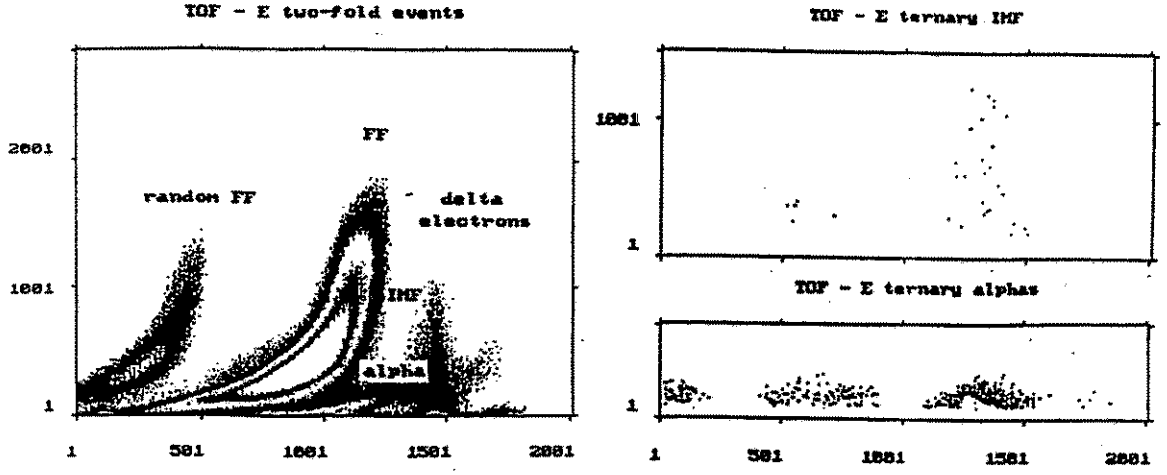

Fig. 3 TOF-E plots of two-fold (left) and triple coincidences (right) for alpha particles (top) and IMF's (bottom).

[1] *Joint Institute for Nuclear Research, Dubna*
[2] *Institut für Kern- und Hadronenphysik, FZR und Joint Institute for Nuclear Research, Dubna*
[3] *Hahn-Meitner Institut Berlin*
[4] *Freie Universität Berlin*

REFERENCES

[1] D. Hilscher and H. Rossner, Annales de Phys. Fr. 17 (1992) 471
[2] D.E. Fields et al., Phys. Rev. Lett., 96 (1992) 3713
[3] H.-G. Ortlepp et al., Proc. Int. Conf. on New Nuclear Physics with Advanced Techniques, Ierapetra, Crete, Greece, 1991 (World Scientific 1992) p. 302
[4] H.-G. Ortlepp et al., Annual Report 1992 (FZ Rossendorf) FZR 93-10 (1993) 97

Measurement of ^{244}Cm (sf) at FOBOS [B]

A.A. Aleksandrov[1], I.A. Aleksandrova[1], M. Andrassy, L. Dietterle[2], V.N. Doronin[1], P. Gippner[2], C.-M. Herbach, E.M. Kozulin[1], A. Matthies[2], D. May[2], H.-G. Ortlepp[2], Yu.V. Petkov[1], G. Renz[2], D.T. Shishkin[1], O.V. Strekalovskij[1], C. Umlauf[2], V.M. Vasko[1], W. Wagner[2]
and the FOBOS-Collaboration

The 4π-fragment spectrometer FOBOS /1/ has come into operation at FLNR Dubna in 1993.

The first experiment aimed to search for cold compact spontaneous fission channels without accompanying neutron emission, which are sensitive to nuclear structure effects /2/. The nuclide ^{244}Cm with its large alpha-decay-to-spontaneous-fission ratio (1.5×10^6) cannot be investigated with methods usually applied for this task, because the huge alpha activity excludes a precise fission fragment (FF) energy measurement. Therefore, a TOF-TOF correlation measurement with the help of the large-area position-sensitive avalanche counters (PSAC) of the FOBOS array seemed us to be a privileged task for a first experiment. Such counters provide a good time resolution ($\approx$ 200 ps) for FF signals at an alpha background of up to several 10^5 s^{-1}, which can easily be discriminated. The energy information of the BRAGG ionization chambers (BIC) located behind the PSAC's has not been taken into account.

Since cold fission is a rare process, stable and high resolution over a long measuring time is required. This was a good possibility to test the reliability of the detector system in complex. The sf source consisted of 4μg ^{244}Cm deposited on a thin backing and housed (for contamination protection) in a closed box equipped at one side with a 1.2μm thick Mylar window and at the opposite side with a parallel-plate avalanche counter (PPAC) as a START detector. Six FOBOS gas modules were covered by the acceptance cone of the START-PPAC.

The coordinate information of the PSAC's has been verified by the requirement to fulfil the angular correlation of FF. The electronics was triggered by a coincidence between the START-PPAC and one of the PSAC's. In the course of three days, about 200 000 fission events have been recorded. The FF TOF-TOF matrix (fig. 1) has to be corrected for the energy losses in the backing and window materials to obtain the mass-TKE matrix (fig. 2). Cold complex fission leads to a fine structure in the mass distributions of FF's for TKE's near the Q value. Further analysis is in progress.

[1] *Joint Institute for Nuclear Research, Dubna*
[2] *Institut für Kern- und Hadronenphysik, FZR und Joint Institute for Nuclear Research, Dubna*

REFERENCES

[1] H.-G. Ortlepp et al., Proc. Int. Conf. on New Nuclear Physics with Advanced Techniques, Ierapetra, Crete, Greece, 1991 (World Sientific 1992) p.302
[2] I.D. Alkhazov et al., J. of Nucl. Phys. Vol. 48 (3) (1988) 655

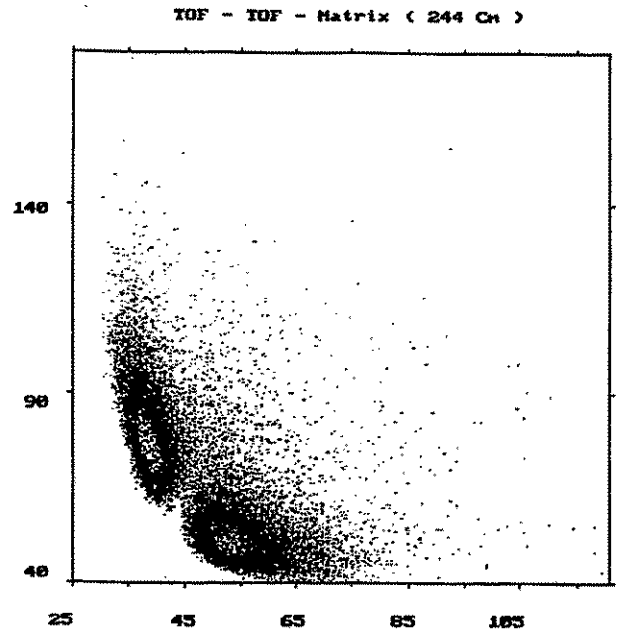

Fig. 1 Time-of-flight (TOF-TOF) correlation matrix for ^{244}Cm (sf) fission fragments

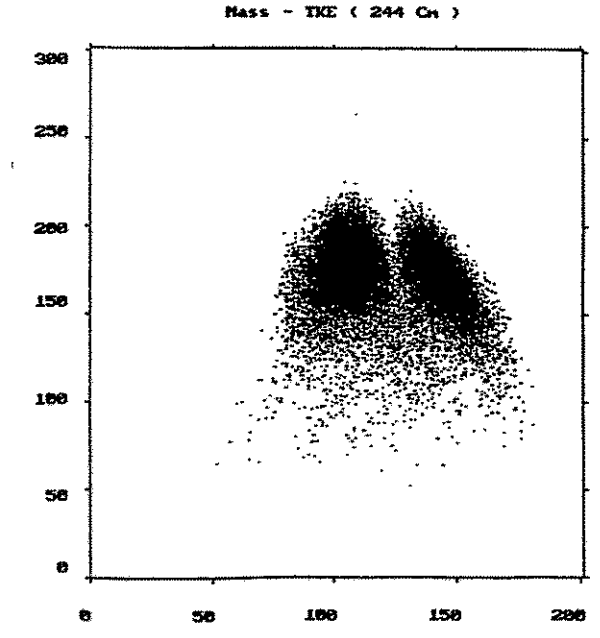

Fig. 2 Mass-TKE (total kinetic energy) plot for ^{244}Cm (sf) fission fragments

Ternary Spontaneous Fission of ^{244}Cm [B]

W. WAGNER[1], P. GIPPNER[1], C.-M. HERBACH, H.-G. ORTLEPP[1]

The spontaneous fission (sf) of ^{244}Cm has been investigated in a first experiment with the new 4π-fragment spectrometer FOBOS /1/.
In addition to the 6 position-sensitive avalanche counters (PSAC: 1+28, 11+18, 6+24) for registration of the fission fragments (FF) /2/, a CsI(Tl) detector modul (4) of the FOBOS scintillator shell /3/ had been positioned at about 90° relative to the symmetry axis of the acceptance cone of the START counter (fig. 1) to detect additionally emitted light charged particles (LCP).

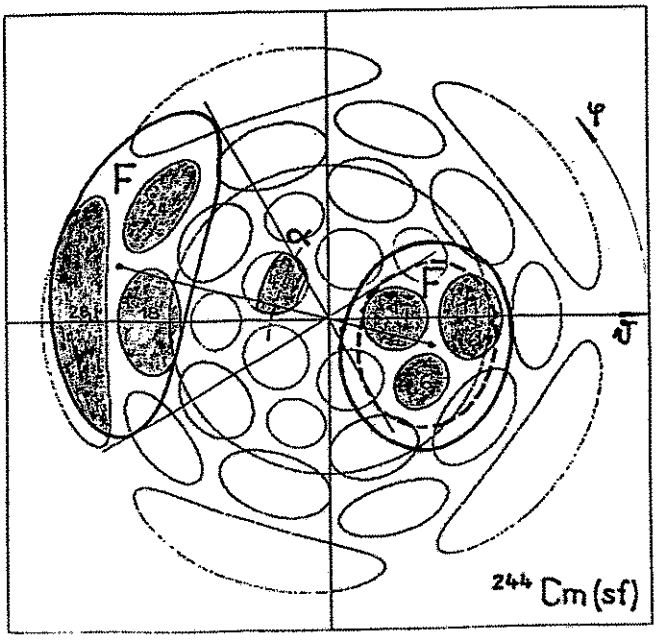

Fig. 1: Acceptances of the FOBOS modules used in the ^{244}Cm(sf) experiment (shaded). The acceptance cones due to the START counter (full lines) and in the case of FF coincidences (dotted line) were calculated analytically.

The main component of LCP in ternary fission turns out to be alpha particles emitted during the scission process from the neck region of the fissioning nucleus under nearly 90° relative to the fission axis /4/. They have a slightly asymmetric GAUSSIAN-like energy distribution with a mean value of 16 MeV and a width of 10 MeV.
Therefore, the CsI(Tl) counters have been shielded against the high alpha activity of ^{244}Cm by use of a 40μm thick Mylar absorber foil, what results in an energy threshold of 6 MeV for neck alpha particles. According to an accurate measurement of its energy distribution /5/, this leads to counting losses of 6%.
Applying the pulse-shape discrimination method /6/, the alpha particles were well separated from prompt fission and background gamma rays in the CsI(Tl) detectors (fig. 2).

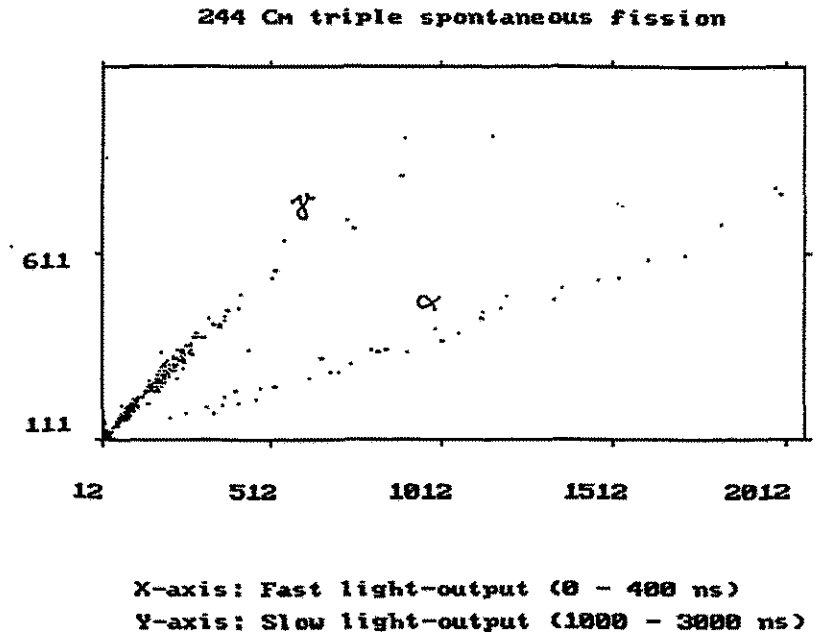

Fig. 2: Pulse-shape discrimination matrix for the large-area CsI(Tl) detector

During the experiment, 198859 sf events have been recorded as coincidences between the START counter and one of the 6 PSAC's, while 36 events could be identified as coincidences between one fission fragment and an additionally emitted alpha particle hitting one of 5 CsI(Tl) detectors of the scintillator module, which could geometrically accept LCP. Correcting for the coincidence efficiency for FF and integrating over the total solid angle, a value of $2.7 \cdot 10^{-3}$ long-range alpha particles per fission event has been deduced. It is obvious to convert this value into a ratio of ternary to binary fission asuming the same relations between the emission probabilities of LCP as has been observed for ^{252}Cf /7/. This results in a preliminary value of 3.1 LCP per 10^3 binary fissions, which is in rather good agreement with the only available value for ^{244}Cm (3.18 ± 0.20 /8/) and confirmes the systematics of ref. /7/, although the uncertainty of about 10% is relatively high due to the poor statistics and the angular distribution of neck alpha particles has not been taken into account.

[1] *Institut für Kern- und Hadronenphysik, FZR und Joint Institute for Nuclear Research, Dubna*

[1] H.-G. Ortlepp et al., Proc. Int. Conf. on New Nuclear Physics with Advanced Techniques, Ierapetra, Crete, Greece, 1991 (World Scientific 1992)p.302
[2] A.A. Aleksandrov et al., this Annual Report
[3] W. Wagner et al., Annual Report 1992 (FZ Rossendorf)FZR 93-10 (1993) 124
[4] C. Wagemans, Particle Emission from Nuclei, Vol.3, CRC Press Inc. (1989)
[5] W. Loveland, Phys. Rev. C9 (1974) 395
[6] J. Alarja et al., Nucl. Instr. and Meth. A242 (1986) 352
[7] J.F. Wild et al., Phys. Rev. C32 (1985) 488
[8] R.A. Nobles, Phys. Rev. 126 (1962) 1508

Investigation of IMF Emission and Projectile Fragmentation in the System ^{32}S (960 MeV) + ^{197}Au with the Extended ARGUS Detector

J. Krüger, A. Budzanowski[4], H. Fuchs[1], C.-M. Herbach, H. Homeyer[1], D. Kamanin[1], A. Matthies, H.-G. Ortlepp, G. Pausch[2], G. Röschert[1], W. Seidel, W. Shuchko[3], A. Siwek[4], W. Trofimov[3], A. Tutay[1], W. Wagner, R. Wolski[3], P. Ziem[1]

The phoswich multidetector-array ARGUS in Berlin had been extended by several silicon detectors and a prototype of a FOBOS gas-detector module [1]. The reaction ^{32}S (960 MeV) + ^{197}Au was investigated with this arrangement. Besides methodical aspects, the aim of this experiment was to clearify the origin of intermediate-mass fragments (IMF) and to study the process of projectile fragmentation as a function of the linear momentum transfer, obtained by the classical method of folding-angle analysis for pairs of fission fragments from the excited target-like system. For all the 14 silicon detectors arranged in the reaction plane, $\phi = 0^0$, we calibrated the energy scale considering the ionization defect [2] and calculated the mass of the detected particles from energy and time of flight. The particle masses in the Bragg ionization chamber were obtained by means of an iterative procedure [3].

Light charged particles (LCP), IMF and products from binary fission (FF) were observed at any angle, whereas the detection of projectile-like fragments (PLF) and heavy residues (HR) is restricted to small angles. By demanding a coincident registration of an IMF ($4 < A < 40$) at $\theta = -123^0$ the mass spectrum in the detector at $\theta = 14^0$ changes drastically (fig.1). IMF are identified as binary partners of HR. The spectrum of relative velocities allows an interpretation of the IMF and HR as products from deeply inelastic collisions as well as from IMF evaporation.

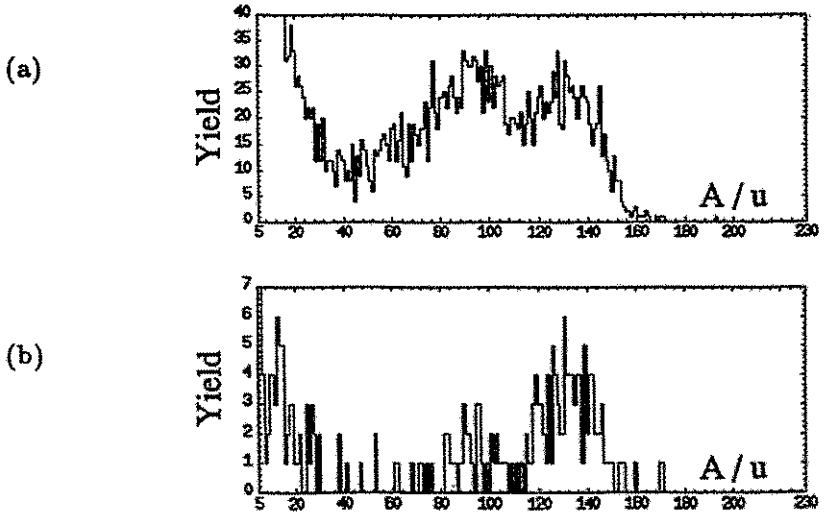

Fig. 1 Mass spectra of a semiconductor detector at $\theta = 14^0$ (a) and with the demand of a coincident registration of an IMF at $\theta = -123^0$ (b)

To study the projectile fragmentation as a function of the dissipated energy, we identified pairs of (symmetric) fission fragments by setting gates in plots of the sum mass versus the relative velocity for all possible pairs of silicon detectors. From calibrated velocities and masses of these FF we computed the velocity vector of the fissioning system, i.e. of the targetlike nucleus. The velocity component in beam direction is a measure of the linear momentum transfer and of the dissipated energy. Fig.2 shows detection probabilities of three coincident protons or alpha particles in the phoswich-array ($5.5^0 < \theta < 23.5^0$), respectively, normalized to the number of corresponding fission fragment pairs, as a function of the reconstructed velocity of the fissioning system. The dashed line at v=1.06 cm/ns indicates the full momentum transfer. It is obvious that the multiplicity of protons detected in a cone around the beam axis is increasing with momentum transfer, whereas the multiplicity of alpha particles has a maximum around half of the maximum possible momentum transfer. Whether this is due to the process of projectile fragmentation – a breakup of the sulfur nucleus into several alpha cluster – will be investigated by comparison with theoretical predictions [4].

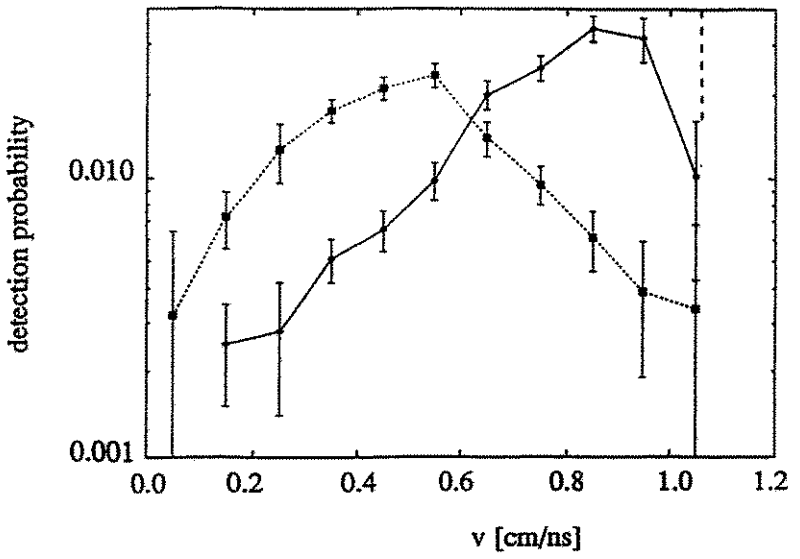

Fig. 2 Detection probabilities of three protons (solid line) and three alpha particles (dashed line). For further explanation see text.

([1]HMI Berlin, [2]FU Berlin, [3]VIK Dubna, [4]IPN Krakow)

REFERENCES

[1] G. Pausch et al., Annual Report 1992, HMI-Bericht 507(1993)87.

[2] J. B. Moulton, J. E. Stephenson, R. P. Schmitt, and G. J. Wozniak, Nucl. Instr. and Meth. 157 (1978) 325.

[3] C.-M. Herbach, H.-G. Ortlepp, Jahresbericht IKH Rossendorf (1991), p.56.

[4] K. Möhring, T. Srokowski, and D. H. E. Gross, Nucl. Phys. A533 (1991) 333

Radial and transversal blast scenarios for central collisions of Au + Au at E = 150 A·MeV[B]

R. KOTTE, B. KÄMPFER[1], J. MÖSNER, W. NEUBERT, D. WOHLFARTH

Intermediate mass fragments (IMF) produced in central Au+Au collisions at 150 A·MeV have been measured with the FOPI detector system at SIS in GSI Darmstadt [1]. Experimental velocity correlations have been analysed and compared with results of a N-body Coulomb trajectory model [2]. This Coulomb dominated final state interaction model is intented to determine the space-time structure of the fragmenting source of the reaction products. The code is also well suited as event generator for studying the influence of the detector acceptance on global event characteristics and single-particle observables. Only a few parameters allow the description of the asymptotic momentum distributions by propagation of an initial configuration characterized by

(i) the total charge of the source Z_{source},

(ii) a slope parameter α describing the experimental charge distribution, which can be well approximated by an exponential function $dN/dZ \sim exp(-\alpha Z)$ for IMFs with $Z \geq 3$ from central events, plus two additional up-scale parameters $A_{1,2}$ for $Z = 1$ and $Z = 2$ particles,

(iii) a temperature parameter T determining the random initial motion with Maxwellian velocity distribution,

(iv) a collective expansion with linear velocity profile between the center and the surface of the source which gives rise to an averaged flow energy $< E/A >_{flow}$,

(v) the radius of the source R (which can be translated into a breakup density), which is the essential parameter extracted from IMF velocity correlation functions (see ref. [2] and subsequent contribution).

Fig. 1 displays two-dimensional plots of cross sections of $Z = 1 - 4$ particles generated with the Coulomb trajectory code for the reaction Au+Au at 150 A·MeV using the parameters $Z_{source} = 2 \cdot 79$, $R = 14$ fm, $\alpha = 0.8$, $A_1 = 3$, $A_2 = 2$, $T = 35$ MeV, and either a purely transversal expansion scenario or a radial one. In both cases $< E/A >_{flow} = 12$ MeV and the total energy per nucleon residing in the system amounts to 37 MeV which is just the available c.m. energy of a symmetric collision at 150 A·MeV projectile energy.

In fig. 2 one observes that a radial blast is compatible with the data of central collisions characterized by the ERAT5 event selection criterion with maximum inpact parameters of $b \simeq 3$ fm in sharp cut-off approximation [2,3], whereas the purely transversal expansion scenario fails to reproduce the kinetic energy distributions. Other event selection criteria point to the possibility of a purely transversal blast [4].

[1]Institut für Theor. Physik, TU Dresden, und Institut für Kern- und Hadronenphysik, FZR

REFERENCES

[1] A. Gobbi et al., NIM **A324** (1993) 156, J.P. Alard et al., Phys. Rev. Lett. **69** (1992) 889

[2] B. Kämpfer, R. Kotte, J. Mösner, W. Neubert, D. Wohlfarth, Phys. Rev. **C48** (1993) 955

[3] S. C. Jeong et al., preprint GSI-93-38 (1993), W. Reisdorf, Contribution to Mazurian Lake Summer School, Piaski, Poland, 1993

[4] C. Kuhn et al., C. Roy et al., GSI Annual Report 1993, GSI-94-1, J. Konopka, private communication

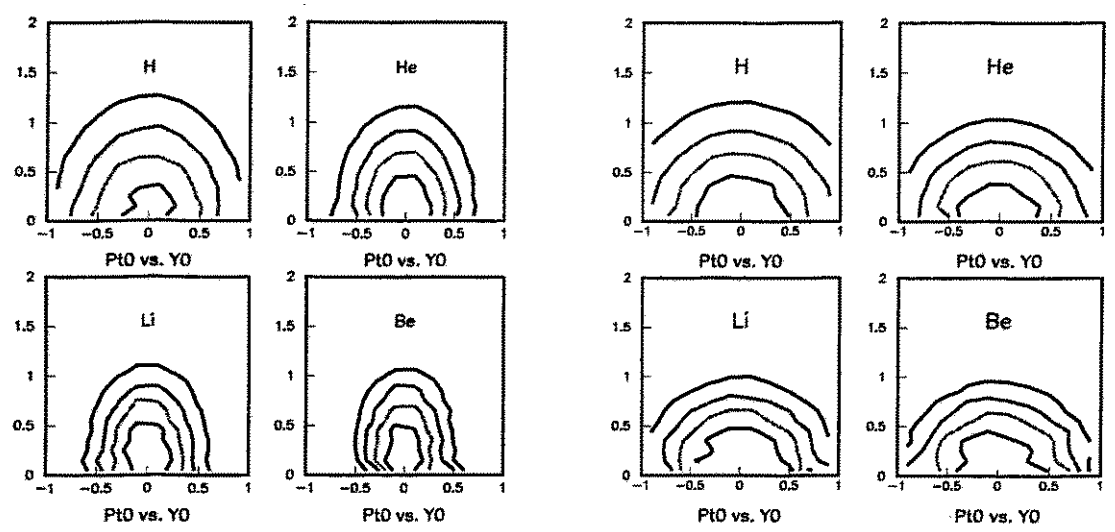

Fig. 1: Contour plots of the invariant cross section $d^2N/p_t^{(0)}dp_t^{(0)}dY^{(0)}$ (for definition of $p_t^{(0)}$ and $Y^{(0)}$ see ref. [3]) of Z=1 - 4 particles generated in Coulomb trajectory simulations relying on a transversal (left panel) or a radial (right panel) initial expansion. The isolines represent equal intensities of 20, 40, 60, and 80% of the maximum value.

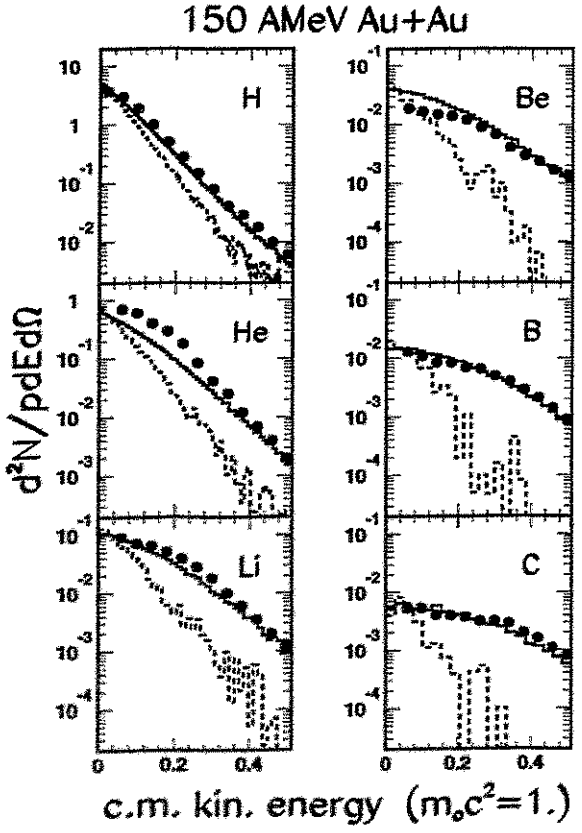

Fig. 2: Kinetic energy distributions (invariant cross section, normalized to the number of events, integrated over the full azimuthal angle and over the c.m. polar angle range $25^\circ < \Theta_{cm} < 45^\circ$ of $Z = 1 - 6$ particles generated with the Coulomb trajectory code. The full and dashed lines represent results of calculations with radial and transversal expansion, respectively (cf. fig. 1). The experimental data from central ERAT5 events [3] are displayed as dots.

Velocity correlations of intermediate mass fragments produced in central collisions of Au + Au at E = 150 - 400 A·MeV[B]

R. KOTTE, B. KÄMPFER[1], J. MÖSNER, W. NEUBERT, D. WOHLFARTH

The intensity interferometry has proven useful to get information on the space-time structure of a disassembling highly excited nuclear system. We apply it to intermediate mass fragment (IMF) data of central collisions of Au+Au at 150, 250, and 400 A·MeV. The data are taken with the high-granular, azimuthally symmetric component "outer plastic wall" of the FOPI (stage I) detector system at SIS in GSI Darmstadt [1]. Supplementing informations concerning event characteristics and one-body IMF observables can be found in refs. [2,3] and in the preceding contribution.
Let be $Y_{12}(\vec{v}_1, \vec{v}_2)$ the coincidence yield of IMF pairs with charges $Z_{1,2} \geq 3$ and velocities $\vec{v}_{1,2}$. Then the two-particle correlation function is defined as

$$1 + R_{12}(\vec{v}_1, \vec{v}_2) = \mathcal{N} \frac{\sum_{events,pairs} Y_{12}(\vec{v}_1, \vec{v}_2)}{\sum_{events,pairs} Y_{12,mix}(\vec{v}_1, \vec{v}_2)}, \qquad (1)$$

where the subscript "mix" means event mixing. $\mathcal{N}$ is a normalization factor fixed by the requirement to have the same number of true and mixed pairs. The correlation function (1) is projected onto the hypersurface $v_{12} = |\vec{v}_{12}| = |\vec{v}_1 - \vec{v}_2|$. Displaying $1+R$ vs. $v_{red} \equiv v_{12}/\sqrt{Z_1 + Z_2}$, instead vs. v_{12}, we find that different charge combinations result in rather similar Coulomb flanks at small v_{red} (see fig. 1). The distribution of the velocity values for which the correlation functions cross the line $1 + R \equiv 0.5$ shows a dispersion of 6.9 (12.5) % when representing $1 + R$ as function of v_{red} (v_{12}). This scaling, predicted and first verified experimentally in ref. [4], is surprisingly well reproduced within the N-body Coulomb trajectory calculations [2] (see fig. 2). All particles ($Z_{tot} = 2Z_{Au}$) are initially randomly distributed in a sphere of radius R with a Maxwellian velocity distribution characterized by a temperature parameter T, and we assume $A = 2Z$. The used charge distribution is exponentially decreasing, i.e. $dN/dZ \sim exp(-\alpha Z)$, for $Z \geq 3$, and has two additional up-scale parameters for $Z = 1$ and $Z = 2$ particles which are adjusted to the observed charged particle and IMF multiplicity distributions after applying the experimental filter. A collective radial expansion with linear velocity profile $v(r) = (r/R)v_{surf}$ is superimposed on the random initial motion. The parameter v_{surf} can be translated into an averaged radial flow energy $< E/A >_{flow}$. For central events the parameter T and the radial expansion energy (which are related to each other due to energy conservation) are fixed by reproducing the single-particle c.m. kinetic energy distributions of $Z = 1...6$ particles in a phase space region $25^o < \theta_{cm} < 45^o$. This region is expected to be essentially unbiased by the apparatus. Within the outer wall acceptance, two-particle relative-velocity distributions of different IMF charge combinations from $Z_{1,2} = 3$ up to $Z_{1,2} \geq 7$ could be determined experimentally. In our corresponding simulations, after Coulomb evolution, the source is boosted in longitudinal direction to account for the *cms* motion. Finally, the only free parameter R is fixed by fitting the experimental IMF correlation functions. For all three projectile energies considered, we find an optimum agreement with the data of central ERAT5 events [2] with the parameter set displayed in table 1 when using source radii of $R = 12(^{+2}_{-1})$ fm which correspond to break-up densities of $\sim 40(^{-15}_{+10})\%$ of nuclear matter saturation density.

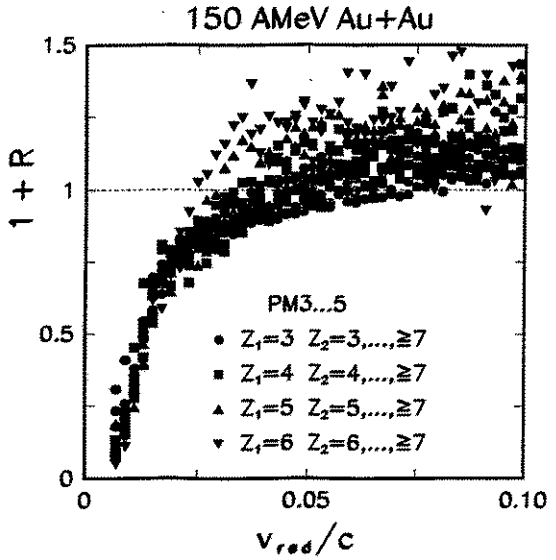

Fig. 1: Experimental correlation function (1) as function of the reduced velocity v_{red} for 14 different IMF combinations from events characterized by the charged particle multiplicity bins PM3 - PM5 [2,3]. To exclude the disturbing influence of the directed sideward flow the events are rotated into a unique reaction plane before determining the mixed event yield. The data should demonstrate the unique scaling at $v_{red}/c < 0.025$, while details of the spreading at $v_{red}/c > 0.025$ needs still an interpretation.

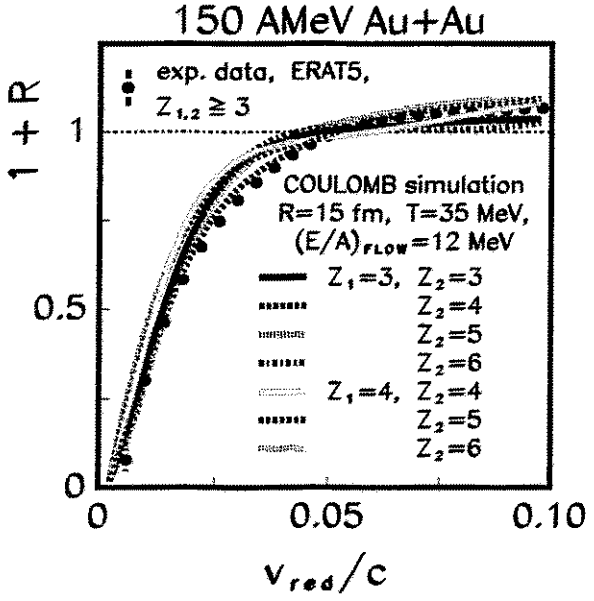

Fig. 2: Correlation function (1) of 7 different IMF combinations as function of the reduced velocity v_{red} generated with the COULOMB trajectory code for the reaction 150 A·MeV Au+Au. The dots represent the experimental correlation function of all IMF combinations in central events characterized by the ERAT5 event selection criterion [2].

Table 1:

projectile energy E/A [MeV]	charge distribution steepness α	temperature parameter T [MeV]	radial flow energy $< E/A >_{flow}$ $[MeV]$
150	0.8	35	12
250	0.9	45	25
400	1.1	55	40

[1]Institut für Theor. Physik, TU Dresden, und Institut für Kern- und Hadronenphysik, FZR

REFERENCES

[1] A. Gobbi et al., Nucl. Instrum. and Methods **A324** (1993) 156
[2] B. Kämpfer, R Kotte, J. Mösner, W. Neubert, D. Wohlfarth, Phys. Rev. **C48** (1993) 955
[3] J.P. Alard et al., Phys. Rev. Lett. **69** (1992) 889
[4] Y.D. Kim et al., Phys. Rev. **C45** (1992) 387, 338

An estimation of the sideways flow in a BUU approach for the reaction Au+Au in the energy region 150-1000 AMeV[B]

B. KÄMPFER[1], R. KOTTE, J. MÖSNER, W. NEUBERT, D. WOHLFARTH AND GY. WOLF[2]

Recently a systematic study of the reaction Au+Au was performed at the SIS accelerator of the GSI Darmstadt using phase I of the 4π-detector facility FOPI [1]. The event structure of a heavy ion collision is expected to depend on the impact parameter b. Other criteria additional to the traditional charged-particle multiplicity binning have been used to establish an approximate correlation with b [2]. The directed sideways flow F_s has been considered as such a global observable [3]. This quantity gives information on the balance of the transverse momenta in the forward c.m.s. hemisphere and does not require the construction of a reaction plane. It is defined as $F_s = \frac{N_c}{N_c-1} * \frac{(\Sigma \vec{p}_t)^2 - \Sigma p_t^2}{(\frac{p_{proj}}{A_{proj}} * \Sigma A)^2}$ and represents approximately the square of the directed momentum per nucleon, which is scaled to the projectile momentum per nucleon in the c.m.s.

Here we report on preliminary estimations of the directed sideways flow using a code basing on a BUU approach [4]. Though this transport theory for the time evolution of the nucleon one-body phase-space distribution does not deliver information on fragment formation, the model is expected to give reasonable discription of the collision up to the time instant of the onset of multifragmentation .

In the model, the nucleons interact with a selfconsistent time-dependent mean field and pairwise with each other through two-body collision including the Pauli blocking. The fragmentation process is supposed to begin at a certain break-up time, after which only such parts of nuclear matter with densities larger than a tenth of nuclear saturation density are to be taken into consideration [5]. This cut excludes fast particles from the subsequent fragmentation process which move within highly diluted matter and leave the collision region early. The break-up time was chosen approximately as the moment of separation of the reaction partners' density distribution.

In the upper panel of fig. 1 the computed averaged value of the directed sidewards flow as function of impact parameter is given for several energies, whereas in the lower panel its maximum values as function of the beam energy is shown together with preliminary experimental data [3]. At all considered energies the asymmetry of the transverse momenta is largest at impact parameter $b \sim 3$ fm. The maximum value extracted from the model is found to be approximately constant for energies $E_{lab} > 150$ AMeV.

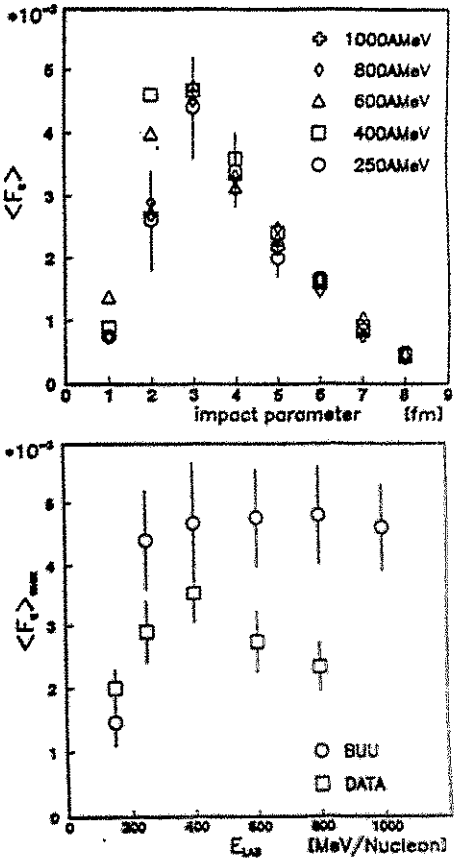

Fig. 1 Sideways flow as function of impact parameter and incident energy.

[1]Institut für Theoretische Physik, TU Dresden und Institut für Kern- und Hadronenphysik, FZR
[2]GSI Darmstadt

REFERENCES:

[1] A. Gobbi et al., Nucl. Instr. Meth. A324 (1993) 156
[2] W. Reisdorf, Proc. Int. Workshop, Hirschegg (1992) H. Feldmeier, p.38
[3] D. Pelte, W. Reisdorf, T. Wienold, GSI-Nachrichten 09-93 (1993)
[4] Gy. Wolf, W. Cassing, U. Mosel, Nucl. Phys. A552 (1993) 549
[5] H.W. Barz et al., Nucl. Phys. A561 (1993) 466

The reaction Au + Au at 150 AMeV simulated by the Copenhagen Statistical Multifragmentation Model [B]

W. NEUBERT, H.W. BARZ[1], J. MÖSNER, R. KOTTE, D. WOHLFARTH
AND THE FOPI COLLABORATION

The applicability of the Copenhagen Statistical Multifragmentation Model (SMM) is tested which supposes an equilibrated state prior to freeze-out. Here we refer to data of the reaction Au+Au at 150A· MeV measured with the 4π phase I setup installed at the SIS at GSI Darmstadt [1]. Central collisions were selected by the ERAT5 criterion [2]. If maximum centrality is assumed it is necessary to start the calculations with the full mass and charge of the Au+Au system. For this purpose the Copenhagen code was upgraded in such a way that systems up to A=400 can be handled. The present code version contains an isotropic radial flow with a collective expansion increasing linearly from the center towards the surface of the freeze-out volume. The calculations reported here refer to a freeze-out density $\rho/\rho_0 = 0.25$. The decisive point in the choice of the physical relevant input parameters of the SMM code is the constraint of energy conservation. The thermal excitation energy was found to be mainly responsible for the steepness of the charge distribution of the fragments. The approximately exponential slope of this distribution found for central ERAT5 events can be reproduced with a thermal excitation energy from 11 to 12 MeV/u. The remaining part of the available c.m. energy ($\simeq$37 MeV/u) is released into Coulomb and binding energies and collective flow where only the latter one can be choosen as input parameter. In fig. 1 we compare the measured and the calculated mean c.m. velocities of different fragments. Fig. 2 shows the corresponding velocity profiles for four selected charges. The SMM with $E_{flow} = 19 MeV/u$ gives a reasonable reproduction of the experimental distributions. A similar analysis was carried out for the c.m. kinetic energies for $25^0 < \Theta_{c.m.} < 45^0$. Nearly the same value of E_{flow} reproduces the averaged kinetic energies $\langle E/A \rangle$ of clusters with Z$\geq$5 (see fig. 3). These findings are in fair agreement with recent results obtained with the extended code FREESCO [2]. Comparing figs. 1 and 2 we found a better overall agreement between calculation and experimental data if we consider mean c.m. velocities instead of the mean c.m. kinetic energies. We found agreeable values of the radial flow within the two hitherto exploited statistical models independent of the specific treatment of fragment formation. Another notifiable point in favour of the extracted radial flow represents a comparison of the mean kinetic energies per nucleon found in very asymmetric collisions of protons [4] and α-particles [5] with Au. These data show the typical 1/A decrease expected for fragments in a common thermal equilibrium (see lower part of fig. 3).

[1]Institut für Theoretische Physik, TU Dresden und Institut für Kern- und Hadronenphysik, FZR

REFERENCES:

[1] A. Gobbi et al., Nucl. Instr. Meth. **A324**, (1993)156
[2] S.C. Jeong et al., preprint GSI-93-38 (1993)
[3] D. Pelte, W. Reisdorf, T. Wienold [FOPI collaboration], GSI-Nachrichten 09-93 (1993)
[4] E.N. Volnin et al., LNPI report 105, Gatchina 1975
[5] V. Lips, Thesis, TH Darmstadt, D17 (1993)

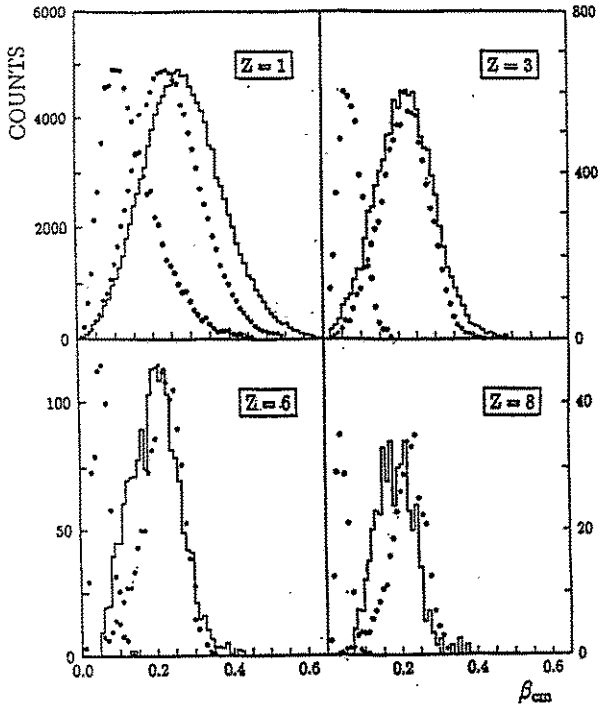

Fig.1 Mean c.m. velocities with the corresponding dispersions as function of the fragment charge. The dots are slightly shifted to show the error bars.

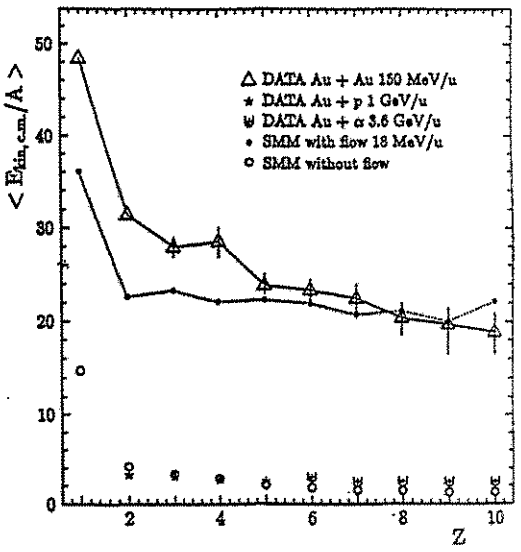

Fig.3 Mean values of the c.m. kinetic energy per nucleon in dependence of the fragment charge, experimental data (⋆)[2], (•)[4] and (⊎)[5]. Calculated values with and without flow are given as triangles and open circles, respectively.

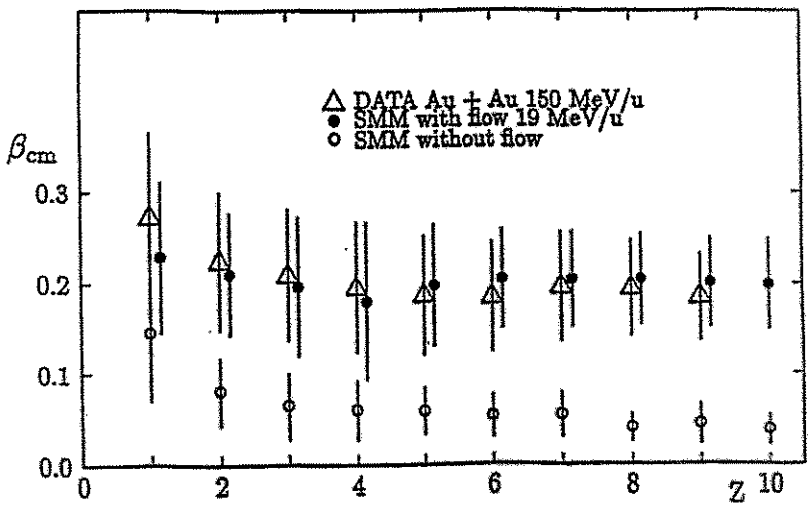

Fig.2 Distributions of c.m. velocities for selected fragment charges. The histograms show the experimental data integrated over the c.m. angle range $25^0 < \Theta_{c.m.} < 45^0$ using the ERAT5 cut [3]. Open circles (o) show calculated distributions for $E^* = 11 MeV/u$ without flow and with $E_{flow} = 19 MeV/u$ (•).

Comparison of two Statistical Models with Reference to Entropy and Isotopic Yield Ratios [B]

W. Neubert, R. Kotte, J. Mösner and D. Wohlfarth

At present the generation of entropy in heavy ion reactions at intermediate energy is a frequently debated issue. Observables like the multiplicity and the yield distributions of intermediate mass fragments (IMF) and the corresponding isotopic yield ratios have been found to be sensitive to the baryonic entropy S/A [1,2]. The entropy can only be determined with respect to the prediction of a certain model. Here, we compare the outcome of the Quantum Statistical Model (QSM) and the Copenhagen Statistical Multifragmentation Model (SMM). The analysis is restricted to the disassembling nucleus $A_0 = 109$, $Z_0 = 48$ motivated by a bulk of experimental data obtained from both proton and heavy ion induced reactions on the target nucleus Ag.

The QSM calculations have been carried out using the standard code version [3] with the option of quantum statistics. One run supplies immediately fragment yields as function of both the nuclear temperature T and the density ρ/ρ_0. More effort requires the calculations with the SMM where the corresponding fragment yields can be obtained only step by step with fixed input pairs of the thermal excitation energy E^* and breakup radius parameter dr_0. In each point the output refers to a certain temperature and breakup density. The calculations have been carried out with the standard variable-volume version of the SMM code [4]. About 70 grid points scattered over the $T - \rho/\rho_0$ plane ($2.5\ MeV \leq T \leq 8\ MeV,\ \ 0.1 \leq \rho/\rho_0 \leq 0.9$) were necessary to get regular surface structures representing physical quantities like the isotopic yield ratios.

Baryonic entropies S/A calculated with both models are compared in fig.1. The QSM gives a rather regular behaviour of the entropy whereas the SMM shows pecularities in the region $3\ MeV < T < 6\ MeV$ around $\rho/\rho_0 = 0.3$ which are supposed to be connected with the liquid-gas phase transition. We remark additionally that compound nucleus formation and contributions to the isotopic yields which are related to this process become very small at temperatures above T= 4 MeV. The QSM does not regard to both of these pattern.

In the framework of the QSM the behaviour of the isotopic ratio and the entropy is very similar since the statistical weight of a final state (e.g. a certain isotope) is proportional to exp(S/A). In fig.2 we compare the predictions of the QSM and the SMM in the range $0.1 \leq \rho/\rho_0 \leq 0.5$ which is expected to be relevant for clusterization. The predictions of the SMM differ considerably from those of the QSM.

In the framework of the SMM multifragmentation is expected to become the dominant process above T = 4 MeV and the $^7Li/^6Li$ ratio is supposed to increase. However, we found a nearly constant isotopic ratio. The essential point of these deviations seems to be the statistical treatment of the secondary decay of hot fragments by the SMM code. The decay channel $^7Li^* \rightarrow\ ^6Li + n$ becomes energetically possible at T>4 MeV leading to a strong affection of the primordial Li isotope yields. Thus, ^6Li production is favoured and the ratio becomes smaller. The calculated value $^7Li/^6Li \simeq 0.7$ is lower than the averaged mean experimental value $^7Li/^6Li = 1.09 \pm 0.03$ [5] indicating an overestimation of the secondary decay channel in the SMM.

In fig.3 we compare τ values obtained from power law fits $dN/dZ \sim Z^{-\tau}$ or $(A^{-\tau})$ of fragment distributions generated by both models. The QSM predicts steeper fragment distributions whereas the SMM gives an enhanced IMF production. In summary, we are aware of ambiguous entropy determination if different models are used. Moreover, in the SMM the ratios of Li isotopes seem to be insensitive to the entropy scince above a limiting temperature there are dominant secondary decays.

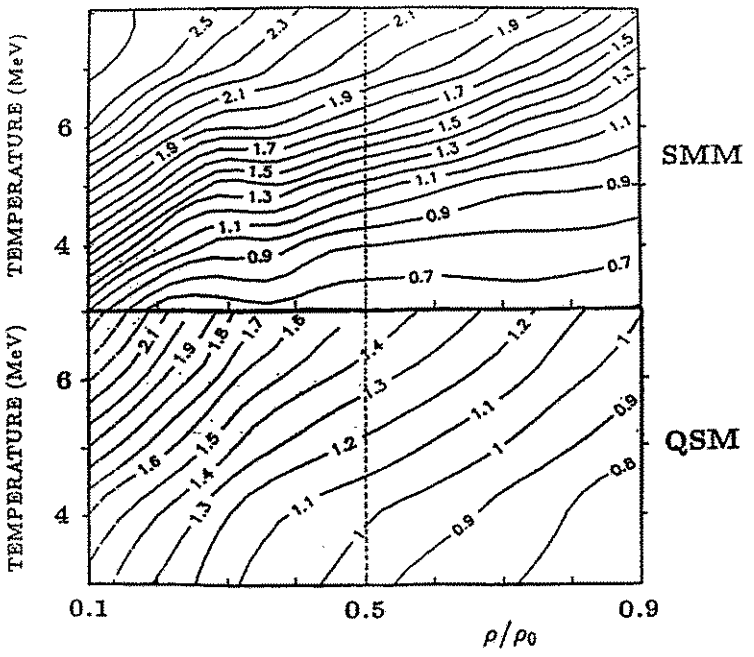

Fig.1 Baryonic entropies in the temperature T versus nuclear density ρ/ρ_0 plane, SMM-top, QSM-bottom of the figure.

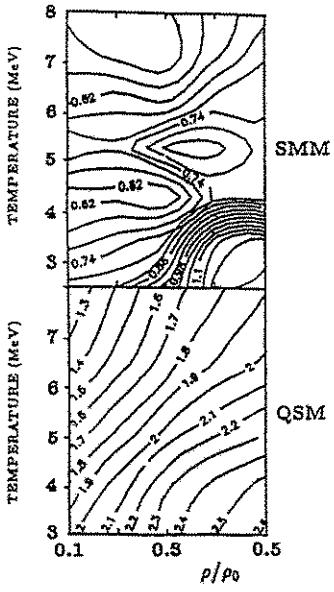

Fig.2 Contours of constant isotopic yield ratios $^7Li/^6Li$ calculated with the SMM (top) and the QSM code (bottom), respectively.

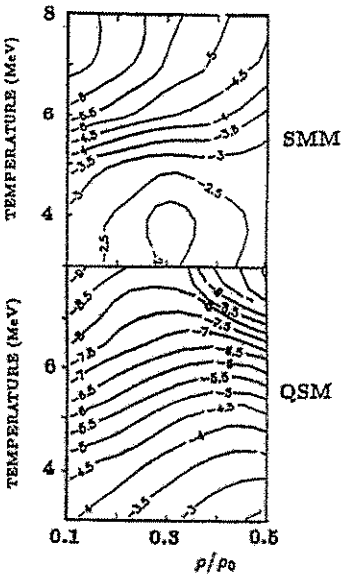

Fig.3 Contour plots of constant power law parameters. The upper part represents results of fits of fragment distributions $4 \leq A \leq 25$ generated by the SMM code. The lower part shows the same for QSM events within $2 \leq Z \leq 13$.

REFERENCES:
[1] C. Kuhn et al., Phys.Rev. C48,(1993)1232
[2] R. Wada et al., Phys.Rev.Letters58,(1987) 1829
[3] D. Hahn and H.Stoecker, Nucl.Phys. A476,(1988) 718
[4] J.P. Bondorf et al., Nucl.Phys.A443,(1985) 321
[5] L.N. Andronenko et al., to be published in Z.f.Phys.

QMD Simulation of Multifragment Production in Heavy Ion Collisions at E/A = 600 MeV
(Prog. Part. Nucl. Phys. 30 (1993) 181)

Begemann-Blaich, M., W.F.J. Müller, J. Aichelin, J.C. Adloff, P. Bouissou, J. Hubele, G. Imme, I. Iori, P. Kreutz, G.J. Kunde, S. Leray, V. Lindenstruth, Z. Liu, U. Lynen, R.J. Meijer, U. Milkau, A. Moroni, C. Ngô, C.A. Ogilvie, J. Pochodzalla, G. Raciti, G. Rudolf, H. Sann, A. Schüttauf, W. Seidel, L. Stuttge, W. Trautmann and A. Tucholski

Abstract: With the ALADIN forward spectrometer the fragmentation of gold nuclei at 600 MeV per nucleon after interaction with carbon, aluminium, copper and lead targets has been investigated. The results are compared to Quantum Molecular Dynamics calculations using soft and hard equations of state.

Quantum molecular dynamics simulation of multifragment production in heavy ion collisions at E/A = 600 MeV
(Phys. Rev. C48 (1993) 610)

Begemann-Blaich, M., W.F.J. Müller, J. Aichelin, J.C. Adloff, P. Bouissou, J. Hubele, G. Imme, I. Iori, P. Kreutz, G.J. Kunde, S. Leray, V. Lindenstruth, Z. Liu, U. Lynen, R.J. Meijer, U. Milkau, A. Moroni, C. Ngô, C.A. Ogilvie, J. Pochodzalla, G. Raciti, G. Rudolf, H. Sann, A. Schüttauf, W. Seidel, L. Stuttge, W. Trautmann and A. Tucholski

Abstract: With the ALADIN forward spectrometer the fragmentation of gold nuclei at 600 MeV per nucleon after interaction with carbon, aluminium, copper, and lead targets has been investigated. The results are compared to quantum-molecular-dynamics (QMD) calculations using soft and hard equations of state as well as a soft equation of state with momentum-dependent forces. Whereas the QMD has been successfully applied to heavy ion collisions at lower energies, it is not possible to reproduce the fragment distributions and the light-particle multiplicities observed in this experiment at relativistic energies. To study the reasons for the discrepancy between the experimental data and the simulations we investigated the time evolution of the nuclear system after a collision and the disintegration pattern of excited nuclei in the QMD approach.

Velocity correlations of intermediate mass fragments produced in central collisions of Au + Au at E = 150 A MeV
(Phys. Rev. C48 (1993) R 955)

Kämpfer, B., R. Kotte, J. Mösner, W. Neubert, D. Wohlfarth, J.P. Alard, Z. Basrak, N. Bastid, I.M. Belayev, Th. Blaich, A. Buta, R. Caplar, C. Cerruti, N. Cindro, J.P. Coffin, P. Dupieux, J. Erö, Z.G. Fan, P. Fintz, Z. Fodor, R. Freifelder, L. Fraysse, S. Frolov, A. Gobbi, Y. Grigorian, G. Guillaume, N. Herrmann, K.D. Hildenbrand, S. Hölbling, A. Houari, S.C. Jeong, M. Jorio, F. Jundt, J. Kecskeméti, P. Koncz, Y. Korchagin, M. Krämer, C. Kuhn, I. Legrand, A. Lebedev, C. Maguire, V. Manko, T. Matulewicz, G. Mgebrishvili, D. Moisa, G. Montaru, I. Montbel, P. Morel, D. Pelte, M. Petrovici, F. Rami, W. Reisdorf, A. Sadchikov, D. Schüll, Z. Seres, B. Sikora, V. Simion, S. Smolyankin, U. Sodan, K. Teh. R. Tezkratt, M. Trzaska, M.A. Vasiliev, P. Wagner, J.P. Wessels, T. Wienord, Z. Wilhelmi and A.L. Zhilin

Abstract: Velocity correlations of intermediate mass fragments (IMFs), produced in central collisions of Au + Au at 150 A MeV beam energy, are extracted from measurements with the FOPI (phase I) detector system at SIS in GSI Darmstadt. The IMF correlation function for semicentral events is found to be affected by the directed sideward flow. When rotating the events into a unique reaction plane an enhancement of correlations, resulting from event mixing effects, vanishes. Selecting violent collisions with a high degree of azimuthal symmetry the correlation function appears nearly independent of additional event or single particle gate conditions. The comparison of the data with a Coulomb dominated final-state interaction model points to an expanding and multifragmenting source with radius R ~ 14 fm.

Charge correlations as a probe of nuclear disassembly
(Nucl. Phys. A556 (1993) 672)

Kreutz, P., J.C. Adloff, M. Begemann-Blaich, P. Bouissou, J. Hubele, G. Imme, I. Iori, G.J. Kunde, S. Leray, V. Lindenstruth, Z. Liu, U. Lynen, R.J. Meijer, U. Milkau, A. Moroni, W.F.J. Müller, C. Ngô, C.A. Ogilvie, J. Pochodzalla, G. Raciti, G. Rudolf, H. Sann, A. Schüttauf, W. Seidel, L. Stuttge, W. Trautmann and A. Tucholski

Abstract: We have studied multi-fragment decays of Au projectiles after collisions with C, Al, Cu and Pb targets at a bombarding energy of 600 MeV/nucleon. We examine the correlations between the charges emitted in these reactions. These correlations are given as a function of the total charge in bound fragments, Z_{bound}, at forward angles, which is a measure of the violence of the collision and can be related to the impact parameter.
The charge distributions have been fitted by a power law and the extracted τ parameter exhibits a minimum as a function of Z_{bound}. We observe a strong reduction in the maximum charge, Z_{max}, of the event with decreasing Z_{bound}. For those events where Z_{max} is less than half Z_{bound}, the relative sizes of the two largest charges within the event cover the full spectrum of possibilities. The charge-Dalitz plots indicate that the multi-fragmentation events are not an extension of symmetric fission reactions. The event-by-event charge moments are examined to measure the size of the charge fluctuations. All of the charge correlations are independent of the target when plotted as a function of Z_{bound}.
The results are compared to both nuclear statistical and percolation calculations. The model predictions differ from each other, establishing that the observables are sensitive to how the available phase space is populated. The sequential nuclear model predicts too asymmetric a decay, while the simultaneous model predicts too symmetric a break-up. The percolation model, which was adjusted to reproduce the size of Z_{max}, correctly predicts the mean behaviour and the fluctuations of the lighter fragments.

Entropy production in the Au + Au reaction between 150 A and 800 A MeV
(Phys. Rev. C48 (1993) 1232)

Kuhn, C., J. Konopka, J.P. Coffin, C. Cerruti, P. Fintz, G. Guillaume, A. Houari, F. Jundt, C.F. Maguire, F. Rami, R. Tezkratt, P. Wagner, Z. Basrak, R. Caplar, N. Cindro, S. Hölbling, J.P. Alard, N. Bastid, L. Berger, S. Boussange, I.M. Belayev, T. Blaich, A. Buta, R. Donà, P. Dupieux, J. Erö, Z.G. Fan, Z. Fodor, R. Freifelder, L. Fraysse, S. Frolov, A. Gobbi, Y. Grigorian, N. Herrmann, K.D. Hildenbrand, S.C. Jeong, M. Jorio, J. Kecskeméti, P. Koncz, Y. Korchagin, R. Kotte, M. Krämer, I. Legrand, A. Lebedev, V. Manko, T. Matulewicz, G. Mgebrishvili, J. Mösner, D. Moisa, G. Montarou, I. Montbel, W. Neubert, D. Pelte, M. Petrovici, S. Ramillien, W. Reisdorf, A. Sadchikov, D. Schüll, Z. Seres, B. Sikora, V. Simion, S. Smolyankin, U. Sodan, K.M. Teh, M. Trzaska, M.A. Vasiliev, J.P. Wessels, T. Wienold, Z. Wilhelmi, D. Wohlfarth and A.V. Zhilin

Abstract: The entropy per nucleon (S/A) has been extracted for the Au [(150-800) A MeV] + Au reaction by using the phase I setup of the 4π facility at GSI, Darmstadt. The entropy has been obtained from the comparison of various observables characterizing the dM/dZ fragment multiplicity distributions, extending up to Z ~ 15, with those calculated with the quantum statistical model. It is the first time that S/A values are determined by considering the full ensemble of charged products detected in the reaction. Consistent values of S/A are found from different methods. These entropy values are shown to be fairly independent of the volume of the "participant" region considered. They are somewhat lower than those extracted in earlier works but are in good agreement with hydrodynamic calculations and suggest a low viscosity for the hot and dense nuclear matter.

Exclusive Studies of Neutron and Charged Particle Emission in Collisions of $^{197}Au + ^{197}Au$ at 400 MeV/Nucleon
(Phys. Rev. Lett. 71 (1993) 963)

Leifels, Y., Th. Blaich, Th.W. Elze, H. Emling, H. Freiesleben, K. Grimm, W. Henning, R. Holzmann, J.G. Keller, H. Klingler, J.V. Kratz, R. Kulessa, D. Lambrecht, S. Lange, E. Lubkiewicz, E.F. Moore, W. Prokopowicz, R. Schmidt, C. Schütter, H. Spies, K. Stelzer, J. Stroth, E. Wajda, W. Walus, M. Zinser, E. Zude and the FOPI Collaboration

Abstract: We present data on collective flow of neutrons in collisions of $^{197}Au + ^{197}Au$ at 400 MeV/nucleon. The azimuthal distribution about the beam axis is investigated with respect to the reaction plane as determined from light charged particles. The "squeezeout" of neutrons, perpendicular to the reaction plane, is observed for the first time. Quantitative agreement to a high level of accuracy is found between the behavior of neutrons and hydrogen ions.

Multi-fragment Events as a Probe of Nuclear Disassembly
(Nucl. Phys. A553 (1993) 271c)

Ogilvie, C.A., J.C. Adloff, M. Begemann-Blaich, P. Bouissou, J. Hubele, G. Imme, I. Iori, P. Kreutz, G.J. Kunde, S. Leray, V. Lindenstruth, Z. Liu, U. Lynen, R.J. Meijer, U. Milkau, A. Moroni, W.F.J. Müller, C. Ngô, J. Pochodzalla, G. Raciti, G. Rudolf, H. Sann, A. Schüttauf, W. Seidel, L. Stuttgé, W. Trautmann and A. Tucholski

Abstract: We review the recent results on the multi-fragment decay of heated nuclear systems that are formed in asymmetric heavy-ion collisions. Particular emphasis is placed on those observables that are sensitive to the fluctuations in the decaying system and their possible role in extracting the physics of phase transitions in nuclear systems.

First Observation of the Coulomb-Excited Double Giant Dipole Resonance in ^{208}Pb via Double-γ Decay
(Physical Review Letters 70 (1993) 533)

Ritman, J., F.-D. Berg, W. Kühn, V. Metag, R. Novotny, M. Notheisen, P. Paul, M. Pfeiffer, O. Schwalb, H. Löhner, L. Venema, A. Gobbi, N. Herrmann, K.D. Hildenbrand, J. Mösner, R.S. Simon, K. Teh, J.P. Wessels and T. Wienold

Abstract: The photon decay of the realtivistic Coulomb excitation of the single and double giant dipole resonance (GDR) in the target has been observed in the system 1A GeV ^{209}Bi on ^{208}Pb. For peripheral events which are dominated by relativistic Coulomb excitation, a large Lorentzian structure in the photon energy spectrum is peaked at 13.3±0.1 MeV with a width of 4.1±0.1 MeV, corresponding to the single GDR in the ^{208}Pb target. The sum energy of coincident γ-γ pairs shows a broad feature at 25.6±0.9 MeV with a Lorentzian width of 5.8±1.1 MeV, which we assign to the double GDR observed via the two-γ decay channel.

Onset of Nuclear Vaporization in $^{197}Au + ^{197}Au$ Collisions
(Physical Review Letters 71 (1993) 1502)

Tsang, M.B., W.C. Hsi, W.G. Lynch, D.R. Bowman, C.K. Gelbke, M.A. Lisa, G.F. Peaslee, G.J. Kunde, M.L. Begemann-Blaich, T. Hofmann, J. Hubele, J. Kempter, P. Kreutz, W.D. Kunze, V. Lindenstruth, U. Lynen, M. Mang, W.F.J. Müller, M. Neumann, B. Ocker, C.A. Ogilvie, J. Pochodzalla, F. Rosenberger, H. Sann, A. Schüttauf, V. Serfling, J. Stroth, W. Trautmann, A. Tucholski, A. Wörner, E. Zude, B. Zwieglinski, S. Aiello, G. Immé, V. Pappalardo, G. Raciti, R.J. Charity, L.G. Sobotka, I. Iori, A. Moroni, R. Scardoni, A. Ferrero, W. Seidel, Th. Blaich, L. Stuttge, A. Cosmo, W.A. Friedman and G. Peilert

Abstract: Multifragmentation has been measured for $^{197}Au + ^{197}Au$ collisions at E/A = 100, 250, and 400 MeV. The mean fragment multiplicity increases monotonically with the charged particle multiplicity at E/A = 100 MeV, but decreases for central collisions with incident energy, consistent with the onset of nuclear vaporization. Molecular dynamics calculations follow some trends but underpredict the observed fragment multiplicities. Including the statistical decay of excited residues improves the agreement for peripheral collisions but worsens it for central collisions.

Azimuthal Asymmetry of Neutral Pion Emission in Au + Au Reactions at 1 GeV/Nucleon
(Physical Review Letters 71 (1993) 835)

Venema, L.B., H. Braak, H. Löhner, A.E.Raschke, R.H. Siemssen, M. Sumbera, H.W. Wilschut, F.-D. Berg, W. Kühn, V. Metag, M. Notheisen, R. Novotny, M. Pfeiffer, J. Ritman, O. Schwalb, A. Gobbi, K.D. Hildenbrand, S. Hlavác, R. Holzmann, R.S. Simon, U. Sodan, K. Teh, J.P. Wessels, N. Herrmann, T. Wienold, R. Kotte, J. Mösner, W. Neubert, D. Wohlfarth, R. Ostendorf, Y. Schutz, N. Brummund and R. Santo

Abstract: The azimuthal angle distributions of neutral pions at midrapidity from Au + Au reactions at 1 GeV/nucleon incident energy have been measured. An enhanced emission of π^0's perpendicular to the reaction plane is observed. The azimuthal asymmetry is dependent on the π^0 momentum: the π^0 spectrum perpendicular to the reaction plane is harder than in the reaction plane. The strength of the observed asymmetry appears to be more pronounced for π^0 than for charged particles and neutrons.

5. Technical and Methodic Developments

First Considerations about a Shower Detector for the COSY-TOF-Spectrometer[B,K]

B. NAUMANN, L. NAUMANN

To obtain a clear signal from the proton-proton-Bremsstrahlung at beam energies above the pion production threshold with the COSY-TOF-Spectrometer it seems necessarily to detect not only the two scattered protons but also the outcoming photon, because the missing mass distribution calculated from times of flight and trajectories of the protons have insufficient resolutions to eliminate background processes ($pp \rightarrow pp\pi^0$, $pp \rightarrow d\pi^+$ etc.). A shower detector combined with the COSY-TOF-Spectrometer should fulfil the following requirements

- a large phase space registration;
- a rotational symmetric detector arrangement;
- high trajectory and energy resolutions;
- a high detection efficiency;
- a short response time;
- no perturbation of the scattered protons and
- moderate costs.

We started our considerations by a simulation of the detector efficiency and energy resolution for a single setup consisting of a converter material layer (Fe,Pb) following by a scintillator layer. The Monte-Carlo calculations were carried out with the GEANT package of the CERN Program Library [1] using the standard event generator FOWL [2]. An incident beam with a momentum of 0.8 GeV/c was chosen for the investigation of the Bremsstrahlung near pion threshold. The detector efficiency depends on the converter thickness given in units of the radiation length of the converter material X_0 as shown in Fig.1. The maximum for a single setup is achieved between $2X_0$ and $3X_0$ up to 50%. The energy loss in the scintillator layer for a detector configuration with a Pb-converter of $3X_0$ thickness doesn't reflect the photon energy, what is seen in Fig.2.

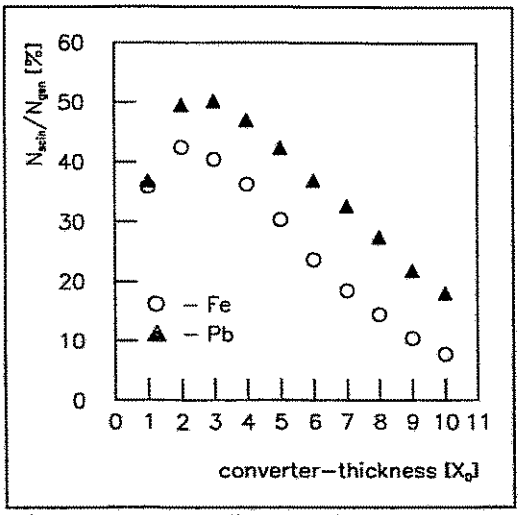

Fig.1 Detector efficiency in dependence on the converter thickness

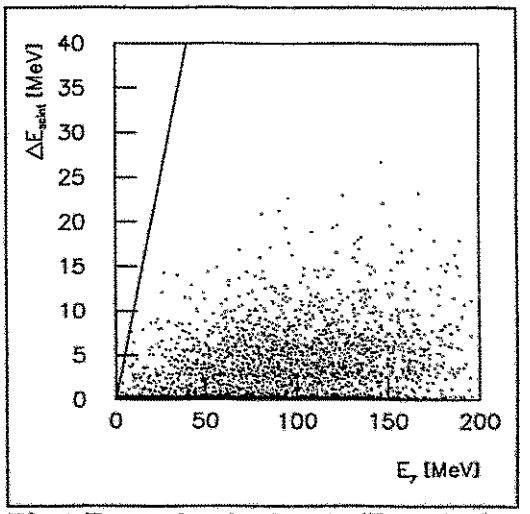

Fig.2 Energy loss in the scintillator in dependence on the photon energy

The photon energy distribution has been simulated for possible COSY-TOF geometrical constraints in relation to all events in full phase space. For a single setup photons were detected with detector efficiency shown above. Supposing the third barrel of the COSY-TOF-Spectrometer would be used as a shower detector, the photons could be registrated in a range of scattering angle from $30° \leq \theta_\gamma \leq 85°$. Both scattered protons could be detected

in the forward direction between $2° \leq \theta_{proton} \leq 30°$. After the transformation in the CM-System θ^*_γ lies between 40° and 110° and the Bremsstrahlung energy distribution shows an enrichement of the high energy photons, see Fig.3.

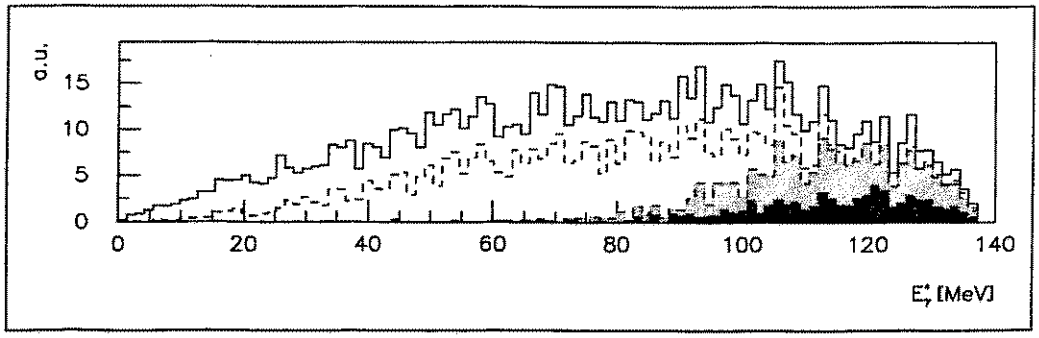

Fig.3 Weighted photon energy distribution for a single detector with Pb-thickness of $3X_0$

solid line	:	all events in full phase space	
dashed line	:	detected events in full solid angle	
gray shape	:	$2° \leq \theta_{proton} \leq 30°$	$0° \leq \theta_\gamma \leq 180°$
black shape	:	$2° \leq \theta_{proton} \leq 30°$	$30° \leq \theta_\gamma \leq 85°$

The situation is completely changed in a multilayer system consisting of 50 converters and scintillators. For different Pb-converter thicknesses the efficiency and the energy resolution were considered (see Fig.4). The detector efficiency is for the chosen thicknesses better than 90%. The best energy resolution could be achieved with Pb-layers of 1 to 2mm thickness, where $\frac{\sigma}{E_0} \approx 8\% \cdot \frac{1}{\sqrt{E[GeV]}}$.

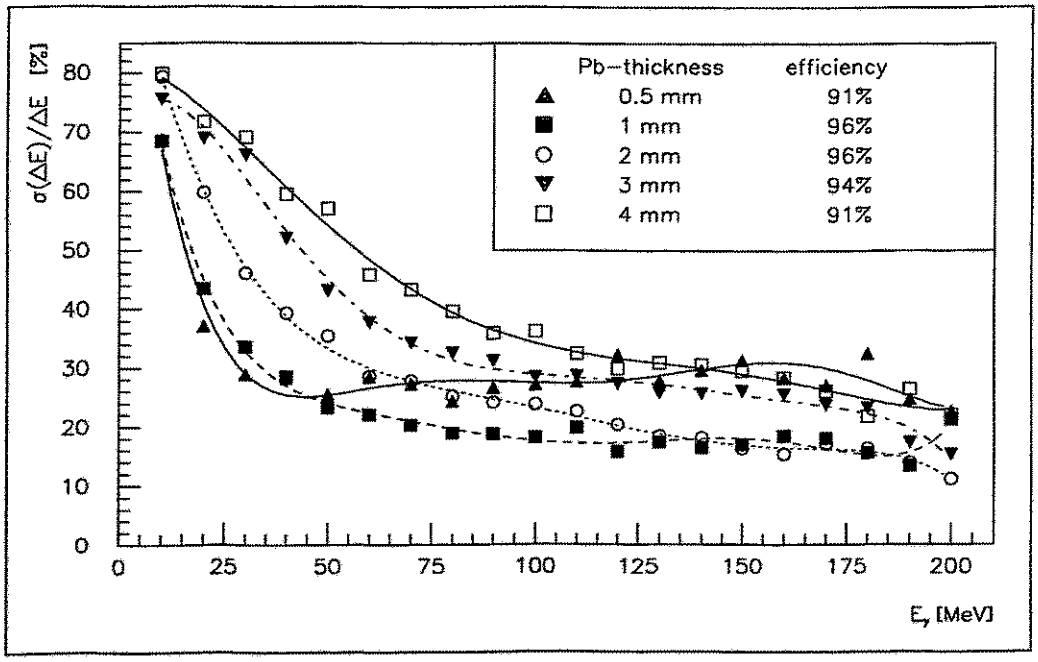

Fig.4 Energy resolution in dependence on the photon energy

REFERENCES:

[1] GEANT, CERN Program Library Q123 (1993)
[2] FOWL , CERN Program Library W505 (1972)

Some Aspects of the Laser based Test System for the COSY-TOF-Spectrometer[B,K]

P. Hermanowski[1], J. Krug[1], R. Loke[1], B. Naumann, L. Naumann

The laser based test system for the COSY-TOF-Spectrometer is under development [1][2]. The UV-light pulse is led to the scintillation counters by optical fibres and through different optical elements. The light intensity for each fibre output should be as uniform as possible with its height approximately that of signals from particle detection. A bundle of fibres to be connected with the 32 start counters was tested. The nonuniformity for these fibres is demonstrated in Fig.1. We constructed a special reflector head to adjust the light intensity as shown in the photograph (Fig.3). It consists of a holder, a support to fix the fibre output window and a mirror to bend the light to a photomultiplier. A rough intensity correction is realized by tilting the mirror surface in relation to the light direction; fine adjustment is possible by shifting the mirror along the light direction. The 36 fibres of the bundle were adjusted to the lowest ADC-value of the original intensity distribution. The result is presented in Fig.2 where the nonuniformity amounts to 5%.

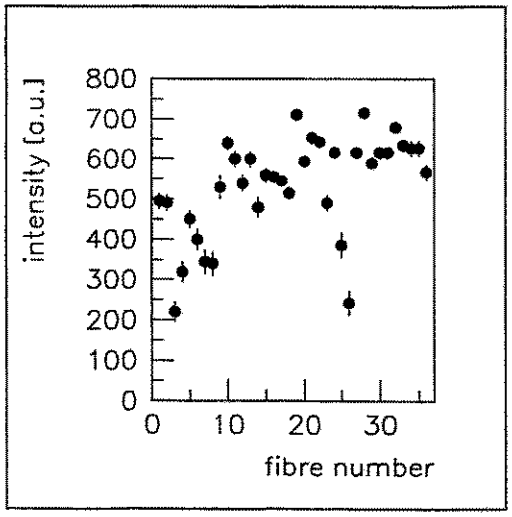

Fig.1 light intensity for each fibre output before adjustment

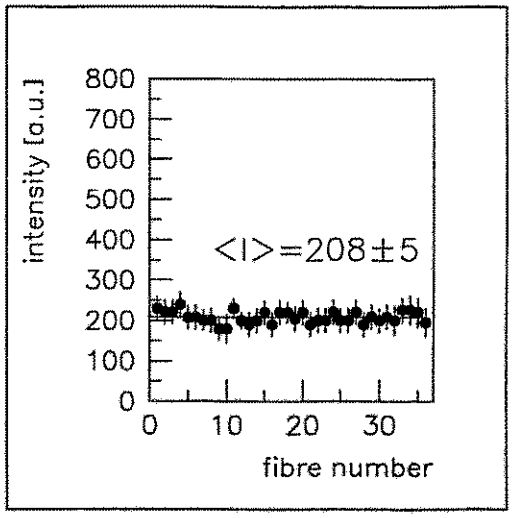

Fig.2 light intensity for each fibre output after adjustment

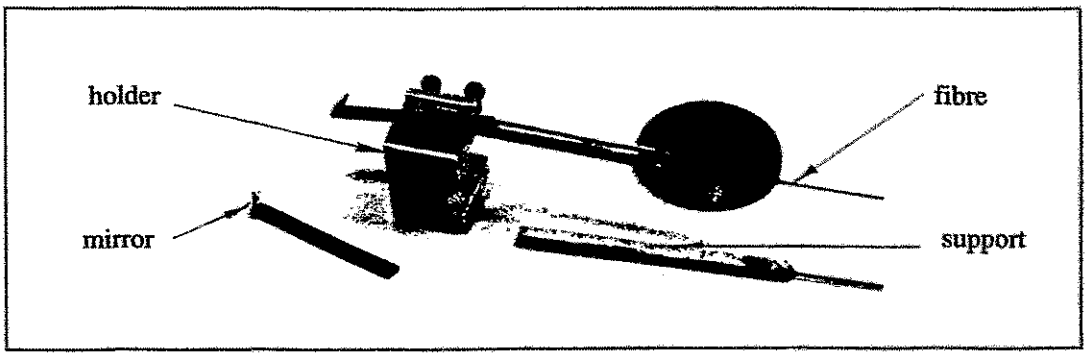

Fig.3 Photograph of the special reflector head

[1] *Ruhr-Universität Bochum, Institut für Experimentalphysik I*

REFERENCES:

[1] P. Hermanowski, Diplomarbeit,Bochum (1993)
[2] P. Hermanowski et al., Annual Report 1992, FZR 93-10(1993),120

Some Aspects of the Installation of the Liquid Hydrogen Target in the Start Detector Device of the COSY-TOF-Spectrometer[B,K]

K. Kilian[1], R. Klein[1], Ch. Nake[1], B. Naumann, L. Naumann, A. Schamlott and P. Turek[1]

The installation of the LH_2 target [1] in the start detector vessel [2] of the COSY-TOF-Spectrometer requires a sufficiently low vacuum pressure, to suppress the growth of residual gas condensates at the target windows. In a first step the components of the residual gas inside the start detector vessel were analyzed after a long pumping duration, when the total pressure reached the asymptotic limit of approximately $3 \cdot 10^{-6}$mbar. This measurement was carried out with the Transpector Gas Analysis System from the Leybold Inficon Inc.[3]. The mass spectrum of the residual gases is shown in Fig.1 as a pattern of peaks on a plot of ion current as a function of ion mass to charge ratio. To calibrate the mass to charge ratio, nitrogen gas was additionally filled in the vacuum vessel. The dashed line in the mass spectrum shows a growth of peaks in the channels for nitrogen. The partial pressures of the major residual gases were calculated from the mass spectrum and are shown in Table 1.

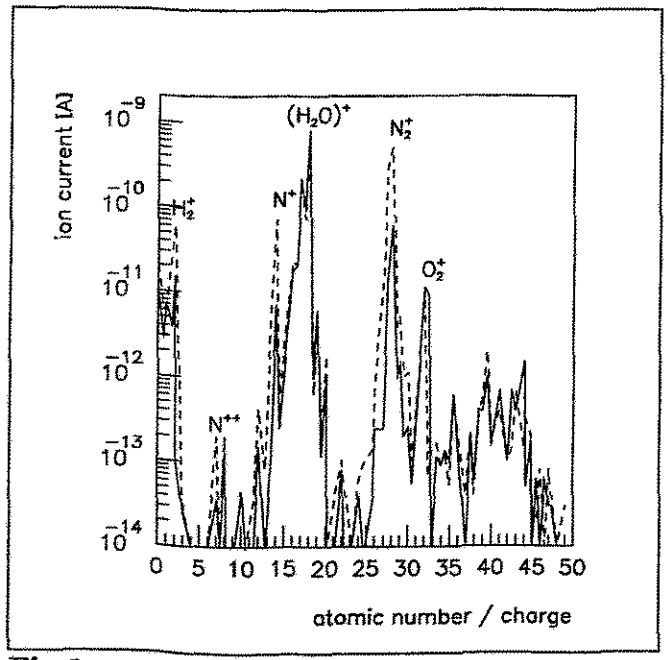

Fig.1
Mass spectrum of residual gases in the start detector device [4]

residual gas molecules	partial pressure [mbar]
H_2O	$6.8 \cdot 10^{-7}$
N_2	$1.3 \cdot 10^{-6}$
O_2	$3.1 \cdot 10^{-7}$

Tab.1
The partial pressure of residual gases calculated from the spectrum in Fig.1.

In a second step the contamination of the windows of the liquid hydrogen target (see Fig.2) with the main residual gas components was investigated . The target cell filled with liquid hydrogen at 16K and 200mbar was mounted in the start detector vessel with a total pressure of 10^{-5}mbar. Water, nitrogen and oxygen were frozen out on the cold target surface and an ice layer became visible. The contamination of the hydrogen target increases with the exposure time for 10^{-5}mbar as shown in Fig.3.

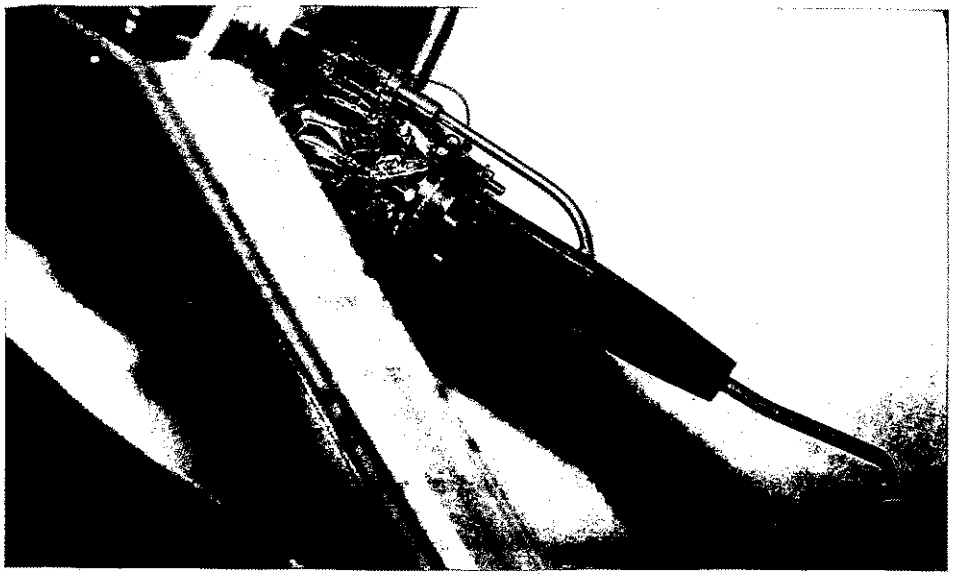

Fig.2 Photograph of the LH_2 target cell

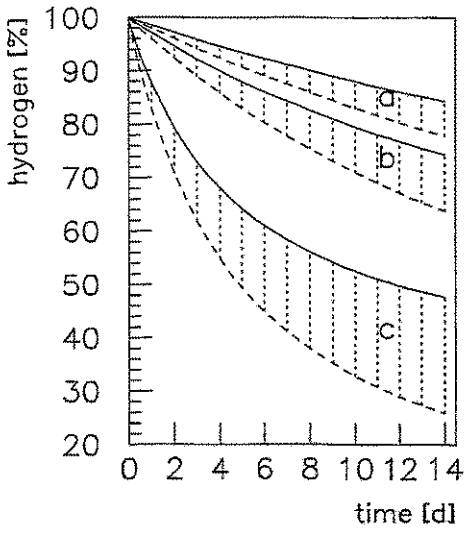

Fig.3
Calculated percentage of hydrogen atoms to all atoms in the target region for various target length
a - 10 mm,
b - 5 mm and
c - 1 mm
at total pressure 10^{-5}mbar for window foil thickness of 2μm;
solid lines :
all hydrogen atoms were considered ;
dashed lines :
only the well defined number of hydrogen atoms from the target volume and the foils are taken into account [4].

Because proton-proton cross section measurements with high accuracy at the COSY-TOF-Spectrometer require well defined hydrogen targets of high purity, the target contamination must be suppressed. There are some possibilities to do that :
- to improve the vacuum ($p \leq 10^{-7}$mbar);
- to eliminate the ice layer by heating ($T \geq 170K$) or
- to surround the LH_2 cell by gaseous hydrogen.

[1] *Forschungszentrum Jülich, Institut für Kernphysik*

REFERENCES:
[1] V.G. Jaeckle,Diplomarbeit,Jül-2633(1992)
[2] K. Kilian et al.,Annual Report 1991, Jül-2590(1992),p.5-6
[3] Manual of the Transpector Gas Analysis System, Leybold Inficon Inc.(1993)
[4] L.Naumann et al.,COSY-TOF-Notes-RO-3-1993(1993)

Investigation of Light-Readout from Long Straight Scintillating Stripes for the COSY-TOF Stop Detector[B]

P. MICHEL, K. MÖLLER[1], A. SCHAMLOTT AND A. SCHÜLKE

The feasibility of two-sided readout of long scintillating stripes was investigated for the realization of the COSY-TOF stop detector barrel section.
The following requirements have to be fulfilled for the stop detector [1]:

- spatial resolution $\sigma = 6...7\,\mathrm{cm}$
- time resolution $\sigma = 0.5\,\mathrm{ns}$
- 100% acceptance, i.e. no gaps in the scintillating material of the detector
- easy handling for assembly and disassembly of the TOF spectrometer

Different methods of light-readout (Fig.1, 0°-readout as reference) were analysed with respect to light output efficiency and time and spatial resolution, to obtain a basis for the decision on the concept of the barrel section for the stop detector.

The tests were carried out with minimal ionizing pions at CERN. The test arrangement consisted of an original TOF start detector module, a long scintillating stripe 6 m from the start detector and a beam defining scintillating detector ($3x3\,\mathrm{cm}^2$) in front of the stripe. To change the hit position of beam particles on the stripe the mechanical support of the stripe could be moved perpendicular to the beam axis.

The time difference of light output pulses from the stripe had to be digitized electronically to get an information on the hit position for on-line trigger processing. For this reason a Real-Time-to-Digital-Converter (RTDC) was developed [2]. The qualitiy of the time measurement of the RTDC was compared (off-line) to conventional TDC. The accuracy of the time measurement with the RTDC proved to be comparable to conventional TDCs.

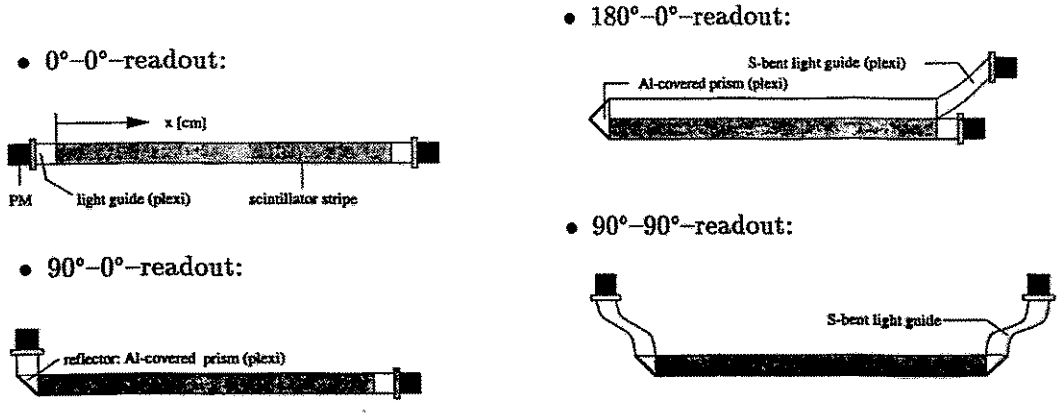

Fig.1 Schematic representation of the configuration layout

The 0°-readout version was shown to be acceptable from the physical point of view but is not doable in the stop detector barrel configuration for constructional reasons. The 180°-readout through a long light guide is very interesting because of technical practicability since it can be integrated in the barrel construction at minimal expense. Utilizing 180° reflection through a prism loss of light occurs so that time and spatial resolution do not meet the qualitiy requirements. In addition, Cerenkov light is created inside the long light

guide which causes an error in hit position determination. The measurements have shown that the requirements concerning efficiency, spatial and time resolution are also satisfied by the two-side light-readout at 90° (tab.1,2). These values are nearly constant over the whole length of the scintillator comparable to 0°-readout (Fig.2,3).

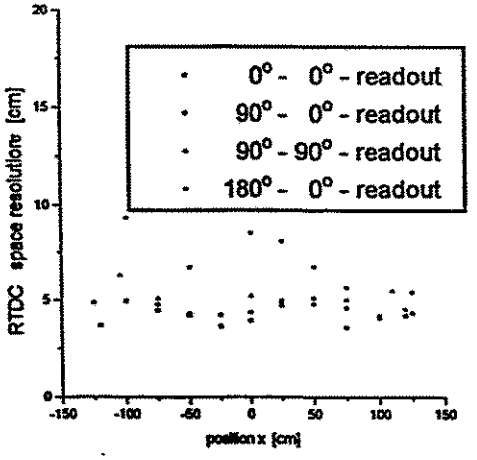

Fig.2 Spatial resolution of configuration layout, measured with RTDC and with conventional TDCs

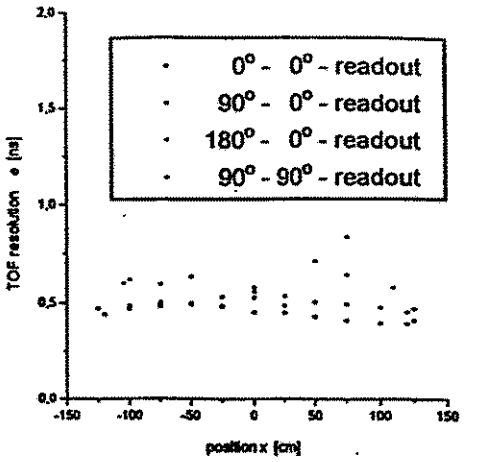

Fig.3 Time resolution Δt_{TOF} of configuration layout

In view of the technical practicability one should use the two-side readout method with S-bent light guide as an alternative to previous configurations of the stop detector. The measurements have shown that the RTDC module is a fast on-line device to determinate the spatial information for trigger processing. The measured spatial resolution is comparable to values reached with conventional TDCs. A sample of modules for fast space determination is available.

	0°	90°	90° S	180°
efficiency [%]	100	74.5	57.9	15.6

Tab.1 Light efficency for the different layouts

	0° − 0°	0° − 90°	90° − 90°	0° − 180°
TDCs σ_x[cm]	4.6	5.3	6.8	~7.7
RTDC σ_x[cm]	4.3	4.6	5.4	~7.5
σ_t[ns]	0.37	0.41	0.45	~0.6

Tab.2 Spatial and time resolution for the different layouts

With the two-side 90° configuration it seems possible to realize a gap-free arrangement with a single layer of 96 scintillating stripes in the TOF stop detector.

[1] Institut für Kern- und Teilchenphysik, TU Dresden und
Institut für Kern- und Hadronenphysik, FZR

REFERENCES:

[1] COSY-Proposal #9

[2] F. Gabriel et.al., this Annual Report

Start Counters for Time-of-Flight Measurements at the 0° Facility[B]

R. Esser[1], D. Kopyoto[1], K. Meyer[1], H. Müller, H. Ohm[1], B. Prietzschk, B. Rimarzig, K. Sistemich[1]

Particle identification and the first-level trigger decision at the COSY 0° Facility will mainly be based on a time-of-flight measurement. The start counters must be positioned as close as possible to the spectrometer dipole D2 in order to obtain the longest possible flight paths for the ejectiles, see Fig.1. Since the stop counters will be placed near the focal surface the length of the flight path is short in particular in the low momentum region. Therefore, in K^+ measurements, the best possible time resolution is necessary for maximal reduction of the expected huge background of protons and pions. The start scintillators must be as thin as 1 and 2 mm for lower and higher momenta, respectively, in order to avoid large effects of particle scattering and hadronic interaction. Long light guides have to be used since there is little space between the magnet and the first wire chamber and since the multipliers have to be placed in a region where the magnetic stray field is small enough so that an efficient shielding is feasible. Small photomultipliers will be used in order to facilitate the shielding.

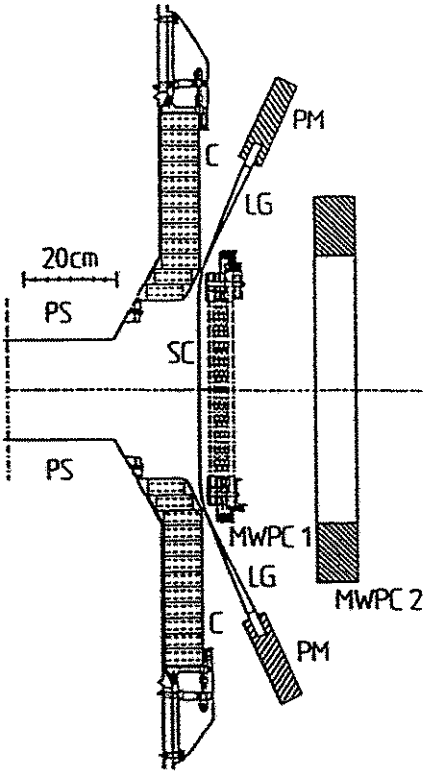

Fig.1 Arrangement of the start scintillators (SC) with light guides (LG) and photomultipliers tubes (PM) between the pole shoes (PS) and coils (C) of the spectrometer dipole D2 and the muti-wire proportional chambers (MWPC) of the 0° Facility.

Scintillators will be 5 cm wide and 30 cm long strips of Pilot U which has a sufficiently large attenuation length and a very short decay time. They will be coupled to light-guide strips made out of ultraviolet-transmitting Plexiglas (Röhm) which makes sure that the short-wavelength component of the Pilot U scintillation light is not absorbed. Near the PM tube the light guides are cut into smaller strips which are bent such that the ends can be put on top of each other. In this way the cross section of the light guide can be accomodated most efficiently on the photocathode of small PMs (see Fig.2). Photomultiplier tubes Hamamatsu R 3478, Philips XP 2972 and XP 2982 with effective photocathode diameters of 15 mm (Hamamatsu) and 23 mm (Philips) have been taken into consideration. Recent test measurements have lead us to the conclusion that both Philips PMs are sufficiently good although the transit time difference is bigger. We have decided to use the XP 2972 or XP 2982 tubes since they are cheaper and offer comparative timing resolution. Moreover, the gain of the Philips tube is higher whilst it is necessary to operate the Hamamatsu tube at the highest allowed supply voltage in order to obtain a sufficiently high amplitude.

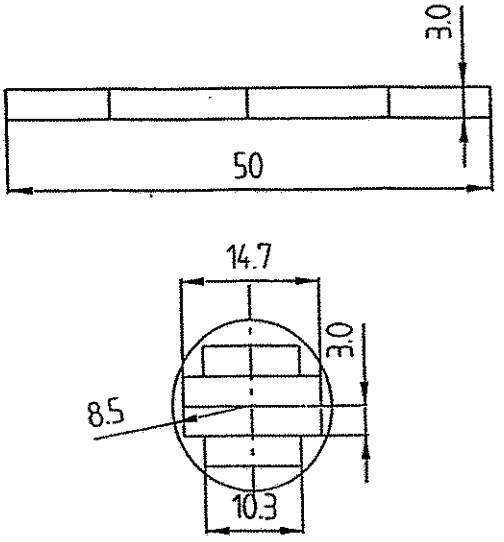

Fig.2 Cross section of the flat part of the light guide indicating the position of the cuts (upper part) and the shape of the end to be coupled to the PM. Dimensions are given in mm.

Monitoring of the scintillation counters with light-emitting diodes is foreseen in order to check for gain and timing variations and to perform off-line corrections during data analysis. This system will also be used for setting the fast TOF trigger by injecting pulses into the system which are separated in time by the flight-time of the particle under consideration. A fast pulse generator is presently being developed at FZ Rossendorf. Prototypes of start counters and two stop counter telescopes are under preparation for a test planned to be performed at ITEP Moscow.

[1] Forschungszentrum Jülich, Institut für Kernphysik

Test of the CLUSTER detector [B]

S. Skoda, L. Käubler, H. Prade, J. Reif, W. Schulze, R. Schwengner, A. Uhlmann, G. Winter, J. Eberth[1], H.G. Thomas[1] and P. von Brentano[1]

The EUROBALL cluster detector [1] consists of seven encapsulated Germanium detectors mounted in a common cryostat which is surrounded by 18 Bismuth Germanate (BGO) detectors serving as an escape-suppression-shield. The High Purity n-type Ge detectors of about 60 % efficiency are protected against the environment by an evacuated aluminium capsule. This encapsulation technique was developed by a collaboration of IKP Cologne, manufacturer Intertechnique and KFA Jülich [2,3]. The Ge detectors are hexaconical shaped to maximize the solid angle covered by Ge. The total efficiency of the cluster detector is enhanced by the add-back technique: the total energy of a Compton-scattered γ ray can be reconstructed by summing up the energy signals of all coincident Ge detectors.

Table 1. Resolutions of encapsulated hexaconical Ge detectors

E_γ	FWHM (keV)							
(keV)	det 1	det 2	det 3	det 4	det 5	det 6	det 7	mean value
122	1.3	1.0	0.9	1.1	1.0	1.3	1.1	1.1(1)
1333	2.2	2.3	2.3	2.1	2.1	2.2	2.1	2.2(1)

The BGO shield detects γ-rays escaping the Ge-detector which are a result of two kinds of γ-e^- interaction. The first process is Compton-scattering and the second is e^-e^+ annihilation (two 511 keV γ rays) after pair production caused by incident γ-rays with energies higher than 1 MeV. Suppression of both kinds of event enhances the peak to background ratio for the full energy peaks. Further, reconstruction of the second type of event will enhance the efficiency of the Cluster detector.
The BGO shield consists of 18 individual BGO scintillator detectors. Mounted behind the Ge-cluster are 6 thick and compact backcatchers used to detect forward scattered γ-rays of nearly incident energy. The Ge cluster is further surrounded by 12 lateral shield detectors. They protrude inward beyond the Ge detector front surface to be sensitive to backscattered γ-rays. The outer shape of the shield is hexaconical as for a single encapsulated Ge detector because the honeycomb structure allows the densest packing of detector material. The 12 lateral BGO detectors exhibit less resolution power. Their thin and long shape causes the light emitted by the BGO scintillator to scatter more often on its way up to the photomultiplier. The side shield consists of 6 BGO detectors on the corners of the honeycomb and 6 BGO detectors between the corners (straight sides). The properties of the three different BGO types are given by the mean values for the respective 6 detectors. The energy resolution was measured with ^{137}Cs at 662 keV. The time resolution was measured against an encapsulated hexaconical Ge detector using the γ-ray sources ^{22}Na and ^{60}Co. The Constant Fraction threshold was set below 60 keV (^{241}Am).

Table 2. Energy and Time Resolutions for different BGO detector types

BGO type	Energy resolution	Time resolution
back catcher	12(1)%	10.0(5) ns (5ns against NE213)
lateral shield, straight side	17(1)%	13.7(5) ns
lateral shield, corner	21(1)%	15.2(7) ns

[1] *Institut für Kernphysik der Universität zu Köln*

REFERENCES:

[1] EUROBALL III proposal, GSI 1992, ed. J. Gerl and R.M. Lieder
[2] J. Eberth et al., Progr. Part. Nucl. Phys. 28, Pergamon Press, Oxford 1992, p. 495
[3] J. Eberth, Phys. Bl. 11 (1993) 1016

Internal Support and Tabletop Frame for a Single EUROBALL CLUSTER Detector

J. STEPHAN[1], M. FREITAG

An internal support for a single CLUSTER detector has been constructed in cooperation of the department of design and construction and the detector laboratory. This support enables the movement of the cryostat (the common holder of seven encapsulated hexagonal tapered Ge detectors [1]) independently from the BGO shield. The movement is necessary for servicing. Furthermore, the support is used to fix the BGO back catcher. The internal support and the mechanism of movement allow the distance between the extremely thin cryostat covering and the lateral BGO shield to be minimized to 1 mm.
The whole detector system is held by a flange that substitutes an EUROBALL honeycomb in experiments with single CLUSTER detectors. At this flange the lateral BGO shield is immovably mounted while the BGO back catcher and the cryostat including the Ge detectors can be moved on slide rails.
In order to test the components of the internal support and of the slide rails, a model of the CLUSTER detector was constructed to a scale of 1:1 and with the approximate mass of a real CLUSTER detector. At this model tests of different guide bushes were carried out.
Several tabletop frames that enable a safe setting up of the assembled CLUSTER detector of ca. 80 kg mass have been designed and constructed. In the standard frame shown in figure 1 the CLUSTER detector can be tilted downward by up to 30°. A special frame has been developed for experiments at the electron linear accelerator S-DALINAC of the TH Darmstadt. This frame has a minimized height and allows two CLUSTER detectors to be positioned at observation angles with a minimum difference of 30° using a target-detector distance of 44 cm. For the operation of a CLUSTER detector as part of the detector array OSIRIS CUBE at the tandem accelerator of the University Cologne an adapter has been constructed to optimize the target-detector distance.

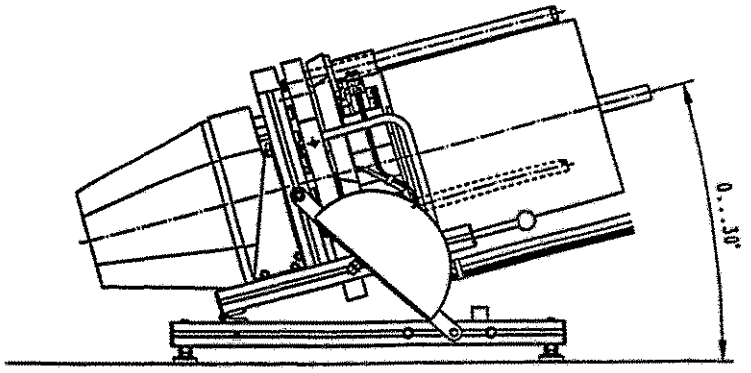

Figure 1. Tabletop frame with honeycomb substitute flange and CLUSTER detector

[1] *Zentralabteilung Forschungs- und Informationstechnik, FZ Rossendorf*

REFERENCES:

[1] EUROBALL III, Eds.: J. Gerl and R.M. Lieder, GSI Darmstadt 1992

The Gas Supply System of the FOBOS Avalanche Counters [B]

G. Renz[2], V.M. Vasko[1], P. Gippner[2], M. Andrassy,
V.N. Doronin[1], D.I. Shishkin[1]

The pentane gas supply system for the position-sensitive avalanche counters (PSAC) (see fig. 1) has been completed. Its status is controlled by a SIMICRO-SX microcomputer system and visualized on a colour X-Terminal /1/. Careful tests have been provided during the two experimental periods of altogether 2 months. The vapour of the liquid pentane stored in glass flasks at room temperature flows through the regulating valve V 11.9, which adjusts the gas flow q. The second valve V 11.0 allows to stabilize the pressure in a range of 1 to 6 mbar inside the FOBOS gas collector rings which up to 30 PSAC's can be connected to. Special sensors SS in combination with minivalves MV protect the PSAC's from critical pressure to avoid a destruction of the thin (1.2 μm polypropylene) window foils. The MV's are usually closed and open if p inside the PSAC's exceeds a value of about 6.6 mbar. In the first experiments, 10 PSAC's have been supplied simultaneously. A special technique has been developed to determine the leakage rate Q of each PSAC before mounting it to FOBOS. Therefore, Q of the entire PSAC configuration could be limited to a resonable value, which is only about one order of magnitude higher than the leakage rate of the central FOBOS vacuum chamber.

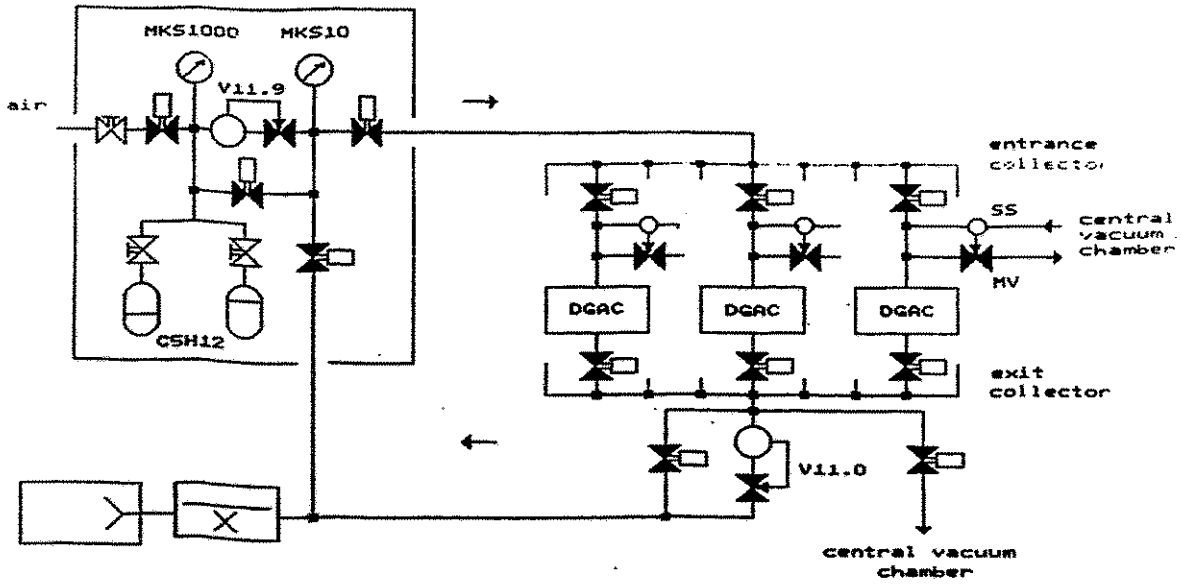

Fig. 1 The scheme of the pentane gas supply system of FOBOS

[1] *Joint Institute for Nuclear Research, Dubna*
[2] *Institut für Kern- und Hadronenphysik, FZR und Joint Institute for Nuclear Research, Dubna*

REFERENCE

[1] G. Renz et al., FLNR Scient. Report, JINR, Dubna (1992) 246

The Gas Supply System of the FOBOS Bragg Ionizations Chambers [B]

G. Renz[2], V.M. Vasko[1], P. Gippner[2], A. Matthies[2], M. Andrassy,
V.N. Doronin[1], D.I. Shishkin[1], Sh. Heinitz[2]

The gas supply system shown in fig. 1 has been designed for on-line mixing of P10 [Ar(90%) + CH_4 (10%)] to get the optimal mixture for operation of the Bragg ionization chambers (BIC). It is controlled by a SIEMENS-SX-MULTIBUS microcomputer system. Three steely gas cylinders contain highly cleaned and compressed technical gases which flow into the tube system with original pressures measured by the sensors S1 - S3. The gases are expanded down to about 2 atm with the help of the mechanical reducers R1 - R3. At this pressure, both components move through the flow control valves V6 and V7, respectively, which determine on-line the mixing ratio of the components. A combination of the sensor S4 and the valve V4 prevents the following elements of the system from mechanical damage because of overpressure.

The distribution of the P10 mixture among the BIC's in operation is performed by the entrance collector ring, which is connected to 10 detector groups each consisting of 3 BIC's and two valves regulating gas flow and pressure, respectively. Such a group is shown in fig.2. The arrangement chosen is capable to stabilize the pressure individually in each group within a region of 133 - 1000 mbar.

During the first experiments, the mixing process has been performed off-line. The pressure within the 12 BIC's in operation was p = 266 mbar. The stabilization mechanism has been found to work reliable over a period of about two months. A stabilization accuracy of better than 2% has been achieved. The flow rate allowed a complete gas exchange within the 12 BIC's during a time interval of 3 hours.

However, the composition of the off-line mixed gases obviously deteriorates during the measuring period, as has been observed by an increase of the electron drift time. Therefore, on-line mixing of the detector gases will now be realized. The mixing process will be controlled by a gas analyser just coming into operation.

The leakage rate of the window foils of the BIC's has been observed to be higher by more than 2 orders of magnitude in comparison with the expected gas diffusion rates. This effect is caused by micro holes in the thin 1.2μm polypropylene entrance window foils. In order to achieve a vacuum of at least 10^{-1} Pa inside the central vacuum chamber, an additional pumping system consisting of a dual-stage rotary pump, a roots pump and three turbo molecular pumps has been installed. The latter ones have a pumping capacity of altogether 3000 l/s.

With the increasing number of FOBOS modules, a more reliable test procedure for the BIC window foils has to be elaborated for pressure values of higher than 200 mbar.

[1] *Joint Institute for Nuclear Research, Dubna*
[2] *Institut für Kern- und Hadronenphysik, FZR und Joint Institute for Nuclear Research, Dubna*

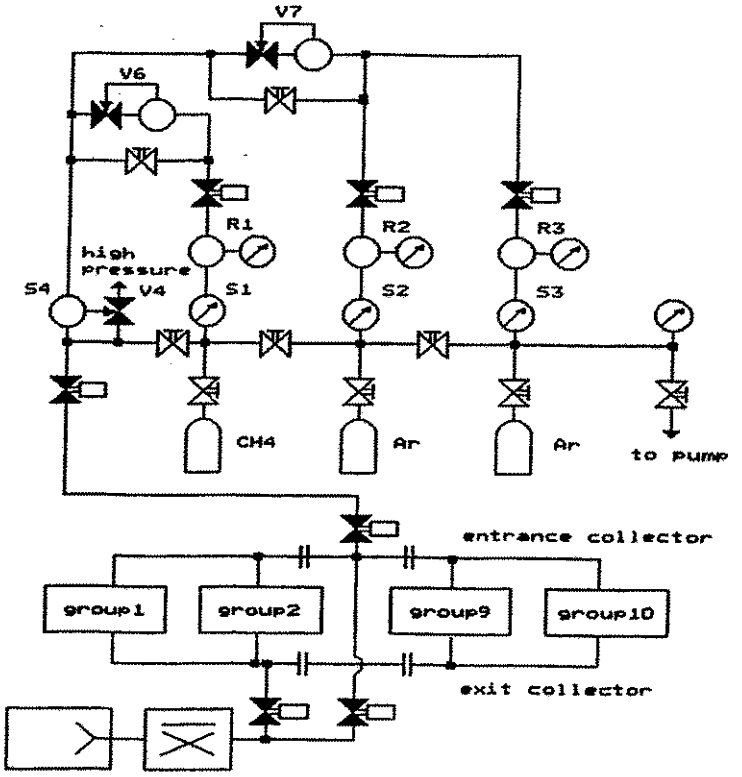

Fig. 1 The scheme of the gas supply system of the Bragg ionization chambers

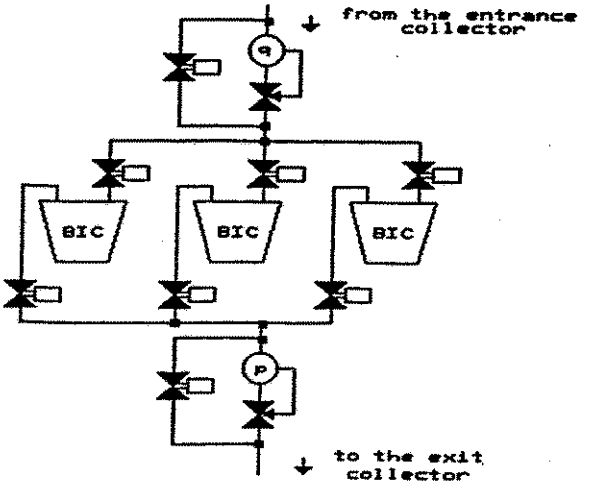

Fig. 2 Schematic arrangement of ionization chambers and regulating valves within a detector group

The Light Output of CsI(Tl) for Low-Energy Alpha Particles [B]

W. WAGNER[1], H.-G. ORTLEPP[1]

The light output L of CsI(Tl) is a non-linear function of the particle energy E. For low-energy particles with a high stopping power dE/dx, the relation

$$L \approx \frac{S}{kB} \cdot R$$

can be deduced from the semi-empirical formula of Birks /1/, where R is the range in the scintillator, S is the absolute scintillation efficiency and kB is the quenching parameter.
The dependence of the light output on the alpha particle energy has been measured with a large-area CsI(Tl) detector of the FOBOS scintillator shell /2/ by applying the foil method. The energy of alpha particles from ^{238}Pu and ThC sources has been varied using a different number of thin (2μm) Mylar absorber foils. The current pulses of the photomultiplier were intergrated within a time interval of 2μs. The light output is then proportional to the pulse height. The measured values are shown in fig. 1. (the dashed line is to guide the eye).
The range of alpha particles in CsI has been calculated according to the STOPPOW code /3/ (fig.1, full line). The experimental points are, indeed, well fitted by the range curve, if the measured data are corrected for the energy loss in the dead layer of the entrance surface of the CsI(Tl) crystal originating from the polishing procedure. From this measurement, one can deduce a dead layer of about 4μm. Such a value is in rather good agreement with earlier measured data for commercial CsI crystals /4/. It results in a lower energy threshold of the FOBOS scintillation detectors and amounts to about 0.6-0.8 MeV in the case of alpha particles.

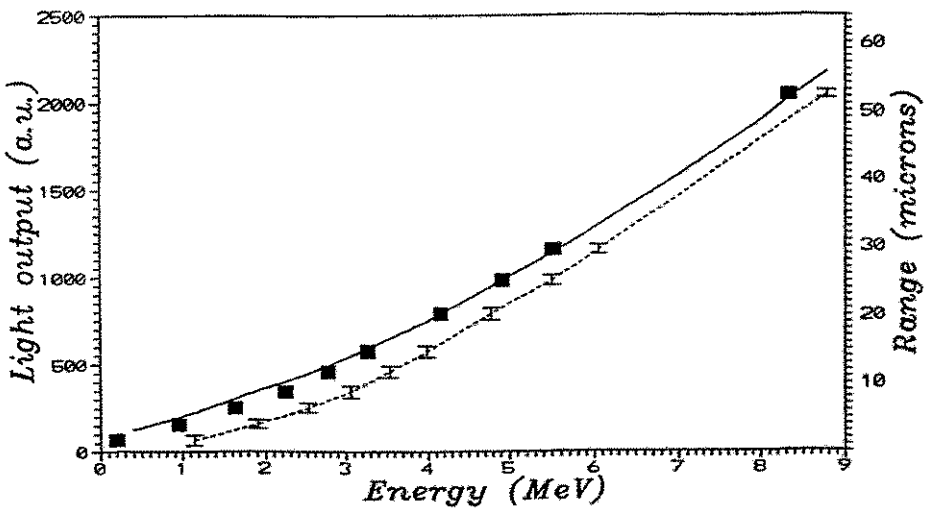

Fig. 1 Measured (dashed curve) and corrected (squares) light output data

[1] *Institut für Kern- und Hadronenphysik, FZR und Joint Institute for Nuclear Research, Dubna*

REFERENCES

[1] J.B. Birks, The Theory and Practice of Scintillation Counting, Pergamon (Oxford, 1964)
[2] W. Wagner et al., FLNR Scient. Report, JINR, Dubna, 1992
[3] J. Henniger et al., Report JINR, 6-84-366 (Dubna, 1984)
[4] D. Dorchoman et al., Report JINR, P1-10910 (Dubna, 1977)

First Tests of the Driftchamber HELITRON [B]

J. Mösner, W. Neubert, D. Wohlfarth, R. Kotte, S. Mohren[1],
L. Göbel and K.H. Hermann

In a further step towards completing phase II of the 4π-detector system FOPI the driftchamber HELITRON (see Refs. [1-5]) has been completed in 1993 as a result of common efforts by GSI Darmstadt, CRIP Budapest and FZ Rossendorf.
During the fall some sectors of the HELITRON have been tested by means of cosmic rays, ^{55}Fe source and Nd:YAG-laser. In December the HELITRON was placed into the superconducting solenoid (B=0.6T) in Cave B and first beam test measurements of three sectors have been performed using the reaction Kr (500 A*MeV) on Pb at the SIS of GSI.
Most of the aspects of wiring, installing and commissioning of the HELITRON have been described already in Refs. [6,7]. Here, we will supplement these reports by presenting some results of the test measurements.
Before installing the HELITRON into the magnet we measured the dependence of the pulse sizes on the potential wire voltage at different drift field voltages using cosmic rays and ^{55}Fe source. The gas mixture was 88% Ar, 2% Methane and 10% Isobuthane. By means of the laser beam we determined the drift velocity (without magnetic field) at different drift field strengthes. Considerable effort was necessary in order to avoid feed back oscillations and to reduce pick-up noise and high frequency disturbances. This task is not finished now. Further improvements have to be undertaken to reduce the noise.
During the beam time a drift voltage of 12.3 kV, corresponding to E=800 V/cm, and a potential wire voltage of 1.6 kV have been used. Data were taken in coincidence with the outer plastic wall (PLAWA) and several runs have been written on tape using part of the Heidelberg FADC system of the central drift chamber (CDC). The evaluation of these raw data is in progress. As an example, fig.1 shows a track crossing the sense wire plane of sector 1 between the wire numbers 20 and 21.
The staggering of ± 0.2 mm of the sense wires causes the time differences between the single hits and a smooth curve fitted to all hits. The result is shown in fig.2, where up to wire # 20 these differences have mainly positive values for even and negative ones for odd wire numbers and vice versa for wire numbers larger than 20. In fig.2 also the distributions of these time differences for odd and even wires are depicted. From a single hit one can deduce a mean standard deviation of about 7 ns which corresponds to a position resolution of 280 μm in the direction of drift velocity. Since this value strongly depends on the signal to noise ratio it should be improved by further reducing the pick-up noise. Nevertheless, fig.2 shows that the staggering should be well suited to distinguish wether the track passes the sector to the left or right side of the sense wire plane.
Fig.3 shows a track crossing the cathode plane separating adjacent sectors. Evaluating such tracks the radial coordinate r can be determined more precisely from drift distance measurements in the two sectors than by the charge division method. Thus, the charge division method can be tested. Moreover, such tracks are suited to determine the socalled Lorentz angle λ which means the drift angle caused by the magnetic field. Since the magnetic field within the volume of the HELITRON is rather inhomogeneous (especially the radial component of B is not negligible) this task is not trivial. A detailed knowledge of B as function of r and z is necessary in order to calculate the cathode crossing point and the angle λ. Evaluations are in progress.

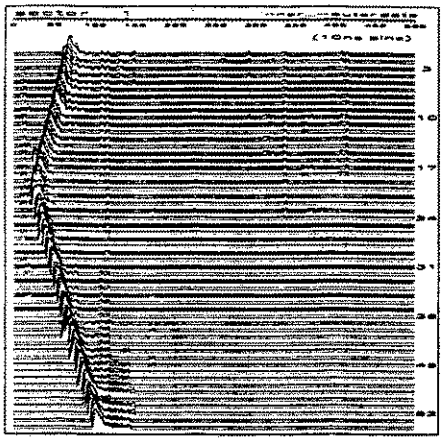

Fig.1 A track which crosses the sense wire plane. Shown are the raw data of the 54 sense wires of sector 1 from the preamplifieres at the inner and outer cylinder of the HELITRON.

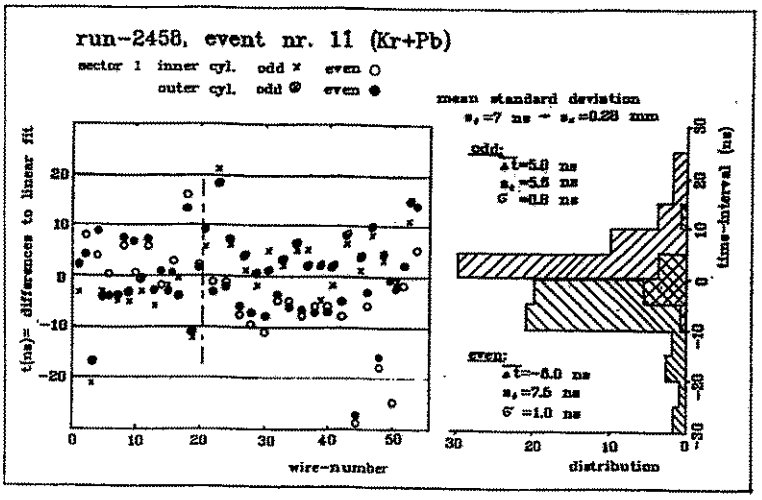

Fig.2 The distribution of the single hits of the track shown in fig.1. For explanation see text.

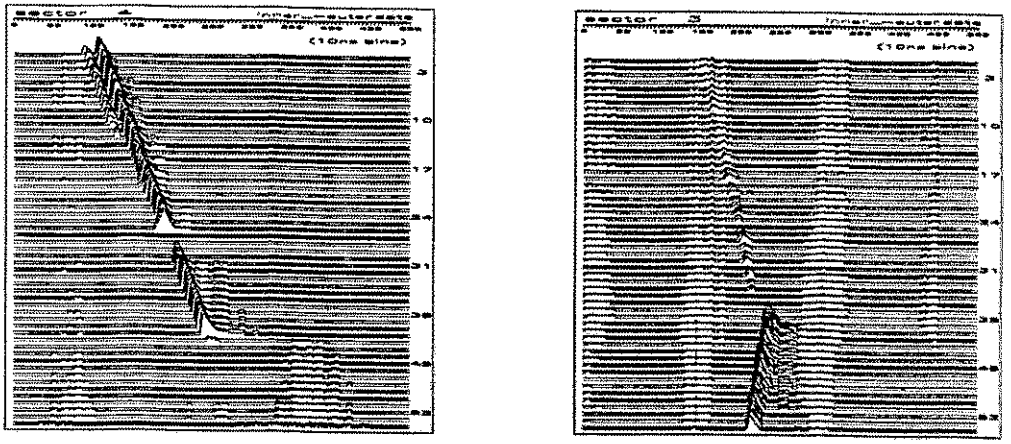

Fig.3 A track which crosses the cathode plane separating sectors 3 and 4. The particle passes from sector 4 to sector 3. Due to the radial component of the magnetic field the sense wires 39 to 41 were hit in both sectors. (The wires 27 to 30 in sector 4 have no signals because there preamplifieres were not connected.)

REFERENCES:

[1] Z. Fodor et al., GSI 91-1, p.302
[2] H.W. Daues et al., GSI 91-1, p.303
[3] J. Erö et al., GSI 92-1, p.352
[4] H.W. Daues et al., FZR 93-10, p.129
[5] G. Augustinski et al., GSI 93-1, p.372
[6] J. Kecskemeti et al., to be publ. in GSI 94-1
[7] H.W. Daues et al., to be publ. in GSI 94-1

Calibration of the FOPI plastic wall detector for Au + Au at 1GeV/u [B]

J. BIEGANSKY

During December 1992 the 4π-detector system was used to investigate collisions of Au on Au with 1 GeV per nucleon beam energy at the SIS of GSI, Darmstadt. Because of changes in the setup of the detectors as well as in the energy range, the calibration procedure for the plastic wall had to be adapted before it was executed. The plastic wall is an arrangement of 512 strips carrying a photomultiplier tube on each end obtaining an energy loss and a time signal from each tube. These raw data undergo several stages of data processing until they contain the information in the desired way (see ref.[1]). The time calibration has to take into account that there are individual differences between the tubes resulting from different strip lengths, aging effects and walk corrections. The walk behaviour is not stable for more than a few hours and has therefore to be corrected several times over the whole period of data aquisition. This requires a correction function for each channel(**Fig.1**). The resulting time distribution for all channels narrows(**Fig.2**). Finally an absolute time offset is determined by extracting the punch-through energy for protons and adapting the timescale until this point equals a value which is derived from energy loss calculations with respect to the given setup conditions.

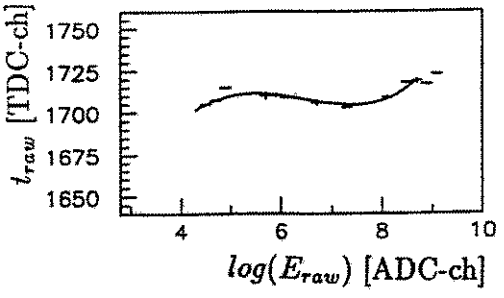

Fig.1: time walk, single tube spectrum with fitted polynom for linearization

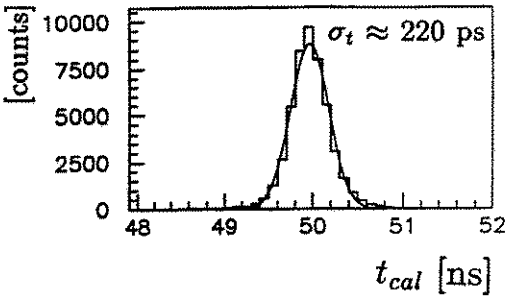

Fig.2: time distribution of 1024 channels after walk correction

The energy loss calibration starts with relative corrections due to different strip lengths and individual tube saturation. This correction is obtained by comparing the phototube signals to signals delivered by two photodiodes. Again a fit function is determined for each channel to correct nonlinearities in the tube amplification. The energy loss is normalized to *mil* units (minimum ionizing light, 1 $mil \Leftrightarrow 3.6\ MeV$) by comparing the measured signals to the Compton edge of γ-quanta emitted by a ^{60}Co source. The last step is to link all calibration parameter sets and provide them in a standard data format to enable our collaborators working with the plastic wall data.

REFERENCES:

[1] Thomas Wienold, thesis, GSI-Report 93-28

TP - MUSIC III: A Tracking Detector for all Elements between He and U [B]

T. Möhlenkamp, W. Seidel, M. Begemann-Blaich[1] Th. Hofmann[1], W. D. Kunze[1], V. Lindenstruth[1], U. Lynen[1,2], W. F. J. Müller[1], J. Pochodzalla[1,2], H. Sann[1], A. Schüttauf[2], W. Trautmann[1], A. Wörner[1] and B. Zwieglinsky[3] for the ALADIN-Collaboration

The TP - MUSIC III tracking detector (Time Projection MUltiple Sampling Ionization Chamber) at the ALADIN - spectrometer measures the position and the charge of the reaction products of heavy ion collisions at relativistic energies [1].
The system consists of a field cage with an active volume of $2 \times 1 \times 1.8\ m^3$ instrumented with 8 ionization chamber sections, each with 8 anodes, and 6 proportional counter modules (Fig.1). The charge Z of the fragments passing through the detector is determined by measuring the energy deposition in the counting gas. The track position parallel to the bending plane of the ALADIN magnet is deduced from the drift time of the electron cloud to the anodes or proportional counters. The track position perpendicular to the bending plane (Y) is determined by a charge division read-out of the proportional counters. One anode section on each side of the MUSIC detector was set up with sawtooth shaped anodes which allowed to determine the Y-position for particles with $Z \geq 10$ independent of the proportional counters. This redundant measurement was used to calibrate the non-linear response of the proportional counter charge division readout.
The anodes and proportional counters have complementary capabilities: The direct ionization measurement with the anodes gives a charge resolution of $\Delta Z = 0.4$ (FWHM) up to Uranium. The signal-to-noise ratio, however, restricts the usage of the anodes to $Z \geq 8$. The proportional counters, operated with a typical gas gain of 600, are sensitive to all particles with $Z \geq 2$. The charge resolution is $\Delta Z = 0.8$ (FWHM) for $2 \leq Z \leq 12$ but deteriorates for heavier fragments due to quenching (Fig.2).
A serious problem in the operation of all TPC-like detectors is the build-up of a space charge due to the drift of positive ions produced in the gas amplification process back into the active gas volume.

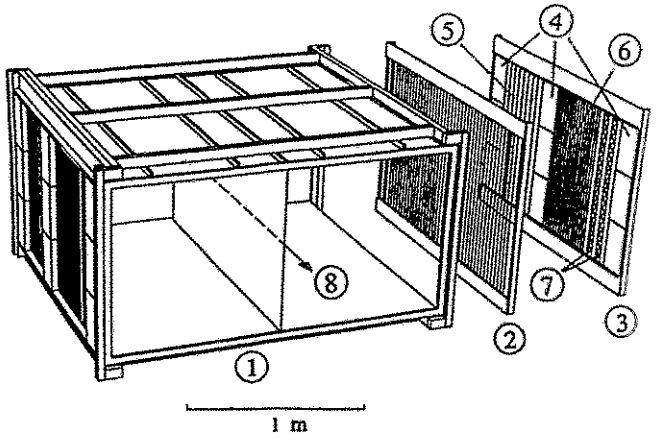

Fig.1 Schematic view of the improved TP-MUSIC III (looking upstream): The cathode is placed in the center of the field cage. The Frisch-grids are mounted at a distance of 1.0 m from the cathode. In each half of the detector, 24 anode stripes and 9 MWPC's measure the charge and two positions of the particles passing through.
1 - field cage separated by central cathode plane;
2 - rigth Frisch-grid; 3 - right anode plane; 4 - the 9 right MWPC's; 5 - anode stripes (8 x 6 cm); 6 - anode stripes (16 x 3 cm); 7 - two sawtooth shaped anode stripes (position sensitive in y-direction); 8 - beam direction

This is exacerbated in the current ALADIN setup by the requirement that the full primary beam passes through the detector. Therefore the proportional counters were equipped with a gating grid placed between anode wires and the Frisch-grid [2]. A potential difference of 160 V between adjacent wires prevents the drift of electrons or ions through the gating grid.

The gate is opened only after an accepted trigger and closed again after the maximal drift time has elapsed. This not only prevents the detection of uninteresting tracks and reduces detector loading but also suppresses the back drift of all positive ions. The gating grid driver circuits were placed inside the metal shielding boxes of the proportional counter modules to minimize cross talk into the ionization sections. The opening of the gate and the subsequent settling of the electronics require about $2\mu s$. Thus, only 10 cm of the drift region in front of the Frisch-grid has become inactive due to the gating.

The large range of primary ionization($\frac{dE}{dx} \propto Z^2, Z = 2, \ldots, 92$) combined with the charge division readout results in a range of proportional counter output signals of about 1:10000. To process this huge dynamic range a special shaping amplifier module was developed by the GSI-Elektronik-Experimente division. Each signal is split threefold and sent with relative gains of 1:6:36 into three sampling ADC channels.

The TP-MUSIC III detector was used in the most recent ALADIN experiment S114 with beams of Au with 600, 800 and 1000 MeV/u, Ar with 1000 MeV/u and U with 600 and 1000 MeV/u. Typical beam rates were 2000 particles/second, limited by the space charge caused by the primary ionization of the beam.

The counters worked reliably and were stable over the whole time of nearly six weeks. Despite the copious production of long-range δ-rays in the counter gas by heavy fragments or beam particles we were able to set the readout threshold of the proportional counters below the amplitude of α-particles. The correlation of the charge measured in the MUSIC detector and the charge measured in the time-of-flight system, which is located behind the MUSIC field cage, is shown in Fig. 3. Both detector systems combined achieve an unambiguous charge determination for all nuclei with $2 \leq Z \leq 92$. The analysis of the data is still in progress. The combination of the fragment velocity deduced from the time-of-flight wall with the momentum inferred from the tracking information of the TP-MUSIC system will allow full kinematic reconstruction of multifragmentation events.

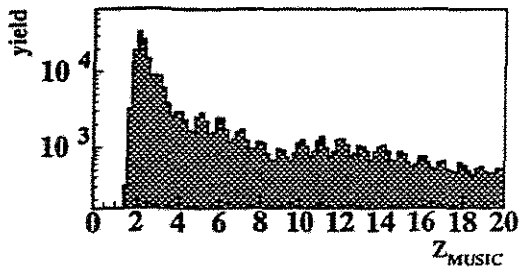

Fig.2 Charge spectrum of fragments detected by the proportional counters for Z<20.

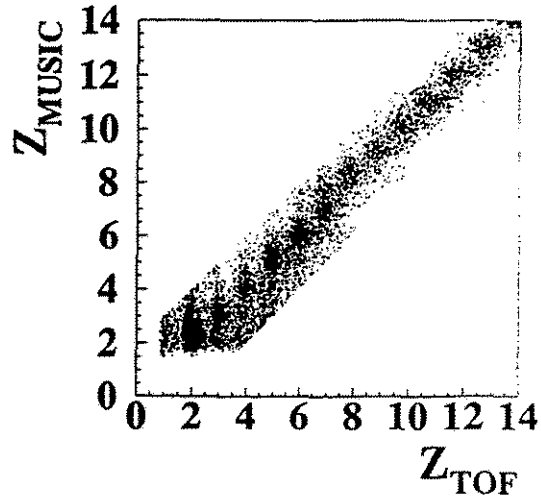

Fig.3 Charge measured by the MUSIC correlated with the charge measured by the TOF wall.

[1]GSI Darmstadt
[2]Uni. Frankfurt/M
[3]SINS Warszawa

REFERENCES:

[1] W. Seidel et al., GSI scientific report 1991 page 359 and Jahresbericht 1991, FZR 92-09, page 73

[2] Z.-A. Lui et al., GSI scientific report 1990 page 298

Particle Identification in a Wide Dynamic Range Based on Pulse-Shape Analysis with Solid-State Detectors

G. PAUSCH[1], W. BOHNE[2], D. HILSCHER[2], H.-G. ORTLEPP, D. POLSTER[2]

The efforts to exploit pulse-shape information for particle identification in solid-state detectors [1] have been continued. Based on a simple simulation code, we studied the influence of detector properties (internal electric field profile) and methods of signal processing on the particle discrimination [2]. A new technique of particle identification resulting from these investigations was tested at the VICKSI accelerator.

We irradiated a commercial 500μm Si-detector (active area: 450 mm^2, transmission mount) with heavy ions produced in reactions of a 698 MeV ^{32}S beam with a mixed {Au + Ni + C} target. The detector was placed at a distance of 16.5 cm from the target with the low-field side (rear side of the detector!) facing the target. We derived the energy information as usual by means of a charge-sensitive preamplifier combined with a spectroscopic amplifier (shaping time: 1μs). As proposed in [2] we exploited for particle identification the time shift t_Q of the first moment, i.e. the centre of gravity of the current pulse, measured with respect to a time-of-flight start signal.

However, instead of scanning the current signals with flash ADC's we used a simple and cheap method to measure t_Q: The bipolar output of a conventional spectroscopic amplifier (SPA) reacts on a delta-like current pulse in the detector (corresponding to a step-like charge signal) with a zero crossing at a fixed time t_0. If the current flow in the detector has a finite duration Δt, and if this Δt is small compared to the linear part of the slope region near the zero crossing of the SPA output signal, the shift of the zero crossing with respect to t_0 is just given by the first moment of the current signal. Therefore we used a second spectroscopic amplifier (bipolar output; shaping time: 0.25μs) followed by a zero-cross trigger, and measured t_Q as the time difference between the zero crossing and the subsequent RF signal from the accelerator. This technique needs no "fast" timing signal from the detector.

The results are illustrated in figs.1–2. The charge numbers of ions up to $Z = 16$ can be identified within a dynamic range of $\approx 1 : 5$ (e.g. 3...14 AMeV for Carbon, 5...23 AMeV for Silicon ions) where the upper limit is given by the maximum energy deposition in a Si detector of 500μm thickness. The lower energy limit for Z identification corresponds to a particle range of 40...50μm. For energies near the punch-through point we were able to resolve isotope lines up to Magnesium. The resolution of the t_Q measurement was found to be $\approx$ 1 ns for Carbon ions of $\approx$ 160 MeV.

The test experiment showed that the dynamic range for particle identification based on pulse-shape analysis can be drastically extended by the technique proposed in [2]. The described scheme of signal processing is well suited and cheap enough to be exploited even in large multi-detector arrays.

[1] Freie Universität Berlin, [2] Hahn-Meitner-Institut Berlin

References:

[1] G. Pausch et al., Nucl. Instr. and Meth. A322 (1992) 43.

[2] G. Pausch, W. Bohne, and D. Hilscher, Nucl. Instr. and Meth. A337 (1994) 573.

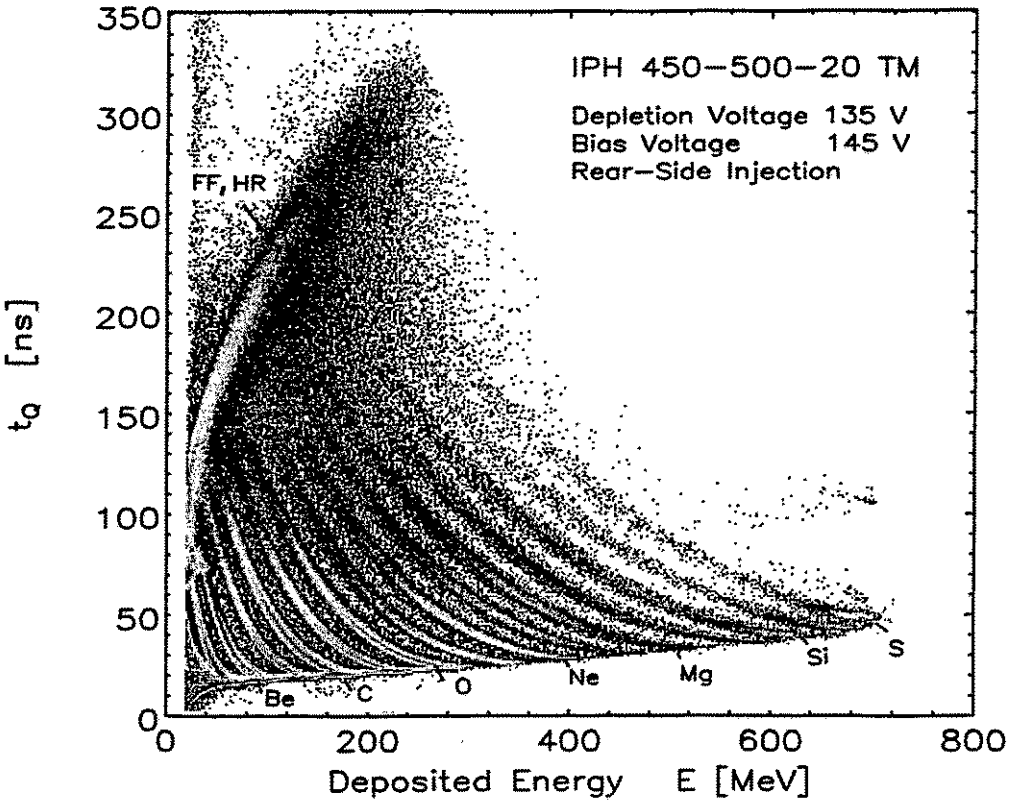

Figure 1. Two-dimensional representation of the count rate versus energy deposition E and the particle-sensitive parameter t_Q (which represents a combination of pulse-shape information and time-of-flight [3]). The resolved lines are due to ions with different Z; to resolve isotope lines one has to zoom the spectrum. The lower limit of Z identification is due to the bump of fission fragments (FF) and heavy residues (HR). The t_Q measurement for these particles is falsified due to the long duration of the current pulses (up to $0.6\mu s$).

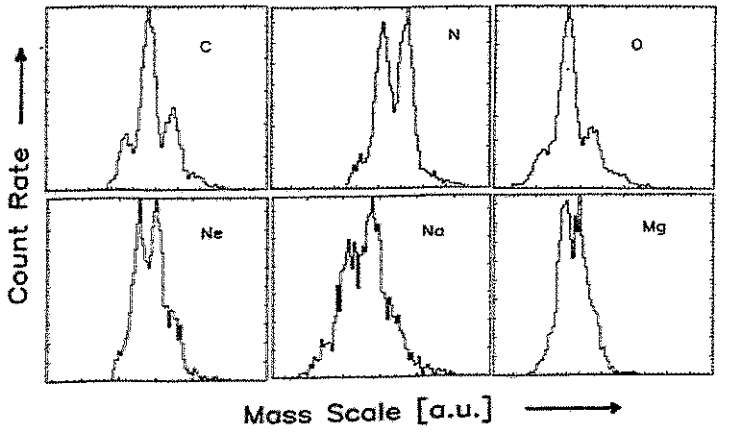

Figure 2. Isotope separation obtained for selected elements and energies near the punch-through point.

COSMIC RAY TRACKING BY STREAMER TUBES [B]

U. Brandt [1], K. Daumiller [1], P. Doll [1], H. O. Klages [1],
P. Kleinwächter, G. Kolb [1], P. Manfrass,
H. Müller [1], L. Smykov [2]

Self quenching streamer tubes of the IAROCCI type [1] are widely used in high energy and cosmic ray physics, especially for muon and electron detection [2]. The KASCADE collaboration [3] intends to take advantage of this kind of detectors in order to distinguish between the electromagnetic and muon component of extensive air showers close to the shower core. In a first test set-up we used three horizontal planes of streamer tubes with the dimensions 1.5m x 1m in a vertical distance of 1m from each other (fig. 1). Typically, a streamer tube has the following characteristic: 8mm x 8mm cell size, 1.50m length, cathode resistivity of about 100 $k\Omega/cm^2$. A twofold 8-cell comb profile is enclosed in a gas tight PVC box. At one end of the streamer tube the anode wires are connected together after passing an end plug of the comb profile. The tubes are filled with an argon/isobutan mixture in the ratio 1:3 at atmospheric pressure. The high voltage applied to the anode wires is 4.9 kV. If a cosmic particle strikes the streamer tube the produced charge cloud will influence signals in Cu-strips which are arranged parallel (x-direction, strip widths 6mm, pitch 10mm) and orthogonal (y-direction, strip width 12mm, pitch 16mm) to the anode wires. In most cases, several adjacent strips give a response per impinging particle depending on a complicated function of capacitances and resistances between wire, cathode, influence strip and ground, respectively. More systematic investigations concerning this problem are in progress.

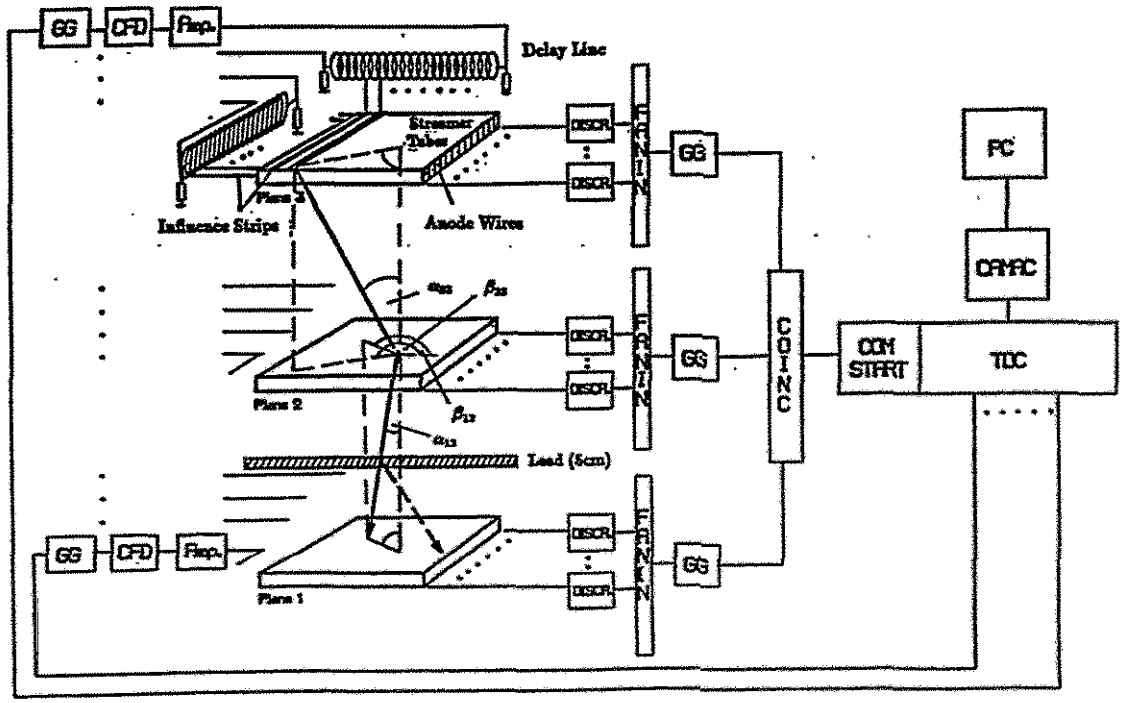

Fig. 1 Scheme of the experimental set-up and the angular relations used in the data processing

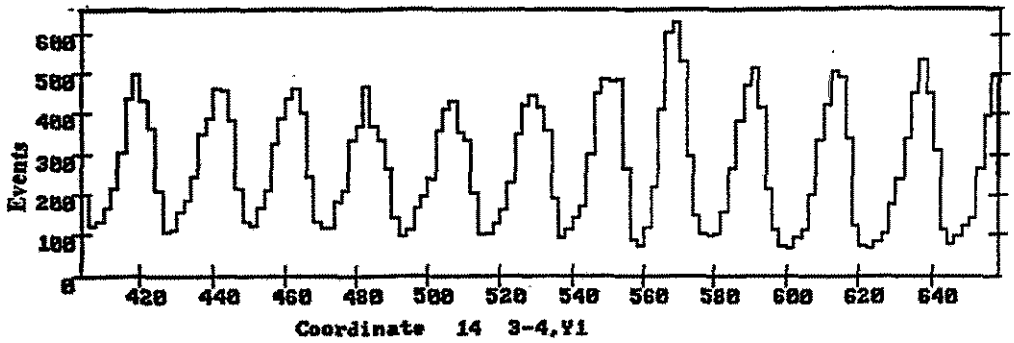

Fig. 2 Streamer tube response function in y-direction as a part of the middle plane measured with cosmic particles

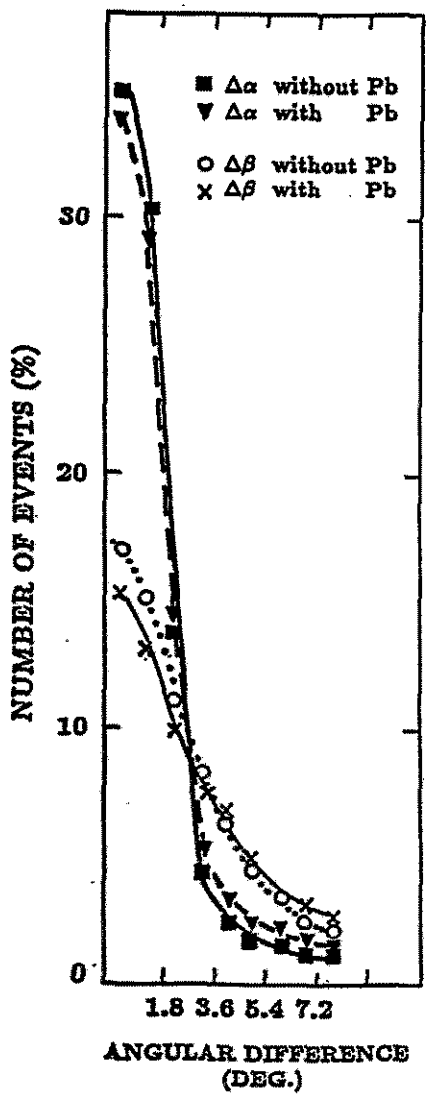

Fig. 3 Distributions of the angular differences $\Delta\alpha$ and $\Delta\beta$ with and without lead layer. The symbols represent mean values of $\pm 0.45^o$.

After anode wire triggering the charge pulses induced in the strips run through delay lines in both directions yielding time coordinates from the TDC which are converted in real position values by subtraction. Fig. 2 shows a typical streamer tube response function for the y-direction pointing to a position resolution in the order of the strip width. For each recorded cosmic particle track the angles α_{ij} and β_{ij} with respect to the middle plane were calculated as well as the angular differences $\Delta\alpha = |\alpha_{12} - \alpha_{23}|$ and $\Delta\beta = \|\beta_{12} - \beta_{23}| - \pi|$ to estimate the ratio of the hard and soft components of the penetrating cosmic particles. About 16.000 tracks were stored without and with a lead layer (5cm thickness) arranged between planes 1 and 2 of the experimental set-up. In fig. 3 the results of statistical calculations are presented. Clearly, the bulk of data ($\sim 65\%$) are forward peaked for $\Delta\alpha < 2^o$ indicating to the hard components (muons) of the cosmic rays as expected [4]. The influence of the lead layer can be recognized as well. The corresponding distributions are broader in comparision to the former case.

[1] *Kernforschungszentr. Karlsruhe, KASCADE Collaboration*
[2] *Joint Institute for Nuclear Research, Dubna, Russia*

REFERENCES:

[1] E. Iarocci, Nucl. Instr. and Meth. 217(1983)30
[2] M. Aglietta et al., Nuovo Cim. 13(1990)353
[3] P. Doll et al., KfK 4686 (1989)
[4] Review of Particle Properties, P.L. B204(1988), p. 61

Improvements of the Winding Machine for Multi Wire Detector Planes

M. Sobiella, M. Freitag, J. Hutsch, H. Krug[1], P. Manfrass

In ref. [1] we reported on the construction of a winding machine suitable for the manufacturing of large multi wire planes for gaseous detectors. There were mentioned several problems that decreased the accuracy in wire positioning and that required efforts for improvement. On the basis of extensive vibration measurements at different components of the machine the frame has been modified to damp these oscillations. Furthermore, the wire supply unit has been optimized.

In order to quantify the wire position accuracy the wire distances of the most of the planes have been measured by means of a PC-coupled high-resolution length measuring system. A few prominent results are displayed in fig. 1. In the diagrams the deviation of the distance D_i between two adjacent wires i and $i+1$ from the mean wire distance $\bar{D} = (\sum_{i=1}^{N} D_i)/N$ is plotted versus the wire number i for planes made from 20 μm thick tungsten wires. The standard deviations of the wire distances are additionally given.

Finally it should be mentioned that the performance, especially the flexibility, of the control software [2] has been considerably improved.

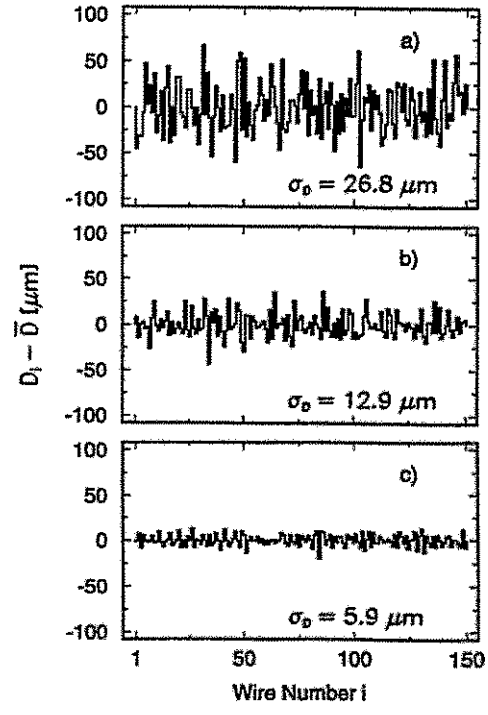

Fig. 1 Development of the accuracy during the optimization of the mechanical construction of the winding machine.

- **a)** Initial status (April 1993)
- **b)** Status (November 1993) after the optimization of the machine
- **c)** As b), but after an additional adjustment of the wires.

[1] *Zentralabteilung Forschungs- und Informationstechnik, FZR*

REFERENCES

[1] M. Sobiella et al., Research Centre Rossendorf, Inst. of Nuclear and Hadronic Physics, Annual Report 1992, **FZR 93-10**, p. 115

[2] H. Krug et al., Research Centre Rossendorf, Inst. of Nuclear and Hadronic Physics, Annual Report 1992, **FZR 93-10**, p. 116

The Integration of Fastbus Components in the Experiment Data Acquisition System at the COSY - Jülich[B]

S. Dienel[1], K.W. Leege[1], W. Oehme[1], H. Müller, B. Prietzschk, B. Rimarzig, Ch. Schneidereit, N. Brummund[2], M. Karnadi[2], R. Nellen[2], K.H. Watzlawik[2], M. Drochner[3], W. Erven[3], J. Holzer[3], P. Wüstner[3] and K. Zwoll[3]

The concept of the Experiment Data Acquisition System is based on distributed computers (Workstation, VME, CAMAC, FASTBUS) arranged in a hierarchical structure. Its basic layout has already been presented in [1,2,3,4] in more detail. All functions of this computer system and the standards of the communication within the system are realized as a client/server model. It is defined in close analogy to the ISO/OSI reference model (layer 7), respectively the MMS standard [5]. The set of definitions developed for the COSY experiments is called Experimental Message Specification (EMS) [6]. The communication is based on TCP/IP via Ethernet and the transfer of measured data is performed using the VICbus. This client/server concept requires clients working as requestors of the EMS-Servers and EMS-Servers working as responders. The clients are mainly processes running at the workstation (master control, instrumentation system control), which enable experiment preparation, experiment control, run control,...[1,2,3]. Each EMS-Server supplies a set of functions which are similar from the clients point of view but specific realized in the front-end area depending on the type of the so called Virtual Experimental Device (VED). The most important functionality of the EMS-Servers consists in the front-end setup, subevent/event readout and in writing events on a tape (event builder). For the experiments at the 0°-facility (ZDF) it was proposed to use FASTBUS modules from Phillips Scientific (TDC's and QDC's) especially for coupling and readout of Start-Stop-Detectors. The contribution of the group at the FZ Rossendorf mainly consists in the integration of these components as so called FBMB instrumentation system in the global concept.

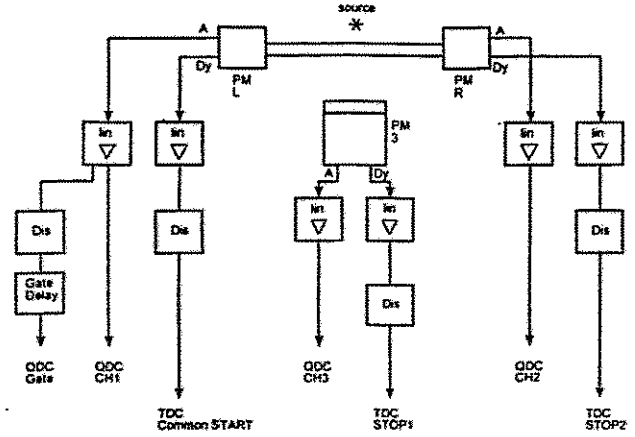

Fig.1 Test arrangement

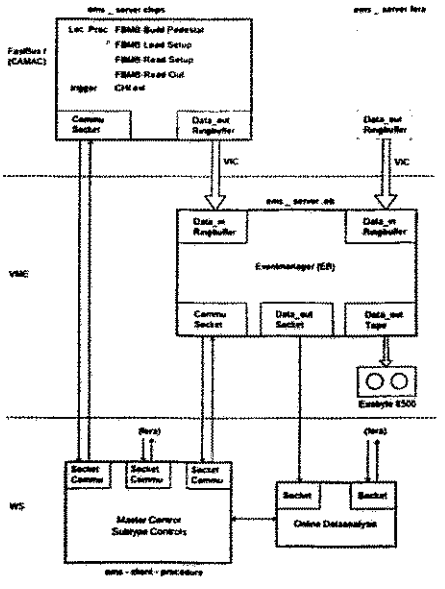

Fig.2 Server structure of the test experiment

This requires a special instrumentation system control process (FBMB) with an OSF/MOTIF interface at the workstation which must be embedded in the environment

of master control and other subcontrol processes at the clients side. On the other hand we have added a set of EMS-Server functions (Readout, LoadSetup, ReadSetup, BuildPedestal, TestFunctions and Trigger routines) at the EMS-SERVERs side running on the intelligent Fastbus Controller (CHI). Additionally we have built in a so called TestReadout function both at workstations and EMS-SERVERs side. The major goal of this feature is to obtain informations about the behaviour of the modules produced by Phillips Scientific.

In order to test the described parts of the data acquisition system a first very simple test experiment has been carried out using the arrangement shown in Fig.1. It consists of a radioactive source in front of two scintillators. The first is coupled to the photomultipliers PML and PMR, the second to PM3. From each photomultiplier two signals for amplitude and time measurements are digitized via QDC and TDC modules. In Fig.2 the server structure of the test experiment and in Fig.3 the data transfer from the FASTBUS modules to the workstation is schematically depicted. The data are stored event by event. Any desired graphical representation can be realized on-line as well as off-line. As an example a two-dimensional scatter plot of the correlated amplitudes of PML and PMR is shown in Fig.4.

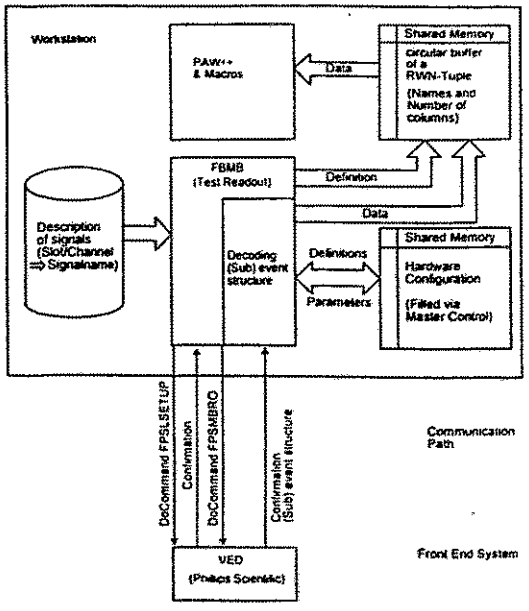

Fig.3 The principle of Test Readout of one Philips Scientific Instrumentation System with a configurable PAW-Interface

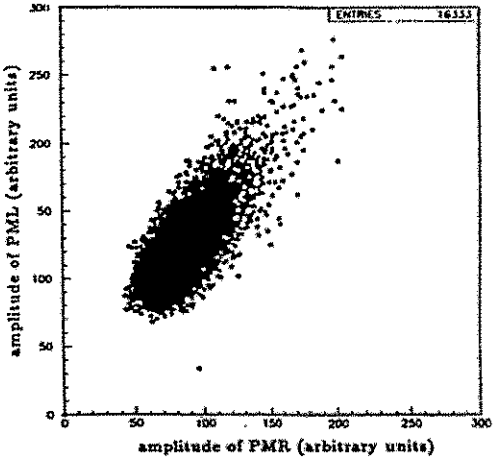

Fig.4 Correlation between the amplitudes in the photomultipliers PML and PMR

[1] Zentralabteilung Forschungs- und Informationstechnik, FZR
[2] Forschungszentrum Jülich, Institut für Kernphysik DV
[3] Forschungszentrum Jülich, Zentrallabor für Elektronik

REFERENCES:

[1] K. Zwoll et al., Conference Record RT93, 8.-11.6.93 Vancouver, BC, Canada

[2] K.H. Watzlawik et al., IKP Annual Report 1991, p. 276, FZ Jülich

[3] K.H. Watzlawik et al., IKP Annual Report 1992, p. 36, FZ Jülich

[4] N. Brummund et al., Annual Report 1992, FZR 93-10, 132

[5] MMS - Manufacturing Message Specification ISO 9506

[6] K. Zwoll et al., FZ Jülich, IB-KFA-ZEL 501293

A Real Time to Digital Converter (RTDC) for on-line Position Measurement applied to the COSY-TOF Stop Detector[B]

F. GABRIEL[1], P. MICHEL, K. MÖLLER[2], A. SCHAMLOTT AND A. SCHÜLKE

A new concept for the design of the stop detector region at COSY-TOF consists in covering the barrels by 96 straight scintillators which are read out at each end via 90° light reflectors and s-bent light guides [1]. The particle coordinate in z-direction (along the scintillator) can be determined by measuring the time difference of light output pulses at both ends. Since the TOF-spectrometer should be optimized for measuring reactions with low cross sections the first level event trigger has to select the hit pattern of interesting processes and to supress the dominant trivial reactions as e. g., elastic scattering. In the TOF stop detector the position along the straight scintillators is related to the reaction angle θ of the ejectiles. Thus, together with the coplanarity contraint an on-line identification of elastically scattered protons is possible. Due to the conversion time of conventional TDC's the information on the position can be obtained only off-line and can not be included in fast trigger processing.

Therefore, we developed a new TDC in real time technique based on a 2.5 GHz clock start-stop counter [2]. Fig.1 shows a simple schematic layout of the TDC. We used electronic circuits of a new ultra high speed ECL-family (Motorola) to operate at this relatively high frequency. These became commercially available and inexpensive some months ago.

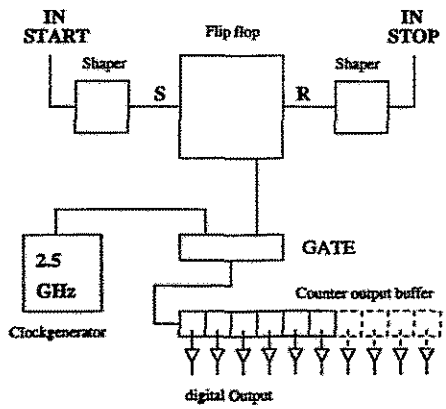

Fig.1 Schematic layout of the GHz-start-stop counter

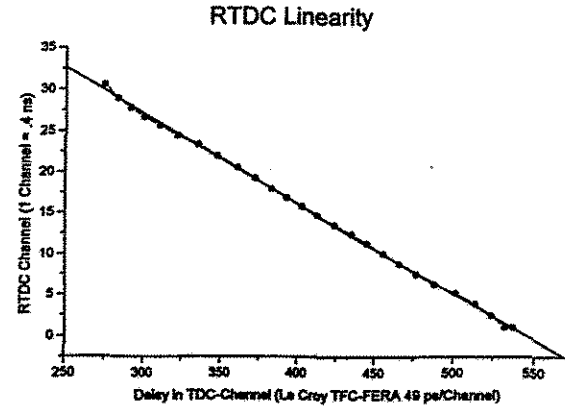

Fig.2 Measured linearity of the RTDC

Fast impulse shaping steps are necessary to process the input signals coming from discriminators . By means of a fast flip flop a gate signal is produced with the length of the start to stop time difference. The spikes of the 2.5 GHz clock are counted in a binary counter cascade during the gate time intervall (LSB=400ps) which is asynchronous to the acquisition clock. Digital outputs are enabled from the stop signal, and the gate length is limited by giving a reset to the flip flop with the start signal trailing egde. To prevent ground problems and feedback effects the layout of the

circuitry has to meet all demands of equipments operating in the GHz region, which could be realized in the present case. Fig.2 shows the measured linearity of the TDC. The differential non-linearity was determined to be ± 50ps. The input (stop signal)-output delay of the module as a result of signal propagation in electronic elements and strips amounts to less than 500 ps.

To test the module we measured the time resolution (sigma) of the delay time distribution which can be calculated precisely by probability theory using the fact of asynchronity of the clock generator. The theoretical sigma ranges quadratically from 0 to 0.5 LSB: $\sigma = \sqrt{\chi - \chi^2}$, where χ is the fractional portion of the time in excess of an integer number of LSB. Fig.3 shows a plot of the standard deviation for each of the mean values plotted in Fig.2 together with the theoretical curve due to the asynchronous clock.

Since the measured points are in a good agreement with this curve, it can be assumed that the RTDC does not cause an additional intrinsic time dispersion at 2.5 GHz. Therefore, the maximum uncertainty for the measurement of time intervalls is 0.5 LSB and corresponds to a σ of 200 ps.

For test purposes we implemented a single channel RTDC in a passive CAMAC module. To apply the fast TDC concept for the TOF trigger processing we are now developing a RTDC CAMAC module containing 16 start stop channels and combining the RTDC function with additional logic operations.

The module will provide a 16 bit output word composed of timing information, binary encoded channel number and fixed bits reflecting system parameters.

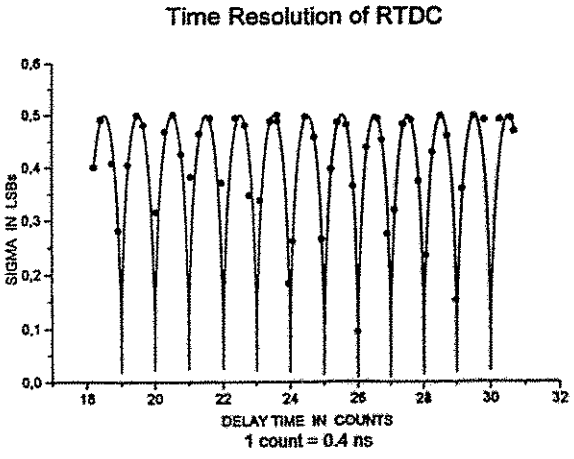

Fig.3 Measured time resolution of the RTDC

[1] Zentralabteilung Forschungs- und Informationstechnik, FZR

[2] Institut für Kern- und Teilchenphysik, TU Dresden und
Institut für Kern- und Hadronenphysik, FZR

REFERENCES:

[1] P. Michel et al., this Annual Report

[2] F. Gabriel, P. Michel, FZR 94 - 30

Software Development for FOBOS [B]

C.-M. Herbach, V.V. Trofimov[1], V.E. Shuchko[1], L. Dietterle[2], D.V. Vakatov[1]

In 1993 the development and implementation of the data acquisition /1/ and analysis system for the first FOBOS experiments /2/ have been finished. The system includes the modified HOOPSY /3/ data acquisition system, the modified OLYMP /4/ data analysis system, the ATHENE /5/ on-line/off-line data analysis program and several newly developed software components providing the data communications between the front-end and back-end electronics.

The experimental data are received via the VSB bus from the read-out system (CAMAC controllers) driven by a VME front-end system (ELTEC operating with the OS9 system). The commands are generated from the HOOPSY system running on a μVAX under VMS and loaded to the VME system via Ethernet. The data storage system is based on a 2 Gbyte disk of a SPARC station running under SUN-OS. The SPARC disk system is included in the logical disk space for the HOOPSY by using the MULTINET package on the VAX computer. All experimental data are stored as raw-data files.

On-line data monitoring and analysis are provided by the ATHENE system running on a PC AT. The on-line access to the experimental data on the SPARC station is realized by NFS and user written routines working with open shared files. These files are accessable for write request from HOOPSY and read request from ATHENE, simultaneously.

Off-line data analysis is available by using ATHENE on the PC's and/or OLYMP on the VAX computer.

[1] *Joint Institute for Nuclear Research, Dubna*

[2] *Institut für Kern- und Hadronenphysik, FZR und Joint Institute for Nuclear Research, Dubna*

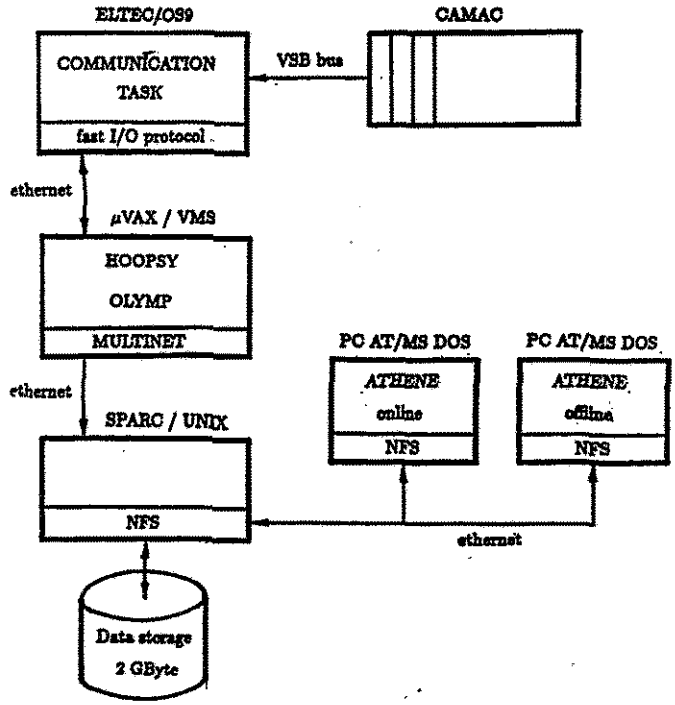

Fig. 1 Data processing of the FOBOS data acquisition system

REFERENCES

[1] O.V. Strekalovskij et al., this Annual Report

[2] A.A. Aleksandrov et al., this Annual Report

[3] G. Roeschert et al., Report HMI-436 (Berlin, 1986)

[4] OLYMP User's Manual, Report HMI (Berlin, 1992)

[5] C.-M. Herbach et al., Annual Report 1991 (FZ Rossendorf) FZR 92-09 (1992) 61

The FOBOS Data Acquisition System in 1993 [B]

O.V. Strekalovskij[1], S.I. Ivanovskij[1], H.-G. Ortlepp[2], G. Pausch[3], G. Renz[2], V.V. Trofimov[1], W. Wagner[2], V.E. Shuchko[1]

The data acquisition system as has been used in the first experiments with FOBOS /1/ is shown in fig. 1. Seven CAMAC crates containing the front-end electronics and STR 610/CBV CAMAC-to-VSB interfaces have been connected via VSB Differential Bus Extension (VDB) to a VME workstation (ELTEC EUROCOM 6, 25 MHz) serving as an event builder. Addressed read-out based on recognized event patterns has been performed.

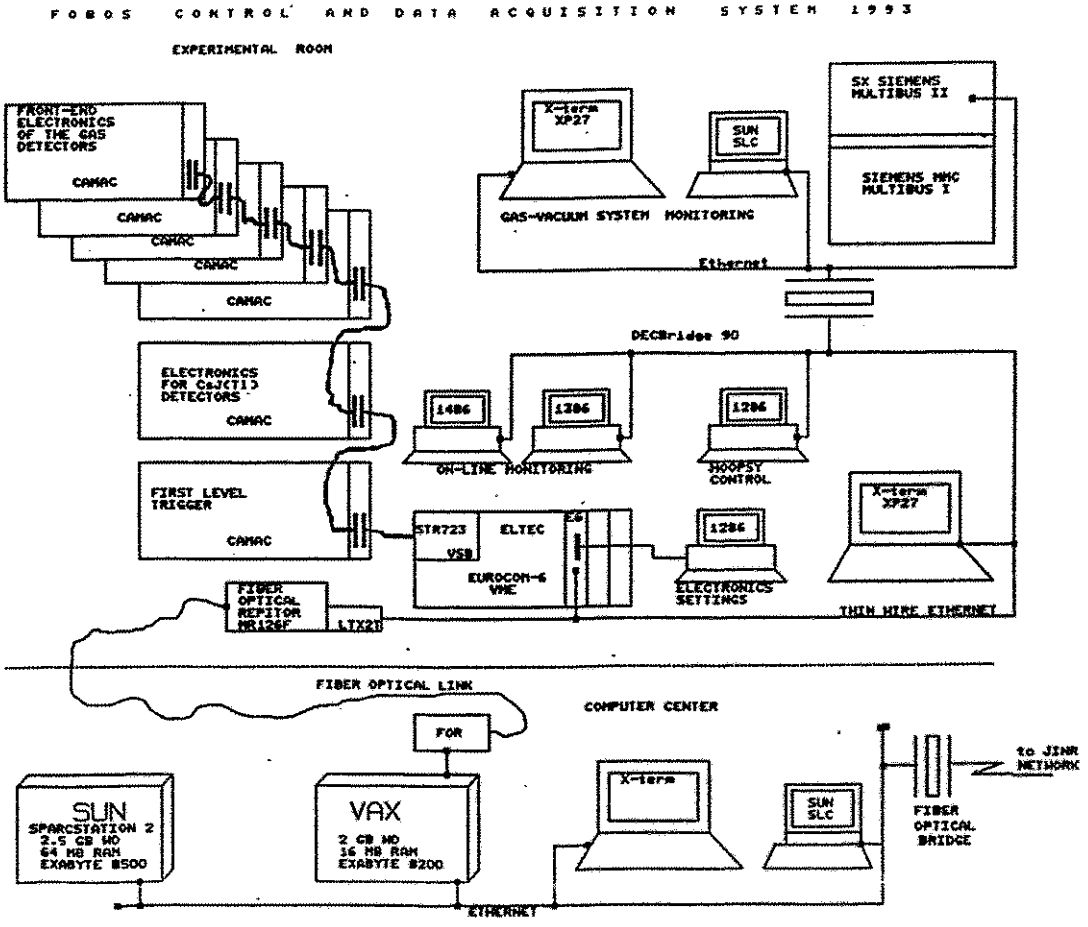

Fig. 1 The FOBOS control and data acquisition system

The ELTEC is connected to a special Ethernet segment and further by a fiber-optic link to a μVAX in the computer center. The HOOPSY data acquisition control software /2/ resident at the μVAX has been modified for VME and successfully applied in a FOBOS-ARGUS experiment at HMI Berlin /3/.

The data collected on the disk of the Sparcstation 2 are stored on Exabyte tape. Quasi-on-line monitoring of collected data is performed by several PC's with the help of the ATHENE data analysis software /4/ having access via LAN to data just written on disk.

A DEC bridge-90 has been installed to connect with a SUN SCL computer, which controls the gas-vacuum system of FOBOS based on SIEMENS-SX- Multibus-II /5/.
The upgrade of the FOBOS data acquisition system by a FASTBUS minicrate containing STR330/CPU CERN Host Interface (CHI) is presently in progress. A STR330/VSB I/O-Port, a STR330/LAN Ethernet module, six 96-channel charge-integrating ADCs (C.A.E.N. F683C) and one 96-channel TDC handle the information of the 210 CsI(Tl) detectors of the FOBOS scintillator shell /6/ and the 92 phoswich detectors of the ARGUS forward array /7/. The STR330/VSB module allowes any VME bus processor to directly access the data memory of STR330/CPU.

[1] *Joint Institute for Nuclear Research, Dubna*
[2] *Institut für Kern- und Hadronenphysik, FZR und Joint Institute for Nuclear Research, Dubna*
[3] *Freie Universität Berlin*

REFERENCES

[1] A.A. Aleksandrov et al., this Annual Report
[2] G. Röschert et al., Report HMI-436 (Berlin, 1986)
[3] G. Pausch et al., Annual Report 1992 (FZ Rossendorf) FZR 93-10 (1993) 99
[4] C.-M. Herbach et al., Annual Report 1991 (FZ Rossendorf) FZR 92-09 (1992) 61
[5] G. Renz et al., this Annual Report
[6] W. Wagner et al., FLNR Scient. Report, JINR, Dubna, 1992
[7] W. Terlau et al., Annual Report 1989 (HMI Berlin) HMI-482 (1990) 93

Status of the Software Development for the FOBOS Gas Vacuum System [B]

C. UMLAUF[1], D. MAY[1], G. RENZ[1]

Last year the existing control software /1/ was extended by several additional features and the graphic visualization of the status of the gas vacuum system on X-terminals was improved. The visualization software worked successfully during the experiments in 1993.
The periodic output of the actual pressure values on the screen was extremly speeded up. The repetition period takes now about 200 ms, what became possible by replacing routines with functions of the XMove-Toolkit by our own routines written using Xlib. Nevertheless, it became obviously that the performance of the SX- multiprocessor system is not efficient enough to run more tasks with extensive graphical output. That's why we decided to develop and run the software for on-line analysis of the pressure-time behaviour separately on a SUN station. The necessary cyclic data transfer to the SUN station is realized via special TCP/IP socket programming.
The use of this workstation offers additionally the possibility for a more comfortable graphic visualization and an effective software design using the CERN PAW package. The pressure-time behaviour of any of the 64 measuring points can now be displayed. Each on-line diagram shows the pressure trend at one of the measuring points during the past 30 minutes (see fig. 1).

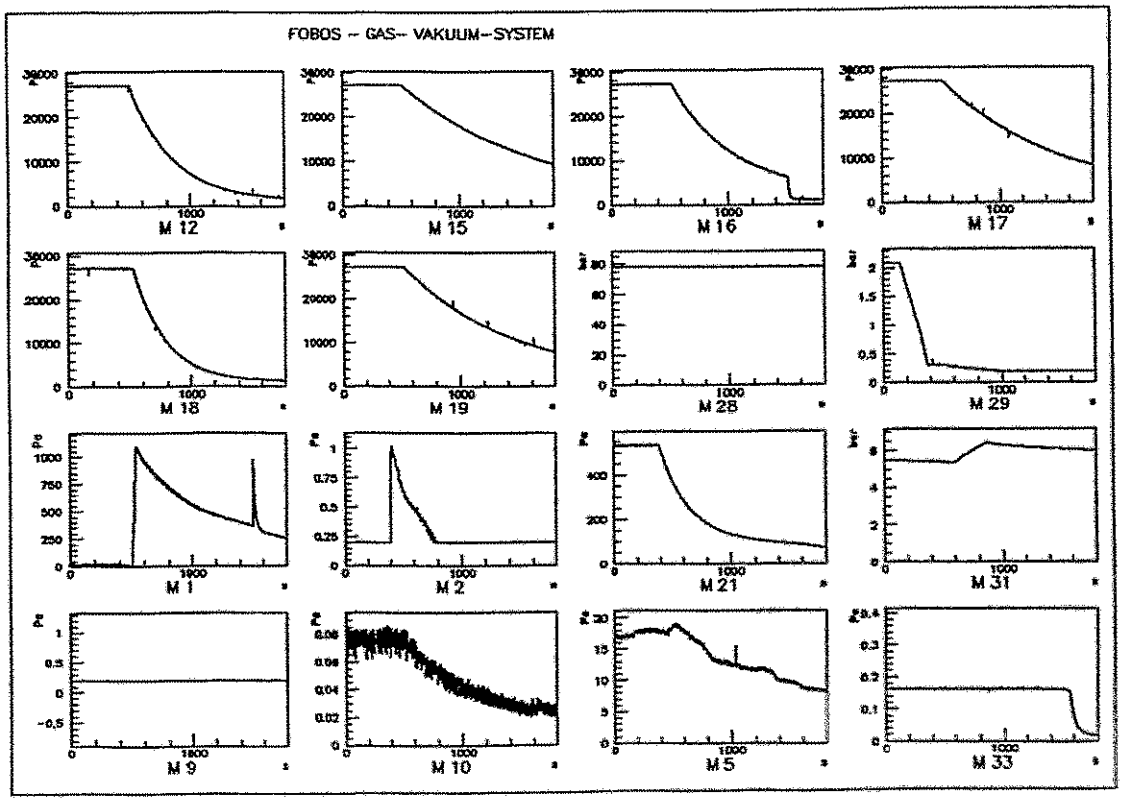

Fig. 1 Pressure-time behaviour during evacuation of FOBOS BIC's

Simultaneously, the data can be written on hard disk for further analysis. Programs for subsequent off-line graphic display and for conversion to PC spread sheet format have been written. Hardcopies are also possible.
On the SX system, first routines and programs for error handling have been implemented. In case of an error, a message window with explaining text for error handling is opened and an acoustic signal warns the user. If the pressure values exceed the permitted range, high voltage is switched off automatically, or switching on is locked by sending kill-signals to the C.A.E.N. high voltage systems.
First utility programs with user-friendly graphic interface for creating and editing the necessary configuration files for the control software have been developed.

[1] *Institut für Kern- und Hadronenphysik, FZR und Joint Institute for Nuclear Reaearch, Dubna*

REFERENCE

[1] G. Renz et al., Annual Report 1993 (FZ Rossendorf) FZR 93-10 (1993) 122

Development of Data Acquisition Electronics for FOBOS

K. Heidel, H.-G. Ortlepp[1]

Constant-Fraction-Discriminator CFT 5386

The development of data acquisition electronics for FOBOS [1] has been continued by building up the Constant-Fraction-Discriminator (CFT) 5386 as CAMAC 1M module. The CFT was designed for the processing of signals provided by a specific preamplifier for the large avalanche counters. Each module contains 3 CFT for the processing of fast timing signals. In the subnanosecond timing region the device has much better properties than a conventional CFT. If the rise and fall times of the detector signals are smaller than 1ns a time resolution of 200ps has been achieved in the large dynamical range of 100 : 1.
The CFT was developed using high performance ECL technology. The input pulse is fed to a dual comparator (Analog Devices 96687). The control of the working conditions is performed via the CAMAC dataway.
The lay-out is manufactured from 4-layer bord designed by PCAD and produced in mixed technology.

Technical data

Input Pulse	-3mV...-3500mV, 50Ω, dc-coupled
Output Pulse	NIM at 50Ω,width 25ns
Threshold	0mV...1000mV, adjustable 1mV/lsb
Delay	external
Walk	internal stabilization
Fraction	0.22, fixed

CAMAC-functions

F(17)A(1,2,3)	write control register CFT1,2,3 W1...W10 Threshold, W11 enable
F(1)A(1,2,3)	read control register CFT1,2,3 R1...R10 Threshold, R11 enable
F(2)A(0)	read response register R1...R3 actual CFT1...CFT3

[1] *Institut für Kern- und Hadronenphysik, FZR, und*
Joint Institute for Nuclear Research, Dubna

REFERENCE:
[1] Heidel,K.,Ortlepp,H.-G., Annual report 1992, FZR 93-10, 136

Depth Distributions of Positron-emitting Nuclei Generated by Ion Beams in Thick Targets[B]

W. Enghardt[1], P. Blochberger[2], B.G. Hasch, G. Kraft[3], K. Lauckner, P. Manfrass, J. Pawelke, D. Schardt[3], M. Sobiella

In ref. [1] we reported on in-beam positron emission tomography (PET) measurements which revealed that the spatial distribution of positron-emitting nuclei generated by a beam of ^{20}Ne with an energy of 406 MeV/u has a prominent peak near to the range of these particles. We assume that this behaviour provides the unique opportunity of an on-line and in-situ control of the tumour therapy with light ion beams by means of PET. A simple calculation [1] predicted that also beams of ^{12}C and ^{16}O, which are of special interest for the therapy, should produce a β^+-emitter distribution with a pronounced maximum.

In order to measure the spatial distribution of the β^+-emitters along the beam direction, experiments with beams of ^{12}C ($E = 85 \ldots 330$ MeV/u), ^{16}O ($E = 200 \ldots 400$ MeV/u) and ^{20}Ne ($E = 300$ MeV/u) have been carried out at the beam of the heavy ion synchrotron SIS at GSI. The beam of stable ions has been stopped in phantoms of polymethylmethacrylate (PMMA) or graphite mounted between two position sensitive block detectors of 8×8 BGO crystals [2]. These detectors operate in coincidence and form a very small limited angle positron camera having a field of view (FOV) with a cross section of 5.4×5.4 cm^2. In order to obtain information on the whole depth distributions of the induced positron emitters, the target has been moved beam up and down through the FOV in steps of 3.125 mm by means of a step motor driven linear table [3].

Annihilation events have been registered in list mode in the pauses between the synchrotron pulses. The list mode data comprise information on the position where the block detectors have been fired, the energy of the detected γ-rays, the coincidence time, the singles and coincidence rates as well as the current phantom position. From these we reconstructed the range distributions (fig. 1) by calculating the intersection points of the event lines with the plane, which is parallel to the detector surfaces and comprises the beam axis, and by projecting these 2D distributions onto the beam axis. The results of figs. 1a,b,c show that the therapeutically relevant beams generate a β^+-emitter distribution with a maximum in the vicinity of the range of the primaries due to projectile fragmentation. It is interesting to note that a clear maximum can be even identified after irradiating a phantom with only one synchrotron pulse of 3×10^7 ^{16}O particles (fig. 1e).

To develop an algorithm for extracting the primary particle range from the positron emitter distributions we refined the simulation program of ref. [1]. The code includes the longitudinal and transverse momentum transfer in the projectile fragmentation, the range and angular straggling during the stopping process, furthermore, all generations of fragments as well as the positron ranges are taken into account, whereas the absorption, scattering and the angular correlation of the annihilation radiation, the time dependence of the beam intensity as well as the efficiency and the spatial resolution of the detector have been neglected during the calculation of fig. 1f. Nevertheless, the shape and the position of the peak is rather well predicted giving rise to the hope to be able to extract the primary beam range from the positron emitter distributions.

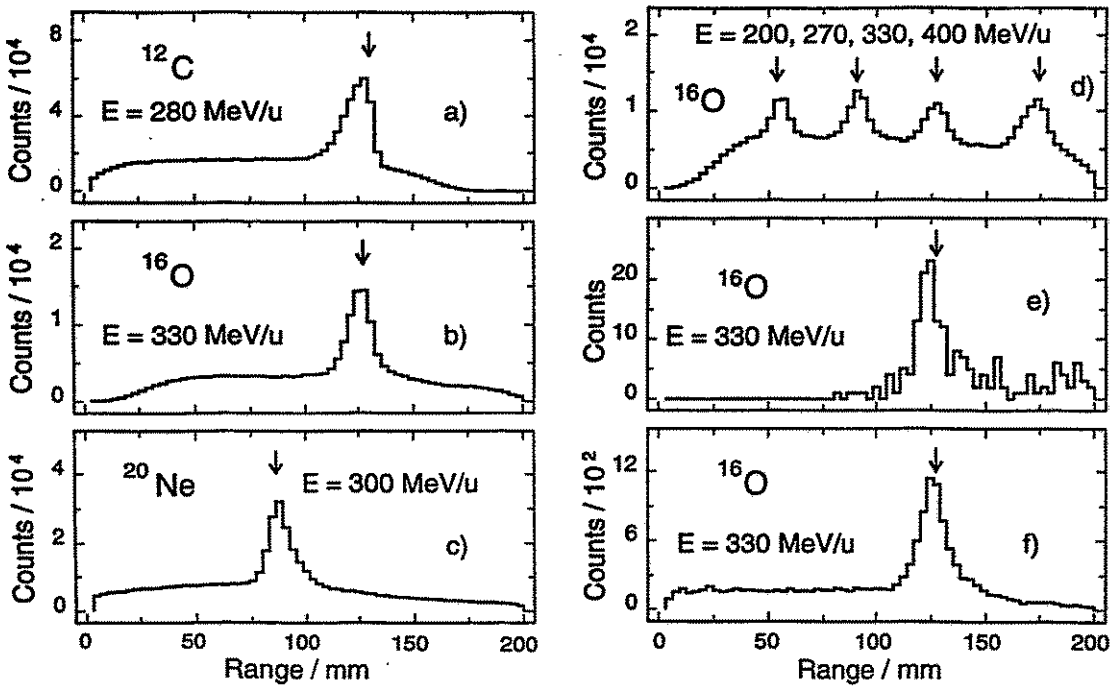

Fig. 1 Range distributions of β^+-emitters induced by beams of light ions in a PMMA phantom. The arrows indicate the calculated ranges of the primary particles.

- **a)** Distribution obtained during 2 hours of irradiation with about 3×10^{10} ^{12}C particles.
- **b)** Distribution obtained during 1 hour of irradiation with about 2×10^{10} ^{16}O particles.
- **c)** Distribution obtained during 2 hours of irradiation with about 4×10^{10} ^{20}Ne particles.
- **d)** Distribution obtained during 2 hours of irradiation with about 3×10^{10} ^{16}O particles of four different energies that were cyclically changed every 2 s from synchrotron pulse to pulse.
- **e)** Distribution obtained from only one beam pulse of 3×10^{7} ^{16}O particles and a subsequent decay measurement of 10 min.
- **f)** Simulation result obtained from 10^5 histories assuming an infinitely short ^{16}O beam pulse and the decay of all produced positron emitters.

[1] *Uniklinikum der TU Dresden und Institut für Kern- und Hadronenphysik, FZR,*
[2] *Uniklinikum der TU Dresden,*
[3] *GSI Darmstadt*

REFERENCES

[1] W. Enghardt et al., Phys. Med. Biol. **37** (1992) 2127
[2] J.G. Rogers et al., IEEE Trans. Nucl. Sci. **NS-39** (1992) 1063
[3] J. Pawelke et al., Research Centre Rossendorf, Inst. of Nuclear and Hadronic Physics, Annual Report 1992, **FZR 93-10**, p. 142

On the Monte-Carlo Simulated Spatial Distribution of Positron-emitting Nuclei Generated by Relativistic Light Ion Beams in Organic Matter[B]

B. G. Hasch, W. Enghardt[1]

For particles heavier than beryllium, fragmentation of swift projectiles penetrating a thick target leads to a spatial distribution of positron-emitting nuclei peaked in the immediate vicinity of the ion beam range. The spatial distribution of the annihilation points of the positrons which are emitted from the β^+-active isotopes created in this fragmentation process can be measured by the techniques of in-beam positron emission tomography (PET) with a BGO positron camera. In order to make use of this distribution measurement for the in-situ control of the tumour therapy with light ions it has to be shown that it is possible to extract precisely the range of the ion beam from the spatial distribution of the positron emitters. Therefore, we have refined the Monte-Carlo simulation of ref. [1] to study this relationship.

The simulation is organized as a chain of three steps. In the first step the spatial distribution of the annihilation points of the positrons emitted from the β^+-active isotopes produced by fragmentation of the projectiles and the target atoms is created. The code for this first step includes the stopping process with straggling of energy loss and angular scattering and the nuclear projectile and target fragmentation with a semiempirical treatment of the reaction kinematics. Furthermore, the range distribution of the positrons depending on the emitting isotopes is taken into account. All caluclations are done in three dimensions considerating all generations of fragments. In addition, this step returns the accompanying three dimensional dose distribution. This dose distribution is shown in fig. 1c as the projection onto the beam axis. In the second step the time dependence of the beam intensity and the fact that only in the pauses between the synchrotron pulses the data accquisition is enabled is taken into consideration. The deviation from co-linearity of the two photons emitted in the annihilation process, the movement of the phantom between the two detector heads of the BGO positron camera, the spatial resolution of the detectors and the scattering and attenuation of the photons are addressed in the third step. Comparing the measured distribution in fig. 1a and the simulated distribution in fig. 1b some differences are obviously. The position of the peaks of figs. 1a,b differ because the stopping process is modelled by using the modified relativistic Bethe-Bloch formula in a simple parametrisation which overestimates the specific energy loss and therefore leads to smaller ranges. The shape depends on the ratio of the partial fragmentation cross section. In considering that the parametrisation [2] of the partial nuclear fragmentation cross sections we are using is developed for the nuclear fragmentation of heavy nuclei with a atomic mass $A > 40$ at very high energies and therefore, the difference between the calculated partial cross sections and the available experimental ones is partly rather large, the peak shapes of the simulated and of the experimental distribution are in quite good agreement. Furthermore, the flat part at low and high ranges caused by target fragmentation is obviously smaller in the simulation than in the experiment. Uncertainties in the partial fragmentation cross sections and a description of the fragmentation process which restricts to only one fragment neglecting all secondary fragments could cause this difference.

All important processes are now implemented in the MC simulation code and we are focussing our further work on the resolving of the referred problems to create a model as the basis for the developement of a reliable algorithm to extract the range of the primary projectiles from the spatial distribution of the positron-emitting isotopes.

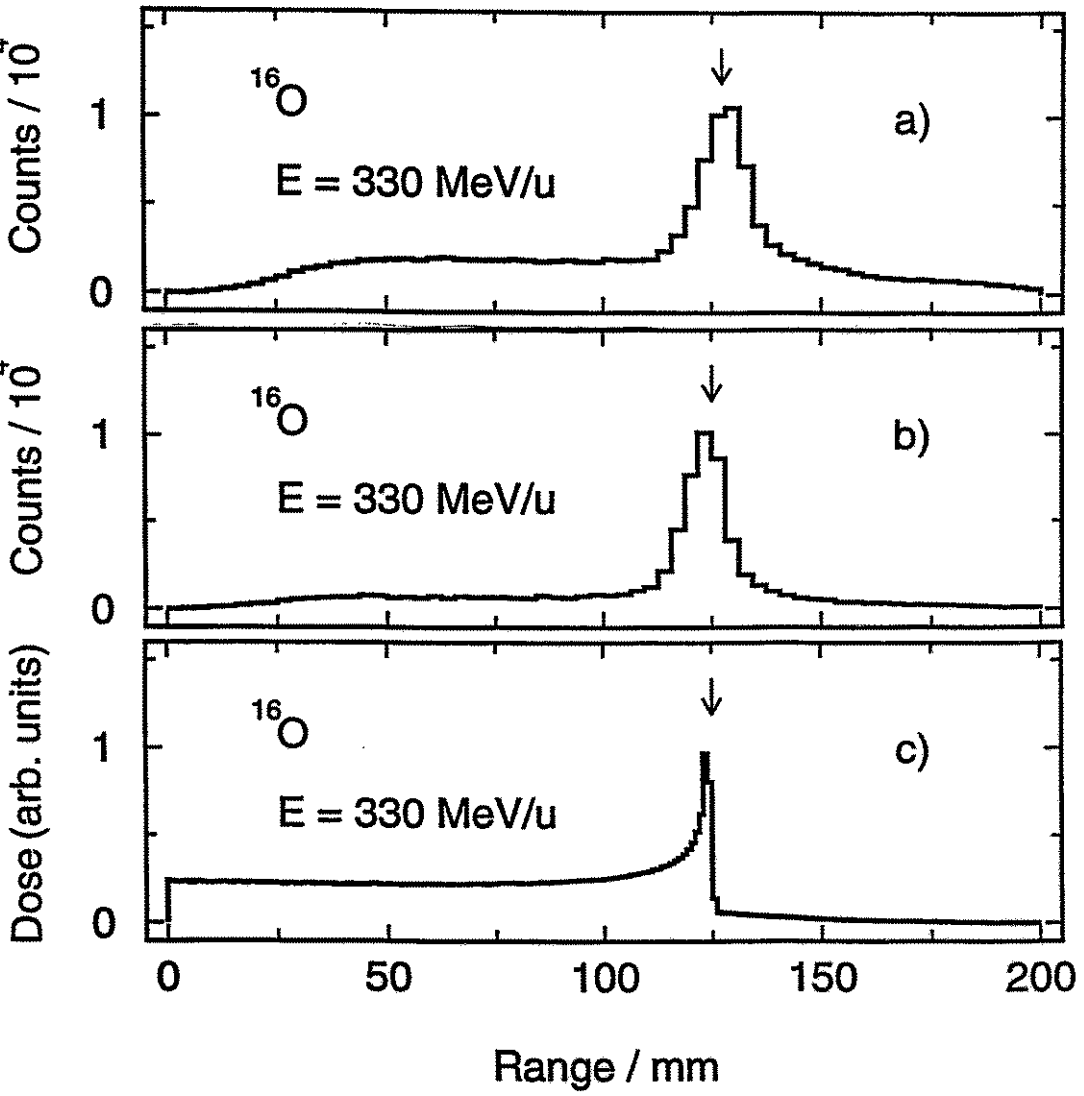

Fig. 1: Comparison between the experiment and the simulation. The arrows indicate the calculated range of the primary projectiles.

- **a)** Range distribution of β^+-emitters induced by a beam of ^{16}O in a PMMA phantom obtained during 1 hour of irradiation with about 2×10^{10} ^{16}O particles.
- **b)** Range distribution of β^+-emitters simulated by the described MC code.
- **c)** Bragg curve corresponding to the simulated range distribution.

[1] *Uniklinikum der TU Dresden und Institut für Kern- und Hadronenphysik, FZR*

REFERENCES:

[1] W. Enghardt et al., Phys. Med. Biol. **37** (1992) 2127
[2] K. Sümmerer et al., Phys. Rev. **C42** (1990) 2546

FASA - A 4π detector setup for the investigation of target multifragmentation in nucleus-nucleus collisions
(Nucl. Instr. Meth. A332 (1993) 149)

Avdeyev, S.P., V.A. Karnaukhov, W.D. Kuznetsov, L.A. Petrov, R. Barth, V. Lips, H. Oeschler, O.V. Bochkarev, L.V. Chulkov, E.A. Kuzmin, I.G. Mukha, V.A. Olkin, G.B. Yankov, W. Karcz, Y.T. Vidaj, W. Neubert and E. Norbeck

Abstract: The FASA setup, installed at the JINR synchrophasotron providing light ion beams with energies up to 3.65 GeV/nucleon, is a fragment multiplicity detector, consisting of 55 scintillation counters made of thin CsI(Tl) films, five time-of-flight telescopes and a large-area position-sensitive parallel-plate avalanche chamber. The basic aim of the device is to determine with high precision the energy, mass, and velocity of the fragments detected in the time-of-flight telescopes (TOF) while for the other fragments global multiplicity information is obtained. Therefore, the TOF telescopes serve as a trigger. In addition, angular correlations and distributions and relative velocity correlations for coincident fragments can be measured with the FASA setup.

A Dedicated 0° Facility for Threshold Particle Production Studies at COSY
(Physica Scripta 48 (1993) 50)

Büscher, M., K. Sistemich, V. Abaev, U. Bechstedt, P. Birien, W. Borgs, W. Cassing, S. Dienel, H. Dombrowski, S.V. Dshemuchadse, J. Ernst, R. Eßer, A. Franzen, D. Gotta, D. Grzonka, A. Hardt, F. Hinterberger, M. Ivanov, L. Jarczyk, B. Kamys, St. Kistryn, H.R. Koch, V.I. Komarov, V. Koptev, S. Kopyto, A. Kozela, A. Krykin, K.W. Leege, H. Müller, W. Oehme, W. Oelert, H. Ohm, R. Santo, Chr. Schneidereit, O.W.B. Schult, H. Seyfarth, V. Shelkov, J. Smyrski, A. Strzalkowski, K.-H. Watzlawik, B.Zh. Zalyhanov, N.I. Zhuravlev and P. Zolnierczuk

Abstract: A universal facility is in preparation for the study of particle production in proton-nucleus reactions below the nucleon-nucleon threshold. The device will be located at the internal target position TP2 at COSY-Jülich and will consist of three dipole magnets. This 0° Facility will separate ejectiles from the circulating proton beam and allow momentum and angle analysis both for positively and negatively charged particles. A major goal of the experimental program is the investigation of the K^+-meson production at projectile energies below the NN threshold. The detector concept for these studies is described and also an overview over further planned experiments is given.

A highly-segmented ΔE-time-of-flight wall as forward detector of the 4π-system for charged particles at the SIS/ESR accelerator
(Nucl. Instr. Meth. A324 (1993) 156)

Gobbi, A., J.P. Alard, G. Augustinski, Z. Basrak, N. Bastid, I.M. Belayev, Th. Blaich, P. Boccaccio, R. Bock, S. Boussange, A. Buta, R. Caplar, C. Cerruti, R.J. Charity, N. Cindro, J.P. Coffin, M. Crouau, F. Daudon, J.F. Devin, P. Dupieux, J. Erö, Z.G. Fan, C. Fayard, P. Fintz, Z. Fodor, L. Fraysse, R. Freifelder, S. Frolov, E. Gimenez, Y. Grigorian, G. Guillaume, N. Herrmann, K.D. Hildenbrand, S. Hölbling, F. Hornecker, A. Houari, S.C. Jeong, M. Jorio, F. Jundt, J. Kecskeméti, P. Koncz, Y. Korchagin, R. Kotte, M. Krämer, C. Kuhn, A. Lebedev, I. Legrand, C.F. Maguire, V. Manko, M. Marquardt, T. Matulewicz, S. Mayade, G. Mgebrishvili, J. Mösner, D. Moisa, G. Montarou, I. Montbel, P. Morel, W. Neubert, R. Neunlist, G. Ortlepp, D. Pelte, M. Petrovici, F. Rami, W. Reisdorf, M.A. Saettel, E. Sahuc, G. Savinel, Z. Seres, D. Schüll, B. Sikora, V. Simion, S. Smolyankin, U. Sodan, M.H. Tanaka, K.M. Teh, R. Tezkratt, B. Tischler, M. Trzaska, M.A. Vasiliev, D. Vincent, P. Wagner, J. Weinert, J.P. Wessels, T. Wienold, Z. Wilhelmi, D. Wohlfarth and A.V. Zhilin

Abstract: At the SIS/ESR accelerator facility at GSI in Darmstadt the 4π-detector system FOPI is under construction at present. It is designed for the investigation of central collisions of heavy ions in the energy range up to 2 A GeV. As phase I of this detector a forward wall has been built and used in various experiments. It comprizes a total number of 764 scintillators with an additional shell of 188 thin ΔE-detectors in front of it and covers the full azimuth of the polar angles from 1° to 30°. The velocity and the nuclear charge of the fragments are determined by a combined time-of-flight and ΔE measurement.

II. Publications and Talks

1. Publications

Argaman, N., F.-M. Dittes, E. Doron, J.P. Keating, A.Yu. Kitaev, M. Sieber and U. Smilansky:
Correlation in the Actions of Periodic Orbits Derived from Quantum Chaos;
Phys. Rev. Lett. 71 (1993) 4326

Avdeyev, S.P. et. al, W. Neubert:
FASA-A 4π detector setup for the investigation of target multi-fragmentation in nucleus-nucleus collisions;
Nucl. Intr. Meth. A332 (1993) 149

Baldsiefen, G., U. Birkental, H. Hübel, N. Nenoff, B.V. Thierumala Rao, P. Willsau, J. Heese, H. Kluge, K.H. Maier, R. Schubart, S. Frauendorf:
First Observation of a Crossing of Oblate Dipole Bands in the A=200 Region;
Phys. Lett. B298 (1993) 54

Barz, H.W., W. Bauer, J.P. Bondorf, A.S. Botvina, R. Donangelo, H. Schulz and K. Sneppen:
Charged-particle correlations in 600 A·MeV gold induced disassembly reactions, a statistical multifragmentation analyses;
Nucl. Phys. A561 (1993) 466

Begemann-Blaich, M. et al.., W. Seidel:
QMD Simulation of Multifragment Production in Heavy Ion Collisions at E/A=600 MeV;
Prog. Part. Nucl. Phys. 30 (1993) 181;

Begemann-Blaich, M., W.F.J. Müller, J. Aichelin, J.C. Adloff, P. Bouissou, J. Hubele, G. Imme, I. Iori, P. Kreutz, G.J. Kunde, S. Leray, V. Lindenstruth, Z. Liu, U. Lynen, R.J. Meijer, U. Milkau, A. Moroni, C. Ngô, C.A. Ogilvie, J. Pochodzalla, G. Raciti, G. Rudolf, H. Sann, A. Schüttauf, W. Seidel, L. Stuttge, W. Trautmann and A. Tucholski:
Quantum molecular dynamics of multifragment production in heavy ion collisions at E / A = 600 MeV;
Physical Review C48 (1993) 610
Preprint GSI 93-29, Apr. 1993

Brokstedt, A., J. Lytkens-Lindén, M. Bergström, L.P. Eckström, H. Ryde, J.C. Barcelar, J.D.Garrett, G.B. Hagemann, B. Herskind, F. R. May, P.O.Tjom, S. Frauendorf:
Interpretation of Bands in ^{163}Er within the Tilted Rotation Scheme;
Nucl. Phys. A557 (1993) 469c

Büscher, M., K. Sistemich, V. Abaev, U. Bechstedt, P. Birien, W. Borgs, W. Cassing, S. Dienel, H. Dombrowski, S.V. Dshemuchadse, J. Ernst, R. Eßer, A. Franzen, D. Gotta, D. Grzonka, A. Hardt, F. Hinterberger, M. Ivanov, L. Jarczyk, B. Kamys, St. Kistryn, H.R. Koch, V.I. Komarov, V. Koptev, S. Kopyto, A. Kozela, A. Krykin, K.W. Leege, H. Müller, W. Oehme, W. Oelert, H. Ohm, R. Santo, Chr. Schneidereit, O.W.B. Schult, H. Seyfarth, V. Shelkov, J. Smyrski, A. Strzalkowski, K.-H. Watzlawik, B.Zh. Zalyhanov, N.I. Zhuravlev and P. Zolnierczuk:
A Dedicated 0° Facility for Threshold Particle Production Studies at COSY;
Physica Scripta 48 (1993) 50

Cassing, W., A. Peter and A. Pfitzner:
A non-perturbative transport approach including particle collisions and density fluctuations;
Nucl. Phys. A561 (1993) 133

Döring, J., J.W. Holcomb, T.D. Johnson, M.A. Riley, S.L. Tabor, P.C. Womble and G. Winter:
Energy of the $4^{(+)}$ isomer and new bands in the odd-odd nucleus ^{74}Br;
Phys. Rev. C47 (1993) 2560

Döring, J., L. Funke, R. Schwengner and G. Winter:
Three-quasiparticle excitations in ^{77}Br;
Phys. Rev. C48 (1993) 2524

Frauendorf, S.:
Tilted Cranking;
Nucl. Phys. A557 (1993) 259c

Frauendorf, S. and V.V. Pashkevich:
Shapes of Na Clusters;
Z. Phys. D26 (1993) 98

Freund, S., J. Altmann, F. Becker, T. Burkardt, J. Eberth, L. Funke, H. Grawe, J. Heese, U. Hermskens, K.H. Maier, T. Mylaeus, H. Prade, S. Skoda, W. Teichert, H.-G. Thomas, A. v. d. Werth and G. Winter:
Identification of excited levels in the N=Z+1 nucleus ^{73}Kr;
Phys. Lett. B302 (1993) 167

Gobbi, A. et al., R. Kotte, J. Mösner, W. Neubert, D. Wohlfarth:
A highly-segmented Δ-E-time-of-flight wall as forward detector of the 4π-system for charged particles at the SIS/ESR accelerator;
Nucl. Instr. Meth. A324 (1993) 156

Gorelik, G. and H. Rotter:
Freiheit gegen Bürgschaft;
zum 25. Todestag von Lew Landau,
Physikalische Blätter 49 (1993) 115

Herzberg, R.D., P. von Brentano and I. Rotter:
Evidence for trapping and collectivization of resonances at strong coupling;
Nucl. Phys. A556 (1993) 107

Iskra, W., I. Rotter and F.M. Dittes:
Hierarchical trapping of resonance states at high level density;
Phys. Rev. C47 (1993) 1086

Iskra, W., M. Müller and I. Rotter:
Selforganization in the nuclear system. I: The slaving principle;
J. Phys. G: Nucl. Part. Phys. 19 (1993) 2045

Jolos, R., P. von Brentano and F. Dönau:
Barrier Pentration Effect on the Angular Momentum Dependence of the Parity Splitting in Actinide Nuclei;
J. Phys. G: Nucl. Phys. 19 (1993) L151

Kämpfer, B., R. Kotte, J. Mösner, W. Neubert, D. Wohlfarth, J.P. Alard, Z. Basrak, N. Bastid, I.M. Belayev, Th. Blaich, A. Buta, R. Caplar et al. (FOPI collaboration):
Velocity correlations of intermediate mass fragments produced in central collisions of Au + Au at E = 150 A MeV;
Phys. Rev. C48 (1993) R955

Kämpfer, B., A.I. Titov, E.L. Bratkovskaya:
Estimates of dielectron produ tion in pp and pd reactions at 1 - 2 GeV;
Phys. Lett. B301 (1993) 123

Kaptari, L.I., A.Y. Umnikov, B. Kämpfer:
Nuclear structure functions;
Phys. Rev. D47 (1993) 3804

Kreutz, P., J.C. Adloff, M. Begemann-Blaich, P. Bouisson, J. Hubele, G. Imme, I. Jori, G.J. Kunde, S. Leray, V. Lindenstruth, Z. Lin, U. Lynen, R.J. Meijer, U. Milkau, A. Moroni, W.F.J. Müller, C. Ngo, C.A. Ogilvie, J. Pochozalla, G. Raciti, G. Rudolf, H. Sann, A. Schüttauf, W. Seidel, L. Stuttge, W. Trautmann, A. Tucholski:
Charge Correlations as a Probe of Nuclear Disassembly;
Nucl. Phys. A556 (1993) 672

Kuhlmann, E., H. Brand, S. Brand, P. Cloth, M. Dahmen, V. Drüke, W. Eyrich, D. Filges, H. Freisleben, A. Fritsche, K. Kilian, M. Kirsch, H. Koch, R.A. Kraft, J. Krug, S. Lange, H. Macher, H. Matthäy, P. Michel, R. Mirz, K. Möller, H.P. Morsch, B. Naumann, L. Naumann, W. Oelert, A. Parsch, N. Paul, P. Ringe, E. Roderburg, K. Röhrich, A. Röser, M. Rogge, G. Schmidt, M. Schmidt, O. Schult, T. Sefzik, M. Steinke, F. Stinzing, R. Stratmann, P. Turek, R. Werding, S. With:
Light meson production and pp.Bremsstrahlung at the COSY Time-of-Flight spectrometer;
Physica Scripta 48 (1993) 226

Kuhn, C. et al., R. Kotte, J. Mösner, W. Neubert, D. Wohlfarth:
Entropy production in the Au+Au reaction between 150 and 800 MeV;
Phys. Rev. C48 (1993) 1232

Leifels, Y., et al., R. Kotte, J. Mösner, W. Neubert, D. Wohlfarth:
Exclusive studies of neutron and charged particle emission in collisions of Au+Au at 400 MeV/nucleon;
Phys. Rev. Lett. 71 (1993) 963

Matsuo, M., T. Dossing, B. Herskind, S. Frauendorf:
Poisson and Porter-Thomas Fluctuations in Off-yrast Rotational Transitions;
Nucl. Phys. A564 (1993) 345

Matsuo, M., T. Dossing, B. Herskind, S. Frauendorf, E. Vigezzi, R.A. Broglia:
Chaotic Behaviour in Warm Deformed Nuclei Induced by Residual Two-body Interactions;
Nucl. Phys. A557 (1993) 211c

Meißner, Th., G. Ripka, R. Wünsch, P. Sieber, F. Grümmer and K. Goeke:
Scale Invarianz and the Stability of a Hedgehog Soliton;
Phys. Lett. B299 (1993) 183

Ogilvie, C.A., J.C. Adloff, M. Begemann-Blaich, P. Bonisson, J. Hubele, G. Imme, I. Iori, P. Kreutz, G.J. Kunde, S. Leray, V. Lindenstruth, Z. Lin, U. Lynen, R.J. Meijer, U. Milkau, A. Moroni, W.F.J. Müller, C. Ngo, J. Pochozalla, G. Raciti, G. Rudolf, H. Sann, A. Schüttauf, W. Seidel, L. Stuttge, W. Trautmann, A. Tucholski:
Multi-fragment Events as a Probe of Nuclear Disassembly;
Nucl. Phys. A553 (1993) 271

Oliveira, J.R.B., S. Frauendorf, M.A. Deleplanque, R.M. Diamond, F.S. Stephens, C.W. Beausang, J.E. Draper, C. Duyar, E. Rubel, J.A. Becker, E.A. Henry, N. Roy:
Rotational-Induced Transition from Superfluid to Normal Phase in Mesoscopic Systems: ^{168}Yb and Adjacent Nuclei;
Phys. Rev. C47 (1993) R926

Ritman, J., F.D. Berg, W. Kühn, V. Metag, R. Novotny, M. Nutheisen, P. Paul, M. Pfeiffer, U. Schwalb, H. Löhner, L. Venema, A. Gobbi, N. Herrmann, K.D. Hildenbrand, J. Mösner, R.S. Simon, K. Teh, J.P. Wessels, T. Wienold:
First Observation of the Coulomb-Excited Double Giant Dipole Resonance in ^{208}Pb via Double-γ Decay;
Phys. Rev. Lett. 70 (1993) 533

Roderburg, E. et al., P. Michel, K. Möller, B. Naumann, L. Naumann, G. Schmidt:
Studies of η and η' Measurements with the Time of Flight Spectrometer at COSY;
Acta Phyisica Polonica B24 (1993) 1629

Tsang, M.B. et al., W. Seidel:
Onset of Nuclear Vaporization in ^{197}Au + ^{197}Au Collisions;
Phys. Rev. Lett. 71 (1993) 1502,
Preprint MSUCL-897 Jun. 1993

Venema, L.B., H. Braak, H. Löhner, A.E. Raschke, R.H. Siemssen, M. Sumbera, H.W. Wilschut, F.D. Berg, W. Kühn, V. Metag, M. Notheisen, R. Novotny, M. Pfeiffer, J. Ritman, O. Schwalb, A. Gobbi, K.D. Hildenbrand, S. Hlavac, R. Holzmann, R.S. Simon, U. Sodan, K. Teh, J. Wessels, N. Herrmann, T. Wienold, R. Kotte, J. Mösner, W. Neubert, D. Wohlfarth, R. Ostendorf, Y. Schutz, N. Brummund, R. Santo:
Azimuthal Asymmetrie of Neutral Pion Emission in Au+Au Reactions at 1 GeV/U;
Phys. Rev. Lett. 71 (1993) 835

Winter, G., R. Schwengner, J. Reif, H. Prade, L. Funke, R. Wirowski, N. Nicoley, A. Dewald and P. von Brentano:
A study of excited states in ^{85}Kr and ^{86}Kr; Evidence for neutron-core excitations in the N=50 nucleus ^{86}Kr;
Phys. Rev. C48 (1993) 1010

Zilges, A., R.-D. Herzberg, P. von Brentano, F. Dönau, R.D. Heil, R.V. Jolos, U. Kneissl, J. Margraf, H.H. Pitz and C. Wesselborg:
First Identification of Dipole Excitation to a $2^+ \otimes 3^- \otimes$ Particle Multiplet in an odd-A Nucleus;
Phys. Rev. Lett. 70 (1993) 2880

2. Conference Contributions and Research Reports

Andrassy, M., G.G. Chubarian, P. Gippner, C.-M. Herbach, A. Matthies, H.-G. Ortlepp, G. Pausch, G. Renz, K.D. Schilling, W. Wagner:
Analyse der Massen- und Impulsbilanz bei der Messung von Fragmenten aus Schwerionenreaktionen;
Poster, Spring Meeting of the German Physical Society (Nuclear Physics), Mainz, Mar. 1993,
Verhandlungen der DPG 4 (1993) 634

Augustinski, G., et al., J. Biegansky, R. Kotte, J. Mösner, W. Neubert, D. Wohlfarth:
Towards the completed FOPI-Facility;
GSI Scientific Report, GSI 93-1, p. 371

Augustinski, G. et al., J. Hutsch, R. Kotte, J. Mösner, W. Neubert, D. Wohlfarth:
The many steps of the HELITRON;
GSI Scientific Report, GSI 93-1, p. 372

Barz, H.W., J.P. Bondorf, R. Donangelo, B. Heide, H. Schulz and K. Sneppen:
Effects of Flow on the Velocity Correlations of Fragments in Nuclear Disassembly Reactions;
Proc. Int. Workshop on Gross Properties of Nuclei and Nuclear Excitations XXI; Hirschegg, Österreich, Jan. 18-23, 1993, (ed.) H. Feldmeier, p. 263

Barz, H.W., P. Danielewicz, H. Schulz and G.M. Welke:
Collisions in an expanding pion gas and the $p_\perp$ spectrum in ultrarelativistic heavy-ion collisions;
Proc. Budapest Workshop on Relativistic Heavy Ion Collisions, Budapest, Hungary, Aug. 1992, (Eds.) T. Csörgö, KFKI Budapest preprint KFKI-1993-11/A (1993) p. 135

Brand, H. et al., COSY-TOF-collaboration:
Status of the Time-of-Flight Spectrometer;
Annual Report 1992, Jül-2590, KFA Jülich, Feb. 1993

Brand, H., S. Brand, S. Chamera, H. Freiesleben, A. Fritsche, P. Hermanowski, H. Koch, J. Krug, E. Kuhlmann, J.S. Lange, H. Matthäy, P. Ringe, A. Röser, M. Steinke, M. Strunk, U. Zielinski, L. Naumann und die COSY-TOF-Kollaboration:
Laserkalibrierungssystem für das COSY-TOF-Spektrometer;
Spring Meeting of the German Physical Society (Nuclear Physics), Mainz, Mar. 1993

Brandt, U., K. Daumiller, P. Doll, R. Gumbsheimer, H. Hucker, H.O. Klages, P. Kleinwächter, G. Kolb, H.J. Mayer, H. Müller:
Streamer Tubes for KASCADE Muon Detectors;
Proc. of the 23. Int. Conf. Cosmic Ray, Calgary, Canada, 1993, Vol. IV, p. 678

Bunatian, G.G., B. Kämpfer:
Properties of ρ , ω mesons in dense and hot nuclear matter near the critical pion mode softening;
Spring Meeting of the German Physical Society (Nuclear Physics), Mainz, Mar. 1993

Bunatian, G.G., B. Kämpfer:
Quasi-particle description of a strongly interacting pion gas;
Preprint FZR-93-28

Cassing, W., A. Peter and A. Pfitzner:
Dynamische Beschreibung von Zweiteilchenstößen und Dichtefluktuationen;
Verhandlungen der DPG 4 (1993) 708

Dittes, F.M., E. Doron, U. Smilansky:
Semiclassical evolution of the baker's map: How long does it last;
WIS 93/74-Aug-PH (Rehovot, Israel)

Dittes, F.M., E. Doron, U. Smilansky:
Semiclassical evolution of the baker´s map: How long does it last;
Poster auf "The Gran Finale", Como, Italien, Sep. 5-10, 1993

Dittes, F.M.:
Transfer operator approach to the semiclassical baker's map;
Meeting on "Applied periodic orbit theory", Bad Honnef, Nov. 2-4, 1993

Enghardt, W.:
Einrichtung einer experimentellen Strahlentherapie bei der Gesellschaft für Schwerionenforschung Darmstadt;
(Herausgeber: G. Kraft, G. Gademann) GSI-Report 93-23

Enghardt, W., B.G. Hasch, P. Manfraß, J. Pawelke, M. Sobiella, P. Blochberger, A. Friedrich, H. Geissel, H. Irnich, G. Kraft, A. Magel, W. Meufels, G. Münzenberg, F. Nickel, P. Poppensieker, I. Schall, D. Schardt, C. Scheidenberger, B. Voss, C. Ziegler:
Positron emission tomography for dose localization and beam monitoring in light ion tumour therapy;
Poster, European Congress of Medical Physics 93, Puerto de la Cruz, Spain, Sep. 1993;

Enghardt, W., B.G. Hasch, P. Manfraß, J. Pawelke, M. Sobiella, P. Blochberger, A. Friedrich, H. Geissel, H. Irnich, G. Kraft, A. Magel, W. Meufels, G. Münzenberg, F. Nickel, P. Poppensieker, I. Schall, D. Schardt, C. Scheidenberger, B. Voss, C. Ziegler:
Anwendung der Positronen Emissions Tomographie für die Kontrolle der Tumortherapie mit leichten Ionen;
Poster, 24. Wissenschaftliche Tagung der Deutschen Gesellschaft für Medizinische Physik, Erlangen, Oct. 1993

Enghardt, W., W.D. Fromm, H. Geissel, H. Keller, G. Kraft, A. Magel, P. Manfraß, G. Münzenberg, F. Nickel, J. Pawelke, D. Schardt, C. Scheidenberger, M. Sobiella:
Results of in-beam PET imaging experiments at the FRS;
GSI Scientific Report, GSI 93-1, p. 334

Fomichev, A.S., I. David, S.M. Lukyanov, Yu.E. Penionzhkevich, N.K. Skobelev, O.B. Tarasov, A. Matthies, H.-G. Ortlepp, W. Wagner, M. Lewitowicz, M.G. Saint-Laurent, J.M. Corre, Z. Dlouhy, I. Pecina:
The Response of a Large CsI(Tl) Detector to Light Particles and Heavy Ions in the Intermediate Energy Range;
GANIL P 93 23, CAEN, France, 1993

Fomichev, A.S., W. Wagner, I. David, Z. Dlouhy, J.M. Corre, M. Lewitowicz, S.M. Lukyanov, A. Matthies, L. Nosek, H.-G. Ortlepp, Yu.E. Penionzhkevich, I. Pecina, M.G. Saint-Laurent, N.K. Skobelev, O.B. Tarasov:
The Resonse of CsI(Tl) Counter to Light and Intermediate Mass Fragments in the Energy Range 2 ÷ 77 MeV/A;
Preprint JINR P13-93-114, Dubna, Russia, 1993

Hofmann, T., A. Wörner, W.D. Kunze, U. Lynen, T. Möhlenkamp, W.F.J. Müller, H. Sann, W. Seidel:
Der TP-MUSIC III Detektor am Aladin-Spektrometer;
DPG Frühjahrstagung Physic der Hadronen und Kerne, Mainz, Mar. 22, 1993;
Verhandlungen der DPG 4 (1993) 654

Iskra, W. M. Müller and I. Rotter:
Selforganization in the nuclear system. I: The slaving principle;
Preprint FZR-93-01

Iskra, W., M. Müller and I. Rotter:
Selforganization in the nucear system. II: Formation of a new order;
Preprint FZR-93-13

Iskra, W., M. Müller and I.Rotter:
Selbstorganisation in Atomkernen;
Verhandlungen der DPG 4 (1993) 672

Iskra, W., M. Müller and I. Rotter:
Resonance states in excited systems;
Verhandlungen der DPG 4 (1993) 708

Iskra, W., M. Müller and I. Rotter:
Hierarchical formation of local resonance structure;
Verhandlungen der DPG 4 (1993) 715

Iskra, W., M. Müller and I. Rotter:
Selforganization in an open quantum system;
Poster auf der Tagung "Dynamic Days", Rydzyna, Poland, Jun. 1993

Iskra, W., M. Müller and I. Rotter:
Collective strength in nuclei resulting from selforganization;
Poster auf der "Gull Lake Nuclear Physics Conference: Giant Resonances", Gull Lake, Michigan, USA, Aug. 1993

Iskra, W., M. Müller and I. Rotter:
Selforganization in an open quantum system;
Poster auf "XXIII Mazurian Lakes Summer School: Frontier Topics in Nuclear, Astronuclear and Astroparticle Physics", Piaski, Poland, Aug. 1993

Iskra, W., M. Müller and I. Rotter:
Selforganization in an open quantum system;
Poster auf der Tagung "Chaos, Order and Patterns, Aspects of Nonlinearity", Como, Italy, Sep. 1993

Jenkovszky, L.L., B. Kämpfer, V.M. Sysoev:
Bubble free energy in a first-order phase transition;
Preprint ITP-92-51E

Jeong, S.C. et al., R. Kotte, J. Mösner, W. Neubert, D. Wohlfarth:
Collective Motion in Selected Central Collisions of Au on Au at 150 A*MeV;
Preprint, GSI-93-38

Kämpfer, B.:
Properties of ρ,ω mesons in dense nuclear matter near critical pion mode softening;
Poster, Spring Meeting of the German Physical Society (Nuclear Physics), Mainz, Mar. 1993

Kämpfer, B.:
Velocity correlations of intermediate mass fragments in central reactions of Au + Au at 100-400 MeV;
Poster, Spring Meeting of the German Physical Society (Nuclear Physics), Mainz, Mar. 1993

Kämpfer, B. and O.P. Pavlenko:
Dilepton radiation from pre-equilibrium parton matter;
Proc. of the Budapest Workshop on Relativistic Heavy Collisions, (Eds.) T. Csörge et al., KFKI-1993-11/A, p. 130

Kämpfer, B. and O.P. Pavlenko:
Probing early parton kinetics by photons, dileptons and charm;
Poc. of Quark Matter '93, FZR-93-16

Kämpfer, B., P. Koch, O.P. Pavlenko:
Dynamics of an expanding dense pion gas and low-mass dilepton emission;
Preprint FZR-93-07,
Uni Bremen Report No. 47

Kämpfer, B. and O.P. Pavlenko:
Photon production in a gluon-enriched plasma;
Preprint FZR-93-16

Kämpfer, B. and O.P. Pavlenko:
Dilepton radiation from pre-equilibrium parton matter;
Proc. Int. Workshop on Gross Properties of Nuclei and Nuclear Excitation, Hirschegg 1993, (ed.) H. Feldmeier, p. 111

Kämpfer, B., P. Koch, O.P. Pavlenko:
Low-mass dilepton emission from an expanding superdense pion gas;
Proc. Int. Workshop on Gross Properties of Nuclei and Nuclear Excitations, Hirschegg 1993, (ed.) H. Feldmeier, p. 278

Kämpfer, B., R. Kotte for the FOPI-Collaboration:
Velocity correlations of intermediate mass fragments produced in central collisions of Au + Au at E=100,150,250,400 AMeV;
GSI-Nachrichten 10-93

Kämpfer, B., O.P. Pavlenko:
Probing early parton kinetics by photons, dileptons, and charm;
Preprint FZR-93-16,
Proc. of Quark Matter '93

Kämpfer, B., O.P. Pavlenko:
Transverse momentum dependence of dileptons from parton matter produced in ultra-relativistic heavy-ion collisions;
Preprint FZR-93-23

Kämpfer, B., O.P. Pavlenko:
Photon production in an expanding and chemically equilibrating gluon-enriched plasma;
Preprint FZR-93-29

Kämpfer, B., O.P. Pavlenko:
Kinetics of pre-equilibrium parton matter probed by dileptons, in "Particle Procuction in Highly Excited Matter", (Eds.) H.H. Gutbrod, J. Rafelski, Plenum Press, New York and London 1993, NATO ASI series 303B, p. 649

Komarov, V.I., A.Yu. Petrus and H. Müller:
High Excitation of the Few-Nucleon Systems Accompanied by the Meson Cooling;
Deuteron 93, Dubna, Sep. 1993

Kotte, R., B. Kämpfer, J.Mösner, W. Neubert, D. Wohlfarth:
Flow Effects in Cluster Correlations;
International Meeting on FOPI-Activities, LPC Clermont-Ferrand, France, May 1993

Kraft, G., U. Weber, D. Schardt, W. Enghardt, M. Scholz:
Heavy Ion Therapy at GSI (HITAG);
GSI-Nachrichten 11-93, p. 3

Kunde, G.J. et al., W. Seidel:
Multifragmentation of the System Au+Au at SIS-Energies;
GSI Scientific Report, GSI 93-1, p. 51

Lindenstruth, V. et al., W. Seidel:
Breakup Configurations in Multiple Disintegration of Projectile Fragments;
Preprint, GSI-93-54;
GSI-Scientific Report, GSI 93-1, p. 50

Lindenstruth, V. et al., W. Seidel:
Isospin Correlations in Multifragmentation Processes;
GSI Scientific Report, GSI 93-1, p. 52

Lips, V., R. Barth, H. Oeschler, S.P. Avdeyev, V.U. Karnaukhov, W.D. Kuznetzov, L.A. Petrov, O.V. Bachkarev, L.V. Chulkov, E.A. Kuzmin, W. Karez, W. Neubert, E. Norbeck:
Multifragmentation induced by relativistic alpha-projectiles studied with the 4πsetup FASA;
31. International Winter Meeting, Bormio, Italy, Jan. 25, 1993

Lips, V., R. Barth, H. Oeschler, S.P. Avdeyev, V.A. Karnaukhov, W.D. Kuznetsov, L.A. Petrov, O.V. Bachkarev, L.V. Chulkov, E.A. Kuzmin, W. Karez, W. Neubert, E. Norbeck:
Multifragmentation induced by relativistic α-projectiles;
Preprint, Inst. für Kernphysik, Technische Hochschule Darmstadt, IKDA 93/42, Oct. 1993

Michel, P., K. Möller, B. Naumann, L. Naumann, A. Schamlott and A. Schülke:
Test of the Start Detector System for the Investigation of the pp-Bremsstrahlung with the COSY Time-of-flight Spectrometer (TOF);
Annual Report 1992, Jül-2590, KFA Jülich, Feb. 1993

Michel, P., K. Möller, B. Naumann, L. Naumann, A. Schamlott, A. Schülke and the COSY-TOF-Collaboration:
Startdetektor zur Untersuchung der Proton-Proton-Bremsstrahlung am TOF-Spektrometer des COSY-Ringes;
Spring Meeting of the German Physical Society (Nuclear Physics), Mainz, Mar. 1993

Michel, P., K. Möller, A. Schamlott, A. Schülke:
Test des Rossendorfer COSY-TOF-Startdetektors am Zyklotron mit 13 MeV Protonen;
Laborbericht, May 1993;
COSY-TOF-NOTES-RO-1-1993

Michel, P., A.Schülke:
LED-Testsystem für den COSY-TOF-Startdetektor MARS;
COSY-TOF-NOTES-RO-2-1993

Möller, K. and the TOF-Collaboration:
COSY-Flugzeitspektrometer TOF an COSY;
Poster, Spring Meeting of the German Physical Society (Nuclear Physics), Mainz, Mar. 1993

Müller, H.:
Subthreshold Poduction of K^- Mesons in Proton-Induced Reactions at Light Nuclei;
Proc. of the 105th International WE-Heraeus-Seminar on Hadronic Processes at Small Angles in Storage Rings, edited by E. Rössle, O.W.B. Schult, Bad Honnef, Feb. 1993

Naumann, L., B. Naumann, A. Schamlott:
Untersuchung des Einflusses der Restgaskomponenten des Startdetektorvolumens auf das Flüssig-Wasserstoff-Target des COSY-TOF-Spektrometers;
COSY-TOF-Notes-RO-3-1933, Nov. 1993

Neubert, W., R. Kotte, J. Mösner, D. Wohlfarth:
Analysis of isotopic yield ratios by means of the Statistical Multifragmentation Model;
Workshop on Multifragmentation, Copenhagen, Sep. 1993

Ortlepp, H.-G., M. Andrassy, G.G.Chubarian, M. Danziger, L. Dieterle, A.S.Fomichev, P. Gippner, C.-M. Herbach, A.I. Ivanenko, I.V. Kolesov, A. Matthies, D. May, Yu.Ts. Oganessian, Yu.E. Penionzhkevich, V.N. Pokrovskij, G. Renz, L.A. Rubinskaja, V.E. Shuchko, O.V. Strekalovskij, V.V. Trofimov, V.M. Vasko, W. Wagner, K. Heidel, K.D. Schilling, W. Seidel, H. Sodan, H. Fuchs, D. Hilscher, H. Homeyer, W. v. Oertzen, P. Ziem, G. Pausch, B.A.Burova, S.V. Radnev, I.D. Sandrev:
The 4π-Fragmentspectrometer FOBOS - Status and First Preliminary Results -;
Proc. of the Heavy Ion School-Seminar, Dubna, Russia, May 1993

Pawelke, J., W. Enghardt:
A simple and fast reconstruction algorithm for on-line range measurements by means of PET in light ion tumour therapy;
GSI Scientific Report, GSI 93-1, p. 335

Pelte, D., W. Reisdorf, T. Wienold for the FOPI-Collaboration:
FOPI studies of Au on Au collisions at SIS energies;
GSI-Nachrichten, GSI 09-93

Peter, A., W. Cassing and A. Pfitzner:
Probing long- and short-range correlations with giant resonances;
GSI Scientific Report, GSI 93-1, p. 35

Pfitzner, A., W. Cassing, A. Peter:
Vibrations versus collisions and the iterative structure of two-body dynamics;
Preprint FZR-93-26

Protochristov, Chr., L. Kostova, M. Michailova, W. Andrejtscheff, L. Käubler, L. Funke, H. Prade, R. *Schwengner, J. Reif and G. Winter:*
The Proton $g_{9/2}$ Isomer in the N=50 Nucleus ^{87}Rb;
Verhandlungen der DPG 4 (1993) 561

Roderburg, E. et al.:
Studies of η and η' Measurements with the Time of Flight Spectrometer at COSY;
KFA-IKP(I)-1993-6, Oct. 1993

Schülke, A., P. Michel, K. Möller, B. Naumann, L. Naumann, A. Schamlott:
Entwicklung und Test eines Startdetektors für das ppγ-Experiment am COSY-Flugzeitspektrometer TOF;
Poster, Spring Meeting of the German Physical Society (Nuclear Physics), Mainz, Mar. 1993

Seidel, W. et al.:
A new TPC with enlarged dynamic range for tracking in high-energy heavy ion experiments;
Poster auf der Third London Conference on Position-Sensitive Detectors, London, Sep. 1993

Sistemich, K., M. Büscher, W. Cassing, B. Kamys, V. Komarov, V. Koptev, H. Müller and A. Sibirtsev:
Hadronic Processes at Small Angles in Storage Rings;
Proc. of the 105th International WE-Heraeus-Seminar on Hadronic Processes at Small Angles in Storage Rings, edited by E. Rössle, O.W.B. Schult, Bad Honnef, Feb. 1993

Sobeslavsky, E., R. Begmann, M. Kretzschmar, U. Wenzel:
Application of an image processing software for quantitative autoradiography;
FZR 93-12, Institute of bioanorganic and radiopharmaceutical chemistry, Annual Report 1993, p. 30

Trautmann, W. et al., W. Seidel:
Spectrometric Results from ALADIN;
31. International Winter Meeting, Bormio, Italy, Jan. 1993,
GSI-Nachrichten 07-93

Trautmann, W. et al., W. Seidel:
Multifragmentation in Peripheral Nucleus-Nucleus Collisions;
Preprint GSI 93-76

Wagner, W., A.S. Fomichev, H.-G. Ortlepp, C.-M. Herbach, A. Matthies, G. Pausch, O.V. Strekalowskij, M.A. Milovidov, V.A. Vitenko:
A Large Area CsI(Tl) Detector for the Scintillator Shell of FOBOS;
JINR Rapid Communications 4[61]-93, Dubna, Russia, 1993

Wünsch, R.:
Self-Consistent Solutions of the Semibosonized Nambu & Jona-Lasinio Model;
Preprint FZR-93-18

3. Lectures and Seminars

Andrassy, M., G.G. Chubarian, M. Danziger, P. Gippner, L. Dietterle, A.S. Fomichev, H. Fuchs, K. Heidel, C.-M. Herbach, D. Hilscher, H. Homeyer, I.A. Ivanenko, I.V. Kolesov, A. Matthies, D. May, Yu.Ts. Oganessian, W. v. Oertzen, H.-G. Ortlepp, G. Pausch, Yu.E. Penionzhkevich, G. Renz, K.D. Schilling, H. Sodan, O.V. Strekalovskij, V.V. Trofimov, V.M. Vasko, W. Wagner, P. Ziem:
FOBOS - ein 4π-Detektor mit niedriger Energieschwelle für Schwerionenreaktionsprodukte;
Spring Meeting of the German Physical Society (Nuclear Physics), Mainz, Mar. 1993

Barz, H.-W.:
Flavour Kinetic Model for Particle Production in Ultrarelativistic Heavy Ion Collisions;
Interdisciplinary Workshop on Statistical Description of Transport in Plasma, Astro- and Nuclear Physics, Les Houche, France, Feb. 1993

Barz, H.-W.:
Kinetic Theory of an Expanding Pion Gas;
Nordic Workshop on High Energy Reaction Theory, Bergen, Norway, Jun. 1993

Barz, H.-W.:
Transport treatment of an Expanding Pion Gas;
NATO Advanced Study Institute on "Hot and Dense Nuclear Matter", Bodrum, Turkey, Sep./Oct. 1993

Barz, H.-W. and R. Schmidt:
Moderne Probleme der Kern- und Clusterphysik;
Lecture, TU Dresden, Winter semester 1992/93, Summer semester 1993

Dittes, F.M.:
Statistical properties of regular and chaotic open quantum systems;
Seminar, UNAM Mexico-City, Feb. 1993

Dittes, F.M.:
New results on strongly coupled quantum systems;
Seminar, UNAM - Filiale Guernavaca, Mexico, Mar. 1993

Dittes, F.M.:
Long-time behaviour of the semiclassical baker's map;
Seminar, The Weizman Institute of Science, Rehovot, Israel, Apr. 1993

Dittes, F.M.:
Transfer operator approach to the semiclassical baker's map;
Workshop on classical mechanical methods in quantum mechanics, University Milano, Filiale Como, Italy, Jun. 1993

Dittes, F.M.:
Long time accuracy of the semiclassical approximation for the baker's map;
Quantum Chaos Day at the Technion Haifa, Israel, Jul. 1993

Dittes. F.M.:
Semiklassische Behandlung einfacher chaotischer Systeme;
Seminar, FZ Rossendorf, Nov. 1993

Dönau, F.:
Quasiclassische Orbitale in Rotierenden Kernen;
Institut für Theoretische Physik, Universität zu Köln, Feb. 1993

Enghardt, W.:
Positron emission tomography for dose localization and beam monitoring in light ion tumour therapy;
Int. Workshop of the EORTC Heavy Particle Therapy Group, Brussels, Belgium, Mar. 1993

Enghardt, W.:
PET für die Dosislokalisation und Bestrahlungskontrolle bei der Leichtionen-Tumortherapie;
Seminar, Forschungszentrum Jülich, Sep. 1993

Enghardt, W.:
PET für die Dosislokalisation und Bestrahlungskontrolle bei der Leichtionen-Tumortherapie;
Seminar, Inst. für Strahlenschutzphysik, TU Dresden, Nov. 1993

Frauendorf, S.:
Cluster binding energies calculated with the Strutinsky method;
Clusterworkshop, NBI Copenhagen, Denmark, Jan. 1993

Frauendorf, S.:
Orientation of the angular momentum at high spin;
Seminar, FZ Rossendorf, Jan. 1993

Frauendorf, S.:
Orientierung des Drehimpulses in schnell rotierenden Atomkernen;
Seminar, FZ Rossendorf, Jan. 1993

Frauendorf, S.:
$\Delta I = 1$ band in the light Pb nuclei;
Seminar, Institut of Nuclear and Radiation Physics, University Bonn, Feb. 1993

Frauendorf, S.:
Strutinsky claculations of the shapes and binding energies of alkali clusters;
Seminar, Institute for Theoretical Physics, University Regensburg, Feb. 1993

Frauendorf, S.:
M1-Bands in Light Pb-Isotopes;
Spring Meeting of the German Physical Society (Nuclear Physics), Mainz, Mar. 1993

Frauendorf, S.:
The Shape of Quantal Droplets: Alkali Atom Clusters Compared with Nuclei;
Nuclear Physics Seminar, University of Tennessee, USA, Apr. 1993

Frauendorf, S.:
Rotation about a Nonprincipal Axis;
Theoretical Physics Seminar, Oak Ridge National Laboratory, USA, Apr. 29, 1993

Frauendorf, S.:
The Onset of Chaos in Rotating Nuclei;
Nuclear Physics Division Seminar, Oak Ridge National Laboratory, USA, Apr. 1993

Frauendorf, S.:
Rotationsdämpfung - ein Signal für den Übergang zu chaotischem Verhalten von warmen rotierenden Kernen;
Seminar, FZ Rossendorf, May 1993

Frauendorf, S.:
The Decline of K-Forbiddeness;
Workshop on Nuclear Spectroscopy at the New Arrays, University of Lund, Sweden, Jun. 1993

Frauendorf, S.:
The Decline of K-Forbiddeness;
International Conference on the Future of Nuclear Spectroscopy, Crete, Jun./Jul. 1993

Frauendorf, S.:
The Spin Orientation Degree of Freedom;
3 Lectures Lawrence Berkeley Laboratory, Berkeley, USA, Jul./Aug. 1993

Frauendorf, S.:
Thermodynamic Properties of the Electron System in Alkali Clusters;
ICW-93, International Workshop on Clusters as a Local Probe of Bulk Phenomena, Michigan State University, East Lansing, USA, Aug. 1993

Frauendorf, S.:
The Decline of K-Forbiddeness;
Nuclear Physics Division Seminar, Oak Ridge National Laboratory, USA, Sep. 1993

Heide, B.:
Mittelenergetische Schwerionenstöße im Rahmen eines Botzmann-Ühling-Uhlenbeck-Kopenhagen Hybridmodells;
Theorie-Treffen SIS, Rauischholzhausen, Jun. 1993

Heide, B.:
Schwerionenstöße im Hybridmodell;
Seminar, Institut für Theoretische Physik der TU Dresden, Jul. 1993

Kämpfer, B.:
Probing non-equilibrated parton matter by dileptons;
XXI Int. Workshop, Hirschegg, Austria, Jan. 1993

Kämpfer, B.:
Kosmische Phasenübergänge;
Spring Meeting of the German Physical Society (Nuclear Physics), Mainz, Mar. 1993

Kämpfer, B.:
Dileptonen von Nichtgleichgewichtspartonenmaterie;
Spring Meeting of the German Physical Society (Nuclear Physics), Mainz, Mar. 1993

Kämpfer, B.:
Dilepton yields of of-equilibrium parton matter;
International Workshop, Bergen, Norway, Jun. 1993

Kämpfer, B.:
Probing parton matter by dileptons, photons and charm;
Quark Matter '93, Borlänge, Sweden, Jun. 1993

Kämpfer, B.:
Theorie des Atomkerns;
Lecture, TU Dresden, Summer semester 1993;
Quantenelektrodynamik;
Lecture, TU Dresden, Winter semester 1993/94

Kotte, R., B. Kämpfer, J. Mösner, W. Neubert, D. Wohlfarth:
Flow Effects in Cluster Correlations;
International Meeting on FOPI-Activities, LPC Clermont-Ferrand, France, May 1993

Lauckner, K.:
Entwicklung eines Verfahrens zur Verbesserung der Schwächungskorrektur von PET-Bildern;
Seminar, FZ Rossendorf, Jun. 1993

Meng, L.:
Berry phase and diabolic pair transfer;
Seminar, FZ Rossendorf, Oct. 1993

Michel, P.:
Konzept einer schnellen TDC zur Online-Datenerfassung am COSY-TOF-Spektrometer;
Seminar, Universität Bochum, Jun. 1993

Michel, P.:
Detektorkonzeption für Ringelemente des COSY-TOF-Spektrometers;
TOF-Meeting, KfA Jülich, Nov. 1993

Möller, K.:
Kernreaktionen I;
Lectures TU Dresden,
Winter semester 1993/94

Müller, H.:
Subthreshold Production of K^- Mesons in Proton-Induced Reactions at Light Nuclei;
105th International WE-Heraeus-Seminar on Hadronic Processes at Small Angles in Storage Rings, Bad Honnef, Feb. 1993

Müller, M.:
Selbstorganisation in Atomkernen;
Spring Meeting of the German Physical Society (Nuclear Physics), Mainz, Mar. 1993

Müller, M.:
Hierarchische Bildung von lokaler Resonanzstruktur;
Spring Meeting of the German Physical Society (Nuclear Physics), Mainz, Mar. 1993

Müller, M.:
Selbstorganisation in Atomkernen;
Seminar, Technische Universität Dresden, Institut für Theoretische Physik, Apr. 1993

Müller, M.:
Selforganization in the nuclear system;
Intern. Workshop on Time Reversal Invariance and Parity Violation in Neutron Reactions, Dubna, Russia, May 1993

Müller, M.:
Selforganization in an open quantum system;
XXIII Mazurian Lakes Summer School: Frontier Topics in Nuclear, Astronuclear and Astroparticle Physics, Piaski, Poland, Aug. 1993

Müller, M.:
Selbstorganisation am Beispiel eines offenen Quantensystems;
Seminar, WE-Heraeus-Ferienkurs "Ordnung und Quantenchaos", Dresden, Sep. 1993

Müller, M.:
Selbstorganisation in Atomkernen;
Chaos und Strukturbildung, München, Nov. 1993

Naumann, B.:
Vergleich von Simulationsrechnungen für das COSY-TOF-Spektrometer mit einem Barrel bzw. einem dreilagigen Konsus;
TOF-Meeting, KfA Jülich, Nov. 1993

Naumann, L.:
Untersuchung der NN-Bremsstrahlung unter Berücksichtigung von Polarisationsvariablen;
Seminar, FZ Rossendorf, Jun. 1993

Naumann, L.:
Die Untersuchung des Einflusses der Restgaskomponenten des Startdetektorvolumens auf das Flüssig-Wasserstoff-Target des COSY-TOF-Spektrometers;
TOF-Meeting, KfA Jülich, Nov. 1993

Ortlepp, H.-G.:
The 4π-Fragment Spectrometer FOBOS - Status and First Preliminary Results;
School-Seminar on Heavy-Ion Physics, Dubna, Russia, May 1993

Ortlepp, H.-G.:
FOBOS - First Experiments and Program for 1994;
FLNR-Conference about the Program of Fundamental and Application Research at the FLNR in 1994 Ratmino, Russia, Dec. 1993

Pawelke, J.:
Positronen Emissions Tomographie in der Leichtionen-Tumortherapie;
Seminar, TU Dresden, Institut für Strahlenschutzphysik, Jun. 1993

Rotter, H.:
Zwischen Gunst und Gewalt, Physikerschicksale in der Sowjetunion;
Kolloquium Physik, Universität Marburg, Jul. 1993

Rotter, I.:
Resonanzzustände in angeregten Systemen;
Spring Meeting of the German Physical Society (Nuclear Physics), Mainz, Mar. 1993

Rotter, I.:
Quantum chaos and neutron resonances;
Scientific Council on Physics at Low and Intermediate Energies, JINR Dubna, Russia, Apr. 1993

Rotter, I.:
Selborganization in nuclei and irreversibility;
1993 Yukawa International Seminar, Quantum and Chaos: How Incompatible?, Kyoto, Japan, Aug. 1993

Rotter, I.:
Selbstorganisation im nuklearen System;
Lecture, WE-Heraeus-Ferienkurs "Ordnung und Quantenchaos", Dresden, Sep. 1993

Rotter, I.:
Synergetik;
Lecture, TU Dresden, Summer semester 1993

Schülke, A.:
Test des Rossendorfer COSY-TOF-Startdetektors am Zyklotron mit 13 MeV Protonen;
TOF-Meeting, Helmsdorf/Dresden, May 1993

Schülke, A.:
Das Bremsstrahlungsexperiment am COSY/TOF-Spektrometer;
FHG-Doktorandenseminar, TU Dresden, Jun. 1993

Schülke, A.:
Vorstellung des COSY-TOF-Startdetektors;
FHG-Doktorandenseminar, TU Dresden, Jun. 1993

Schülke, A.:
Methodische Untersuchungen zur zweiseitigen Auslese 2,50 m langer Szintillatorstreifen;
CANU-Meeting, Bad Honnef, Dec. 1993

Schwengner, R.:
High-Spin States built on the $17/2^+$ Isomer in ^{85}Kr;
Spring Meeting of the German Physical Society (Nuclear Physics), Mainz, Mar. 1993

Seidel, W.:
Si-CsI detectors for target rapidity fragments;
ALADIN Collaboration Meeting, Gargnano, Italy, Nov. 1993

Wagner, W.:
First experiments with the FOBOS-detector;
Advisory Committee for Low and Intermediate Energy Physics of JINR Dubna, Russia, Nov. 1993

Winter, G.:
Hochspinzustände in ^{85}Kr und ^{86}Kr;
Seminar, Institut für Strahlenphysik, Universität Stuttgart, May 1993

Wünsch, R.:
Untersuchungen zu Form und Tiefe des mittleren Potentials und zur Schwerpuntksbewegung der Quarks im Nukleon im Rahmen des Nambu & Jona-Lasinio-Modells;
Seminar, FZ Rossendorf, May 1993

Wünsch, R.:
Zero-Mode Corrections of the average meson fields in the Nambu & Jona-Lasinio Model;
Int. Workshop on the Quark Structure of Baryons, Trento, Italien, Oct. 1993

Wünsch, R.:
Zero-mode corrections to the NJL soliton;
Seminar, Universität Tübingen, Dec. 1993

Wünsch, R.:
Struktur der Hadronen;
Lecture, TU Dresden, Summer semester 1993

4. Talks of Visitors

Yu. Ts. Oganessian, Dubna:
Statusbericht und Perspektiven der Forschungsaufgaben im FLNR;
Jan. 19, 1993

M.P. Chavleishvili, München:
Spinphänomene in Hochenergiehadronenreaktionen;
Feb. 1, 1993

P. Geltenbort, Grenoble:
Neueste Ergebnisse mit Mikrostreifen-Proportionalzählern;
Feb. 3, 1993

W.I. Furman, Dubna:
Neutronenresonanzen;
Feb. 8, 1993

V.V. Pashkevich, Dubna:
Interpretation of Λ-attachment probabilities in hyperonic fission;
Feb. 15, 1993

H.J. Krappe, Berlin:
Spaltung heißer Kerne in Konkurrenz zur Verdampfung leichter Fragmente;
Mar. 1, 1993

S. Kolomeizev, Moskau:
Zur Pionenerzeugung in mittelenergetischen Schwerionenstößen;
Mar. 29, 1993

O.P. Pavlenko, Kiev:
Kinetics of parton matter in ultra-relativistic heavy-ion collisions;
Apr. 13, 1993

W. Lauth, Mainz:
Optische Spektroskopie an Spaltisomeren;
Apr. 19, 1993

M. Büscher, Jülich:
Die 0°-Facility - ein universelles Spektrometer für Experimente der Mittelenergiephysik am COSY;
Apr. 26, 1993

J. Rasmussen, Berkeley:
Large-matrix diagonalization studies of ^{154,156,158}Gd and neutron pair transfer;
May 3, 1993

T. Seligman/Mexico-City:
Statistische Kernphysik;
Jun. 14, 1993

H. Plendl, Florida:
Ladungsaustauschexperimente am LAMPF mit gestoppten negativen Pionen;
Jun. 28, 1993

M. Kirchbach-Arenhoevel, Darmstadt:
Kurzreichweitige Mesonenaustauschströme;
Jul. 5, 1993

W. Cassing, Giessen:
Neue theoretische Entwicklungen in der Schwerionenphysik;
Aug. 16, 1993

A. Peter, Giessen:
Mikroskopische Analyse der 2-Teilchen-Korrelationen in leichten Atomkernen;
Aug. 20, 1993

K. Holinde, Jülich:
Die Nukleon-Nukleon-Wechselwirkung im Mesonen-Austauschmodell;
Aug. 30, 1993

H. Börner, Grenoble:
Hochauflösende Gammaspektroskopie: Ein Werkzeug zur Erforschung von Atomkernen und Festkörpern;
Aug. 30, 1993

L.L. Jenkovszky, Kiev:
Das Pomeron-Modell der Nukleon-Nukleon-Streuung;
Sep. 28, 1993

H. Reinhardt, Tübingen:
QCD-motivierte effektive Hadronenmodelle;
Oct. 4, 1993

L. Kaptari, Dubna:
Electron scattering off nuclei (an introduction);
Oct. 11, 1993

K. Neergard, Copenhagen:
Spin-polarisation in rotierender Kernmaterie;
Oct. 18, 1993

A.I. Titov, Dubna:
Di-electron production in pp and pd reactions at 1 - 2 GeV;
Nov. 8, 1993

S. Lenz, Erlangen:
Projektileinfang an festen Streuzentren;
Nov. 10, 1993

A. Umnikov, Vancouver:
Deep-inelastic scattering on the deuteron within the Bethe-Salpeter formalism;
Nov. 12, 1993

K.R. Schubert, Dresden:
Experimente mit B-Mesonen - ein perspektivreiches Programm;
Nov. 22, 1993

A. Pelster, Stuttgart:
Theorie und Anwendungen nicht-integrabler Raum-Zeit-Transformationen;
Nov. 29, 1993

W. Reisdorf, Darmstadt:
Schwerionenreaktionen: Zentrale Stöße von Goldkernen bei SIS-Energien (Fragmentbildung und Fluß);
Dec. 6, 1993

Bao Li, Berlin:
Dynamical and statistical aspects of nuclear multifragmentation;
Dec. 13, 1993

S. Frauendorf:
Orientierung des Drehimpulses in schnell rotierenden Atomkernen;
Seminar, Rossendorf, Jan. 25, 1993

R. Wünsch:
Untersuchungen zu Form und Tiefe des mittleren Potentials und zur Schwerpunktsbewegung der Quarks im Nukleon im Rahmen des Nambu - Jona-Lasinio - Modells;
Seminar, Rossendorf, May 3, 1993

S. Frauendorf:
Rotationsdämpfung - ein Signal für den Übergang zu chaotischem Verhalten von warmen rotierenden Kernen;
Seminar, Rossendorf, May 24, 1993

L. Naumann:
Untersuchung der NN-Bremsstrahlung unter Berücksichtigung von Polarisationsobservablen;
Seminar, Rossendorf, Jun. 7. 1993

T. Meng:
Berry phase and diabolic pair transfer;
Seminar, Rossendorf, Oct. 25, 1993

F.M. Dittes:
Semiklassische Behandlung einfacher chaotischer Systeme;
Seminar, Rossendorf, Nov. 15. 1993

III. Personnel

Scientific Staff

Dr. Barz, H.W. [1)]
Dietterle, L. [2,4)]
Dr. Dittes, F.M.
Dr. Dönau, F.
Dr. Dshemuchadse, S.
Dr. Enghardt, W. [1)]
Dr. Frauendorf, S.
Dr. Gippner, P. [4)]
Dr. Herbach, C.-M.
Dr. Kämpfer, B. [1)]
Dr. Käubler, L. [1)]
Dr. Kleinwächter, P.
Dr. Kotte, R.
Dr. Manfraß, P.
Dr. Matthies, A. [4)]
May, D. [4)]
Dr. Meng, J.
Dr. Michel, P.
Dr. Möller, K. [1)]
Dr. Mösner, J.
Dr. Müller, H.
Dr. Naumann, B. [2)]
Dr. Naumann, L.
Dr. Neubert, W.
Dr. Ortlepp, H.-G. [4)]
Dr. Pfitzner, A.
Dr. Prade, H.
Dr. Reif, J.
Renz, G. [2,4)]
Richter, H. [3)]
Dr. Rotter, H. [3)]
Prof. Rotter, I. [1)]
Schamlott, A. [2)]
Dr. Schilling, K.D.
Dr. Schlett, M.
Dr. Schwengner, R.
Dr. Seidel, W.
Dr. Skoda, S.
Dr. Sobeslavsky, E.
Dr. Wagner, W. [4)]
Dr. Winter, G.
Wohlfarth, D.
Dr. Wünsch, R.

Technical Staff

Altus, M.
Angermann, H.
Baumann, U.
Berlin, J.U.
Boeck, M.
Böse, M.
Fiedler, J.
Förster, R.
Freitag, M.
Göbel, L.
Heidel, K.
Herrmann, K.H.
Hutsch, J.
Kerber, J.
Kluge, E.
Koslowsky, M.
Langer, M.
Lauckner, K.
Meier, B.
Prietzschk, B.
Probst, I.
Rimarzig, B.
Römer, H.
Scheinpflug, M.
Schneidereit, Chr.
Schulze, W.
Sobiella, M.
Uhlmann, A.
Umlauf, C. [4)]

Postgraduate Students

Biegansky, J.
Hasch, B.-G.
Heide, B.
Kolomeizew, J.
Krüger, J.
Möhlenkamp, T.
Müller, M.
Pawelke, J.
Schleif, M.
Schneider, Chr.
Schülke, A.

[1)] Finanzierung KAI(WIP)
[2)] Drittmittelstelle
[3)] Finanzierung ABM
[4)] z.Z. VIK Dubna